A NEW SUBSTRUCTURING METHOD FOR MODEL UPDATING OF LARGE-SCALE STRUCTURES

by

Shun WENG

B. Eng., M. Sc.

A Thesis Submitted for the Degree of **Doctor of Philosophy**

Department of Civil and Structural Engineering

The Hong Kong Polytechnic University, Hong Kong

June, 2010

THE HONG KONG POLYTECHNIC UNIVERSITY

Department of Civil and Structural Engineering

A NEW SUBSTRUCTURING METHOD FOR MODEL UPDATING OF LARGE-SCALE STRUCTURES

by

Shun WENG

A Thesis Submitted in Partial Fulfillment of the Requirements for the

Degree of **Doctor of Philosophy**

June, 2010

DECLARATION

I hereby declare that this dissertation entitled "***A New Substructuring Method for Model Updating of Large-Scale Structures***" is my own work and that, to the best of my knowledge and belief, it reproduces no material previously published or written, nor material that has been accepted for the award of any other degree or diploma, except where due acknowledgement has been made in the text.

Signed

Shun WENG

To My Family

ABSTRACT

In vibration-based model updating, the finite element model is iteratively modified to ensure its vibration properties reproduce the measured counterparts in an optimal way. The finite element model of a large-scale structure usually consists of a large number of degrees of freedom. Calculating the eigensolutions and eigensensitivities of such a finite element model and updating it are very expensive in terms of computation time and memory. The substructuring method is a promising solution for reducing computation load in both of these tasks. This PhD study develops a forward and an inverse substructuring approaches that can be used to update finite element models of large-scale structures.

In the forward substructuring approach, the eigensolutions and eigensensitivities of the global structure are calculated from those of the independent substructures and compared with global structure measurements through an optimization process. Kron's substructuring method for eigensolutions is improved in terms of computational efficiency by retaining only the first few eigenmodes of the independent substructures as master modes to assemble a reduced eigenequation for the global structure. This improvement not only reduces the computational endeavor required in extracting the complete eigenmodes of all the substructures, but also produces a smaller eigenequation that is frequently analyzed during the model updating process. The reduced eigenequation for eigensolutions is subsequently extended to calculate the first-order and high-order eigensensitivities of the global structure with respect to elemental parameters. The eigensensitivity matrices are

determined from the derivative matrices of only those substructures that contain the designed elements, thus realizing a significant reduction in computational cost. In consequence, the calculated eigensolutions and eigensensitivities are used in the practical model updating process. As accurate eigensolutions and eigensensitivities are needed in the final steps of the model updating procedure, an iterative scheme is proposed to calculate the eigensolutions and eigensensitivities more accurately using only a few master modes.

In the second part of the thesis, an inverse substructuring approach is developed by extracting substructural flexibility matrices from the experimental modal data. As a result, the focused substructure is treated as an independent structure to be updated directly using a global model updating method, thus accelerating the conventional optimization process significantly. The model condensation technique is also employed, as the measurement exercise is usually conducted at an incomplete set of points on a practical structure. This inverse substructuring approach allows for the focused substructures to be updated directly based purely on the measurements taken in the local area.

The proposed substructuring-based model updating approaches are applied to a few numerical, laboratory, and real structures. The results verify that these substructuring methods are computationally efficient and accurate in finite element model updating and associated applications.

PUBLICATIONS

Journal Papers:

Weng, S., Xia, Y., Xu, Y.L., Zhou, X.Q. and Zhu, H.P., (2009), "Improved substructuring method for eigensolutions of large-scale structures", Journal of Sound and Vibration, **323**(3-5), 718-736.

Xia, Y., Weng, S., Xu, Y.L. and Zhu, H.P., (2010), "Calculation of the Eigenvalue and Eigenvector Derivatives Using an Improved Kron's Substructuring Method", Structural Engineering and Mechanics, An international Journal, **36**(1), pp. 37-55.

Weng, S., Xia, Y., Xu, Y.L. and Zhu, H.P., (2009), "Substructuring Approach to Finite Element Model Updating", Computers and Structures, In review.

Weng, S., Xia, Y., Xu, Y.L. and Zhu, H.P., (2009), "An Iterative Substructuring Approach to the Calculation of Eigensolution and Eigensensitivity", Journal of Sound and Vibration, In review.

Conference Papers:

Xia, Y., Weng, S. and Xu, Y.L., (2009), "A substructuring method for calculation of eigenvalue derivatives and eigenvector derivatives", The 4th International Conference on Structural Health Monitoring on Intelligent Infrastructure (SHMII-4), 22-24 July, Zurich, Switzerland.

Weng, S., Xia, Y. and Xu, Y.L. (2009), "Model updating with improved substructuring method", The 3rd International Conference of Integrity, Reliability and Failure, 20-24 July, Porto, Portugal.

Weng, S. and Xia, Y., (2008), "First and second order residual flexibility in substructure method for eigensolutions of large scale structure", The Second Faculty Postgraduate Research Conference, 23-25 January, Hong Kong, (Best Paper Award).

Weng, S. and Xia, Y., (2007), "Substructure method in eigensolutions and model updating for large scale structures", The 2nd International Conference on Structural Condition Assessment, Monitoring and Improvement (SCAMI-2), 19-21 November, Changsha, China.

Weng, S., Xia, Y. and Xu, Y.L., (2010), "Model updating using substructural modal data", The 11th International Symposium on Structural Engineering, 18-22 December 2010, Guangzhou, China.

Xia, Y., Weng, S. and Xu, Y.L., (2011), "A substructuring method for model updating and damage identification", The 12th East Asia-Pacific Conference on Structural Engineering and Construction (EASEC-12), 24-26 January, Hong Kong.

ACKNOWLEDGMENT

First and foremost I sincerely thank my supervisor, Assistant Professor Xia Yong, for providing me the unique opportunity to pursue my PhD study, for his enlightening guidance, patient training, extensive discussion and continuous encouragement throughout this journey, and for his invaluable comments and suggestions in completion of this thesis. I have been impressed by his deep insights into scientific problems, meticulous attitudes to research and high responsibility to students, which benefit me inexhaustibly in my future research and work. It is a great honor to study under his supervision. I would like to express my sincere gratitude to my co-supervisor Professor Xu Youlin, for his continuous advice, interest and inspiration on my research, for his efforts in providing me extensive chances of discussion and communication, and for his kindly encouragement during my study in HKPolyU.

I am grateful to the Department of Civil and Structural Engineering of HKPolyU for the provided scholarship and prolific resource. I appreciate the support from the Research Grants Council of Hong Kong under the Project of PolyU 5321/08E.

I would also like to thank Dr. Y.Q. Ni, Dr. Y.L. Wong, Prof. T.T. Soong, Dr. J. Chen and Dr. R. Moore for their interesting classes, which have broadened my insight and enriched my life. I am grateful to all technicians in Laboratory QT005 for their kind assistance in the experimental work. I am grateful to our group members, Mr. Z.L. Wei, Dr. X.Q. Chen, Dr. Y.Q. Bao, Dr. B. Chen, Miss J. Zhang, Dr. Q.X. Wu and Mr. M. Yu. And I am very grateful to all teachers and friends within and outside HKPolyU, who have helped me both in my research and my daily life. It is difficult to list all of them on this single page.

Special gratitude is due to my family and Dr. F.N. Li for all of their love and encouragement during the past years.

CONTENTS

LIST OF FIGURES

LIST OF TABLES

LIST OF SYMBOLS

Symbols

{ }	Vector
$\{\}^T$, $[]^T$	Transpose of the vector or matrix
$\{\}^{-1}$, $[]^+$	Inverse, pseudo-inverse matrix
I	Unity matrix
Diag( )	Diagonal-block assembly of the substructures, Primitive matrices
K	Stiffness matrix
M	Mass matrix
F	Flexibility matrix
H	Frequency response function
R	Rigid body modes
P	Projector of normalization
E	Kron's receptance matrix
Ψ	Equivalent stiffness matrix of reduced eigenequation
G	First-order residual flexibility matrix
ω_i , f_i	i^{th} modal frequency (*rad/s*, *Hz*)
λ_i , **Λ**	i^{th} eigenvalue, matrix of eigenvalues
ϕ_i , **Φ**	i^{th} eigenvector (mode shape), matrix of eigenvectors
$\bar{\phi}_i$, $\bar{\mathbf{\Phi}}$	i^{th} expanded mode shape, matrix of expanded mode shapes
J	Objective function
S	Sensitivity matrix
r	Elemental physical parameter
f	Force

$x,\ \dot{x},\ \ddot{x}$	Displacement, Velocity, Acceleration
N	Degrees of freedom of the global structure
$N^{(j)}$	Degrees of freedom of the *j*th substructure
N^{P}	Size of the primitive matrix
N_S	Number of the substructures
N^{T}	Number of interface DOFs
τ	Interface force along the boundaries of the substructures
$\mathbf{L}$	Geometric operator
$\mathbf{C}$	Connection matrix
$\mathbf{T}$	Transformation matrix
$\mathbf{z}$	Modal modes participation factor
$\mathbf{\Gamma}$	Connection matrix of the substructural eigenmodes

Abbreviations

CFT	Concrete Filled Tube
CMS	Component Mode Synthesis
COED	Correlation of Eigenvector Derivatives
CPU	Central Processing Unit
DOF	Degree of Freedom
ERA	Eigensystem Realization Algorithm
FE	Finite Element
FRF	Frequency Response Function
FRFS	First-order Residual Flexibility Substructuring Method
IOR	Iterative Order Reduction
IRS	Improved Reduced System
MAC	Modal Assurance Criteria
MCS	Monte Carlo Simulation
MSE	Modal Strain Energy
PDF	Probability Density Function
RBM	Rigid Body Mode
SEREP	System Equivalent Reduction Expansion Process
SRF	Stiffness Reduction Factor
SRFS	Second-order Residual Flexibility Substructuring Method

Superscripts

E	Experimentally measured values
A	Analytically or theoretically predicted values
(j)	jth substructure
p	Primitive matrix or vector
$[k]$	The kth step of iteration

Subscripts

a	Master DOF
b	Slave DOF
m	Master modes
s	Slave modes
d	Deformational modes
r	Rigid body modes
g	Variables associated with the global structure
B	Boundary of a substructure
I	Inner part of a substructure
R	Reduced model
S	Static condensation
D	Dynamic condensation

CHAPTER ONE

INTRODUCTION

1.1 Background

Accurate finite element (FE) models are frequently required in a large number of applications such as design optimization, damage identification, structural control, and structural health monitoring. Due to uncertainties in the geometry, material properties, and boundary conditions, the dynamic responses of a structure predicted by a highly idealized numerical model usually differ from its measured responses. For example, Brownjohn *et al*. (2000) reported that the differences between the experimental and numerical modal frequencies of a curved cable-stayed bridge exceeded 10% for most modes and even reached 40% in some cases. Jaishi and Ren (2005) observed differences of up to 20% in the natural frequencies predicted by an FE model and those measured in a steel arch bridge, and reported that modal assurance criteria (MAC) values could be as low as 62%. Similarly, Zivanovic *et al*. (2007) found that the natural frequencies of a footbridge predicted by an FE model in design before updating differed from their experimental counterparts by 29.8%. Therefore, FE models need to be updated effectively to obtain a more accurate model that can be used for various purposes such as response prediction and damage identification.

1.2 Finite Element Model Updating

Model updating methods have been extensively developed in two categories: one-step methods and iterative methods. The former directly reconstruct the system matrices of the analytical model, while latter modify the physical parameters of the FE model repeatedly to minimize the discrepancy between analytical modal properties (such as

frequencies and mode shapes) and their measured counterparts. Iterative methods have become more popular because they allow for the physical meaning of the predicted parameters to be reflected and preserve symmetry, positive-definiteness, and sparseness in the updated matrices.

Most iterative methods employ optimization techniques, which require that the eigensolutions and associated sensitivity matrices of the analytical model be calculated in each iteration. As a result, for a large-scale numerical model, the iterative model updating method is very expensive in terms of computation time and computer memory for the following reasons:

- Large system matrices (stiffness and mass matrices) take up a large amount of storage space;
- Extracting eigensolutions from large system matrices is a time-consuming process, and calculating eigensensitivity consumes significantly more computational resources;
- Many uncertain parameters need to be adjusted in a large-scale numerical model. It takes a long time or is even impractical to calculate eigensensitivity with respect to the large number of updating parameters that the model contains. Moreover, the large number of parameters makes convergence of the large-scale optimization problem much more difficult.

Due to the aforementioned difficulties, updating the model of a large-scale structure usually involves a heavy workload. For example, Xia *et al.* (2006) carried out a model updating exercise for the Balla Balla Bridge in Western Australia, which was modeled with 907 elements, 949 nodes, and 5,400 degrees of freedom (DOFs). Convergence of the optimization took 155 iterations and cost about 420 hours. Within each iteration, calculating the eigensolutions took about 10 seconds, whereas calculating the eigensensitivities with respect to the uncertain parameters took more

than two hours. This indicates that calculation of eigensensitivity dominants the computation time during the model updating. In another study, a fine FE model was established for the Tsing Ma Suspension Bridge that consisted of about 300,000 nodes, 450,000 elements, and 1.2 million DOFs. It took about five hours to obtain the first 100 eigensolutions using a 64-bit Itanium server with eight CPUs of 1.5 GHz each (Duan *et al.* 2006). In this case, it is very difficult to update the model for such a large-scale structure using a conventional approach, even with such a powerful computer.

The computational burden associated with the iterative model updating method has led to a search for new model updating methods for large-scale structures that are both accurate and efficient.

1.3 Substructuring Methods

The substructuring approach can potentially be used an alternative to the conventional iterative model updating method in dealing with large-scale structures. The advantages of the substructuring approach include the following:

- As the global structure is replaced by smaller and more manageable substructures, it is much easier and quicker to analyze small system matrices;
- Substructuring methods allow not only for the identification of local parts, but also reduce the number of uncertain parameters and alleviate the ill-condition problem;
- In practical testing, the experimental instruments can be saved if it is necessary to measure the whole structure only for one or more substructures.

The substructuring approach can be utilized by employing the forward and inverse methods, respectively. In the forward substructuring method, the partitioned substructures are analyzed independently to obtain their designated solutions, which

are assembled to recover the solutions for the global structure by imposing constraints at the interfaces. The forward substructuring method has been employed for the eigensolutions of the global structure. However, its application to the model updating of practical structures is hindered because the conventional substructuring methods require the complete eigenmodes of all substructures to assemble the eigenmodes of the global structure. This is time-consuming and not worthwhile, as only a few eigenmodes of the global structure are generally of interest in model updating.

On the other hand, the substructuring approach can be used in an inverse manner to extract substructural properties from the properties of the global structure, by satisfying the constraints of displacement compatibility and force compatibility. Accordingly, the focused substructure can be treated as an independent structure to be updated using a conventional model updating method, thus improving the efficiency of the optimization process. This type of substructuring method requires an effective decoupling algorithm to ensure the extraction of substructural properties that validly represent the real local area.

Subject to the difficulties encountered in terms of efficiency or accuracy, there is a need to develop a new more efficient and effective substructuring approach to update models of large-scale structures.

1.4 Research Objectives

This study aimed at developing a more efficient substructuring approach for updating models of large-scale structures is motivated by the distinct advantages of substructuring methods in dealing with large-scale structures.

The above goal will be achieved under the two following approaches:

1. Develop an efficient substructuring-based model updating method that employs

the forward substructuring approach as follows:

- Develop a concise-form and efficient substructuring method for calculating eigensolutions for the global structure;
- Extend the efficient substructuring method to calculate the eigensensitivities of the global structure;
- Formulate a substructuring-based model updating procedure.

2. Develop a substructuring-based model updating procedure based on an inverse approach:

- Derive the substructural flexibility matrix from measured modal data of the global structure;
- Formulate a model updating procedure for independent substructures.

1.5 Thesis Organization

This thesis comprises nine chapters as illustrated in Figure 1-1. Chapter 2 summaries the extant literature on various model updating algorithms and substructuring methods and on a range of applications. Three numerical examples and three experimental structures are described in Chapter 3. In Chapter 4, the computational efficiency of Kron's substructuring method is improved to enable the eigensolutions of the global structure to be calculated. The improved substructuring method is then extended to calculate eigensensitivities in Chapter 5. The substructural eigensolutions and eigensensitivities are applied to the sensitivity-based model updating process in Chapter 6. A new iterative scheme is subsequently proposed in Chapter 7 to improve the accuracy of the substructuring method in calculating eigensolutions and eigensensitivities and the scheme is applied to the model updating process. In Chapter 8, an inverse substructuring approach is developed by extracting the substructural flexibility matrices from the experimental modal data. After normalizing the extracted

substructural flexibility, one independent substructure is directly updated instead of updating the global structure. Chapter 9 concludes the thesis and discusses possible future research.

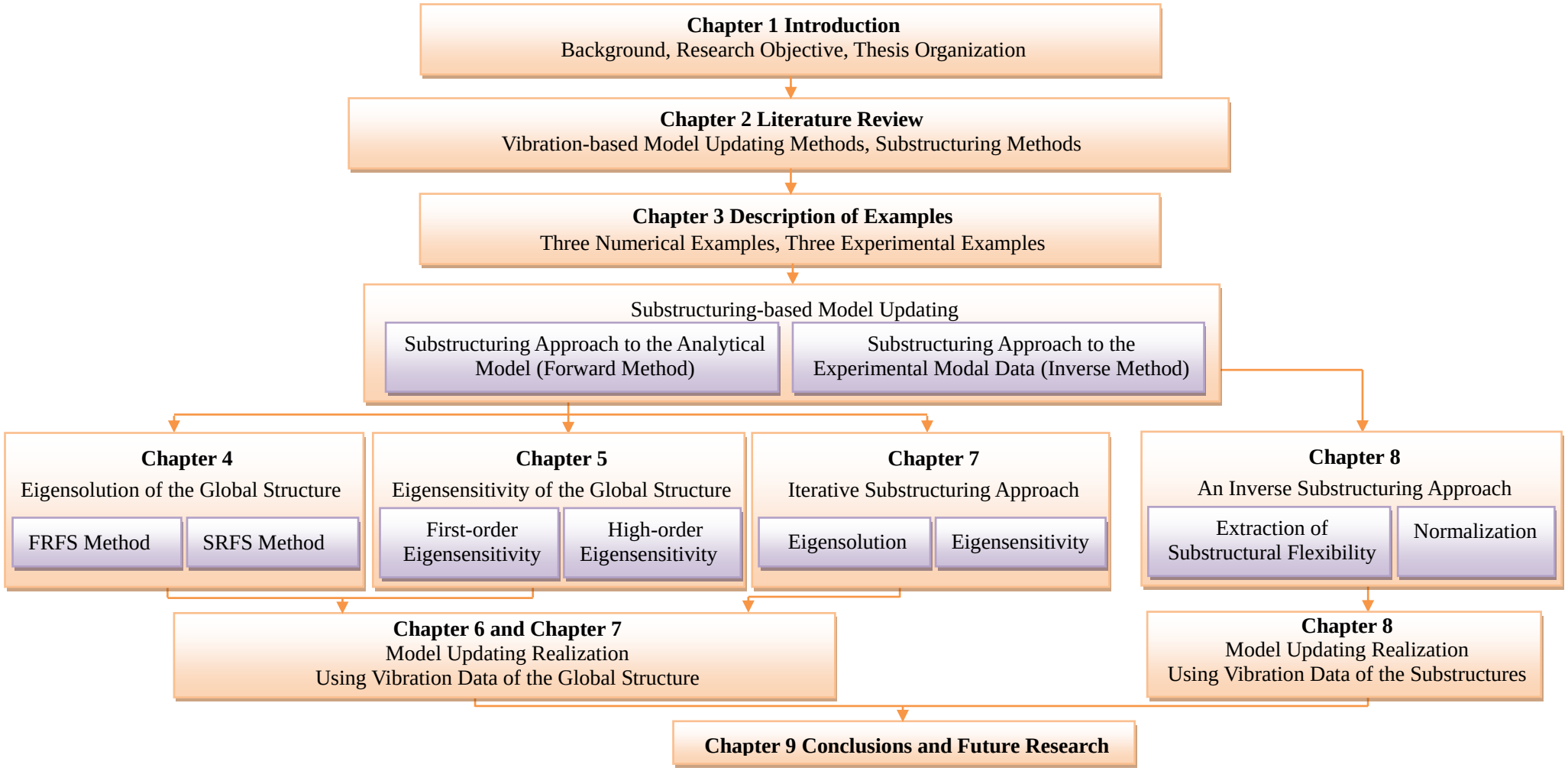

Figure 1-1: Organization of Thesis

CHAPTER TWO

LITERATURE REVIEW

2.1 Introduction

This chapter reviews the technical literatures concerning widely used model updating algorithms and substructuring methods.

Model updating technique has been widely employed in a lot of research works. Most of the practical applications are based on the dynamic measurement, although other kinds of data can be employed in theory (Humar *et al.* 2006; Friswell 2007). The vibration-based model updating methods are usually treated as an optimization problem in terms of minimizing the discrepancy between the analytical prediction and the practical measurement. A model updating process usually contains three aspects: selection of measurement as reference data, selection of parameters to update, and the procedure of model tuning (Brownjohn *et al.* 2001).

According to whether the optimization process is carried out directly from the measured time signals or from the frequency domain information via Fourier transformation, model updating methods are basically categorized into time domain methods and frequency domain methods (Koh and Perry 2010). The former aims to reproduce the structural dynamic responses such as displacement, velocity and acceleration. The frequency domain updating method uses the modal characteristics such as the frequencies, model shapes and modal flexibility, to tune the model parameters. The frequency domain characteristics reflect the global condition of a structure and the input information is not required. The model updating methods using frequency domain data will be concentrated in this chapter. Ljung and Glover

(1981) stated that, the frequency domain methods and the time domain methods can be complementary to each other instead of rival.

Model updating method aims to perturb the system matrices such as mass, stiffness and damping matrices so that the responses of the updated model resemble the measured data as closely as possible. The system matrices can be updated, either by perturbing the items in the matrices directly, or by iteratively modifying the physical parameters such as axial stiffness *EA* and bending rigidity *EI* to indirectly update the system matrices. Accordingly, the model updating methods reviewed in this chapter include the direct updating methods and the iterative updating methods. Particularly, the iterative model updating methods will be studied comprehensively, since it is becoming more popular due to the meaningful interpretation of the predicted parameters and the preservation of the symmetry, positive-definiteness and sparseness in the updated matrices.

The responses of a structure are usually measured at only a limited number of locations and over a limited frequency range, indicating that only a relatively small number of mode shapes with a reduced number of nodes are measured. This inevitable size incompatibility between the analytical and experimental modes makes the direct comparison difficult. The model reduction and data expansion algorithms frequently used in model updating are also reviewed in this report.

As far as the substructuring method is concerned, its theories and wide applications in static analysis, dynamic analysis, nonlinear analysis, and system identification will be reviewed in the final part of the chapter.

2.2 Finite Element Model Updating Methods

2.2.1 Direct Model Updating Methods

The direct model updating methods try to find the updated matrices (stiffness and/or mass) which produce the real responses of a structure as closely as possible by solving an objective function under certain constraints. In these methods, the elements in the system matrices are treated as variables. The direction updating methods have been used extensively for FE model refinement and damage detection, which includes the minimum norm approach, minimum rank approach and matrix mixing updating approach (Abdalla *et al.* 2000).

Model updating often produces sets of equations whose solution are ill-conditioned and extra information is required to produce a well-conditioned estimation problem. One possibility to consider all the uncertain parameters without sufficient extra constraints is taking the minimum norm solution. Berman and Nagy (1983) initiated a formulation of the optimal updating problem, which minimized the Frobenius Norm of global matrix perturbations, using the zero modal force error and the property of matrix symmetry as constraints. Kabe (1985) made sure that the zero coefficients of the analytical stiffness matrix were maintained in the updated stiffness matrix, and adjusted the non-zero elements of the stiffness matrix to reduce the uncertain parameters involved. McGowan *et al*. (1990) employed the mode shape expansion algorithms to extrapolate the incomplete measured mode shapes to be comparable with the analytical modes, thus releasing the ill-conditioned problem. Smith (1998) presented an alternating projection algorithm for system matrix adjustment. Constraints of sparsity and positive definiteness were imposed via successive orthogonal projections onto the convex sets. The definiteness constraints were found to be more effective and computationally efficient if applied after the sparsity constraints rather than simultaneously with them. Other than inclusion of

extra constraints, Friswell *et al.* (1998b) considered only a subset of the parameters to be in error, to deal with the ill-condition problem. The critical decision was then the choice of parameters to include in the subset. Carvalho *et al* (2006; 2007) computed the missing components of the measured experimental eigenvectors in an algorithmic way by using the sophisticated and stable matrix computational techniques, thus avoiding the potential drawback of the ill-conditioned matrix transformation.

Another approach to the direct model updating technique is to minimize the rank of the perturbation matrix instead of the norm of it. Zimmerman and Kaouk (1994) revealed that the perturbation matrices tended to be of small rank because damage was usually located in a few structural members rather than distributed all over the structure. Doebling (1996b) extended the method by updating the elemental stiffness (or substructural stiffness coefficients) rather than the global stiffness matrix. The method computed a minimum rank solution for the perturbations of the elemental stiffness parameters while constraining the connectivity of the global stiffness matrix. Because it computed minimum-rank updates directly to the elemental stiffness parameter, this method was proved to be sensitive to the change of local elemental stiffness parameters. Abdalla *et al.* (1998; 2000) improved the computation efficiency of the minimum rank optimal matrix updating, using an interior point optimization algorithms. The developed methods additionally enforced the constraints such as symmetry, sparsity and positive definiteness. Zimmerman *et al.* (2000) applied the minimum rank updating method to the case where mass, damping and stiffness properties were changed simultaneously. It made use of the cross orthogonality relationships, singular value decomposition, as well as the knowledge gained from the uncoupled damage location algorithm. Yang and Liu (2009) minimized the rank of the perturbed flexibility matrices according to the number of non-zero eigenvalues of the discrepancy of the flexibility matrix.

Matrix mixing update method was developed by Caesar (1987). For the mass normalized mode shapes, the following equations should be satisfied

$$[\mathbf{M}]^{-1} = \sum_{i=1}^{n} \{\phi_i\}\{\phi_i\}^T \tag{2-1}$$

$$[\mathbf{K}]^{-1} = \sum_{i=1}^{n} \frac{1}{\omega_i^2} \{\phi_i\}\{\phi_i\}^T \tag{2-2}$$

If some modes are not measured, the analytical counterparts are in place of them. Then the *m* measured modes and (*n*-*m*) unmeasured modes from analytical model are combined as

$$[\mathbf{M}]^{-1} = \sum_{i=1}^{m} \{\phi_i^E\}\{\phi_i^E\}^T + \sum_{i=m+1}^{n} \{\phi_i^A\}\{\phi_i^A\}^T \tag{2-3}$$

$$[\mathbf{K}]^{-1} = \sum_{i=1}^{m} \frac{\{\phi_i^E\}\{\phi_i^E\}^T}{\left(\omega_i^E\right)^2} + \sum_{i=m+1}^{n} \frac{\{\phi_i^A\}\{\phi_i^A\}^T}{\left(\omega_i^A\right)^2} \tag{2-4}$$

To *et al.* (1990) and Neidbal *et al.* (1990) updated the analytical mass and stiffness matrices with matrix mixing update approach by enforcing orthogonality with respect to the measured mode shapes. The method was extended to satisfy both the eigenequation and the orthogonality relations, which had the advantage of preserving the physical connectivity of the updated model. Hajela and Soeiro (1990) updated the analytical model with matrix mixing update approach again. The static displacement obtained by loads was used to simulate higher modes that were difficult to measure in practice.

In sum, the direct model updating methods have been widely studied by researchers in the past half century, but not limited to the above review documents. Although the direct model updating methods do not require the parametric analytical models, it is apparent by now that those methods have significant disadvantages. The direct model

updating methods reconstruct the system matrices arbitrarily, which may not be meaningful. Indeed, the original purpose of these methods was not model updating or damage detection but often vibration control and stability. However, it is very unlikely that these methods will prove useful in the majority of structural health monitoring (Bakir *et al.* 2007).

2.2.2 Iterative Model Updating Methods

Other than the direct model updating methods, the iterative model updating methods aim to update the physical parameters of the analytical model, such as the material properties (Young's modulus, Poisson's ratio, mass density, etc.) or the physical dimensions of the model. Consequently a parametric model of the structure is required. The iterative methods allow a wide choice of physically meaningful parameters, preserve the matrix properties of symmetry, sparseness and positive-definiteness, and guarantee the structural connectivity. Due to these merits, the iterative methods have been becoming more popularly used in model updating. An FE model updating mainly includes three aspects, the updating parameters, the objective function and the optimization algorithms.

2.2.2.1 Updating Parameters

Selection of parameters to be updated is very critical to a successful model updating and requires engineering judgment. Two important issues deserve considerations, i.e., how many parameters should be selected and which parameters from the many candidates are preferred. The number of updating parameters should be kept as small as possible to guarantee a well-conditioned updating problem, and release the expensive computation of eigensolutions and the associated eigensensitivities (Friswell *et al.* 2001). Besides, it is necessary to select the most effective updating parameters that produce a genuine improvement in the modeling of the structure. If inappropriate model parameters are selected, the updated model either cannot

reproduce the required dynamic properties accurately or does not represent the real structure. In the latter case, although the objective function reduces to below a threshold, the updated model has no real meaning and the obtained parameters are, in effect, the compensation for the real model parameters. Therefore, the analyst should first know what inaccuracy of the model comes from and which part of the model needs updating, based on the features of the measurement data and his knowledge of the model. The parameters can be the elemental axial stiffness (*EA*) and bending rigidity (*EI*) (Xia *et al.* 2008), or the geometric dimension (Mottershead *et al.* 1996), or the stiffness of particular area such as the structure joint (Law *et al.* 2001). Apparently the selection of parameters is closely associated with the modelling of the structure of interest.

2.2.2.2 Optimisation Algorithms

The widespread up-to-date optimization algorithms in iterative model updating methods mainly include the sensitivity-based model updating method and the evolutionary method such as the genetic algorithm (GA) and the neural network algorithm. In this study, the sensitivity-based algorithm will be concentrated.

Basically, the sensitivity-based model updating is an inverse procedure to correct the uncertain parameters of the analytical model, which is usually posed as a minimization problem to find the optimimum r^* such that (Bakir *et al.* 2007)

$$J\left(r^*\right) \le J\left(r\right), \quad \forall r \tag{2-5}$$

$$r_{li} \le r_i \le r_{ui}, \ (i=1, 2, \ldots, n)$$

where r is the design variables, with r_{li} and r_{ui} representing the lower and upper bounds, respectively. For example, the general objective function combining the modal properties of the frequency and the mode shape is usually denoted as (Brownjohn *et al.* 2001)

$$J(r)=\sum_i W_{\lambda i}^2\left[\, f_i\left(\{r\}\right)^A - f_i^{\,E}\,\right]^2+\sum_i W_{\phi i}^2\sum_j\left[\,\phi_{ji}\left(\{r\}\right)^A-\phi_{ji}{}^E\,\right]^2 \qquad (2\text{-}6)$$

where f_i^E and $\phi_{ji}{}^E$ represent the experimental *i*th natural frequency and the *i*th mode shape at the *j*th point, f_i^A and $\phi_{ji}{}^A$ represent the frequency and mode shape counterparts from the analytical FE model which are expressed as the function of the uncertain physical parameters $\{r\}$, $W_{\lambda i}$ and $W_{\phi i}$ are the weight coefficient due to the different measurement accuracy of the frequencies and mode shapes. The objective function is minimized by adjusting continuously the parameters $\{r\}$ of the initial FE model through optimization searching techniques.

To find the optimal searching direction, sensitivity analysis is usually conducted to compute the rate of the change of a particular response quantity with respect to the change in a physical parameter. For example, the sensitivity matrix of the frequency and mode shape with respect to the parameter *r* can be expressed as

$$\left[S_\lambda(r)\right]=\frac{\partial\lambda(r)}{\partial r},\ \left[S_\phi(r)\right]=\frac{\partial\phi(r)}{\partial r} \qquad (2\text{-}7)$$

Brownjohn *et al.* (2001) explicitly described the sensitivity-based FE model updating method and its application to structure condition assessment, particular for bridge structure. Teughels and De Roeck (2004) addressed the general sensitivity-based model updating method using damage functions and the trust region approach. The detailed procedures and applications were then presented in a companion work (Bakir *et al.* 2007). Zivanovic *et al.* (2007) generalized the complete sensitivity-based model updating process mainly into five phrases, including the initial FE modeling, modal testing, manual model tuning, automatic updating, and physical interpretation of all parameter changes. The standard procedure was implemented on a lively steel box girder footbridge.

As regards the aforementioned algorithm, the main task of the sensitivity-based model updating procedure includes the construction of the objective function and calculation of the sensitivity matrix. The objective function is usually evolved from the eigensolutions of the analytical model and the measured eigenmodes. The basic algorithm in calculation of eigensolutions of an analytical model is standard. The various types of objective functions are addressed in the following section.

2.2.2.3 Objective Functions

Selection of the objective functions has a profound impact on the optimization problem. The updating objective should be sensitive to small changes in the parameters. Otherwise, the difference between the analytical model and experimental observation may be reconciled by the changes in other more sensitive parameters which might be less in need of updating. In that case, the updated model replicates the measurements but does not represent the real model.

There are commonly five expressions possibly used to be model updating objectives which are the frequency residual, mode shape related function, modal flexibility residual, modal strain energy, and frequency response function (Humar *et al.* 2006).

The advantage of the frequency-based model updating approach can be concluded as the following aspects. i) Since frequency measurements can be cheaply acquired, the approach could provide an inexpensive structural assessment technique. ii) The measurement of natural frequencies can be quickly conducted and is often reliable. iii) Moreover, the natural frequencies are the global property of a structure and thus can be measured at a few locations or even at one point. However, the frequency-based model updating is limited in widespread application since the changes in natural frequencies cannot provide the spatial information (Salawu 1997). Multiple

frequencies shifts can provide the spatial information because changes in the structure at different locations will cause different combinations of changes in the modal frequencies. But there is often an insufficient number of frequencies with significant enough changes to determine the location uniquely (Doebling 1996a).

Mode shapes inherently contain the spatial information about structural changes, and therefore utilization of the differences in mode shapes represents another subgroup of objective function in model updating. Allemang and Brown (1982) proposed the Modal Assurance Criteria (MAC) to estimate the degree of correlation between the mode shapes of the analytical model and experimental measurement.

$$\mathrm{MAC}\left(\phi^A, \phi^E\right) = \frac{\left|\left\{\phi^A\right\}^T \phi^E\right|^2}{\left(\left\{\phi^A\right\}^T \phi^A\right)\left(\left\{\phi^E\right\}^T \phi^E\right)} \tag{2-8}$$

There has been a significant amount of works selecting the combination of the frequencies and model shapes as objective for FE model updating over the past years. Wu and Li (2004) updated the FE model of an existing 310 m tall Nanjing TV Tower based on frequencies and mode shapes from ambient vibration measurements. Jaishi and Ren (2005) updated a half-through arch bridge with the modal frequencies and mode shapes from the ambient vibration testing. Bakir *et al.* (2007) attempted to minimize the MAC values and the relative differences of the frequencies to update a multistorey complex structure with a complex damage pattern. A sensitivity-based FE model updating scheme with a trust region algorithm was applied to an actual residential building from Turkey that had been subjected to the 1999 Kocaeli and Duzce earthquakes. Daniell and Macdonald (2007) updated the FE model of a cable-stayed bridge, in which the natural frequencies and mode shapes were compared with those from ambient vibration tests. Weber and Paultre (2010) performed a sensitivity-based model updating procedure on a three-dimensional truss tower tested in the laboratory. A number of mathematical techniques were combined

in a consistent way, including regularization of the nonlinear updating problem and its linearization.

It should be noted that, the successfully updating procedure with the natural frequencies and mode shapes is heavily affected by the environmental factors. Many researchers observed that, the modal frequencies varied significantly in a single day due to the temperature change, and it was necessary to discriminate the variation of the modal properties due to the environmental change from those caused by the structural change (Xia *et al.* 2006). Roberts and Pearson (1998) monitored a 9-span, 840m long bridge. They found that the changes due to the environment could account for the changes in frequencies as much as 3% ~ 4% during a year. Farrar *et al.* (1997) reported that, the first three frequencies of the Alamosa Canyon Bridge varied approximately 5% during a 24 h time period, and a regression model that described the variation of frequencies due to the change of temperature were provided by Sohn *et al.* (1999), to establish the confidence intervals of the frequencies with respect to the varied temperatures. Peeters and Roeck (2001) presented the results of almost one year monitoring of the Z24-Bridge in Switzerland, and reported that the first four frequencies varied more than ten percent during the testing period. Xia *et al.* (2006) periodically tested a laboratory reinforced concrete slab nearly two years to investigate the variation of the frequencies, mode shapes and damping with respect to the temperature and humidity changes. They found that the frequencies bore a strong negative correlation with the temperature and humidity, the damping ratio possessed a positive correlation, and no obvious correlation from the mode shapes. Ni *et al.* (2009) eliminated the temperature effect in vibration based structural damage detection of Ting Kau Bridge. A neural network models was established based on 770 hours frequency and temperature data.

It is commonly understood that the natural frequencies and mode shapes of a

structure have different sensitivities on the updated parameters, and the degrees of accuracy of the measured natural frequencies and mode shapes are also different. In general, the natural frequency is less sensitive to the structural parameters, but can be measured more accurately than the mode shape. To take into consideration of their contributions in model updating, different weights can be assigned to the natural frequency and mode shape in the objective function and the sensitivity matrix [*S*]. Baruch and Bar-Itzhack (1978) firstly introduced the concept of the weighted coefficient. The weights of the mode shapes were chosen to be smaller than those of the frequencies (Ricles and Kosmatka 1992). Friswell *et al.* (1998d) chose the weighted coefficient for each individual frequency and mode shape to construct the objective according to the measured vibration data. Christodoulou and Papadimitriou (2007) established the weighted residuals metric to update the elemental parameters. A Bayesian statistical framework was then used to rationally select the optimal values of the weights based on the measured modal data.

Derivatives of the mode shapes (the mode shape curvatures) are proved to be more sensitive to small perturbations than the mode shapes, and therefore, can also serve as objective indices in model updating. The mode shape curvature is written by the central difference approximation in the work of Pandey *et al.* (1991) as

$$\phi_j'' = \frac{\left(\phi_{i+1,j} - 2\phi_{i,j} + \phi_{i-1,j}\right)}{h^2} \tag{2-9}$$

where *h* is the distance between two successive measured locations. Abdel Wahab and De Roeck (1999) used the mode shape curve to identify the change of the elemental parameters before and after updating, which was further applied to the Z24 bridge.

Changes in strain energy are also used as an optimization objective in some research work. In fact, the mode shape curvature is correspondent to the strain energy at that

location. The modal strain energy (MSE) for the *j*th mode is

$$U_j = \frac{1}{2}\{\phi_j\}^T \mathbf{K} \{\phi_j\} \tag{2-10}$$

The modes that yield the highest value of strain energy are the modes that tend to stretch the stiffness matrix the most, which has the most significant contribution to the stiffness matrix, and thus provides the best information about changes to the elemental stiffness parameters of the structure. Sanayei and Saletnik (1996a) used the strain residual function as objective to minimize the difference between the analytical strains and measured ones, and applied this method to a truss and a frame to estimate the elemental parameters (Sanayei and Saletnik 1996b). Shi *et al.* (2000) derived the sensitivity of MSE with respect to the elemental parameters, and proved that the use MSE was more sensitive to local damage than other mode shape based indices. Jaishi and Ren (2007) used the eigenfrequency residual and MSE residual as two objective functions of the multiobjective optimization. The gradient of the proposed modal strain energy objective function was derived with the help of the eigenvalue and eigenvector derivatives.

Since each entry of the modal flexibility component consists of the coupling of the mode shapes and frequencies for different modes, the scope of measured data is greatly enlarged compared with the use of the natural frequencies and mode shapes. Therefore, more and more researchers incorporate the modal flexibility index in their model updating process. Aktan *et al.* (1994) firstly proposed the use of the measured flexibility as a 'condition index' to indicate the relative integrity of a bridge. Pandey and Biswas (1994) applied the modal flexibility based model updating to several numerical examples, and to the damage identification of an actual spliced beam. They showed that the estimates of the damage condition and the location of the damage could be obtained from just the first two measured modes of the structure. Zhao and Dewolf (1999) presented a comparison on the use of the natural frequencies, mode shapes, and modal flexibility matrix for structure condition

assessment. The results demonstrated that the modal flexibility were more likely to indicate the local change of the elemental parameters than the other two. Topole (1997) developed an algorithm to calculate the contribution of the flexibility to the sensitivity of the model parameters, and applied it to detect the damage of a simulated structure with truss member. Similarly, Reisch and Park (2000) refined the elevated highway bridge column based on the relative changes in localized flexibility properties. Wu and Law (2004a) studied the truncated sparse modal flexibility obtained from the incomplete measurements and derived explicitly its sensitivity with respect to the elemental generic parameter. In the companion paper, Wu and Law (2004b) reported on the experimental verification of the above-mentioned truncated modal flexibility based model updating method. Jaishi and Ren (2006) chose the modal flexibility residual as the objective function for model updating, and derived its gradient explicitly. In their research, all the elements in the FE model were used as updating parameters, which was the extreme adverse condition in practical FE model updating. Jaishi *et al.* (2007) applied the FE model updating method in real bridge structures. An eigenvalue sensitivity study was feasible to see the effect of various parameters to the concerned modes, according to which the most sensitive parameters were selected for the flexibility-based model updating. Duan *et al.* (2005) assembled the proportional flexibility matrix with arbitrarily scaled modal shapes for model updating in ambient vibration. The damage locating vector method was proposed to the case of ambient vibration with incomplete measured DOFs, when the normalized flexibility matrices were not available (Gao *et al.* 2007). Catbas *et al.* (2008) combined the flexibility and flexibility curvature for structural health monitoring.

Frequency response data is another kind of objective function that can be used in model updating, since it includes a great deal of information. Lin and Ewins (1994) tackled the model updating problem by using the measured FRF data directly, which

was incomplete in both the measured modes and coordinates. Ziaei-Rad (1997) developed a FRF-based model updating by expanding the inverse matrix of FRF as a Taylor series function with respect to the structural parameters. Modak *et al.* (2002) obtained the updated models by both a direct model updating method and an iterative model updating method based on the FRF data. Esfandiari *et al.* (2009) used the FRF and natural frequencies data for finite element model updating. Sensitivity formula, normalization and proper selection of measured frequency points improved the accuracy and convergence of model updating.

Intending to extract as much as information from the limited experimental test, some researchers propose multi-objective model updating technique, which attempts to minimize two or more objectives simultaneously. Jaishi and Ren (2007) used a multi-objective optimization technique to minimize the natural frequency residual and modal strain energy residual simultaneously. Perera and Ruiz (2008) carried out the multistage FE model updating based on the residuals of flexibility and the residuals of the frequencies and mode shapes. In the research of Christodoulou and Papadimitriou (2007) , a weighted residuals metric was firstly established to update the elemental parameters. Standard optimization techniques were then used to find the optimal values of the structural parameters that minimized the weighted residuals metric.

2.2.2.4 Sensitivity Matrix

The sensitivity matrix serves for indicating the searching direction of the optimization algorithm, which endows the more sensitive parameter (with respect to the objective function) a higher priority. Calculation of the eigensensitivity is the most computationally expensive component of model updating.

1) First-order Eigensolutions Derivatives

The sensitivity matrix [*S*] can be computed for all physical elemental parameters using the finite difference method, modal method and Nelson's method (Sutter *et al.* 1988).

The finite difference method uses a difference formula to numerically approximate the derivative, which calculates the eigensolutions at one or more perturbed design points and compares the differences at those points (Choi and Kim 2005). This method is sensitive to round off and truncation errors associated with the step size used. Zivanovic *et al.* (2007) used the forward finite difference approach with an assumed parameter change of +1% for all updating parameters.

The modal method approximates the eigenvector derivatives as a linear combination of the eigenvectors. Fox and Kapoor (1968) firstly utilized the modal method to determine the eigenvalue and eigenvector derivatives by considering the changes of the physical parameters in the mass and stiffness matrices, which set a solid foundation for the eigensensitivity analysis of dynamic systems. It required all modes of the system to calculate the interested eigenvalue and eigenvector derivatives, which was computationally expensive for large-scale structures. Wang (1985; 1991) developed the modified modal method to reduce the number of modes required. The eigenvector derivatives were represented by the truncated eigenvectors together with a residual static mode, accounting for the contribution of the discarded higher modes approximately. The coefficients of the residual modes were computed by a Bubnov-Galerkin method from the governing equation. Alvin (1997) proposed an iterative approach to determine the eigenvector derivatives. The modal superposition solution was used as the initial point, and then the iterative sensitivity computation was performed with the existing set of eigenmodes.

Nelson’s method (1976) is an exact method for calculating the eigenvector derivatives. It calculates the eigenvector derivative of one mode just using the modal data of that mode solely. Additionally, it preserves the banded nature of the system mass and stiffness matrices, and thereby significantly reduces the computational cost. Sutter *et al.* (1988) compared various sensitivity methods, including the difference method, modal method, improved modal method and Nelson’s method. They concluded that Nelson's method was the most powerful one since it was exact and computationally efficient.

The original Nelson’s method supposed that the target structure was grounded and did not contain repeated frequencies. Many researchers have developed it to deal with the general structures which might include the repeated frequencies or the rigid body modes. Ojalvo (1988), Mills-Curran (1988) and Dailey (1989) generalized Nelson’s method to solve the eigensolution derivatives of the real symmetric eigensystems with repeated eigenvalues, by deleting the rows and columns of the singular matrix $[\mathbf{K}-\lambda\mathbf{M}]$ to form a reduced full-rank coefficient matrix. Song *et al.* (1996) introduced a set of non-modal vectors which were mass orthogonal with respect to the repeated eigenvectors, based on the generalized Schmidt orthogonalization. The non-modal vectors served to span the subspace of the eigenvector derivatives for the repeated eigenpairs. Wu *et al.* (2006; 2007) used only the eigenvectors corresponding to the repeated eigenvalues to form a non-singular coefficient matrix. The improvement preserved the symmetry of the coefficient matrix and had exactly the same bandwidth as the original eigenequation. Lin and Lim (1996) calculated the eigenvalue and eigenvector derivatives when considering the rigid body modes. A small shift was introduced on both the stiffness and mass matrices.

Computation efficiency of Nelson’s method is improved by a few researchers. Lin *et*

al. (1996) represented the eigenvector derivative of a separate mode by the eigenvalue and eigenvector of the mode itself and an inverse of the system matrix. The method retained all the computational advantages of Nelson's method, but avoided the tedious procedure to select properly the eigenvector element and the inversion of the system matrices which were required by Nelson's method. Lin and Lim (1995) combined the eigensensitivity analyses with the static model reduction technique. They reduced the order of the original analytical FE model, yet enabled the design sensitivity analysis to be performed efficiently by suitable selection of the master and slave coordinates.

Based on the Nelson's method, the sensitivity matrix for the modal flexibility and strain energy were derived in the work of Jaishi *et al.* (2007) and Jaishi and Ren (2007), in which the flexibility matrix and strain energy matrix were used as the objective function in model updating.

2) Second-order and High-order Eigensolutions Derivatives

The computation of the second-order eigensensitivity or high-order eigensensitivity is sometimes required for the large variations of the design parameters or the repeated natural frequencies. Friswell (1995) extended Nelson's method to calculate the second- and high-order eigenvector derivatives, by repeatedly differentiating Nelson's eigenequation. Choi *et al.* (2004) computed the first-, second- and higher-order derivatives of eigenvalues and eigenvectors associated with repeated eigenvalues. Repeated eigenvectors and orthonormal conditions were adopted to compose an algebraic equation, which was then used to compute the high-order derivatives of eigenvalues and eigenvectors simultaneously. Guedria *et al.* (2007) calculated the high-order derivatives of both left and right eigenvectors for damped, symmetric as well as asymmetric systems, and generalized the application of Nelson's method.

2.2.3 Stochastic Model Updating Methods

The above-mentioned literatures assume that the analytical FE model is precise enough to represent the vibration properties of the structure and the measurements are accurate as well. In reality, both assumptions are not true.

The measured data and the initial FE model inevitably contain uncertainties that might lead to unreliable or even false parameter updating. The sources of modeling uncertainties mainly include: the variations in the material properties during manufacture, inexact modeling of the material constitutive behavior, uncertainties introduced during the construction process, inexact modeling of the boundary conditions, errors because of the spatial discretization of the structure, and unmodeled features such as neglected 'nonstructural' components (Sohn 2007). The sources of measurement uncertainties mainly include two parts, the measurement noise and the identification errors. The former is due to the noise from the experimental equipments and test environment. The latter one is introduced during the data processing, and the simplification of a nonlinear, complex system into a linear, real system.

Because of these inevitable uncertainties, model updating can be tackled in a stochastic manner. Three commonly used approaches considering the uncertainty in model updating are the Monte Carlo simulation (MCS) method, the perturbation method, and the Bayesian method (Khodaparast *et al.* 2008).

In the MCS method, a large number of samples following the given probability density functions (PDFs) of modal data are generated and repeatedly used for model updating. The desired statistics are eventually estimated from these updating results. Neal (1993) discussed the Markov Chain Monte Carlo method and used it for the

solution of integrals arising in Bayesian inference. Mosegaard and Tarantotla (2002) provided an introduction and thorough discussion of the Monte Carlo sampling techniques and their application in probabilistic parameter estimation problems. Mares *et al.* (2006) and Mottershead *et al.* (2006) described the theory of the stochastic model updating using a Monte Carlo inverse procedure with multiple sets of experimental results. The Monte Carlo inverse propagation and multivariate multiple regressions were employed to solve a set of analytical models with randomized updating parameters. The main disadvantage of the MCS method is that, it is computationally intensive as it requires a large number of simulations to obtain an accurate and valid statistics.

An alternative approach to estimate the effect of uncertainty is the perturbation method. This approach expands each term in the model updating equation with a truncated Taylor series expansion around the mean value and then proceeds the approximation with the moments of solutions (Hua *et al.* 2008). The second moment solution is usually applied to evaluate the mean and standard deviation of the response, or to evaluate the failure probabilities. Liu (1995) investigated the measurement noise effect on the damage detection with the perturbation method. Xia *et al.* (2002) and Xia and Hao (2003) took into account the effects of random noise in both the vibration data and analytical model. The structural stiffness parameters in the intact state and damaged state were evaluated with a two-stage model updating process. The statistical FE model of the structure at the undamaged state was derived in the first-stage updating, by considering the statistical uncertainties of the initial analytical model and the noise in the measured frequencies. The second stage was to update the improved model to derive a statistical FE model in the damaged state, considering the measurement noise in the damaged structure. Probability of damage existence was estimated by comparing the probability distributions of the stiffness parameters in the undamaged and damaged states. Hua *et al.* (2008) derived two

recursive equations to estimate the first two moments of the random structural parameters from the statistics of the measured modal data. Khodaparast *et al.* (2008) omitted the correlation between the updated parameters and measured data of Hua's work (Hua *et al.* 2008), and the intensive computation of the second-order sensitivities was then saved. Based on the work of Hua and Khodaparast, Govers and Link (2010) adjusted the mean values of the design parameters and their associated covariance matrix from multiple sets of experimental modal data other than a single set of data. In fact, the limitation of the perturbation method is that the initial starting estimate should be close to the true value, similar to the conventional deterministic sensitivity-based model updating.

The third widely used statistical model updating method adopts the Bayesian theory. Beck and Karafygiotis (1998) and Karafygiotis and Beck (1998) provided a general Bayesian statistical framework for updating a structural model and its associated uncertainties. A Bayesian probabilistic framework for modal updating allows obtaining not only the optimal (most probable) values of the updated parameters but also their uncertainties from their joint probability distribution. Katafygiotis *et al.* (2001) and Yuen and Katafygiotis (2001) proposed the Bayesian probabilistic approach to estimate the uncertainties using ambient testing data. Yuen and Katafygiotis (2002) considered both the input error (input measurement noise) and output error (output measurement noise and modeling error). The input error and output error were modeled by independent white noise processes and contributed towards the uncertainty. Lam *et al.* (2004) and Johnson *et al.* (2004) applied the Bayesian based model updating to the structural health monitoring of the Phase I IASC–ASCE benchmark study. Yuen and Katafygiotis (2005) extended Bayesian probabilistic approach to the case without considering any input measurements or any information regarding the stochastic model of the input. It did not require the response to be stationary and did not assume any knowledge of the parametric form

of the spectral density of the input. The Bayesian probabilistic approach was subsequently combined with a substructure concept, allowing for the identification and monitoring of some critical substructures only (Yuen and Katafygiotis 2006). Cheung and Beck (2009) developed the Hybrid Monte Carlo method (Hamiltonian Markov chain method) to solve the Bayesian model updating problem. It showed high potential for solving model updating problems in higher-dimensional parameter spaces without restriction on the model (linear or nonlinear) and on the type of data. In essence, one of the most useful applications of Bayesian model updating is to predict the future events based on the past observations (Cheung and Beck 2009).

Schueller and Jensen (2008) stated that the stochastic search algorithms would be the most promising technique for analyzing complex problems. Efficient procedures to deal with optimization considering uncertainties should become the rule and not the exception in future engineering design.

2.2.4 Model Updating for Damage Identification

Structural damage can be defined as changes in structural parameters which adversely affect the current or future performance of the structure whereas structural damage detection aims to find such changes in the structure using measurement data (Friswell 2007). The methods for damage identification can be usually found as the damage index methods, signal based methods and model updating methods.

The damage index methods make use of the measured modal properties of a structure at both intact and damage states. The natural frequency shifts (Friswell *et al*. 1994; Salawu 1997), mode shape changes (Parloo *et al*. 2003), mode shape curvatures/strain mode shapes (Pandey *et al.* 1991), modal flexibility changes (Pandey *et al.* 1994), modal strain energy changes (Shi *et al*. 2002) and frequencies response functions (Ni *et al.* 2006) are usually used as indicator to identify the

structural damage location and extend.

Damage is typically a local phenomenon which tends to be captured by higher frequency modes. Many signal based identification methods such as wavelet transform (Wang and Deng 1999), wavelet packets transform (Chang and Sun 2005), Hilbert-Huang transform (Huang 2000; Liu 2006) have been developed to decompose a signal using a short-duration wave/function, thus allowing a refined decomposition rather than decomposition with infinite-duration sinusoids such as Fourier transforms. The main advantage in using the signal based damage identification method is the ability to perform local analysis of a signal (Reda Taha *et al*. 2006).

With the model updating technique, the damage can be identified by comparing the differences between the updated model and the original one (usually the reduction of the stiffness parameters) (Friswell and Mottershead 1995). The model updating method cannot only detect the structural damage, but also quantify the damage severity. The model updating methods and their application in damage identification have been reviewed in the former part of this section. The model updating methods that will be proposed in the following chapters can be used for damage identification as well. In a word, model updating is one way to perform damage identification analysis, and damage identification is one application for model updating. Actually model updating can be used for a range of applications but not limited to the damage identification, such as optimization design, prediction of response and so on (Friswell 2001).

2.3 Model Condensation and Data Expansion

The outcome of the modal experiments is incomplete in two senses. First, it contains only a partial set of the natural frequencies and mode shapes. Second, the measured

mode shapes consist of a limited number of DOFs, typically much smaller than the number of DOFs in the analytical model. It means that only a relatively small number of mode shapes with limited points are measured. To compare the analytical modal properties with the experimental ones, either the analytical model needs to be condensed or the experimental data enlarged.

Matching the mode shapes in modal dimension is usually achieved by applying the modal assurance criterion and thus selecting the analytical mode shapes that have a counterpart in the experimental set. Matching the mode shapes in spatial dimension, i.e., the number of DOFs, is not as obvious. Most model updating techniques require a one-to-one correspondence between the analytical model and experimental measurement, and hence either a reduction or expansion procedure must be employed to resolve the inconformity between them.

2.3.1 Model Condensation

If the objective is to assess the degree of correlation between the experimental and analytical models, a reduction of the analytical mode shape to the size of the measured one is probably the wisest route because of its simplicity and accuracy (Friswell and Mottershead 1995).

1) Condensation with the Stiffness and Mass Matrices

The classical eigenequation is divided according to the master and slave DOFs as

$$\begin{bmatrix} \mathbf{K}_{aa} & \mathbf{K}_{ab} \\ \mathbf{K}_{ba} & \mathbf{K}_{bb} \end{bmatrix} \begin{Bmatrix} \phi_a \\ \phi_b \end{Bmatrix}_i - \lambda_i \begin{bmatrix} \mathbf{M}_{aa} & \mathbf{M}_{ab} \\ \mathbf{M}_{ba} & \mathbf{M}_{bb} \end{bmatrix} \begin{Bmatrix} \phi_a \\ \phi_b \end{Bmatrix}_i = \begin{Bmatrix} 0 \\ 0 \end{Bmatrix} \tag{2-11}$$

where the subscripts '*a*' and '*b*' relate to the master and slave coordinates, respectively, and the master DOFs are usually regarded as the measured coordinates. The full-DOF eigenvector is expressed by the eigenvector of master DOFs with transformation as

$$\begin{Bmatrix} \phi_a \\ \phi_b \end{Bmatrix} = \mathbf{T}\{\phi_a\} \tag{2-12}$$

The corresponding reduced mass and stiffness matrices are given by

$$\mathbf{M}_R = \mathbf{T}^T\mathbf{M}\mathbf{T}\ ,\quad \mathbf{K}_R = \mathbf{T}^T\mathbf{K}\mathbf{T} \tag{2-13}$$

Guyan reduction (Guyan 1965) is one of the most popular and basic condensation techniques. This method neglects the inertia terms and gives the transformation matrix of

$$\mathbf{T} = \begin{bmatrix} \mathbf{I} \\ -\mathbf{K}_{bb}^{-1}\mathbf{K}_{ba} \end{bmatrix} \tag{2-14}$$

With this static condensation algorithm, the modal responses obtained are exact only at zero frequency. As the interested frequency increases, the neglected inertia terms become more significant (O'Callahan 1989). The dynamic reduction is an extension of Guyan's method. The transformation matrix is modified to include the inertia forces at the chosen eigenvalue λ_0, and given by

$$\mathbf{T} = \begin{bmatrix} \mathbf{I} \\ -\left(\mathbf{K}_{bb} - \lambda_0\mathbf{M}_{bb}\right)^{-1}\left(\mathbf{K}_{ba} - \lambda_0\mathbf{M}_{ba}\right) \end{bmatrix} \tag{2-15}$$

If this shift frequency λ_0 is equal to zero, this method is equivalent to the static condensation. O'Callahan (1989) developed an improved reduced system (IRS) condensation method, which included a higher-order term in Taylor series expansion of the inverse of the dynamic stiffness matrix. The transformation matrix is expressed as

$$\mathbf{T} = \begin{bmatrix} \mathbf{I} \\ \mathbf{t} \end{bmatrix} = \begin{bmatrix} \mathbf{I} \\ \mathbf{t}_S + \mathbf{t}_D \end{bmatrix} \tag{2-16}$$

where

$$\mathbf{t}_D = \mathbf{K}_{bb}^{-1}\left(\mathbf{M}_{ab} + \mathbf{M}_{aa}\mathbf{t}_S\right)\mathbf{M}_R^{-1}\mathbf{K}_R$$

$$\mathbf{M}_R = \mathbf{T}^T \begin{bmatrix} \mathbf{M}_{aa} & \mathbf{M}_{ab} \\ \mathbf{M}_{ba} & \mathbf{M}_{bb} \end{bmatrix} \mathbf{T}, \quad \mathbf{K}_R = \mathbf{T}^T \begin{bmatrix} \mathbf{K}_{aa} & \mathbf{K}_{ab} \\ \mathbf{K}_{ba} & \mathbf{K}_{bb} \end{bmatrix} \mathbf{T} \tag{2-17}$$

Friswell *et al.* (1995) developed an iterative IRS strategy to get more accurate results. The transformation matrix (Eq. (2-16)) is expressed as an iterative form

$$\mathbf{t}^{[k]} = -\mathbf{K}_{bb}^{-1}\mathbf{K}_{ba} + \mathbf{K}_{bb}^{-1}\left(\mathbf{M}_{ba} + \mathbf{M}_{bb}\mathbf{t}^{[k-1]}\right)\left(\mathbf{M}_R^{[k-1]}\right)^{-1}\mathbf{K}_R^{[k-1]}$$

$$\mathbf{M}_R^{[k-1]} = \left[\mathbf{T}^{[k-1]}\right]^T \mathbf{M}\mathbf{T}^{[k-1]}, \quad \mathbf{K}_R^{[k-1]} = \left[\mathbf{T}^{[k-1]}\right]^T \mathbf{K}\mathbf{T}^{[k-1]} \tag{2-18}$$

The convergence of this iteration was proved mathematically (Friswell *et al.* 1998a). The disadvantage of this reduction method is that the estimated results are acceptable only in the domain of (0, f_c), where the cut-off frequency f_c is the smallest frequency of the structure with all the master DOFs grounded.

Xia and Lin (2004b) improved the Friswell's method by including all the inertia terms in the transformation matrix without any approximation, and proposed the iterative order reduction (IOR) method. The reduced eigenequation is formulated as

$$\mathbf{K}_S\mathbf{\Phi}_a = \lambda\mathbf{M}_D\mathbf{\Phi}_a \tag{2-19}$$

where the reduced stiffness matrix $\mathbf{K}_S$ is the same as that in Guyan reduction. The reduced mass matrix $\mathbf{M}_D$ is composed by the mass matrix in Guyan reduction with an iterated perturbation. $\mathbf{M}_D$ is iteratively updated by

$$\mathbf{t}_D^{[k]} = \mathbf{K}_{bb}^{-1}\left(\mathbf{M}_{ba} + \mathbf{M}_{bb}\mathbf{t}_S + \mathbf{M}_{bb}\mathbf{t}_D^{[k-1]}\right)\left(\mathbf{M}_D^{[k-1]}\right)^{-1}\mathbf{K}_S \tag{2-20}$$

$$\mathbf{M}_D^{[k]} = \mathbf{M}_S + \left(\mathbf{M}_{ba} + \mathbf{t}_S^T\mathbf{M}_{bb}\right)\mathbf{t}_D^{[k]} \tag{2-21}$$

Afterwards, Xia and Lin (2004a) modified the reduced eigenequation based on the same iteratively updated transformation matrix (Eq. (2-20) and Eq. (2-21)). The reduced eigenequation is given by

$$\mathbf{K}_R\mathbf{\Phi}_a = \lambda\mathbf{M}_R\mathbf{\Phi}_a \tag{2-22}$$

$$\mathbf{M}_R^{[k-1]} = \left[\mathbf{T}^{[k-1]}\right]^T \mathbf{M}\mathbf{T}^{[k-1]}, \quad \mathbf{K}_R^{[k-1]} = \left[\mathbf{T}^{[k-1]}\right]^T \mathbf{K}\mathbf{T}^{[k-1]}$$

This modification preserved the symmetric property of the stiffness and mass matrices.

Choi *et al.* (2008) performed the iterative dynamic condensation at the substructural level. Since the iterative dynamic condensation spent a lot of computation time to construct the transformation matrix, it was more efficient if the transformation matrix was constructed for the substructures instead of the global structure.

2) Condensation with Eigensolutions

O'Callahan *et al.* (1989) presented the system equivalent reduction expansion process (SEREP). The analytical eigensolutions take the place of the system matrices to recover the unmeasured DOFs. The analytical eigenvectors are partitioned into the master and slave coordinates

$$[\boldsymbol{\Phi}] = \begin{bmatrix} \boldsymbol{\Phi}_a \\ \boldsymbol{\Phi}_b \end{bmatrix} \tag{2-23}$$

and the transformation matrix is introduced by a generalized inverse of the analytical eigenvectors as

$$\mathbf{T} = [\boldsymbol{\Phi}][\boldsymbol{\Phi}_a]^+ = \begin{bmatrix} \boldsymbol{\Phi}_a \\ \boldsymbol{\Phi}_b \end{bmatrix} [\boldsymbol{\Phi}_a]^+ \tag{2-24}$$

2.3.2 Data Expansion

Reducing the analytical model to the size of the experimental model is not always recommended since the measurement coordinates are unlikely to be the best master coordinates from a reduction viewpoint. In addition, if the objective is to estimate the rotational DOFs using the measured data, the expansion of the measured mode shapes to the size of the analytical model is required.

There are mainly three kinds of methods for data expansion in spatial dimension. The

first approach employs the extrapolation of the measured DOFs to those of the full model. The second route uses the mass and stiffness matrices of the analytical model to compute the mode shape values at the DOFs missed in the measurement. The third alternative utilizes the analytical mode shapes directly with the assumption that the unmeasured mode shapes can be expressed as the linear combinations of the measured ones.

1) Spatial Curve Fitting

Measurement of rotation is usually much more difficult and expensive than that of the translational movement. The rotations of two closely spaced points can be estimated as their translations divided by the distance. To avoid too densely arranged transducers, the curve fitting can also be used to estimate the translation values at some interior points.

Williams and Green (1990) utilized the cubic polynomial to fit the measured translational mode shapes, and then differentiated it to obtain the required rotations. Ng'andu *et al.* (1993) employed the curve fitting for the beam-like structures and the surface fitting for the plate or shell structures, to estimate the rotational responses. In later work, Ng'andu *et al.* (1995) adopted the spline functions to estimate the rotational coordinates. They investigated the influence of the smoothing factor and the distribution of the measurement points, both of which were proved to control the accuracy of estimation. The measurement noise was smoothed in their method.

Although it is quick, cheap, and does not require prior knowledge of the analytical model, the spatial curve fitting technique is not often used since the structures with complex spatial formations or sudden changes of structural geometry are difficult to be evaluated with the spatial curve fitting technique.

2) Expansion with the Stiffness and Mass Matrices

The second method expands the measured mode shapes to the analytical size, making use of the analytical system matrices. In essence, the mode shape expansion is the inverse of model reduction. Accordingly, the aforementioned model condensation techniques can be employed reversely. The primary task of mode shape expansion is to estimate the transformation matrix **T** for the slave DOFs and master DOFs.

$$\phi = \begin{Bmatrix} \phi_a \\ \phi_b \end{Bmatrix} = \mathbf{T}\phi_a \tag{2-25}$$

Guyan expansion is the reverse procedure of the static condensation described previously (Balmes 2000). Corresponding to the Guyan condensation, the slave DOFs is estimated by

$$\phi_b = -\mathbf{K}_{bb}^{-1}\mathbf{K}_{ba}\phi_a \tag{2-26}$$

From the dynamic reduction based on Eq. (2-11), the slave DOFs of the *i*th mode is given by

$$\phi_{bi} = -\begin{bmatrix} \mathbf{K}_{ab} - \lambda_i \mathbf{M}_{ab} \\ \mathbf{K}_{bb} - \lambda_i \mathbf{M}_{bb} \end{bmatrix}^{+} \begin{bmatrix} \mathbf{K}_{aa} - \lambda_i \mathbf{M}_{aa} \\ \mathbf{K}_{ba} - \lambda_i \mathbf{M}_{ba} \end{bmatrix} \phi_{ai} \tag{2-27}$$

3) Expansion with Eigensolutions

The third kind of expansion methods is that use only the analytical eigenvectors, but not the system matrices (**K**, **M**). The simplest method of mode shape expansion is to substitute the elements of the mode shapes from the FE model for the DOFs that have not been measured.

$$\phi = \begin{Bmatrix} \phi_a^{\,E} \\ \phi_b^{\,A} \end{Bmatrix} \tag{2-28}$$

This simple method can be used only if the analytical and measured mode shapes have been scaled in the same way.

In the model coordinate method, the relationship between the experimental mode shapes and the analytical mode shapes at the master DOFs are expressed as follows.

$$\boldsymbol{\Phi}_a^E = \boldsymbol{\Phi}_a^A \mathbf{t} \tag{2-29}$$

Eq. (2-29) gives the transformation matrix

$$\mathbf{t} = \left(\boldsymbol{\Phi}_a^A\right)^+ \boldsymbol{\Phi}_a^E \tag{2-30}$$

The unmeasured DOFs can be estimated from the transformation matrix of

$$\boldsymbol{\Phi}_b^E = \boldsymbol{\Phi}_b^A \mathbf{t} \tag{2-31}$$

Retroactively, the transformation matrix **t** can also be used for full model directly, which smooth the measured mode shapes (Lipkins and Vandeurzen 1987).

In SEREP expansion method (O'Callahan *et al.* 1989), the full mode shapes are expressed as a linear combination of the measured eigenvectors, on the basis of the transformation matrix

$$\left\{\boldsymbol{\Phi}\right\} = \mathbf{T}\left\{\boldsymbol{\Phi}_a^E\right\} \tag{2-32}$$

T is regarded as a global curve-fitting function which projects the eigenvector elements from the measured part to the full system. The transformation matrix **T** can be constructed in various manners as

$$\mathbf{T} = \boldsymbol{\Phi}^A \left(\boldsymbol{\Phi}_a^A\right)^+, \quad \mathbf{T} = \boldsymbol{\Phi}^A \left(\boldsymbol{\Phi}_a^E\right)^+, \quad \mathbf{T} = \begin{bmatrix} \boldsymbol{\Phi}_a^E \\ \boldsymbol{\Phi}_b^A \end{bmatrix} \left(\boldsymbol{\Phi}_a^A\right)^+, \mathbf{T} = \begin{bmatrix} \boldsymbol{\Phi}_a^E \\ \boldsymbol{\Phi}_a^A \end{bmatrix} \left(\boldsymbol{\Phi}_a^E\right)^+ \tag{2-33}$$

Gysin (1990) compared the above methods to check their accuracy when applied to a spring mass structure. Both expansion error and damage localization capability were evaluated for each technique. It was concluded that no expansion method was satisfactory for all cases. If the expansion was utilized for model updating or damage identification and the maximum discrepancy were located at the measured DOFs, the dynamic expansion method performed best among them. Imregun and Ewins (1993)

employed the dynamic expansion and the model coordinate method to compare the system matrices based expansion and the eigensolution based expansion, using a spring-mass system, a cantilever beam, and a free-free plate. They also concluded that the quality of the expanded mode shapes was case-dependent. Random errors of the measured data did not affect the quality of the expanded mode shapes. The complexity of the mode shapes, however, was a significant adverse factor. Therefore, it was unlikely that acceptable results could be obtained in the case of markedly complex mode shapes.

4) Orthogonal Procrustes Expansion

Another problem associated with the experimental mode shapes is orthogonalization, i.e., looking for the minimal modification that will transform the set of mode shapes into an orthogonal state with respect to the mass matrix.

$$\left[\boldsymbol{\Phi}^{E}\right]^{T}\mathbf{M}^{A}\boldsymbol{\Phi}^{E}=\mathbf{I} \tag{2-34}$$

Baruch and Itzhack (1978) presented an optimal orthogonalization technique to adjust the measured modes orthogonal to the mass matrix. Kenigsbuch and Halevi (1998) proposed both a direct and an iterative method for computing the orthogonal modes, which were closest to the measured ones in a weighted Euclidean sense. Smith and Beattie (1990) expanded the measured mode shape vectors from the orthogonal Procrustes algorithm. The orthogonal Procrustes problem can be viewed as a search for a linear relationship between the original analytical eigenvectors and the measured eigenvectors (Smith and Beattie 1990).

$$\begin{bmatrix}\boldsymbol{\Phi}_{a}^{E}\\ \boldsymbol{\Phi}_{b}^{E}\end{bmatrix}=\begin{bmatrix}\boldsymbol{\Phi}_{a}^{A}\\ \boldsymbol{\Phi}_{b}^{A}\end{bmatrix}\mathbf{P}_{op} \tag{2-35}$$

The orthogonal Procrustes problem can then be formally stated as

$$\min_{\mathbf{P}_{op}}\left\|\boldsymbol{\Phi}_{a}^{E}-\boldsymbol{\Phi}_{a}^{A}\mathbf{P}_{op}\right\|,\ \text{subject to}\ \ \mathbf{P}_{op}^{T}\mathbf{P}_{op}=\mathbf{I} \tag{2-36}$$

The expanded and mass orthogonal eigenvectors are then given by Eq. (2-35).

Accurate expansion results depend on the accuracy of the measured mode shapes, the selection of the measured DOFs, as well as the magnitude of error in the original model.

2.3.3 Information Enlargement

Due to the limitation of instruments, the experimental information may not satisfy the requirement of system identification or model updating. It is necessary to enlarge the information from the limited instruments.

Doebling (1995) and Doebling *et al.* (1996) estimated the residual flexibility from the experimental vibration data. The FRF of the response at DOF *i* due to an excitation at DOF *j* can be written as a sum over all of the modal modes as

$$\mathbf{H}_{ij}(\omega) = -\omega^2 \left(\sum_{k=1}^{\infty} \frac{\phi_k^i \phi_k^j}{\omega_k^2 - \omega^2} \right) \tag{2-37}$$

Suppose that there are n_1 modes below the measured bandwidth (including rigid-body modes) and n_2 modes in the measured bandwidth, Eq. (2-37) can be represented by

$$\mathbf{H}_{ij}(\omega) = -\omega^2 \left(\sum_{k=1}^{n_1} \frac{\phi_k^i \phi_k^j}{\omega_k^2 - \omega^2} + \sum_{k=n_1+1}^{n_1+n_2} \frac{\phi_k^i \phi_k^j}{\omega_k^2 - \omega^2} + \sum_{k=n_1+n_2+1}^{\infty} \frac{\phi_k^i \phi_k^j}{\omega_k^2 - \omega^2} \right) \tag{2-38}$$

When the structure is free and the rigid body modes are considered, the first term of Eq. (2-38) is rewritten as

$$\lim_{\frac{\omega_k}{\omega} \to 0} \left\{ -\omega^2 \sum_{k=1}^{n_1} \frac{\phi_k^i \phi_k^j}{\omega_k^2 - \omega^2} \right\} = \sum_{k=1}^{n_1} \phi_k^i \phi_k^j \tag{2-39}$$

And the third part is

$$\lim_{\frac{\omega}{\omega_k} \to 0} \left\{ -\omega^2 \sum_{k=n_1+n_2+1}^{\infty} \frac{\phi_k^i \phi_k^j}{\omega_k^2 - \omega^2} \right\} = -\omega^2 \sum_{k=n_1+n_2+1}^{\infty} \frac{\phi_k^i \phi_k^j}{\omega_k^2} \tag{2-40}$$

which is often referred to as the residual flexibility. The residual flexibility term can be obtained by curve fitting algorithm.

Rade and Lallement (1998) examined several strategies for the enrichment of experimental data, based on the exploitation of different boundary conditions. Kwon and Lin (2004) proposed a frequency selection method for efficient FRF-based model updating. The selected frequencies can carry as much information as possible with a limited number of frequencies. Cottin and Reetz (2006) repeated different sets of the measured natural frequencies to improve the accuracy of the parameter estimation.

2.4 Substructuring Methods

As stated by Klerk *et al.* (2008), analysis of a structural system in substructure manner has some important advantages over the global method.

1) The substructuring method allows evaluation of large or complex structures, which might be inefficient or even prohibited for global method.

2) It allows identification of local problems and elimination of local subsystem behavior that has no significant impact on the assembled system.

3) It allows combination of distinct modeled parts in an efficient way and solving only one or several parts at a time.

4) It allows sharing and combining substructures from different project groups.

Due to these advantages, the substructuring methods have been widely used in aerospace, mechanical and civil engineering with a range of applications.

2.4.1 Substructuring Methods for Eigenproperties

The substructuring methods for eigenproperties are usually utilized in three domains, the physical, frequency and modal domains.

1) In the physical domain, a structure is characterized by its mass, stiffness, and damping matrices for a discretized linearized model. The substructuring method

applied in physical domain mainly aims to divide the large mass, stiffness and damping matrices into smaller ones, and subsequently releases the computational load.

2) A structure in the frequency domain is seen through its frequency response functions. It is widely used in experimental substructuring method, when the FRFs of the substructures have been experimentally determined.

3) In the modal domain, the dynamic behavior of a structure is interpreted as a superposition of modal responses. That is, the displacement in the physical domain is projected to the modal basis, usually the substructural eigenmodes.

2.4.1.1 Physical Domain

The global structure with N DOFs is divided into N_S substructures. The motion equation of the jth substructure may be written as

$$\mathbf{M}^{(j)}\left\{\ddot{x}^{(j)}(t)\right\}+\mathbf{C}^{(j)}\left\{\dot{x}^{(j)}(t)\right\}+\mathbf{K}^{(j)}\left\{x^{(j)}(t)\right\}=\left\{f^{(j)}(t)\right\}+\left\{g^{(j)}(t)\right\} \quad (2\text{-}41)$$

where $\mathbf{M}^{(j)}$, $\mathbf{C}^{(j)}$, and $\mathbf{K}^{(j)}$ are the mass, damping, and stiffness matrices of the jth substructure, $\left\{x^{(j)}(t)\right\}$ denotes the displacement vector, $\left\{f^{(j)}(t)\right\}$ is the external force vector, and $\left\{g^{(j)}(t)\right\}$ is the connecting forces between the adjacent substructures. The motion equations are coupled for the N_S substructures and can be rewritten in a block-diagonal format as

$$\mathbf{M}^{p}\{\ddot{x}\}+\mathbf{C}^{p}\{\dot{x}\}+\mathbf{K}^{p}\{x\}=\{f\}+\{g\} \quad (2\text{-}42)$$

with the compatibility condition and equilibrium condition

$$\mathbf{B}\{x\}=\mathbf{0},\ \ \mathbf{L}^{T}\{g\}=\mathbf{0} \quad (2\text{-}43)$$

where the matrix **B** operates on the interface DOFs and is a signed Boolean matrix if the interface DOFs are matching, and the matrix **L** is a geometric operator to connect the DOFs in the global structure with those in the independent substructures. $\mathbf{M}^{p}$, $\mathbf{C}^{p}$ and $\mathbf{K}^{p}$ denote the primitive matrices which directly assemble the mass,

damping and stiffness matrices of the substructures. If the interface force are expressed in Lagrange multiplier form of

$$\{g\} = -\mathbf{B}^T \{\tau\} \tag{2-44}$$

The assembled matrix is expressed as

$$\begin{bmatrix} \mathbf{M}^p & \mathbf{0} \\ \mathbf{0} & \mathbf{0} \end{bmatrix} \begin{Bmatrix} \ddot{x} \\ \tau \end{Bmatrix} + \begin{bmatrix} \mathbf{C}^p & \mathbf{0} \\ \mathbf{0} & \mathbf{0} \end{bmatrix} \begin{Bmatrix} \dot{x} \\ \tau \end{Bmatrix} + \begin{bmatrix} \mathbf{K}^p & \mathbf{B}^T \\ \mathbf{B} & \mathbf{0} \end{bmatrix} \begin{Bmatrix} x \\ \tau \end{Bmatrix} = \begin{Bmatrix} f \\ \mathbf{0} \end{Bmatrix} \tag{2-45}$$

Choi *et al.* (2008) applied this substructural concept in model condensation technique. The global stiffness and mass matrices were handled instead by the substructural matrices, which save much computation cost in construction of the transformation matrix **T** (Eq. (2-16)) that is expensive in conventional model condensation technique.

2.4.1.2 Frequency Domain

Performing a Fourier transform on Eq. (2-42) and Eq. (2-43) gives the following set of governing equations in the frequency domain (Gordis *et al.* 1991).

$$\begin{cases} \mathbf{H}^p(\omega)\{x(\omega)\} = \{f(\omega)\} + \{g(\omega)\} \\ \mathbf{B}x(\omega) = \mathbf{0} \\ \mathbf{L}^T g(\omega) = \mathbf{0} \end{cases} \tag{2-46}$$

where $\{x(\omega)\}$, $\{f(\omega)\}$, $\{g(\omega)\}$ represent the amplitude of the harmonic response and forces, $\mathbf{H}^p$ is a block-diagonal matrix containing the dynamic stiffness matrices of the substructures, i.e.,

$$\mathbf{H}^p(j\omega) = -\omega^2 \mathbf{M}^p + j\omega \mathbf{C}^p + \mathbf{K}^p \tag{2-47}$$

Similar to the physical domain substructuring method, the interface force can be expressed in Lagrange multiplier form of $\{g(\omega)\} = -\mathbf{B}^T \tau(\omega)$. Consequently, Eq. (2-46) can be re-written in a coupled form as

$$\begin{bmatrix} \mathbf{H}^p & \mathbf{B}^T \\ \mathbf{B} & 0 \end{bmatrix} \begin{Bmatrix} x \\ \tau \end{Bmatrix} = \begin{Bmatrix} f \\ 0 \end{Bmatrix} \tag{2-48}$$

where ω is omitted for brevity. The displacement can be obtained in the receptance formula as

$$\{x\} = \left(\mathbf{H}^p\right)^{-1}\{f\} - \left(\mathbf{H}^p\right)^{-1}\mathbf{B}^T\left(\mathbf{B}\left(\mathbf{H}^p\right)^{-1}\mathbf{B}^T\right)^{-1}\mathbf{B}\left(\mathbf{H}^p\right)^{-1}\{f\} \tag{2-49}$$

Classically, frequency domain substructuring is performed by primarily coupling the dynamic stiffness $\mathbf{H}^p$. As dynamic stiffness matrix $\mathbf{H}^p$ is hard to obtain directly in practice, they are obtained by inverting the measured receptance matrix and usually carried out as coupling the impedance matrix $\left(\mathbf{H}^p\right)^{-1}$ directly (Imregun and Robb 1992; D'Ambrogio and Sestieri 2004).

2.4.1.3 Modal Domain

The displacement vector $\{x\}$ in Eq. (2-45) can be decoupled in modal domain as $\{x\} = \mathbf{\Phi}^p\{q\}$, and the undamped eigenproblem with dynamic substructuring method can be obtained as

$$\begin{bmatrix} \mathbf{K}^p & \mathbf{B}^T \\ \mathbf{B} & \mathbf{0} \end{bmatrix} \mathbf{\Phi}^p q - \lambda \begin{bmatrix} \mathbf{M}^p & \mathbf{0} \\ \mathbf{0} & \mathbf{0} \end{bmatrix} \mathbf{\Phi}^p q = \begin{Bmatrix} \mathbf{0} \\ \mathbf{0} \end{Bmatrix} \tag{2-50}$$

The substructuring method in modal domain is usually used to extract the eigensolutions and eigensensitivities. The substructural eigensolution methods mainly include the component mode synthesis (CMS) method, Kron's substructuring method, Rayleigh-Ritz based substructuring method.

(a) Component Mode Synthesis Method

In CMS method, the component modes for each substructure can be classified into four groups according to the boundary conditions, which include the rigid body modes, normal modes, constraint modes and attachment modes (Craig 2000).

1) The rigid body modes (RBMs) describe the rigid body movement of a free

substructure. It can be obtained either by numerically extracting a null basis from the free stiffness **K**, or by considering its self-equilibrium. With the former manner, the rank deficient **K** is determined and rearranged as

$$\mathbf{K} = \begin{bmatrix} \mathbf{K}_{II} & \mathbf{K}_{IB} \\ \mathbf{K}_{BI} & \mathbf{K}_{BB} \end{bmatrix} \tag{2-51}$$

where $\mathbf{K}_{II}$ is a square matrix with a full rank. The subscript '*I*' represents the inner DOFs and the subscript '*B*' represents the interface DOFs. A generalized inverse is computed as

$$\left(\mathbf{K}\right)^{+} = \begin{bmatrix} \mathbf{K}_{II}^{-1} & \mathbf{0} \\ \mathbf{0} & \mathbf{0} \end{bmatrix}, \quad \mathbf{R} = \begin{bmatrix} -\mathbf{K}_{II}^{-1}\mathbf{K}_{IB} \\ \mathbf{I} \end{bmatrix} \tag{2-52}$$

where **R** is the rigid body modes. For a free structure with a large number of DOFs, the above calculation is not only expensive but also inaccurate. Alternatively, the self-equilibrium method can be used (Felippa and Park 1997). For a two-dimensional structure having *N* nodes, the three independent RBMs are the *x* translation ($\mathbf{R}_x$ = 1, $\mathbf{R}_y$ = 0), the *y* translation ($\mathbf{R}_x$ = 0, $\mathbf{R}_y$ = 1) and the *z* rotation ($\mathbf{R}_x$ = -*y*, $\mathbf{R}_y$ = *x*), i.e.,

$$\mathbf{R}^T = \begin{bmatrix} 1 & 0 & 0 & 1 & \cdots & 0 & 0 \\ 0 & 1 & 0 & 0 & \cdots & 1 & 0 \\ -y_1 & x_1 & 1 & -y_2 & \cdots & x_N & 1 \end{bmatrix} \tag{2-53}$$

The columns of **R** are naturally orthogonal by construction, and can be normalized by dividing $N^{1/2}, N^{1/2}$ and $\left[\sum\left(x_i^2 + y_i^2 + 1\right)\right]^{1/2}$, respectively.

2) The normal modes are obtained using the general eigenequation for both the fixed boundary condition and free boundary condition. The fixed interface normal modes are obtained by restraining all boundary DOFs and solving the following eigenequation.

$$\left(\mathbf{K}_{II} - \lambda_i \mathbf{M}_{II}\right)\left\{\phi_I\right\}_i = \left\{\mathbf{0}\right\} \tag{2-54}$$

The complete fixed interface normal modes are expressed as

$$\underset{N\times N_i}{\boldsymbol{\Phi}_n} = \begin{bmatrix} \boldsymbol{\Phi}_I \\ \mathbf{0}_B \end{bmatrix} \tag{2-55}$$

where N_i is the number of normal modes, which is equal to the quantity of the inner DOFs. Only the inner DOFs are used to construct the normal modes for the fixed interface condition. When normalized with respect to the mass matrix $\mathbf{M}_{II}$, the fixed interface modes satisfy

$$\boldsymbol{\Phi}_I^T \mathbf{M}_{II} \boldsymbol{\Phi}_I = \mathbf{I}, \;\; \boldsymbol{\Phi}_I^T \mathbf{K}_{II} \boldsymbol{\Phi}_I = \boldsymbol{\Lambda} \tag{2-56}$$

The free interface normal modes are obtained by releasing all boundary DOFs and solving the eigenequation

$$\left(\mathbf{K} - \lambda_j \mathbf{M}\right)\{\phi\}_j = 0 \;\; (j = 1, 2 \ldots N_d = N - N_r) \tag{2-57}$$

where N_d and N_r are the number of the deformational modes and the rigid body modes, respectively.

3) A constraint mode is defined as the force to generate a unit displacement to one coordinate of a specified 'constraint' coordinate ***C***, while the remaining coordinates of that set ***C*** are restrained, and the remaining DOFs of the structure are free. The force equilibrium satisfies

$$\begin{bmatrix} \mathbf{K}_{II} & \mathbf{K}_{IB} \\ \mathbf{K}_{BI} & \mathbf{K}_{BB} \end{bmatrix} \begin{bmatrix} \boldsymbol{\Phi}_{IB} \\ \mathbf{I}_{BB} \end{bmatrix} = \begin{bmatrix} \mathbf{0} \\ f_{BB} \end{bmatrix} \tag{2-58}$$

The constraint mode matrix is given by

$$\underset{N\times N_b}{\boldsymbol{\Phi}_c} = \begin{bmatrix} \boldsymbol{\Phi}_{IB} \\ \mathbf{I}_{BB} \end{bmatrix} = \begin{bmatrix} -\mathbf{K}_{II}^{-1}\mathbf{K}_{IB} \\ \mathbf{I}_{BB} \end{bmatrix} \tag{2-59}$$

where N_b is the number of constraint modes, and equal to the number of the inner DOFs. The constraint modes are stiffness orthogonal to all of the fixed interface normal modes, that is

$$\boldsymbol{\Phi}_n^T \mathbf{K} \boldsymbol{\Phi}_c = \mathbf{0} \tag{2-60}$$

4) An attachment mode is regarded as the displacement vector due to a single unit force applied at one of the given coordinates *A*, which is therefore acquired by

$$\begin{bmatrix} \mathbf{K}_{II} & \mathbf{K}_{IB} \\ \mathbf{K}_{BI} & \mathbf{K}_{BB} \end{bmatrix} \begin{Bmatrix} \mathbf{\Phi}_I \\ \mathbf{\Phi}_B \end{Bmatrix} = \begin{Bmatrix} \mathbf{0} \\ \mathbf{I}_B \end{Bmatrix} \tag{2-61}$$

Based on the four groups of mode components, applications of the CMS methods are reviewed as follows.

Fixed Interface CMS

The fixed interface CMS was initially proposed by Hurty in 1965 (Hurty 1965), in which the interface DOFs were fixed by using constraint modes associated with the static response due to the unit displacements on the interface DOFs. Craig and Bampton (1968) (for the discrete case) and Morand and Ohayon (1979) (for the continuous case) expressed the eigenmodes of each substructure with the fixed coupling interfaces and the static boundary functions associated with the coupling interfaces, which made the fixed interface CMS method known widely. Suarez and Singh (1992) improved the computation accuracy of the method by using the mode superposition algorithm to account for the truncated normal modes.

Qiu *et al.* (1997) proposed an exact fixed interface CMS method, in which the exact residual constraint modes were constructed based upon an incomplete set of normal modes of the substructures. In this regard, the exact constraint modes were expressed in two parts: the static constraint modes and a residual term, with which it represented exactly the effect of the discarded normal modes. Shyu *et al.* (1997) improved the computation accuracy of the fixed interface approach by retaining the higher-order term. Instead of the static constraint mode, quasi-static modes were used to capture the inertial effects of the truncated modes, which depended on the value of a centering frequency parameter.

Heo and Ehmann (1991) calculated the eigensensitivity of the global structure based on the derivative matrices of the constraint modes and fixed normal modes of the substructures. Hassis (2000) proposed a projection basis for the fixed interface CMS method. For each fixed boundary, a 'boundary structure' was associated and determined by applying the normal modes of the associated boundary structure to the interface boundary. Takewaki and Uetani (2000) proposed an inverse fixed interface CMS procedure to enhance the computational efficiency for updating damped large structural systems. Bennighof and Lehoucq (2004) presented an automatically multilevel substructuring method for the eigenvalue computations in linear elastodynamics, which was accomplished by dividing a structure recursively into substructures on multiple levels. They solved the fixed interface eigenvalues on the substructures and interfaces.

Free Interface CMS

MacNeal (1971) and Rubin (1975) initially proposed the free interface CMS method, in which the free interface normal modes and the attachment modes were combined to express the substructural modes, and a linking force was used to enforce the rigid/weak connection between the substructures.

Arora and Nuyen (1980) combined the free interface CMS technique with the subspace iteration method to obtain the eigensolutions of the global structure. Likewise, Lee and Jung (1995) developed the free interface CMS technique combining with the modified Lanczos method. The obtained natural frequencies and mode shapes were improved in both efficiency and accuracy. Lallemand *et al.* (1999) derived the eigensensitivity formulae of the global structure by enforcing the linking force on the derivative matrices of the substructural rigid body modes, free-interface normal modes and attachment modes.

Felippa *et al.* (1998) studied the attachment modes for both the symmetric and unsymmetrical free stiffness matrices. For the unsymmetrical case two kinds of attachment modes, one preserving the Penrose conditions and the other the spectral properties, were examined. Rixen (2004) assembled the free substructures using the dual assembly of the interface force and enforced only weak interface compatibility. The constraint of weak interface compatibility was more natural than classical free interface CMS procedures and led to simpler reduced matrices. Markovic *et al.* (2007) derived the free interface CMS formula in an inverse procedure, which partitioned the entire structure via the localized Lagrange multiplier method. Unlike the majority of the available CMS approaches, where one retained the full dimension of the interface boundary DOFs, this method allowed the reduction of the interface DOFs.

Hybrid Substructuring Methods

Liew *et al.* (1996) stated that the fixed interface CMS method could achieve more accurate results but take longer computation time than the free CMS method. Some researchers proposed the hybrid CMS method to combine the fixed interface and free interface cases.

Liew *et al.* (1993) proposed a hybrid CMS method for analysis of the free vibration of a rectangular plate with mixed interface conditions. Several plate cases were solved to demonstrate the applicability and accuracy of the hybrid method.

Farhat and Geradin (1994) constructed a substructure interface impedance operator with a spectral analysis. The procedures for ‘gluing’ the non-conforming and incompatible substructure models were proposed. They considered the CMS method for assembling heterogeneous substructures and recast it into a hybrid variational formulation.

Qiu *et al.* (2003) expressed the substructural displacements exactly as linear combination of the fixed and free interface modes. The higher free interface modes were expressed in terms of some lower mixed modes by means of an exact expression.

Morgan *et al.* (2003) combined the fixed interface and free interface modes for identification of non-proportionally damped systems. The fixed interface method was applicable when the finite element matrices were employed for analytical implementation. The free interface method was used within an experimental implementation with test data.

Shanmugam and Padmanabhan (2006) proposed a hybrid fixed-free interface method, in which the analyst could decide which boundary was to be fixed and which to be free, in order to achieve the full potential of this method.

(b) Kron's Substructuring Method

Kron (1963) first proposed a substructuring method to study the eigensolutions of systems with a large number of variables in a piecewise manner. This method partitioned and reconnected the substructures in their natural manner, without intentionally constraining the boundary coordinates or releasing the boundary coordinates. It constituted the receptance matrix by imposing displacement constraints at the interface coordinates of the adjacent substructures via the Lagrange multiplier technique and virtual work theorem. Simpson and Tabarrok (1968) initiated Kron's complicated electrical notation into its structural receptance form, and searched the eigenvalues by the bisection scanning and the sign count algorithm. They described the complicated process of Kron's substructuring method with a simple case study, and extended to cover various problems such as the complex

eigenproblem of damped structure (Simpson 1973b). To render the Kron's procedure more attractive in design applications, the eigenvalue and eigenvector derivative formulae were then derived based on the Kron's receptance matrix (Simpson 1973a). Mackenzie (1974) validated this substructuring method and showed that the in-core requirements and operational counts of Kron's substructuring method were very competitive and advantageous, comparing with other substructuring methods.

Afterwards, Simpson (1982) replaced the receptance formula with a transcendental dynamic stiffness matrix. The Newtonian process was utilized to accelerate the computation. Sehmi (1985) further improved it with a quadratically convergent Newtonian procedure. The procedure was integrated with the Strum sequence algorithm, so that the eigensolutions were obtained in ascending order without missing. Williams and Kennedy (1988) proposed a multiple determinant parabolic interpolation method to ensure the successful convergence of the required eigenvalues in all circumstances.

Turner (1983) attempted to reduce the computational load of the Kron's method via static condensation, but the results were not precise enough to satisfy the requirement of usual applications. Subsequently, this method was ignored by researchers, because it was not comparable to other fast developing eigensolvers at the global structure level, such as the Lanczos method and Subspace Iteration method. Sehmi transformed the Kron's receptance matrix and combined the eigenproblem with numerical solutions of the Lanczos method (Sehmi 1986) and Subspace Iteration method (Sehmi 1989). This improvement renders the Kron's substructuring method new value, although it requires calculating all eigenpairs of each substructure primarily.

Zhao and Simpson (1988) applied Kron's substructuring procedure in analysis of a

stable damped spinning structure, with the presence of the centrifugal force and steady-state internal force. Lui (1998) discussed some theoretical aspects of the Kron's receptance matrix, such as the zeros and poles of the eigenvalues, and summarized detailed characteristics of Kron's substructuring method.

(c) Rayleigh-Ritz Based Substructure Approach

For a continuum system, an exact analytical solution is not always possible and an approximate solution via some kinds of structural discretization is undertaken, which divides the continuum system into several substructures. With the substructure manner, the solution of the global structure can be formed from the space of the admissible functions to constrain the substructures. Admissible functions, which are determined by the global shape function, need satisfy only the geometric interface conditions. This approach is known as the Rayleigh-Ritz based substructure method. Basically, each substructure is approximated by a set of admissible trial vectors, and an iteration process is employed so that the eigensolutions converge to the accurate ones of the continuum system (Meirovitch 1997).

Meirovitch and Kwak (1990) stated that, the use of mere admissible functions was characterized by poor or slow convergence, which in turn was likely to demand relatively large numbers of substructures. In addition, while analyzing individual substructure, a finite linear combination of the admissible functions of the same class was not capable of satisfying the natural boundary conditions. They conceived quasi-comparison functions, which were the linear combinations of the admissible functions capable of approximating the differential equation and the natural boundary conditions to any degree of accuracy by merely increasing the orders of the variables in the approximated solution.

Meirovitch and Kwak (1991) employed a consistent kinematical procedure in the

Reyleigh-Ritz based substructure method to ensure the geometric compatibility conditions at interface points automatically. The mathematical proof of convergence of this substructure synthesis was presented later (Meirovitch and Kwak 1992). Morales (2000) extended the Rayleigh-Ritz based substructure synthesis method to analyze more general structures, including the complex variables. Johnson (2003) intended to amount the admissible functions to a series of constraints on the system variables. The geometric compatibility was verified to be the equivalent of generating underlying admissible shape functions.

(d) Modes Selection Scheme

In modal domain analysis of the dynamic substructuring methods, some modes are retained while the others are discarded. Intrinsically, the modes associated with the lowest frequencies are suggested to be retained. But this is not always correct.

Spanos and Tsuha (1991) proposed a two-stage method to encompass the optimal modes in the substructures. In the first stage, Rayleigh-Ritz algorithm was utilized to eliminate the unimportant and unreliable high modes. In the second stage, a modal balancing method further eliminated the modes that were least affected by the actuators, disturbances and interface forces, and that contributed least to the motions at the sensors and substructure interface locations. Tournour *et al.* (2001) investigated the convergence properties with respect to the quantity of the retained modes, from which a convergence criterion was proposed. Six test cases were used to evaluate the number of necessary modes in the substructures ensuring the accuracy of the free interface CMS method. Givoli *et al.* (2004) proposed a criterion of ‘modal importance’ to choose the modes to be retained in the linear dynamical substructures. A norm indicator was proposed, and the important modes of the substructures were those whose coupling matrices had the highest norm.

In sum, all the three substructuring methods in modal domain (CMS method, Kron's substructuring method and the Rayleigh-Ritz based substructuring method) are fundamentally inspired from the concept of Ritz method, in which different types of modes are chosen as Ritz vectors for each substructure. In Rayleigh-Ritz based substructuring method, the Ritz vectors are designated by the shape functions of the independent substructures and enforced by the shape function of the global structure. The CMS method either constrains all boundaries of the partitioned substructures or releases all of them intentionally. In the former case, the Ritz vectors are represented by fixed normal modes and enforced by the constraint modes. In the later case, the Ritz vectors encompass the rigid body modes and the free normal modes, which are enforced by the linking forces. Kron's substructuring method partitions and reconnects the substructures in their natural manner, without intentionally constraining the boundary coordinates or releasing them. The Ritz vectors are the eigensolutions of the independent substructures, which are assembled to represent the global structure by a determined geometric matrix. As a result, the Kron's substructuring method requires less computer memory and much fewer operational counts, and thereby is adopted in this research.

2.4.2 Generic Substructure Method

A generic element is a family of elements that encompasses all possible element formulations described by the same displacement field. Once a member of the family is defined (the baseline element), it is possible to obtain any other elements in the family, by modifying the baseline eigenvalues and transforming the baseline eigenvectors (Gladwell and Ahmadian 1995). Accordingly, model updating consists of two parts: defining the generic family of the elements and finding the appropriate parameter values to specify the model in this family. Similarly, a substructure could be regarded as a generic element.

Doebling (1995) decomposed the measured stiffness matrix or flexibility matrix into the component stiffness matrices of the underlying structural elements. Assuming that an N DOF global structure is divided into N_S elements or substructures, the stiffness matrix of the jth element/substructure, which has the size of $N^{(j)}$ and rank of $q^{(j)}$, can be decomposed as

$$\mathbf{K}^{(j)} = \mathbf{\Phi}^{(j)} \mathbf{\Lambda}^{(j)} \left[\mathbf{\Phi}^{(j)} \right]^T \tag{2-62}$$

where $\mathbf{\Phi}^{(j)}$ is regarded as the static eigenvector with the size of $N^{(j)} \times q^{(j)}$, and $\mathbf{\Lambda}^{(j)}$ is the diagonal matrix of the nonzero static eigenvalues of the jth element. If the elemental displacements are related to the global DOFs by $\left\{ x^{(j)} \right\} = \mathbf{T}^{(j)} \left\{ x_g \right\}$, and the global stiffness matrix is formed by assembling the elemental stiffness matrices as $\mathbf{K}_g = \sum_{j=1}^{N_S} \left[\mathbf{T}^{(j)} \right]^T \mathbf{K}^{(j)} \mathbf{T}^{(j)}$, the global matrix can be written as

$$\mathbf{K}_g = \sum_{j=1}^{N_S} \left[\mathbf{T}^{(j)} \right]^T \mathbf{\Phi}^{(j)} \mathbf{\Lambda}^{(j)} \left[\mathbf{\Phi}^{(j)} \right]^T \mathbf{T}^{(j)} = \mathbf{\Phi}_T^p \mathbf{\Lambda}^p \left[\mathbf{\Phi}_T^p \right]^T \tag{2-63}$$

where $\mathbf{\Phi}_T^p$ is regarded as the 'connectivity matrix' of the generic elements and defined by

$$\mathbf{\Phi}_T^p = \left[\left[\mathbf{T}^{(1)} \right]^T \mathbf{\Phi}^{(1)} \quad \left[\mathbf{T}^{(2)} \right]^T \mathbf{\Phi}^{(2)} \quad \cdots \quad \left[\mathbf{T}^{(N_S)} \right]^T \mathbf{\Phi}^{(N_S)} \right] \tag{2-64}$$

The superscript 'p' denotes the primitive matrices of the diagonally assembled substructures, subscript 'g' denotes the variables associated with the global structure, and $\mathbf{\Lambda}^p$ is a diagonal assembly of the elemental static eigenvalues $\mathbf{\Lambda}^{(j)}$, which can by expressed by the elemental physical properties, such as *EI*, *EA*, and *GJ*. The static eigenvector $\mathbf{\Phi}^{(j)}$ is determined for a group of elements, such as the Bernoulli-Euler beam elements. In model updating or damage identification, the changes in elemental parameters can be determined from the variation of $\mathbf{\Lambda}^p$. The elemental eigenvalues and eigenvectors can be used for a substructure as well, in which the substructure is regarded as a super-element.

Ahmadian *et al.* (1997) selected the updated parameters based on the generic elements, and compared with those of traditional selection strategy. The selection strategy based on generic element was proved to produce a structure more consistent with the test data. Friswell *et al.* (1997) updated the physical parameters in a scheme combining the genetic substructure algorithm and the sensitivity method for the location and quantification of damage. The updating parameters were chosen to be the static eigenvalues of the genetic substructure. Later, they used the generic substructure technique to improve the dynamic models of the golf clubs (Friswell *et al.* 1998c). The club shaft was modeled with a generic beam substructure and the eigenvalues of the substructure were chosen as uncertain parameters to be updated.

Zimmerman *et al.* (1999) applied the Ritz vectors in a modified minimum rank perturbation to the genetic substructure algorithm. The static eigenvalues of the substructures were employed to represent the effect of damage. Ratcliffe *et al.* (2000) applied the generic substructure approach to the joint identification. The number of generic parameters was limited by enforcing symmetry of elemental system matrices and persevering coupling of the uncoupled modes. Law *et al.* (2001) employed the generic substructure method to update the semirigid joints together with other parameters of a structural system. Titurus *et al.* (2003) defined a T-joint as generic substructure, in which the first two eigenvalues of the substructure were chosen as parameters to update a welded frame.

Terrell *et al.* (2007) mentioned that unconstrained generic substructure transformations may change the connectivity of the system matrices. They utilized the constrained generic substructure transformations in finite element model updating. The substructural eigenvalues were the uncertain parameters used in the global updating procedure and the substructural eigenvector matrix was optimized to

enforce the connectivity constraints. Di and Law (2007) decomposed the elemental matrices of a frame element into the eigenvalue and eigenvector matrices. The generic eigenvectors reflected the different load-carrying capacities of the generic element. The eigenvalues represented physically the stiffness of the generic element corresponding to its different deformational mode shapes. The eigen-parameters were then included in a flexibility-based and sensitivity-based model updating algorithm for the condition assessment of the plane frame structure.

2.4.3 System Identification with Substructure Method

Koh *et al.* (1991) used a substructure approach to estimate the structural parameters in time domain. For the substructure considered, the equations of motion may be extracted as

$$\begin{bmatrix}\mathbf{M}_{IB} & \mathbf{M}_{II}\end{bmatrix}\begin{Bmatrix}\ddot{x}_B(t)\\ \ddot{x}_I(t)\end{Bmatrix}+\begin{bmatrix}\mathbf{C}_{IB} & \mathbf{C}_{II}\end{bmatrix}\begin{Bmatrix}\dot{x}_B(t)\\ \dot{x}_I(t)\end{Bmatrix}+\begin{bmatrix}\mathbf{K}_{IB} & \mathbf{K}_{II}\end{bmatrix}\begin{Bmatrix}x_B(t)\\ x_I(t)\end{Bmatrix}=\left\{f_I(t)\right\} \quad (2\text{-}65)$$

in which, subscript '*I*' and '*B*' denotes the internal coordinates and interface boundary coordinates of a substructure, respectively. Treating interaction effects at the interface ends as 'input', Eq. (2-65) can be re-arranged as

$$\mathbf{M}_{II}\left\{\ddot{x}_I(t)\right\}+\mathbf{C}_{II}\left\{\dot{x}_I(t)\right\}+\mathbf{K}_{II}\left\{x_I(t)\right\}=\left\{f_I(t)\right\}-\mathbf{M}_{IB}\left\{\ddot{x}_B(t)\right\}-\mathbf{C}_{IB}\left\{\dot{x}_B(t)\right\}-\mathbf{K}_{IB}\left\{x_B(t)\right\} \quad (2\text{-}66)$$

Koh *et al.* (1991) formulated and solved the state and observation equations for the substructures by the extended Kalman filter method with a weighted global iteration algorithm. The substructures with and without overlapping members were considered respectively.

Koh *et al.* (2003) adopted the 'quasi-static displacement' vector to release the requirement of time signals including the displacement, velocity and acceleration at the interface in Eq. (2-66). The displacements of the internal DOFs are separated into

the quasi-static displacements $\left\{x_I^s(t)\right\}$ and the relative displacements $\left\{x_I^*(t)\right\}$,

$$\left\{x_I(t)\right\} = \left\{x_I^s(t)\right\} + \left\{x_I^*(t)\right\} \tag{2-67}$$

where

$$\left\{x_I^s(t)\right\} = -\mathbf{K}_{II}^{-1}\mathbf{K}_{IB}\left\{x_B(t)\right\} = \mathbf{r}\left\{x_B(t)\right\}$$

Without considering the damping force, the motion equation of the substructure gives,

$$\mathbf{M}_{II}\left\{\ddot{x}_I^*(t)\right\} + \mathbf{C}_{II}\left\{\dot{x}_I^*(t)\right\} + \mathbf{K}_{II}\left\{x_I^*(t)\right\} = \left\{f_I(t)\right\} - \left(\mathbf{M}_{IB} + \mathbf{M}_{II}\mathbf{r}\right)\left\{\ddot{x}_B(t)\right\} \tag{2-68}$$

Accordingly, only accelerations (no displacements or velocities) at the interface DOFs are required to compute the interface motion forces. They extended this method to progressive structural identification. Once the unknown structural parameters of the former substructure were identified, an extended substructure was identified based on the former recognized substructure. The substructure was enlarged gradually, until the entire structure or the necessary part was identified. Sometimes the interface points are located at the places where the sensors are unapproachable. Koh and Shankar (2003) related the response at a point to the excitation at another point by a receptance function, and eliminated the interface forces by using different sets of measurement in the focused substructure under the same excitation condition.

Yun and Lee (1997) developed a substructural identification method by employing the sequential prediction error method and auto-regressive and moving average with exogenous inputs (ARMAX) model to process the observation data on the substructures. Yun and Bahng (2000) adopted a backpropagation neural network in substructural identification of a complex system.

Tee *et al.* (2005) proposed two system identification methods at the substructural level. The first one was based on the first-order state space formulation of the

substructures where the eigensystem realization algorithm (ERA) and the observer/Kalman filter identification (OKID) were used. Identification at the global level was then performed to obtain the second-order model parameters. In the second method, identification was performed at the substructural level in both the first- and second-order model identification. Tee *et al.* (2009) incorporated the substructural identification with model condensation technique. The SEREP condensation was adopted, and the stiffness parameters were recovered from the identified condensed stiffness matrices (Koh *et al.* 2006). The method allowed fewer sensors and actuators involved conversion from the first-order to second-order models.

Yang and Huang (2007) and Huang and Yang (2008) employed the substructure concept in the proposed sequential nonlinear least-square estimation with unknown inputs and unknown outputs, to identify damages at critical locations of the complex structures.

2.4.4 Disassembly of the Global Structure into Substructures

Nearly all of the above-mentioned literatures on dynamic substructuring methods include both the disassembling and reassembling procedure, to recover the property of the global structure. During the model updating process, the analytical model of the global structure is iteratively reproduced with various substructuring methods, and then compared with the experimental counterparts. On the other hand, there is another approach, which inversely extracts the substructural properties from the global structure under some constraints. Although this approach is less used, it has merits in some aspects. For example, the measurement quantities of the substructures are obtained by decomposing the measurement of the global structure. Consequently, the interest substructure can be treated as an independent structure using traditional global methods.

Gordis (1997) firstly related the global flexibility with the substructural flexibility matrices by a force method. For a statically determinate structure, the force method yields the global flexibility by

$$\mathbf{F}_g = \mathbf{B}_0^T \mathbf{F}^p \mathbf{B}_0 \tag{2-69}$$

where $\mathbf{F}_g$ is the global flexibility, $\mathbf{F}^p$ is the diagonal assembly of the substructural flexibility matrices, and $\mathbf{B}_0$ is the load transformation matrix which is obtained from the applied loads to the internal forces for the determinate structures. Based on this relation, the substructural flexibility matrices can be estimated from the global flexibility matrix. As $\mathbf{B}_0$ was rank deficient, the extracted substructural flexibility matrices were further constrained by a mapping matrix. Gordis (1997) examined this disassembly procedure and claimed that the disassembly was only feasible for the determinate beam-like structures.

Felippa and Park (1997) extended the force method to more types of structures, by additionally accounting for the constraints of conservation of the elemental rigid body modes and the block-diagonal character of the resultant substructural matrices. If the structure is statically indeterminate, the redundant load transformation matrix $\mathbf{B}_1$ is additionally constructed so that the global flexibility relates to the substructural flexibility matrix as

$$\mathbf{F}_g = \mathbf{B}_0^T \left[\mathbf{F}^p - \mathbf{F}^p \mathbf{B}_1 \left(\mathbf{B}_1^T \mathbf{F}^p \mathbf{B}_1 \right) \mathbf{B}_1^T \mathbf{F}^p \right] \mathbf{B}_0 \tag{2-70}$$

To determine the substructural flexibility matrix $\mathbf{F}^p$, one must construct the load transformation matrix $\mathbf{B}_0$ and $\mathbf{B}_1$ beforehand. Park *et al.* (1997) used this force method to calculate the interface forces and displacements between the adjacent substructures under predefined loads. With the forces and displacements on the boundaries, one substructure might be singled out for various kinds of analysis.

Based on the load transformation matrix $\mathbf{B}_0$ and $\mathbf{B}_1$, Park and Reich (1998) evaluated three methods in disassembly of the global flexibility matrix, the frequency domain

flexibility method, the deformation-based flexibility method, and the strain-based flexibility method, in which the global flexibility was generated from the FRF data, displacement data, and strain data, respectively. Accordingly, the transformation matrix $\mathbf{B}_0$ and $\mathbf{B}_1$ were constructed based on the connectivity of FRF, displacement and strain data. These methods were applied to a ten-story building with a beam-like model and a laboratory bridge structure. The strain-based substructural flexibility method was proved to be more desirable in the studies since it provided more accurate solutions than the other two.

Doebling *et al.* (1998) developed the disassembly procedures for both the stiffness and flexibility matrices based on the generic substructure concept. The elemental/substructural matrices were decomposed into elemental eigenvectors and eigenvalues. The elemental eigenvectors were dependent only on known quantities such as geometry and assumed shape functions, whereas the elemental eigenvalues needed to be determined. This method projected the experimentally measured flexibility matrix according to the strain energy distribution in the regional generic substructures. Using both the presumed connectivity and strain energy distribution pattern, the method formed a well-determined linear least square problem for the structural eigenvalues.

Alvin and Park (1999) stated that, the force method that was originated by Gordis (1997) heavily depended on the choice of load transformation matrices $\mathbf{B}_0$ and $\mathbf{B}_1$. For the continuum structures, such as plates and shells, matrices $\mathbf{B}_0$ and $\mathbf{B}_1$ were difficult to be uniquely determined if the load path was complicated. They developed a direct flexibility method to extract the substructural flexibility matrices from the measured flexibility matrix. Other than the force method in which the substructural flexibility and the global flexibility were connected based on the load path, Alvin and Park (1999) connected them uniquely by the substructural rigid body modes and the

substructural connectivity topology. The substructural displacement vector $\{x^p\}$ and the substructural forces $\left\{ f^p \right\}$ can be expressed in terms of the global displacement vector $\{x_g\}$ and stiffness matrix as

$$\left\{ x^p \right\} = \mathbf{L}\left\{ x_g \right\}, \quad \mathbf{L}^T \left\{ f^p \right\} = \left\{ f_g \right\} \tag{2-71}$$

$$\left\{ f^p \right\} = \mathbf{K}^p \left\{ x^p \right\} = \mathbf{K}^p \mathbf{L}\left\{ x_g \right\} \tag{2-72}$$

L is determined by the geometric topology. Considering the Lagrange multiplier, the substructural displacement and force can be expressed by the global ones as

$$\left\{ f^p \right\} = \left(\mathbf{L}^T \right)^+ \left\{ f_g \right\} - \mathbf{C}\{\tau\} \tag{2-73}$$

$$\left\{ x^p \right\} = \left(\mathbf{K}^p \right)^+ \left\{ f^p \right\} - \mathbf{R}\left\{ x_r \right\} \tag{2-74}$$

where $\mathbf{C}\{\tau\}$ is the Lagrange expression of the interface force and $\mathbf{R}\left\{ x_r \right\}$ is the rigid body motion. They are constrained by the displacement compatibility and force compatibility, respectively

$$\mathbf{C}^T \left\{ x^p \right\} = 0 \tag{2-75}$$

$$\mathbf{R}^T \left\{ f^p \right\} = 0 \tag{2-76}$$

After $\mathbf{C}\{\tau\}$ and $\mathbf{R}\left\{ x_r \right\}$ are solved, the displacement and external force vectors can be expressed with the substructural flexibility, which is subsequently related to the global flexibility. Alvin and Park (1999) extracted the substructural flexibility matrices with an iterative scheme from the global flexibility. Felippa and Park (2002) extended this direct flexibility method to multilevel substructural analysis, and applied it to parallel computation technique.

2.4.5 Comprehensive Applications of Substructuring Technology

1) Periodic or Repetitive Substructures

A periodic system is comprised of a number of identical substructures arranged sequentially and having identical connection properties between all pairs of adjacent

substructures (Garvey and Penny 1994). Josson *et al.* (1995) introduced recursive substructuring algorithm among periodic structures. In each recursive step, the initial problem was transformed into a new problem involving half the number of the identical substructures. Sunar and Rao (1997) utilized the substructuring method for the active control design of large periodic structure. The free vibration analysis of a periodic structure was reduced to that of a substructure by the wave propagation method. The relations between the interactions of identical substructures were obtained by using the quadratic eigenvalue problem. These relations were then used to assemble the global controller of the entire structure from the sub-controller designed for a reference substructure. Aldraihem (2007) examined the dynamic stability of a collar-stiffened pipe by using the Euler-Bernoulli beam theory. The pipe was considered to be composed of identical substructures and be connected in an identical fashion.

2) Modeling Different Parts in Substructure Manner

A system is often composed of different parts, which have different properties and are coupled with determined connections. The different parts can be analyzed independently in substructure manner. Huang *et al.* (1996) used two substructures to model two parts of a composite tower under wind-induced vibrations, because different damping characteristics arose from the construction of the tower with two kinds of materials. Jia (1999) utilized the substructuring technique to model the coupled bending dynamics of a spinning-shaft-disk system. The shaft, disk and spin were treated as three substructures, respectively. Biondi and Muscolino (2003) modeled a coupled structural systems as a combination of the continuous and FE discretized substructures. The interface condition was assumed to be free for the discretized substructure and to be elastic constraints for the continuous beam. Biondi *et al.* (2005) divided a train-track-bridge system into three substructures due to the different properties of the three parts. The procedure handled the dynamic responses

of the vehicles, rails and bridge simultaneously. Wegner *et al.* (2005) divided a soil-structure interaction model into two substructures. The unbounded soil was modeled by the scaled boundary finite element method, and the structure was modeled by a standard FE method. Cai *et al.* (2008) investigated the dynamic responses of a track-ground system subjected to moving train passages by the substructuring method. The whole system was divided into two separately formulated substructures, the track and the ground.

3) Nonlinear Analysis

Nonlinear analysis is much more computationally intensive than linear analysis. Clough and Wilson (1979) applied the substructuring method to the problems with local nonlinearities. A structure was divided a linear substructure and a nonlinear substructure, respectively. The linear substructure was further divided into more substructures, while the nonlinear substructure was kept as a complete system. Han and Abel (1985) proposed an adaptive substructuring algorithm to handle nonlinear problems. The stresses of the elements within linear substructures were often evaluated during the analysis. If the stresses of an element exceeded a predefined level, the substructure was re-substructured and the overstressed element was re-assigned from the linear substructure to the nonlinear substructure. Chen and Archer (2005) presented a domain decomposition method for nonlinear substructures. The nonlinear behavior of a substructure was updated by adding correcting modes. The efficiency was improved by cooperating with a parallel processing technique.

2.5 Challenges in Model Updating and Substructuring Methods

Although the vibration-based model updating has been investigated extensively, there are a number of issues that need to be addressed to make the method more practical and commonly applied in the civil engineering community, as follows.

1) There is a considerable computational burden associated with the traditional model updating methods if the practical structure is represented by a large model in size (Brownjohn 2007; Farrar and Worden 2007). In iterative model updating methods, the eigensolutions and eigensensitivities are repeatedly required from the large-scale analytical model, which is very inefficient.
2) The number of uncertain parameters that need updating is large for civil structures, which may render the optimization process ill-conditioned or the results physically meaningless (Friswell *et al.* 2007).
3) The effect of uncertainty within a model and the measurement data is difficult to quantify (Sohn 2007). How the uncertainty propagates also deserves investigations.
4) The substructuring methods can reduce the size of the system matrices and decrease the number of updating parameters, and therefore reduce the ill-conditioned difficulty and improve the computational efficiency. The substructuring methods, however, may bear errors to some degree, particularly in modeling the interface forces and displacement compatibility. In addition, the effect of uncertainty due to the modeling or measurement noise may accumulate and propagate across the substructures, as the adjacent substructures interact mutually.

CHAPTER THREE

NUMERICAL AND EXPERIMENTAL EXAMPLES

3.1 Introduction

A few numerical and experimental examples that will be employed in the subsequent chapters are described here together for convenience. The numerical examples include a spring-mass model, a three-span frame, and the Guangzhou New Television Tower, which respectively represent the small, medium and large structures to investigate the accuracy and efficiency of the proposed substructuring methods. Three experimental structures, a cantilever beam, a portal frame, and the Balla Balla River Bridge, serve for the application of the substructuring-based model updating. This chapter will present the detailed description of the numerical and experimental examples.

3.2 Numerical Examples

3.2.1 A Spring-mass Model

A simple spring-mass model with six DOFs (Figure 3-1) will be utilized in this thesis to explicitly describe the details of the substructuring methods. The spring-mass system is a one-dimensional structure, which is fixed at one end and free at the other. The stiffness parameters of the six springs are set to $k_1 = k_2 = k_3 = 10$ N/m, $k_4 = k_5 = k_6 = 20$ N/m. The six masses are set to $m_1 = 1$ kg, $m_2 = 2$ kg, $m_3 = 1$ kg, $m_4 = 2$ kg, $m_5 = 2$ kg, $m_6 = 1$ kg. The stiffness matrix of this structure is

$$\mathbf{K}_g = \begin{bmatrix} 20 & -10 & & & & \\ -10 & 20 & -10 & & & \\ & -10 & 30 & -20 & & \\ & & -20 & 40 & -20 & \\ & & & -20 & 40 & -20 \\ & & & & -20 & 20 \end{bmatrix} \tag{3-1}$$

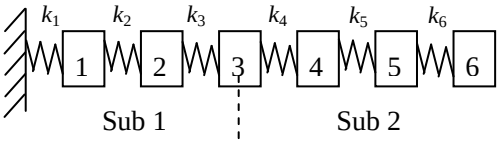

Figure 3-1: Spring-mass Model with Six DOFs

The structure is divided into two substructures at Mass 3 as Figure 3-1. After division, the first substructure is a fixed structure, and the second substructure is free. To be an independent structure, the first substructure has the form as Figure 3-2.

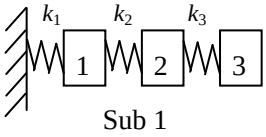

Figure 3-2: First Substructure of the Spring-mass Model

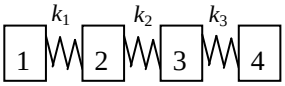

Figure 3-3: Second Substructure of the Spring-mass Model

As usual fixed structure, the first substructure has full-rank stiffness matrix and modal flexibility matrix as

$$\mathbf{K}^{(1)} = \begin{bmatrix} 20 & -10 & \\ -10 & 20 & -10 \\ & -10 & 10 \end{bmatrix}, \quad \mathbf{F}^{(1)} = \begin{bmatrix} 0.1 & 0.1 & 0.1 \\ 0.1 & 0.2 & 0.2 \\ 0.1 & 0.2 & 0.3 \end{bmatrix} \tag{3-2}$$

The second substructure is free and displayed in Figure 3-3 as an independent structure. The stiffness matrix of the second substructure is singular, which is given as

$$\mathbf{K}^{(2)} = \begin{bmatrix} 20 & -20 & & \\ -20 & 40 & -20 & \\ & -20 & 40 & -20 \\ & & -20 & 20 \end{bmatrix} \tag{3-3}$$

And the modal flexibility matrix is

$$\mathbf{F}^{(2)} = \begin{bmatrix} 0.0486 & 0.0069 & -0.0181 & -0.0264 \\ 0.0069 & 0.0153 & -0.0097 & -0.0181 \\ -0.0181 & -0.0097 & 0.0153 & 0.0069 \\ -0.0264 & -0.0181 & 0.0069 & 0.0486 \end{bmatrix} \tag{3-4}$$

3.2.2 A Three-span Frame Structure

A three-span frame (Figure 3-4) is numerically modeled by 160 two-dimensional beam elements each 2.5 m long, which results in 140 nodes and 408 DOFs. The material constants of the beam elements are chosen as: bending rigidity (EI) $=170\times10^6\ Nm^2$, axial rigidity (EA) = $2500\times10^6\ N$, mass per unit length (ρA) = 110 *kg/m*, and Poisson's ratio = 0.3. The elements are labeled as Figure 3-4(a).

The frame is disassembled into three substructures when it is divided at eight nodes as shown in Figure 3-4(b), resulting 51, 55 and 42 nodes in the three substructures. The eight interface nodes introduce 48 interface DOFs (each node has three DOFs) with 24 identical/repeated ones.

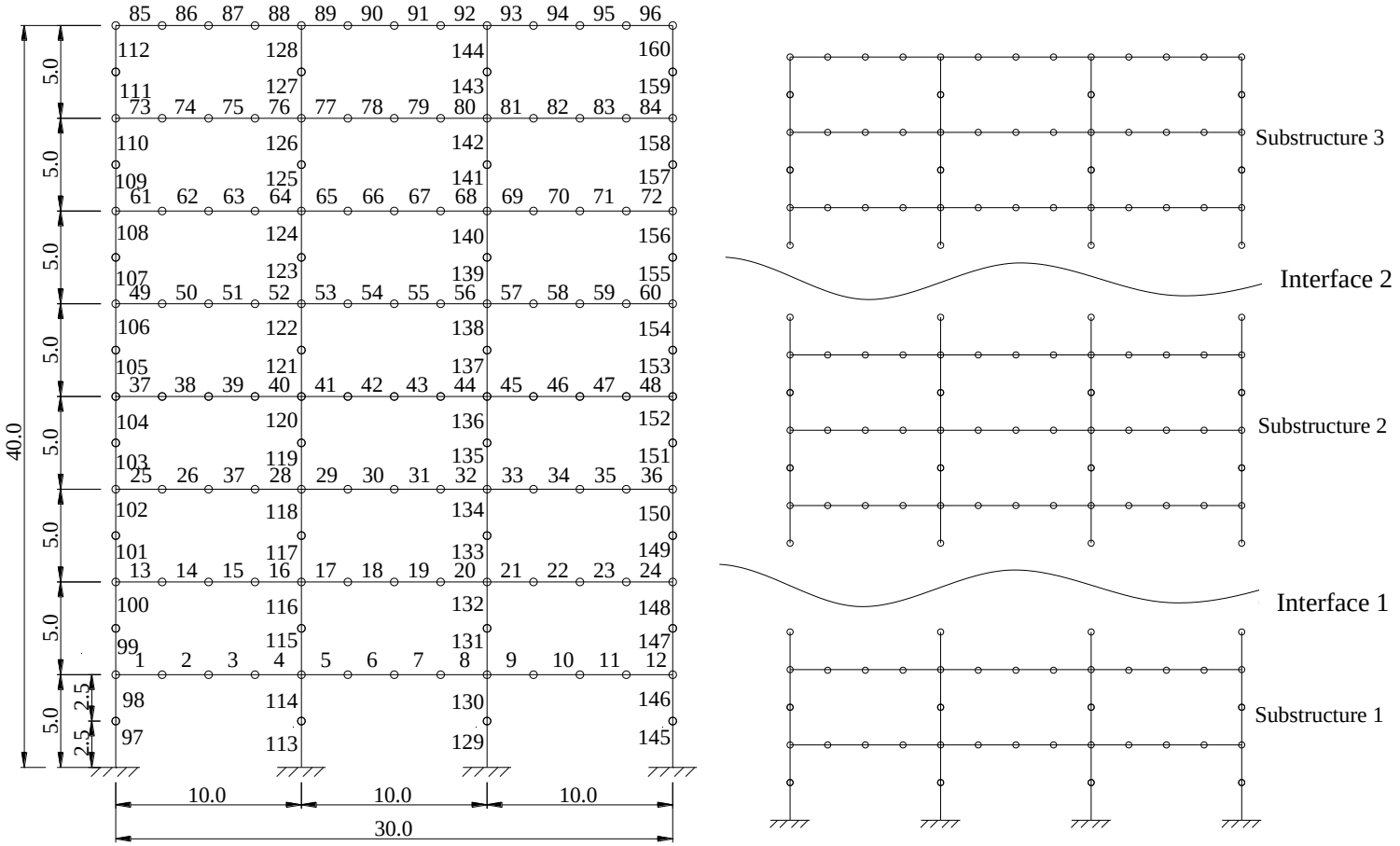

(a) Global Structure (b) Divided Substructures

Figure 3-4: FE Model of the Three-span Frame Structure (Unit: m)

3.2.3 The Guangzhou New Television Tower

The Guangzhou New Television Tower is a 610 m high super-tall structure that consists of a main tower (454 m) and an antennary mast (156 m) as shown in Figure 3-5. The structure comprises a reinforced concrete inner tube and a steel outer tube with concrete-filled-tube (CFT) columns. There are 37 floors connecting the inner tube and the outer tube, which serve for offices, entertainment, catering, tour and mainly emission of television signal.

(a) Landscape View (b) Global Model (c) Substructures

Figure 3-5: Guangzhou New Television Tower and the FE Model

The analytical model of the TV tower shown in Figure 3-5(b) comprises three parts: the outer tube, inner tube, and the connections between them.

The outer tube consists of 24 CFT columns, uniformly spaced in an oval while inclined in the vertical direction. The 24 CFT columns are interconnected transversely by steel ring beams and bracings. The analytical model of the outer tube is composed of 1128 nodes and 3312 three-dimensional beam elements.

The inner tube is an oval shape with a constant dimension of 14m × 17m in plan, but its centroid differs from that of the outer tube. The inner tube is composed of the floors and shear walls, which are modeled by 1440 nodes and 1924 three-dimensional shell elements.

The girder-floor connection between the inner tube and outer tube are modeled by 888 nodes and 2,832 three-dimensional beam elements. Including the mast, the analytical model of the entire structure consists of 8,738 three-dimensional elements, 3,671 nodes (each has six DOFs), and 21,690 DOFs in total.

When applying substructuring method, the global structure is divided into 10 substructures along the vertical direction as shown in Figure 3-5(c). The nodes and elements included in each substructure are listed in Table 3-1.

Table 3-1: Division Formation for the FE Model of the Guangzhou New TV Tower

Substructure index	Sub 1	Sub 2	Sub 3	Sub 4	Sub 5	Sub 6	Sub 7	Sub 8	Sub 9	Sub 10
No. of nodes	336	456	432	432	336	336	432	440	488	487
No. of elements	657	945	873	873	786	786	873	846	990	1109
No. of interface nodes	56	56	56	56	56	56	56	56	56	

3.3 Experimental Examples

3.3.1 Experimental Instruments

Accelerometer Bruel & Kjaer 4370 were used in the laboratory tests to record the acceleration response of a structure. Bruel & Kjaer 4370 is a type of single axis piezoelectric accelerometer sensitive along its Z axis down to nearly 10 μ g, and conventionally useful over a range of 0.1 Hz up to about 1/3 of its mechanical resonance frequency of 15 ~ 21 kHz. It works well for low level and low frequency vibration measurement. The specification of the accelerometer is listed in Table 3-2. Each accelerometer was mounted on the experimental model with a magnetic mounting base (total mass is 77.68 g). The mass of each accelerometer is modeled as a concentrated mass in the FE model. The output charge of the accelerometers is gauged in terms of voltage.

Table 3-2: Specification of Bruel & Kjaer 4370 Accelerometer

Piezoelectric material	pz23
Charge sensitivity	10 pC/ms^{-2} or 98 pC/g (±2%)
Voltage sensitivity	8 mV/ms^{-2} or 80 mV/g (±2%)
Mounted resonance	16 kHz
Frequency range	0.2 Hz ~ 3500 Hz (5%), 0.1 Hz ~ 4800 Hz (10%)
Ambient temperature range	-74 ^{o}C ~ 250 ^{o}C
Dimensions	21 mm diameter 22.6 mm height excluding the top connector
Weight	54 g 77.68 g (including the magnetic mounting base)

The Bruel & Kjaer amplifier 2635 and Bruel & Kjaer amplifier 2692 were employed to amplify the raw signal. The former is a four-stage amplifier consisting of the input amplifier, lowpass filter amplifier, integrator amplifier and output amplifier. The overload detector, test oscillator, and power supply unit are also included. Bruel & Kjaer amplifier 2692 contains up to four modular channels, each consisting of a common module as amplifier 2635. One amplifier 2962 is equivalent to four of

amplifier 2635 in the present testing.

The hammer provides an easy, economical and accurate way to produce excitations for structure dynamic testing. The SINOCERA LC-04A hammer with a rubber tip was employed in the laboratory tests. Its specification is listed in Table 3-3.

Table 3-3: Specification of the Impact Hammer

Sensitivity (pC/N)	4	
Max. shock force (kN)	60	
Head diameter (mm)	30	
Head mass (g)	300	
Frequency responses	Steel tip	10 kHz
	Aluminum tip	3 kHz
	Nylon tip	2 kHz
	Rubber tip	500 Hz

The instruments used in the tests are shown in Figure 3-6.

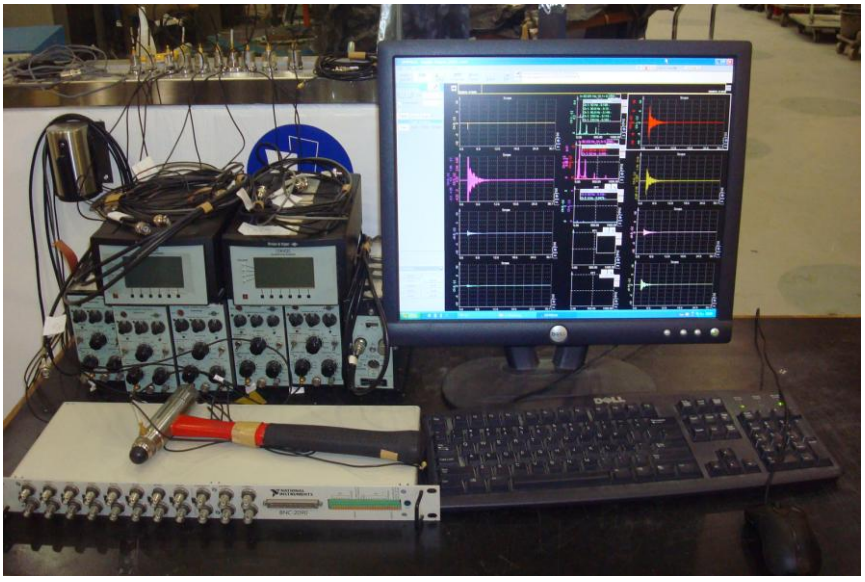

Figure 3-6: Instruments Used in the Experimental Tests

3.3.2 A Cantilever Beam

The first laboratory example is a steel cantilever beam as shown in Figure 3-7. The

beam is 50.1 mm wide, 3.0 mm high and 750 mm long as illustrated in Figure 3-8. The mass density was measured as 8.026×10^3 kg/m^3. To assure that the boundary condition was not altered in each testing, two thick blocks were welded on both sides of the clamped end as shown in Figure 3-7.

The structure was tested in the intact state and four damage configurations, respectively, which are given in Table 3-4. The beam was first tested without introduction of any damage as 'Case 0'. Afterwards, the beam was cut at Location 1 as shown in Figure 3-8, with depth of d = 5 mm, 10 mm, and 15 mm gradually, corresponding to 'Case 1', 'Case 2', 'Case 3', respectively. In 'Case 4', the beam was additionally cut at Location 2 with depth of d = 10 mm. The width of the cuts is b = 5 mm in all of the damage cases. One typical cut is demonstrated in Figure 3-9.

Table 3-4: Configuration of the Damage Scenarios

	Case 0	Case 1	Case 2	Case 3	Case 4
Damage configuration	Intact	Location 1 d = 5 mm	Location 1 d = 10 mm	Location 1 d = 15 mm	Location 1 d = 15 mm Location 2 d = 10 mm

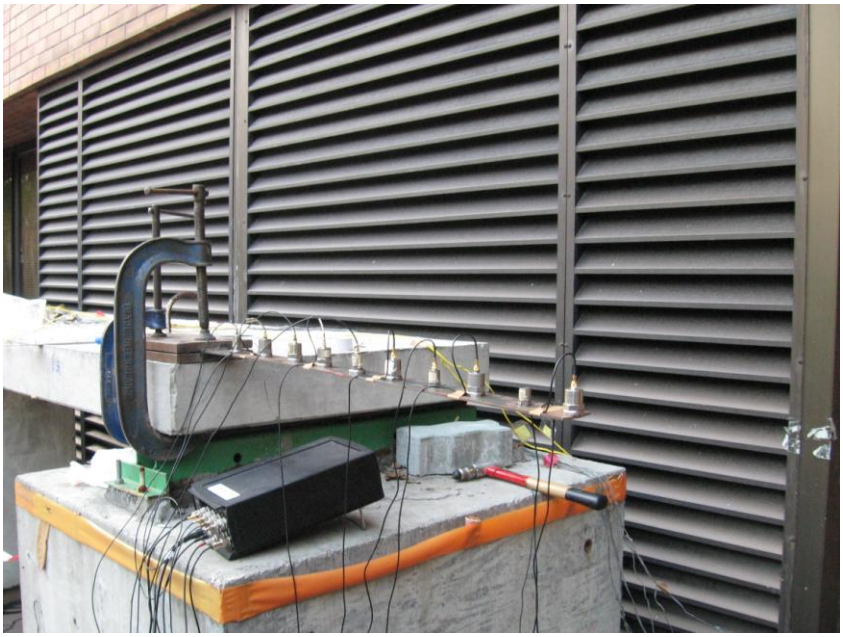

Figure 3-7: Experimental Beam Specimen

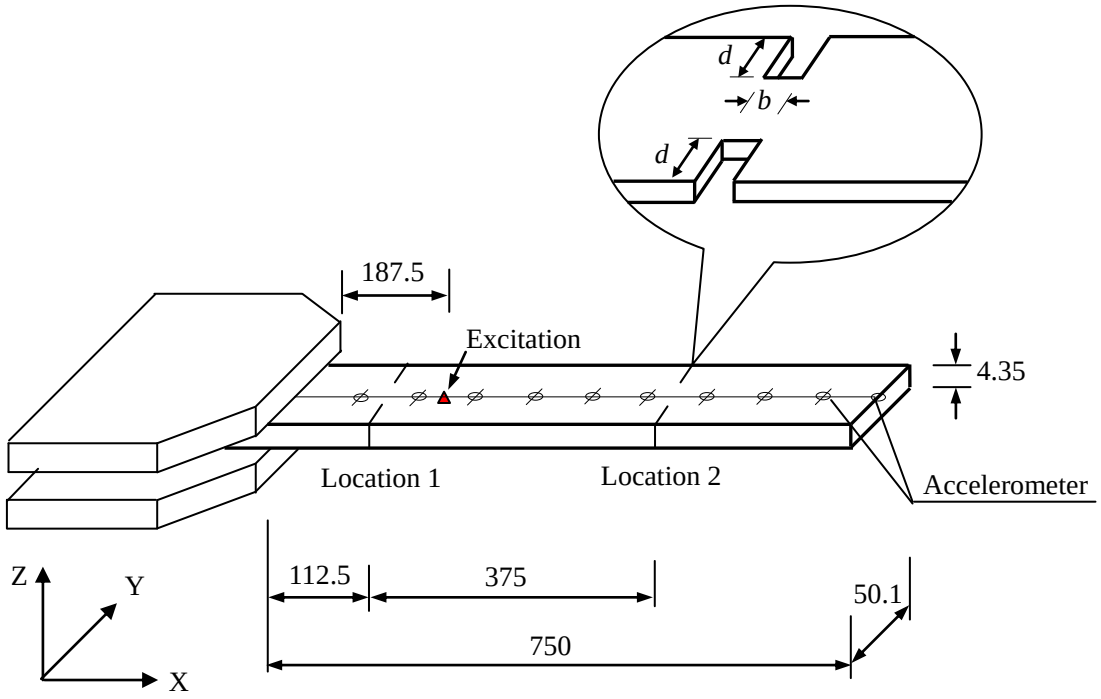

Figure 3-8: Configuration of the Beam Specimen (Unit: mm)

Figure 3-9: One Typical Cut of the Beam Specimen

Ten accelerometers were mounted evenly on the beam as shown in Figure 3-8. The beam was impacted vertically by the hammer at the location of 187.5 mm away from the clamped end. Three hits were imposed on the beam for each damage

configuration to average the signals.

In all cases, time history of input and responses were recorded for about 30 seconds with a sampling frequency of 3000 Hz. One typical set of measurement is shown in Figure 3-10 and Figure 3-11. Diagrams of auto-power spectral density of input, FRF, and coherence function are obtained using software DIAMOND (Doebling *et al.* 1997), and are illustrated in Figures 3-12 to 3-14, respectively. In Figure 3-14, the coherence function values are almost equal to one except at the resonances and anti-resonances in the range of 0 ~ 500 Hz. Therefore, the test data are satisfactory to extract the modal data in the frequency range of 0 ~500 Hz.

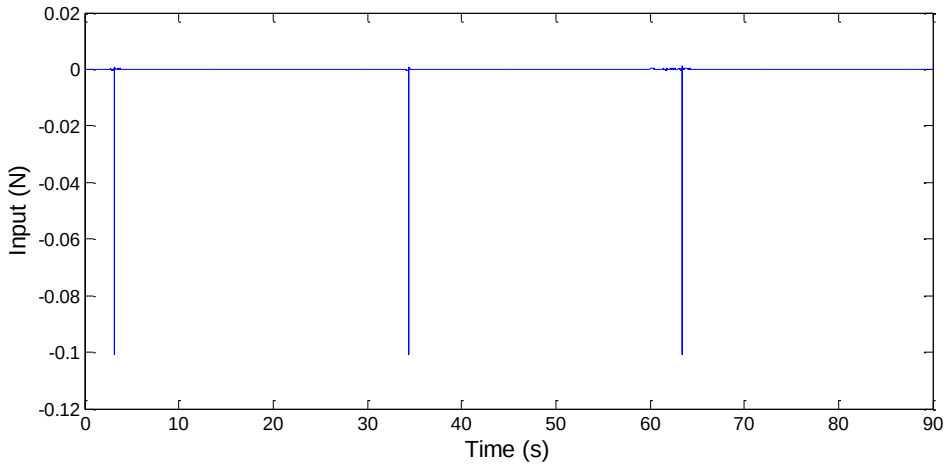

Figure 3-10: Input Force Time History

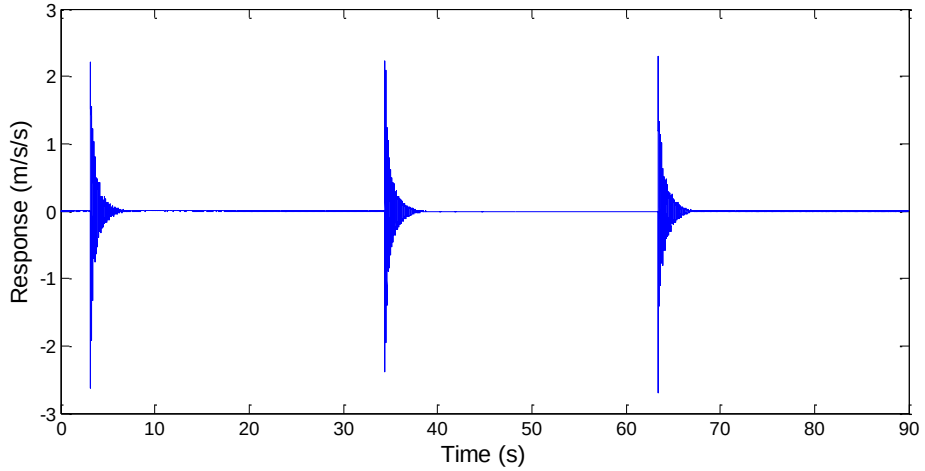

Figure 3-11: Recorded Acceleration Time History

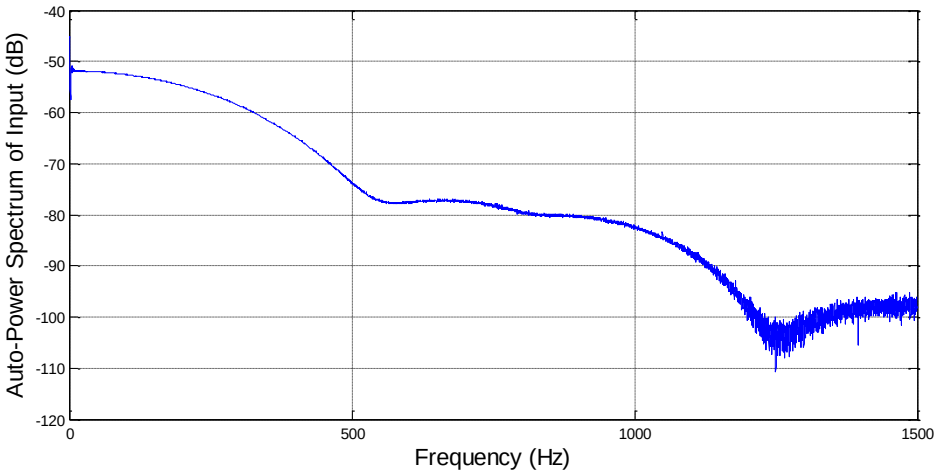

Figure 3-12: Auto-power Spectral Density of the Input Force

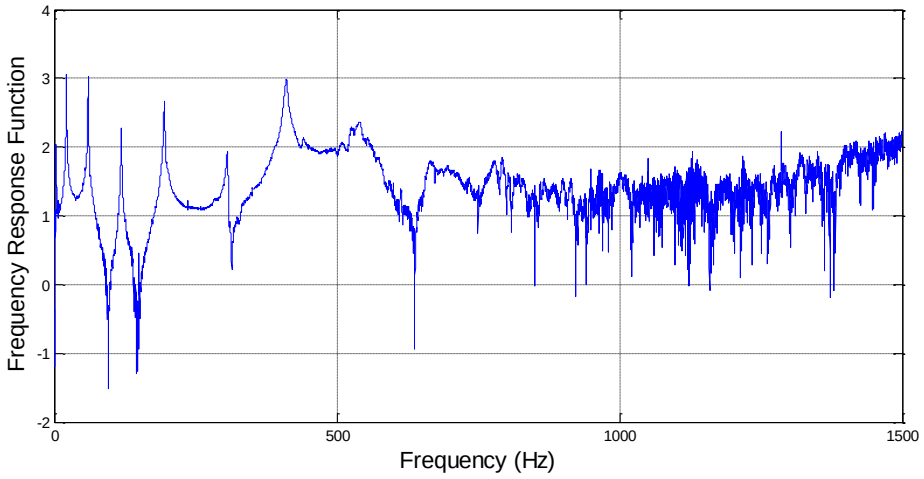

Figure 3-13: Magnitude of Frequency Response Function

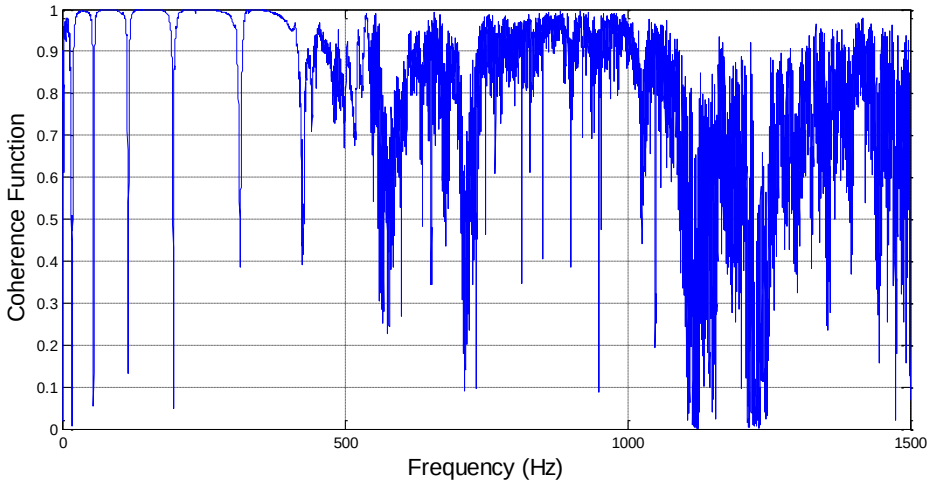

Figure 3-14: Coherence Function

The frequencies and mode shapes were extracted using the rational polynomial curve-fitting with Forsythe orthogonal polynomials (Formenti and Richardson 2002), which is provided in DIAMOND. Six modes could be identified in all of the five states with confidence, and the natural frequencies are listed in Table 3-5 together with the changes of the frequencies as compared to the undamaged state. From the table, it can be seen that nearly all of the frequencies decrease continuously with increase of damage severity.

Table 3-5: Measured Frequencies in the Different States

Modes	Undamaged State	Damaged States							
	Case 0	Case 1		Case 2		Case 3		Case 4	
	Freq. (Hz)	Freq. (Hz)	Diff. (%)	Freq. (Hz)	Diff. (%)	Freq. (Hz)	Diff. (%)	Freq. (Hz)	Diff. (%)
1	3.499	3.438	-1.75%	3.500	0.02%	3.426	-2.09%	3.422	-2.22%
2	21.848	21.851	0.01%	21.518	-1.51%	21.497	-1.61%	21.201	-2.96%
3	60.290	60.280	-0.02%	59.580	-1.18%	59.668	-1.03%	59.003	-2.13%
4	118.819	118.685	-0.11%	117.399	-1.20%	116.817	-1.69%	116.611	-1.86%
5	194.708	193.715	-0.51%	190.254	-2.29%	188.426	-3.23%	187.289	-3.81%
6	306.107	304.317	-0.58%	299.233	-2.25%	295.669	-3.41%	294.385	-3.83%

The mode shapes were normalized with respect to the mass matrix using the Modal Scale Factor (Allemang 2003), and the results are illustrated in Figure 3-15. Mode shapes in the damaged states do not differentiate much from the undamaged ones by visual inspection. The variations of MAC values can reflect the change of mode shapes, and they will be given in the later chapters where model updating approaches are employed to identify the damage.

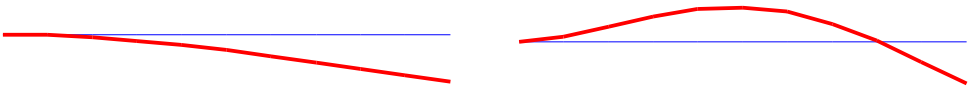

Mode 1 Mode 2

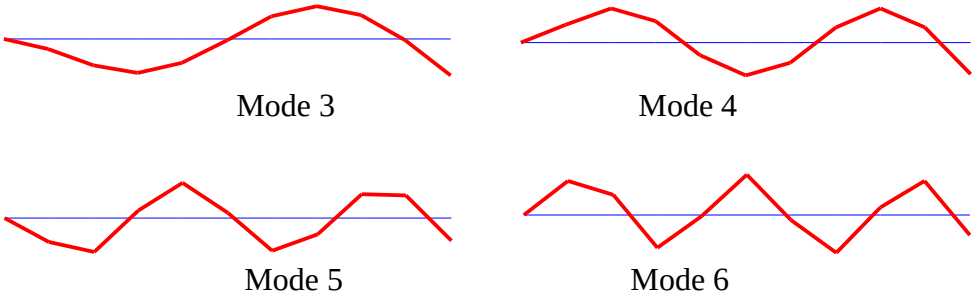

(a) Case 0

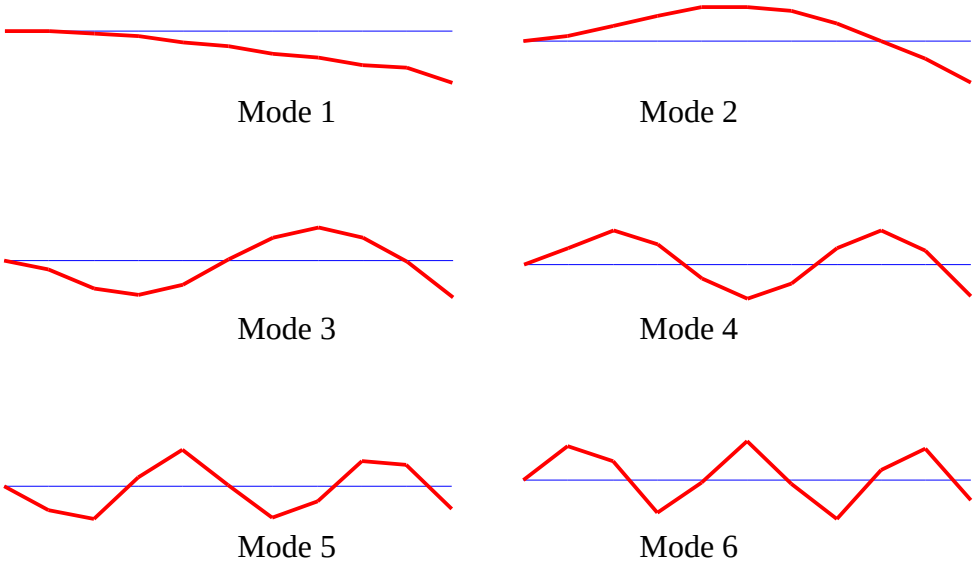

(b) Case 1

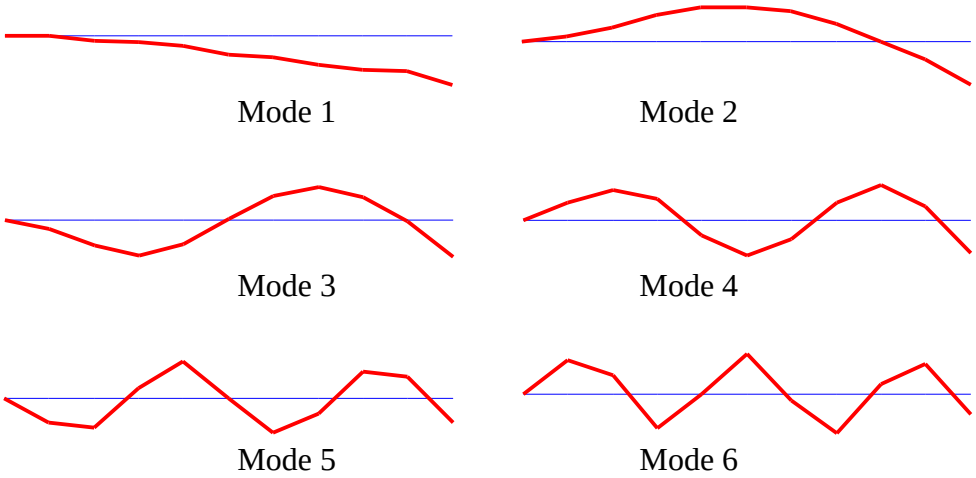

(c) Case 2

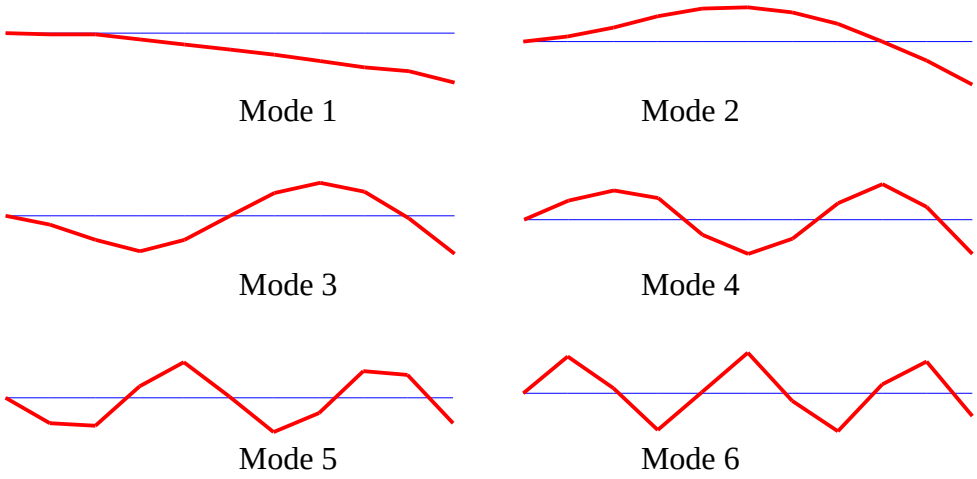

(d) Case 3

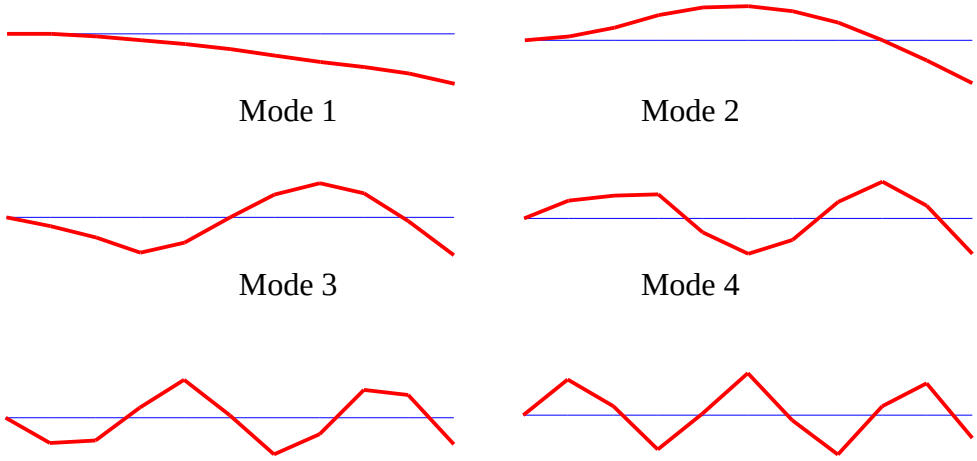

(e) Case 4

Figure 3-15: Measured Mode Shapes in Different Configurations

3.3.3 A Frame Structure

The second laboratory example is a steel frame structure as shown in Figure 3-16. To model the fixed boundary condition, the bottoms of the columns were welded onto a thick plate (size of 700 mm × 150 mm × 30 mm), which was fixed on the strong floor as shown in Figure 3-17. The vibration testing was carried out first in the undamaged states, and subsequently, two damage configurations were introduced.

The cross section of the beam is 50.0 × 8.8 mm^2, and the columns 50.0 × 4.4 mm^2. The mass density was measured as 7.67 × 10^3 kg/m^3. The detailed dimension of the frame is given in Figure 3-18. Since the real structures in civil engineering usually possess low-frequency modes, six steel blocks with each 1.0 kg weight were glued on the bottom of the beam to decrease the natural frequencies of this laboratory model.

Figure 3-16: Overview of the Frame Structure

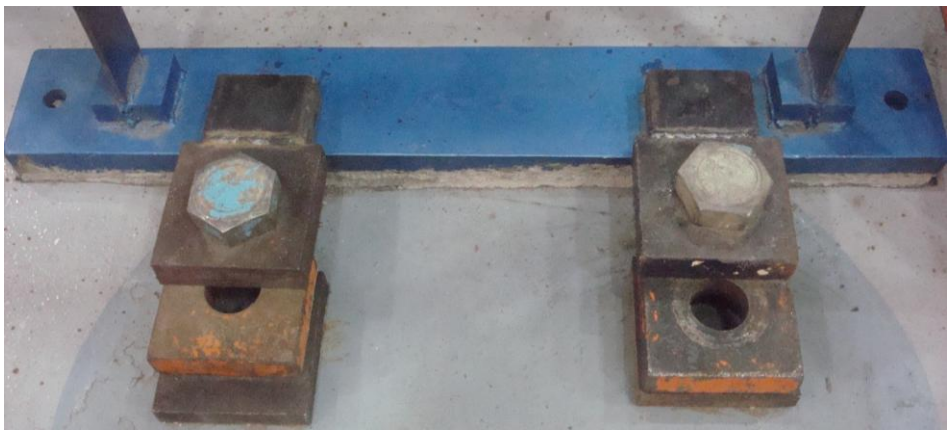

Figure 3-17: Support of the Frame Structure

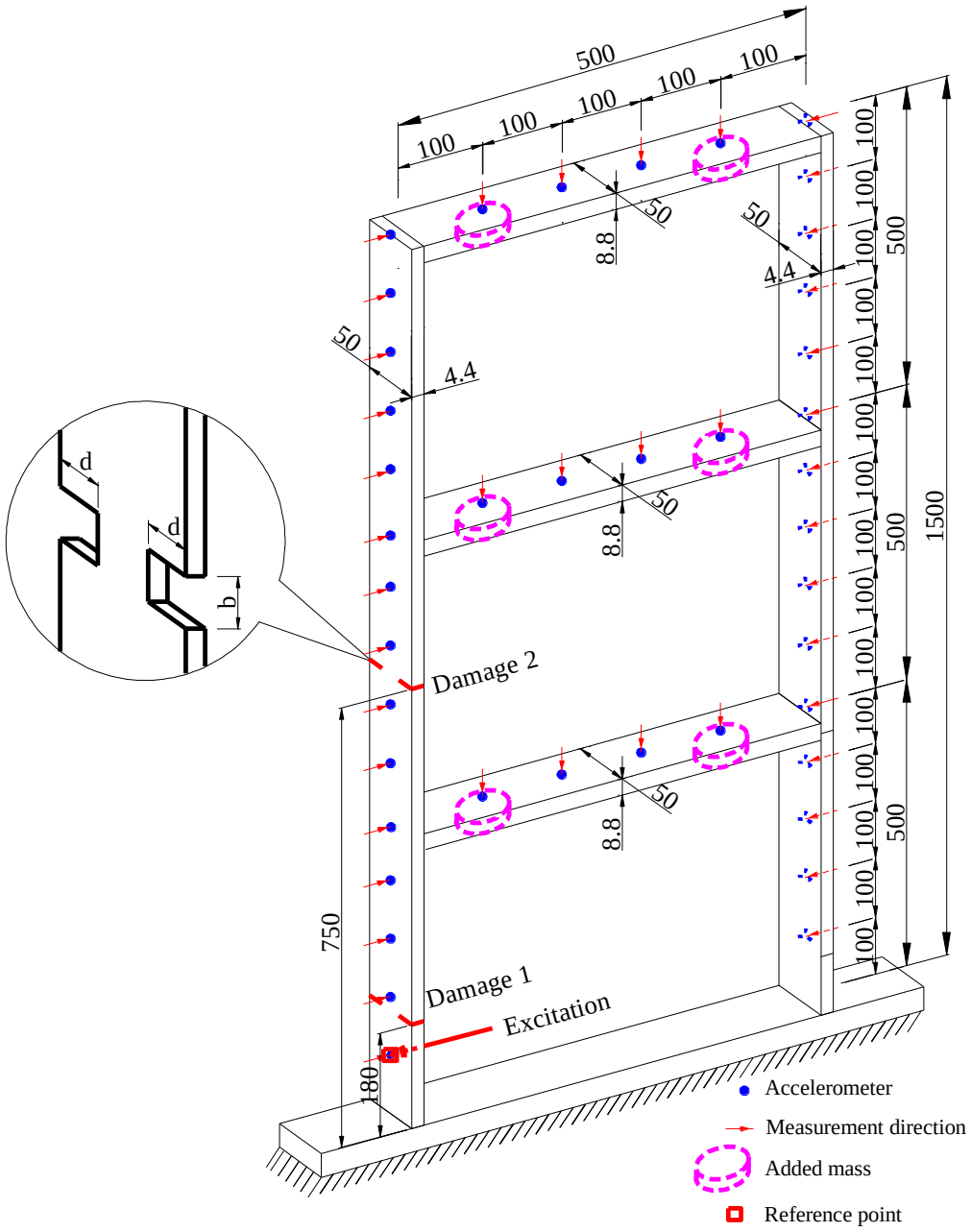

Figure 3-18: Configuration of the Frame Structure (Unit: mm)

A vibration testing was performed in the undamaged state first. The sampling frequency was set to 2000 Hz. To identify the mass-normalized mode shapes, the specimen was excited with the instrumented hammer at the reference point indicated in Figure 3-18, and the response at the excitation point was also recorded by an accelerometer (Schwarz and Richardson 2003).

The frame was impacted three times to average the signals, with each impact lasting

30 seconds. The acceleration responses were recorded at the points and directions denoted in Figure 3-18. The recorded input and output time history were analyzed with DIAMOND software to derive the auto-power spectral density, FRF function and coherence function where the typical curves are displayed in Figures 3-19 ~ 3-23.

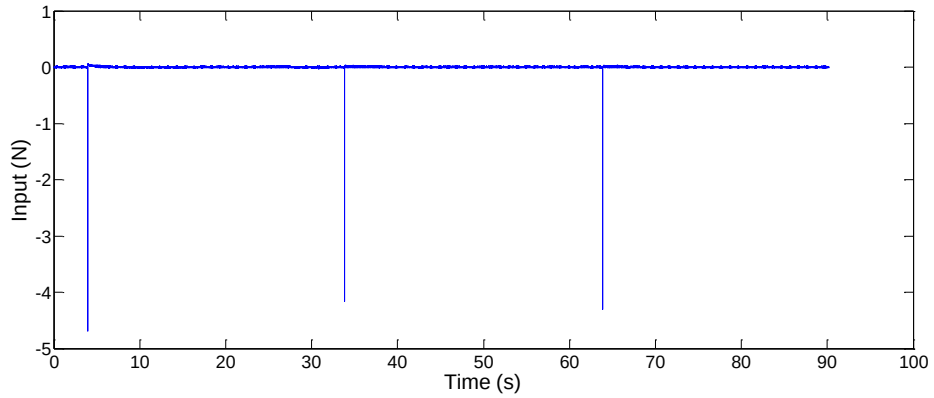

Figure 3-19: Input Force Time History

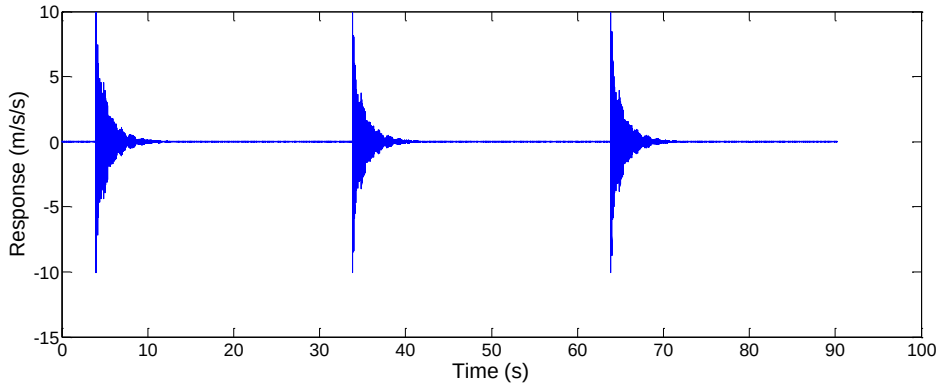

Figure 3-20: Recorded Acceleration Time History

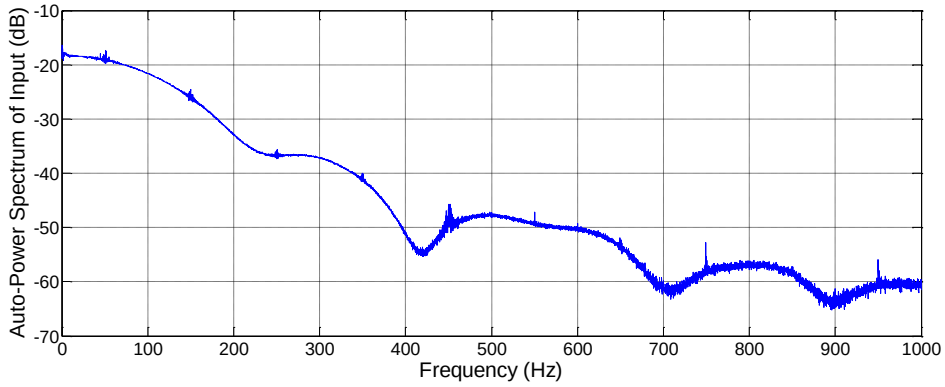

Figure 3-21: Auto-power Spectral Density of the Input Force

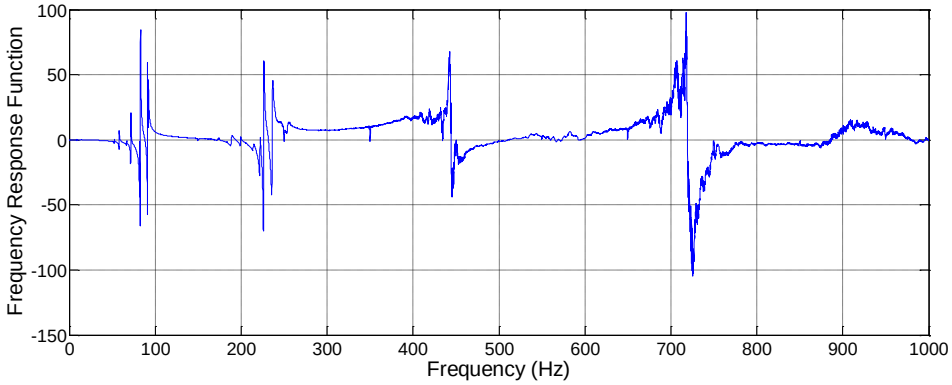

Figure 3-22: Magnitude of Frequency Response Function

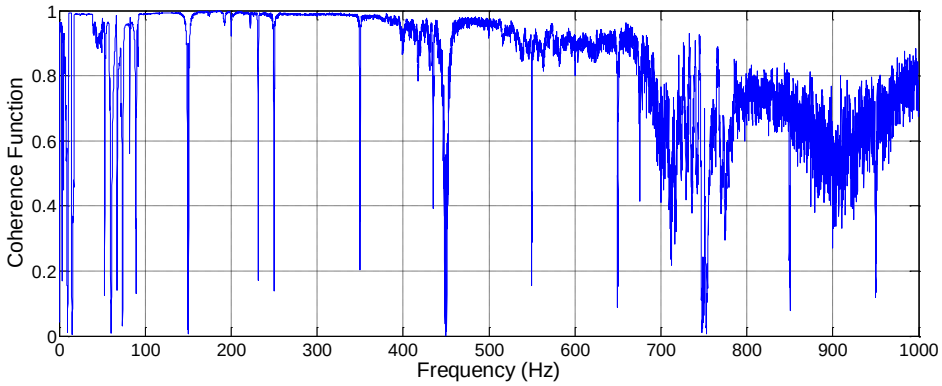

Figure 3-23: Coherence Function

Due to limitation of accelerometers, the accelerometers were moved along the frame to obtain the complete mode shapes of the whole structure. In all groups of tests, one accelerometer located at the reference point in Figure 3-18 kept unaltered as reference when the others moved. Subsequently, the first 14 frequencies and mass-normalized mode shapes are extracted with confidence as shown in Figure 3-24.

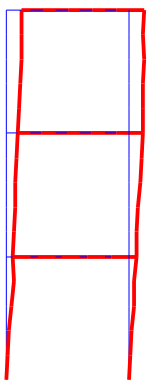

Mode 1 (3.12 Hz)

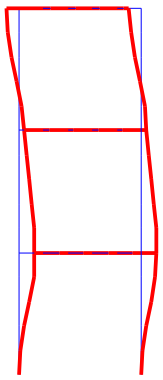

Mode 2 (9.11 Hz)

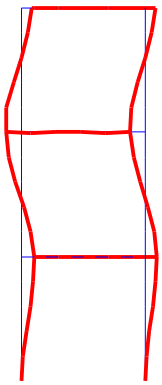

Mode 3 (14.34 Hz)

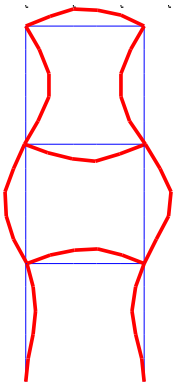

Mode 4 (52.46 Hz)

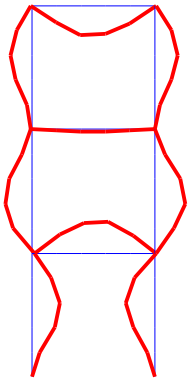

Mode 5 (58.18 Hz)

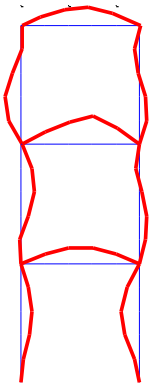

Mode 6 (66.80 Hz)

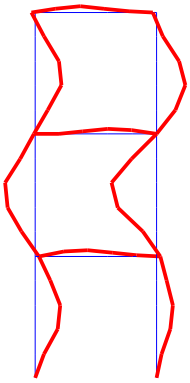

Mode 7 (71.65 Hz)

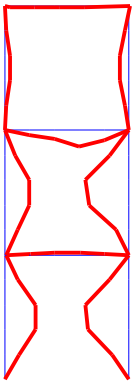

Mode 8 (82.14 Hz)

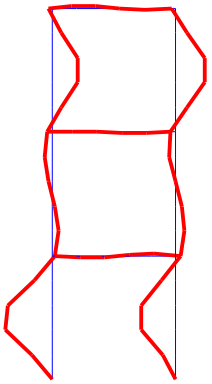

Mode 9 (82.87 Hz)

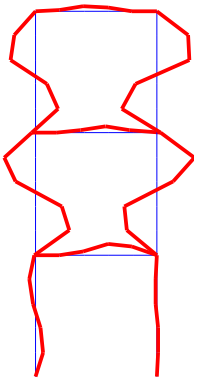

Mode 10 (200.13 Hz)

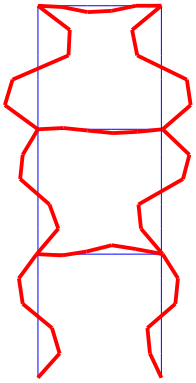

Mode 11 (222.36 Hz)

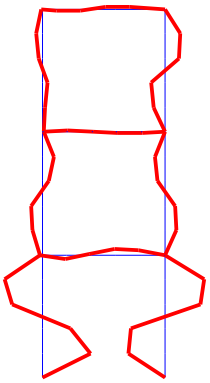

Mode 12 (226.55 Hz)

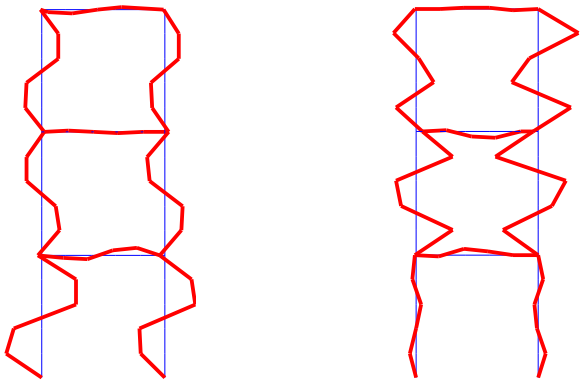

Mode 13 (236.58 Hz) Mode 14 (383.33 Hz)

Figure 3-24: Frequencies and Mode Shapes of the Frame Structure

Next, two damage configurations were introduced in the frame specimen. In the first case, the column of the first storey was cut at 180 mm away from the support as shown in Figure 3-18. The width of the cut is b = 10mm, and the depth d = 15mm. Afterwards, the second storey was cut at 750 mm from the support with a width b = 10mm and depth d = 15mm. The frame was tested again, and the sampling frequencies, impact points, impact times, and the duration of data recording were the same as those in the undamaged state. The input and the responses were picked up at the same points and directions as well. The damages cause little change in mode shapes, which can not be differentiated by visual inspection and not shown herein. The MAC values of mode shapes will be given in later chapters for model updating purpose.

3.3.4 The Balla Balla River Bridge

The Balla Balla River Bridge, as shown in Figure 3-25, is a three-span continuous reinforced concrete bridge located on Coastal Highway over the Balla Balla River in the Shire of Roebourne. An FE model based on design drawings has been established by Xia *et al.* (2008). The FE model of this bridge has 907 elements, 947 nodes each has six DOFs, and 5420 DOFs in total, as shown in Figure 3-26. The elements used in the model are listed in Table 3-6.

Figure 3-25: General view of Balla Balla River Bridge

Table 3-6: Elements of the FE Model of Balla Balla River Bridge

Bridge component	Element type	Quantity
Bearing	Beam	56
Slab	Shell	288
Girder	Shell	252
Stirrup	Beam	231
Diaphragm	Shell	80
Total		907

In the field vibration testing (Xia *et al*. 2008), the instrumented DYTRAN 5803A sledge hammer (12 LB, 1.0 mV/LbF, with 4 additional tips) was used to excite the bridge structure, and Kistler accelerometers model 8330A2.5 and 8330A3 were used to collect the test data. The accelerometers were placed in seven rows corresponding to the seven girders. There are 19 measurement points in each row and 133 in total as shown in Figure 3-27. Ten pairs of natural frequencies and mode shapes were extracted from the FRFs by the Rational Fraction Polynomial method, and are illustrated in Figure 3-28.

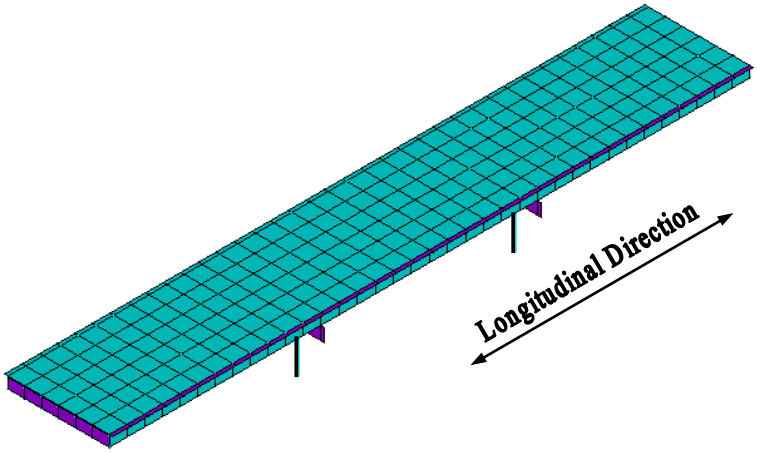

Figure 3-26: FE Model of the Balla Balla River Bridge

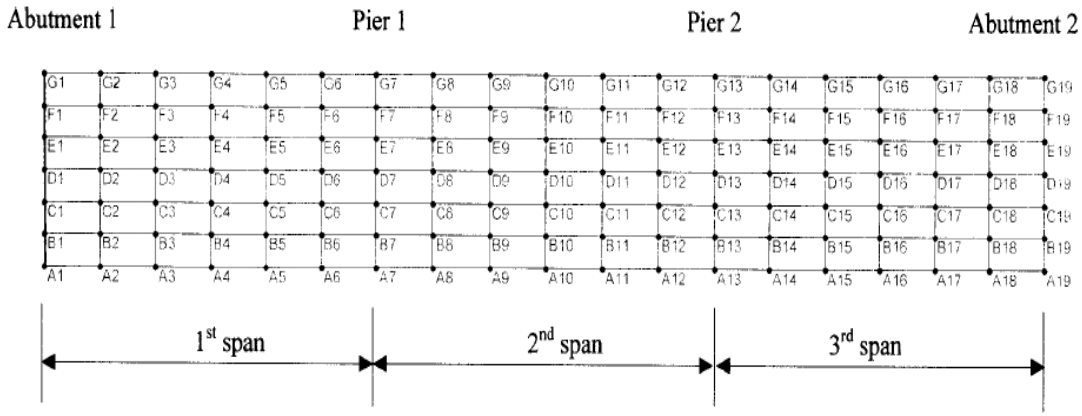

Figure 3-27: Locations of Sensors

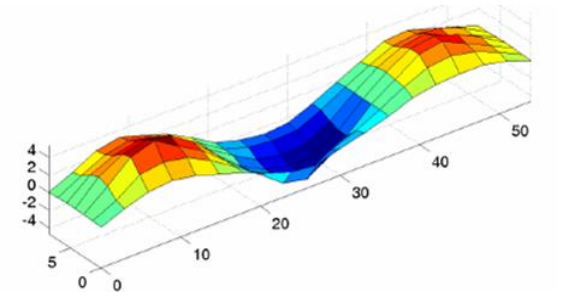

Mode 1:
Freq = 6.7629 Hz Damping = 1.0645 %

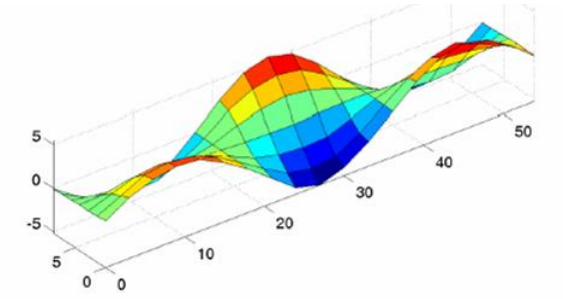

Mode 2:
Freq = 7.9483 Hz Damping = 1.0128 %

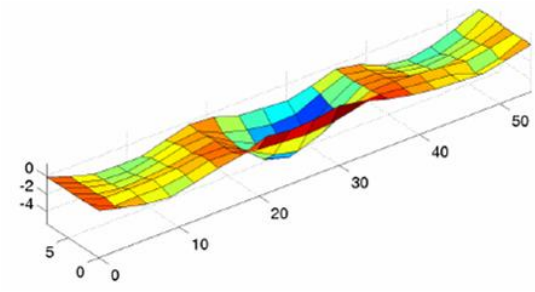

Mode 3:

Freq = 10.0572 Hz Damping = 1.9862 %

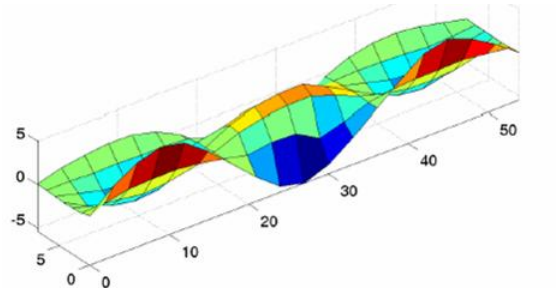

Mode 4:

Freq = 10.7510 Hz Damping = 1.0840 %

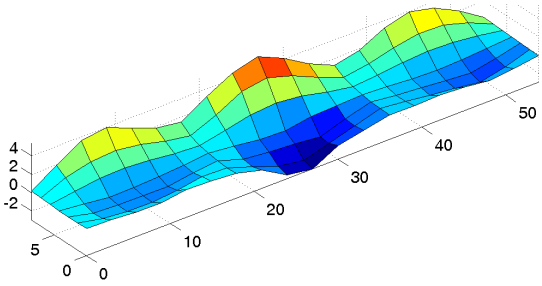

Mode 5:

Freq = 11.0323 Hz Damping = 1.0817 %

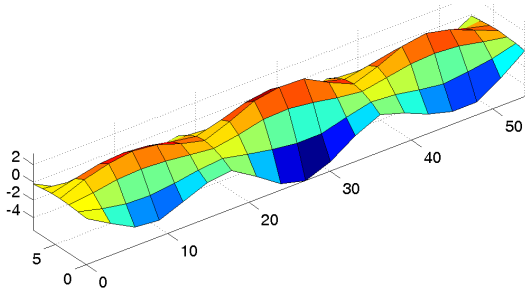

Mode 6:

Freq = 12.6418 Hz Damping = 0.8752 %

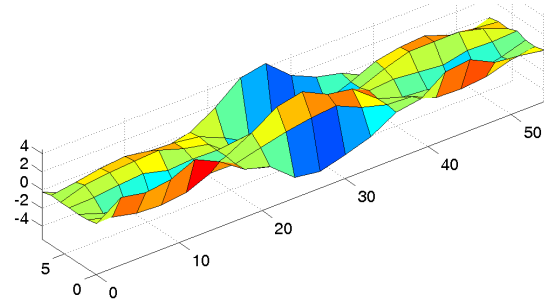

Mode 7:

Freq = 14.7137 Hz Damping = 1.3474 %

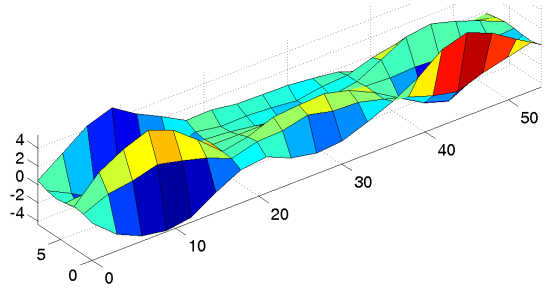

Mode 8:

Freq = 15.7606 Hz Damping = 0.8596 %

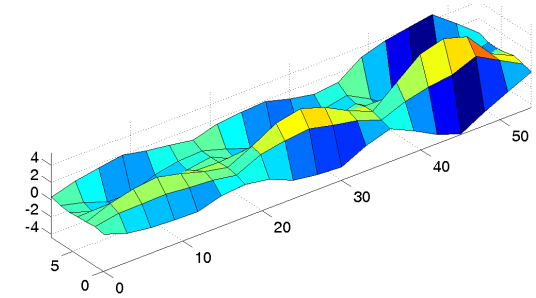

Mode 9:

Freq = 16.3876 Hz Damping = 0.7797 %

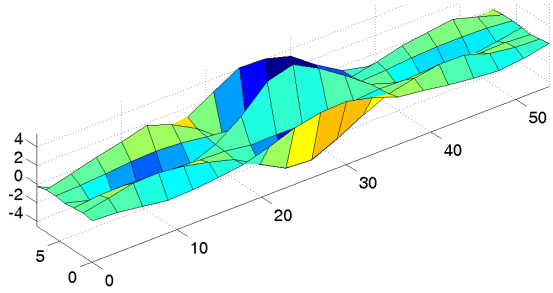

Mode 10:

Freq = 20.1832 Hz Damping = 0.9794 %

Figure 3-28: Measured Frequencies and Mode Shapes of the Balla Balla River Bridge

CHAPTER FOUR

EIGENSOLUTIONS WITH SUBSTRUCTURING METHOD

4.1 Introduction

In the FE model updating field, eigensolutions of an analytical model serve to construct the objective function. The elemental parameters in the FE model are iteratively modified, so that the modal properties (such as frequencies and mode shapes) match the measured counterparts in an optimal way. To achieve this, the eigensolutions of the analytical model need to be calculated repeatedly.

The analytical model of a large-scale structure consists of a large number of elements and nodes to simulate the real structure accurately. Efficiently obtaining the eigensolutions from the large size model is a big challenge. Algorithms that have been developed for the eigensolutions of large-scale structures include the sparse matrix techniques, order reduction methods, and substructuring methods. Sparse matrix techniques exploit the sparsity of the assembled mass and stiffness matrices and perform numerical operations directly on the large-size system matrices mathematically, such as the Lanczos algorithm or Subspace Iteration method (Bath 1982). They are widely used in enormous commercial software such as ABAQUS and ANSYS. Order reduction methods reduce the size of the system matrices by removing some DOFs of the original FE model and retaining a much smaller set. Then the reduced eigenequation is solved to approximate the eigensolutions of the

original structure. Guyan reduction (Guyan 1965), IRS method (Friswell 1997), and IOR method (Xia and Lin 2004) are typical ones in this category. Substructuring methods divide a structure into smaller independent substructures, and the eigensolutions of the original structure are recovered from the eigenproperties of the independent substructures by constraining on the interface of the adjacent substructures (Klerk *et al.* 2008). The substructuring methods possess some benefits for the model updating process. In particular, using the substructuring methods, the optimization process handles one or several substructures only instead of the global structure, and thus improves the computational efficiency significantly. The substructuring method is studied in this research. Calculation of eigensolutions with the substructuring method is presented in this chapter first.

Mackenzie (1974) showed that the in-core requirements and operational counts of Kron's substructuring method were very competitive, comparing with other substructuring methods. The disadvantage of Kron's method is that the complete eigensolutions of all substructures are required to obtain the eigensolutions of the global structure, which is time consuming for a large-scale structure. To improve this computational inefficiency, a modal truncation approximation is proposed, in which only the lowest eigensolutions of the substructures need to be calculated. The discarded higher eigensolutions are compensated by the first-order residual flexibility or the second-order residual flexibility. The division of substructures and the selection of master modes in each substructure are also studied.

4.2 Kron's Substructuring Method for Eigensolutions

Calculation of eigensolutions with the substructuring method consists of three basic

steps: division of a global structure into substructures, calculation of the eigensolutions for the independent substructures, and reconnection of the substructures to the global structure with compatibility equations. In this section, the Kron's substructuring method will be presented first for completeness.

A generalized eigenvalue problem for the *N* DOFs structure has the form of

$$\mathbf{K}\{\phi_i\} = \lambda_i \mathbf{M}\{\phi_i\} \tag{4-1}$$

where **K** and **M** are $N \times N$ stiffness and mass matrices, respectively, λ_i is the *i*th eigenvalue, and $\{\phi_i\}$ represents the corresponding eigenvector.

The global structure is divided into N_S independent substructures, and each substructure has $N^{(j)}$ DOFs ($j = 1, 2, \ldots, N_S$). This division procedure produces N^T interface DOFs. Each interface DOF in the original global structure is shared by two or more substructures that are connected to it. The total number of DOFs of all substructures increases to N^P, which is larger than *N*. For example, if the *n*th ($n = 1, 2, \ldots, N^T$) interface DOF is shared by t_n substructures, it has

$$N^P = N + \sum_{n=1}^{N^T} (t_n - 1) = \sum_{j=1}^{N_S} N^{(j)} \tag{4-2}$$

As an independent structure, each substructure has the stiffness matrix $\mathbf{K}^{(j)}$ and mass matrix $\mathbf{M}^{(j)}$. The generalized eigenequation of the *j*th substructure can be written as

$$\mathbf{K}^{(j)} \left\{\phi_i^{(j)}\right\} = \lambda_i^{(j)} \mathbf{M}^{(j)} \left\{\phi_i^{(j)}\right\} \tag{4-3}$$

Both $\mathbf{K}^{(j)}$ and $\mathbf{M}^{(j)}$ are of order $N^{(j)} \times N^{(j)}$. $\lambda_i^{(j)}$ and $\left\{\phi_i^{(j)}\right\}$ are the *i*th eigenvalue and eigenvector of the *j*th substructure, respectively. Eq. (4-3) yields $N^{(j)}$

pairs of eigenvalues and eigenvectors as

$$\mathbf{\Lambda}^{(j)} = \mathrm{Diag}\left[\lambda_1^{(j)}, \lambda_2^{(j)}, ..., \lambda_{N^{(j)}}^{(j)}\right], \quad \mathbf{\Phi}^{(j)} = \left[\phi_1^{(j)}, \phi_2^{(j)}, ..., \phi_{N^{(j)}}^{(j)}\right] \tag{4-4}$$

Mass normalization of the eigenpairs leads to

$$\begin{cases} \left[\mathbf{\Phi}^{(j)}\right]^T \mathbf{M}^{(j)} \mathbf{\Phi}^{(j)} = \mathbf{I}_{N^{(j)}} \\ \left[\mathbf{\Phi}^{(j)}\right]^T \mathbf{K}^{(j)} \mathbf{\Phi}^{(j)} = \mathbf{\Lambda}^{(j)} \end{cases} \tag{4-5}$$

Diagonally assembling the submatrices to the primitive form gives

$$\mathbf{M}^p = \mathrm{Diag}\left[\mathbf{M}^{(1)}, \mathbf{M}^{(2)}, ..., \mathbf{M}^{(N_S)}\right], \quad \mathbf{K}^p = \mathrm{Diag}\left[\mathbf{K}^{(1)}, \mathbf{K}^{(2)}, ..., \mathbf{K}^{(N_S)}\right]$$

$$\mathbf{\Phi}^p = \mathrm{Diag}\left[\mathbf{\Phi}^{(1)}, \mathbf{\Phi}^{(2)}, ..., \mathbf{\Phi}^{(N_S)}\right], \quad \mathbf{\Lambda}^p = \mathrm{Diag}\left[\mathbf{\Lambda}^{(1)}, \mathbf{\Lambda}^{(2)}, ..., \mathbf{\Lambda}^{(N_S)}\right] \tag{4-6}$$

where superscript '*p*' denotes the variables associated with the primitive form, and the size of the above matrices is $N^P \times N^P$. Due to the orthogonality conditions in Eq. (4-5), it follows that,

$$\begin{cases} \left[\mathbf{\Phi}^p\right]^T \mathbf{M}^p \mathbf{\Phi}^p = \mathbf{I}_{N^P} \\ \left[\mathbf{\Phi}^p\right]^T \mathbf{K}^p \mathbf{\Phi}^p = \mathbf{\Lambda}^p \end{cases} \tag{4-7}$$

Reconnection of the primitive system can be performed by considering the geometric compatibility and force equilibrium at the interface points of the adjacent substructures.

If $\{x\}$ is the displacement vector of the original global structure with the size of $N \times 1$, it is expanded to $\{\bar{x}\}$ with the size of $N^P \times 1$ after substructuring, which includes identical displacements in the interface DOFs. The geometric compatibility is sufficed by applying displacement constraints as

$$\mathbf{C}\{\bar{x}\} = \mathbf{0} \tag{4-8}$$

where **C** is a rectangular matrix containing the general implicit constraints that ensure

the nodes at the interfaces have identical displacements. In matrix **C**, each row contains two non-zero elements. For rigid connections, the two elements are 1 and -1, respectively. If the connected points x_1 and x_2 are not rigidly connected, which have the relation $x_1 = ax_2$, the two non-zero elements are 1 and $-a$. Kron's method considers the connection condition by matrix **C**, instead of adding more items such as the constraint modes or linking force (Hurty 1965; MacNeal 1971).

With the virtual work theorem, the motion equation of the undamped structure is

$$\mathbf{M}^p \left\{\ddot{\bar{x}}\right\} + \mathbf{K}^p \left\{\bar{x}\right\} = \left\{ f_{\text{ext}} \right\} + \left\{ f_{\text{con}} \right\} \tag{4-9}$$

where $\left\{\ddot{\bar{x}}\right\}$ and $\left\{\bar{x}\right\}$ are the acceleration and displacement vectors of the substructures, $\left\{ f_{\text{ext}} \right\}$ is the external force, and $\left\{ f_{\text{con}} \right\}$ is the connection force from the adjacent substructures. For a free vibration system, $\left\{ f_{\text{ext}} \right\} = 0$, and the virtual work done by the connection force along $\{\bar{x}\}$ is

$$\delta \mathbf{W} = \left\{ f_{\text{con}}^T \right\} \{\delta \bar{x}\} \tag{4-10}$$

Considering the connection process to be incomplete, the compatibility is violated at the interface coordinates by an amount of $\{\eta\}$. Eq. (4-8) becomes

$$\mathbf{C}\{\bar{x}\} = \{\eta\} \tag{4-11}$$

In the interface coordinates, there is an associated force vector $\{\tau\}$, representing the internal connection forces due to the 'misfit'. Eq. (4-11) gives

$$\delta \mathbf{W} = \{\tau\}^T \{\delta\eta\} = \{\tau\}^T \mathbf{C}\{\delta \bar{x}\} \tag{4-12}$$

From Eq. (4-10) and Eq. (4-12), one can obtain

$$\left\{ f_{\text{con}}^T \right\} \{\delta \bar{x}\} = \{\tau\}^T \mathbf{C}\{\delta \bar{x}\} \tag{4-13}$$

and thus

$$\{f_{\text{con}}\} = \mathbf{C}^T \{\tau\} \tag{4-14}$$

Consequently, Eq. (4-9) is transformed into

$$\begin{bmatrix} \mathbf{M}^p & \mathbf{0} \\ \mathbf{0} & \mathbf{0} \end{bmatrix} \begin{Bmatrix} \ddot{\bar{x}} \\ \ddot{\tau} \end{Bmatrix} + \begin{bmatrix} \mathbf{K}^p & -\mathbf{C}^T \\ -\mathbf{C} & \mathbf{0} \end{bmatrix} \begin{Bmatrix} \bar{x} \\ \tau \end{Bmatrix} = \begin{Bmatrix} \mathbf{0} \\ \mathbf{0} \end{Bmatrix} \tag{4-15}$$

Assuming the oscillatory solution $\{\bar{x}, \tau\}^T = \{\bar{\phi}, \tau\}^T \exp\left(j\sqrt{\bar{\lambda}}t\right)$, the expanded mode shape of the global structure can be related to the primitive form of the mode shapes $\mathbf{\Phi}^p$ via the modal coordinates **z** as

$$\begin{Bmatrix} \bar{\phi} \\ \tau \end{Bmatrix} = \begin{bmatrix} \mathbf{\Phi}^p & \mathbf{0} \\ \mathbf{0} & \mathbf{I} \end{bmatrix} \begin{Bmatrix} \mathbf{z} \\ \tau \end{Bmatrix} \tag{4-16}$$

where $\bar{\phi}$ is the expanded mode shape of the global structure including the identical values in the interface DOFs. Considering the orthogonality relations in Eq. (4-5), Eq. (4-15) can be transformed into the canonical form (Sehmi 1989)

$$\begin{bmatrix} \mathbf{\Lambda}^p - \bar{\lambda}\mathbf{I} & -\mathbf{\Gamma} \\ -\mathbf{\Gamma}^T & \mathbf{0} \end{bmatrix} \begin{Bmatrix} \mathbf{z} \\ \tau \end{Bmatrix} = \begin{Bmatrix} \mathbf{0} \\ \mathbf{0} \end{Bmatrix} \tag{4-17}$$

where $\mathbf{\Gamma} = \left(\mathbf{C}\mathbf{\Phi}^p\right)^T$ is referred to as the normal connection matrix. Using the above procedure, the nodes at the interface points of the adjacent substructures are constrained to move jointly. Therefore, the eigenvalue $\bar{\lambda}$ obtained from Eq. (4-17) is equal to the eigenvalue λ of the original global structure. As $\bar{\mathbf{\Phi}}$ consists of the expanded eigenvectors $\bar{\phi}$, the eigenvectors of the global structure $\mathbf{\Phi}$ can be obtained after discarding the identical DOFs in $\bar{\mathbf{\Phi}}$. $\mathbf{\Gamma}$ has the order of $N^P \times \left(N^P - N\right)$, where $\left(N^P - N\right)$ is the number of constraint relations and much smaller than N^P.

The first line of Eq. (4-17) gives

$$\mathbf{z} = \left(\mathbf{\Lambda}^p - \bar{\lambda}\mathbf{I}\right)^{-1} \mathbf{\Gamma}\tau \tag{4-18}$$

Substituting Eq. (4-18) into the second line of Eq. (4-17) to eliminate the modal coordinates **z**, one has

$$\mathbf{\Gamma}^T \left(\mathbf{\Lambda}^p - \bar{\lambda}\mathbf{I}\right)^{-1} \mathbf{\Gamma}\tau = 0 \quad \text{or} \quad \mathbf{E}\tau = 0 \tag{4-19}$$

where $\mathbf{E} = \mathbf{\Gamma}^T\mathbf{D}\mathbf{\Gamma}$ and $\mathbf{D} = \left(\mathbf{\Lambda}^p - \bar{\lambda}\mathbf{I}\right)^{-1}$.

Matrix **E** with the size of $\left(N^P - N\right) \times \left(N^P - N\right)$, is known as the *Kron matrix* or *receptance matrix*. Since the above analysis has no approximation in the derivation of **E**, the obtained eigenvalues are exactly those of the original global structure.

4.3 First-order Residual Flexibility Based Modal Truncation

In the original Kron's method, $\bar{\lambda}$ is obtained by scanning the determinant of matrix **E** (Simpson 1974). Obviously, this is very time-consuming as **E** is dependent on the unknown item $\bar{\lambda}$. Sehmi (1986; 1989) applied numerical approaches (Subspace Iteration method and Lanczos method) to Kron's substructuring method, and estimated the eigensolutions more efficiently. Nevertheless, it is onerous to calculate the complete eigensolutions of each substructure to assemble $\mathbf{\Lambda}^p$ and $\mathbf{\Phi}^p$. Moreover, the final eigenequation for searching the eigensolutions has the size of $N^P \times N^P$, which will be very large for large-scale structures.

To overcome this difficulty, the present research will improve the efficiency of Kron's substructuring method by introducing a modal truncation technique. This is based on the fact that the higher modes have little contribution to the receptance matrix. In

consequence, only some lowest modes are retained in the substructures, while the higher modes are discarded and compensated with the first-order residual flexibility.

4.3.1 Method Description

In each substructure, the first few eigensolutions, corresponding to the lower vibration modes, are selected as the 'master' modes. The residual higher modes are treated as the 'slave' modes. Similar to the model reduction technique, the master modes are retained while the slave modes are discarded in the later calculations. Hereinafter, subscript '*m*' and '*s*' will represent the 'master' and 'slave' variables, respectively.

Assuming that the first $N_m^{(j)}$ (j = 1, 2, …, N_S) modes in the *j*th substructure are chosen as the 'master' modes while the residual $N_s^{(j)}$ higher modes are the 'slave' modes, the *j*th substructure has the 'master' eigenpairs and 'slave' eigenpairs as

$$\boldsymbol{\Lambda}_m^{(j)} = \mathrm{Diag}\left[\lambda_1^{(j)}, \lambda_2^{(j)}, ..., \lambda_{N_m^{(j)}}^{(j)}\right], \quad \boldsymbol{\Phi}_m^{(j)} = \left[\boldsymbol{\phi}_1^{(j)}, \boldsymbol{\phi}_2^{(j)}, ..., \boldsymbol{\phi}_{N_m^{(j)}}^{(j)}\right],$$

$$\boldsymbol{\Lambda}_s^{(j)} = \mathrm{Diag}\left[\lambda_{N_m^{(j)}+1}^{(j)}, \lambda_{N_m^{(j)}+2}^{(j)}, ..., \lambda_{N_m^{(j)}+N_s^{(j)}}^{(j)}\right], \quad \boldsymbol{\Phi}_s^{(j)} = \left[\boldsymbol{\phi}_{N_m^{(j)}+1}^{(j)}, \boldsymbol{\phi}_{N_m^{(j)}+2}^{(j)}, ..., \boldsymbol{\phi}_{N_m^{(j)}+N_s^{(j)}}^{(j)}\right],$$

$$N_m^p = \sum_{j=1}^{N_S} N_m^{(j)}, \quad N_s^p = \sum_{j=1}^{N_S} N_s^{(j)}, \quad N_m^{(j)} + N_s^{(j)} = N^{(j)} \quad (j = 1, 2, ..., N_S) \qquad (4\text{-}20)$$

Assembling all 'master' eigenpairs and 'slave' eigenpairs, respectively, one has

$$\boldsymbol{\Lambda}_m^p = \mathrm{Diag}\left[\boldsymbol{\Lambda}_m^{(1)}, \boldsymbol{\Lambda}_m^{(2)}, ..., \boldsymbol{\Lambda}_m^{(N_S)}\right], \quad \boldsymbol{\Phi}_m^p = \mathrm{Diag}\left[\boldsymbol{\Phi}_m^{(1)}, \boldsymbol{\Phi}_m^{(2)}, ..., \boldsymbol{\Phi}_m^{(N_S)}\right]$$

$$\boldsymbol{\Lambda}_s^p = \mathrm{Diag}\left[\boldsymbol{\Lambda}_s^{(1)}, \boldsymbol{\Lambda}_s^{(2)}, ..., \boldsymbol{\Lambda}_s^{(N_S)}\right], \quad \boldsymbol{\Phi}_s^p = \mathrm{Diag}\left[\boldsymbol{\Phi}_s^{(1)}, \boldsymbol{\Phi}_s^{(2)}, ..., \boldsymbol{\Phi}_s^{(N_S)}\right] \qquad (4\text{-}21)$$

Denoting $\boldsymbol{\Gamma}_m = \left[\mathbf{C}\boldsymbol{\Phi}_m^p\right]^T$ and $\boldsymbol{\Gamma}_s = \left[\mathbf{C}\boldsymbol{\Phi}_s^p\right]^T$, Eq. (4-17) can be expanded as

$$\begin{bmatrix} \boldsymbol{\Lambda}_m^p - \bar{\lambda}\mathbf{I} & \mathbf{0} & -\boldsymbol{\Gamma}_m \\ \mathbf{0} & \boldsymbol{\Lambda}_s^p - \bar{\lambda}\mathbf{I} & -\boldsymbol{\Gamma}_s \\ -\boldsymbol{\Gamma}_m^T & -\boldsymbol{\Gamma}_s^T & \mathbf{0} \end{bmatrix} \begin{Bmatrix} \mathbf{z}_m \\ \mathbf{z}_s \\ \tau \end{Bmatrix} = \begin{Bmatrix} \mathbf{0} \\ \mathbf{0} \\ \mathbf{0} \end{Bmatrix} \qquad (4\text{-}22)$$

The second line of Eq. (4-22) gives

$$\{\mathbf{z}_s\} = \left(\mathbf{\Lambda}_s^p - \bar{\lambda}\mathbf{I}\right)^{-1} \mathbf{\Gamma}_s \{\tau\} = \mathbf{t}\{\tau\} \tag{4-23}$$

where $\mathbf{t} = \left(\mathbf{\Lambda}_s^p - \bar{\lambda}\mathbf{I}\right)^{-1} \mathbf{\Gamma}_s$.

The full eigenvector of Eq. (4-22) can be expressed as

$$\begin{Bmatrix} \mathbf{z}_m \\ \mathbf{z}_s \\ \tau \end{Bmatrix} = \begin{bmatrix} \mathbf{I} & 0 \\ 0 & \mathbf{t} \\ 0 & \mathbf{I} \end{bmatrix} \begin{Bmatrix} \mathbf{z}_m \\ \tau \end{Bmatrix} = \mathbf{T}_1 \begin{Bmatrix} \mathbf{z}_m \\ \tau \end{Bmatrix} \tag{4-24}$$

Substituting Eq. (4-24) into Eq. (4-22) and pre-multiplying $\mathbf{T}_1$ on both sides of Eq. (4-22), the full-dimension eigenequation is reduced into

$$\begin{bmatrix} \mathbf{\Lambda}_m^p - \bar{\lambda}\mathbf{I} & -\mathbf{\Gamma}_m \\ -\mathbf{\Gamma}_m^T & -\mathbf{\Gamma}_s^T \left(\mathbf{\Lambda}_s^p - \bar{\lambda}\mathbf{I}\right)^{-1} \mathbf{\Gamma}_s \end{bmatrix} \begin{Bmatrix} \mathbf{z}_m \\ \tau \end{Bmatrix} = \begin{Bmatrix} \mathbf{0} \\ \mathbf{0} \end{Bmatrix} \tag{4-25}$$

In Eq. (4-25), Taylor expansion of the nonlinear item $\left(\mathbf{\Lambda}_s^p - \bar{\lambda}\mathbf{I}\right)^{-1}$ introduces

$$\left(\mathbf{\Lambda}_s^p - \bar{\lambda}\mathbf{I}\right)^{-1} = \left(\mathbf{\Lambda}_s^p\right)^{-1} + \bar{\lambda}\left(\mathbf{\Lambda}_s^p\right)^{-2} + \bar{\lambda}^2\left(\mathbf{\Lambda}_s^p\right)^{-3} + \cdots \tag{4-26}$$

In general, the required eigenvalue $\bar{\lambda}$ corresponds to the lowest modes of the global structure, and is much smaller than the items in $\mathbf{\Lambda}_s^p$ when the master modes is chosen properly. In that case, by retaining only the first item of the Taylor expansion, Eq. (4-25) is approximated as

$$\begin{bmatrix} \mathbf{\Lambda}_m^p - \bar{\lambda}\mathbf{I} & -\mathbf{\Gamma}_m \\ -\mathbf{\Gamma}_m^T & -\mathbf{\Gamma}_s^T \left(\mathbf{\Lambda}_s^p\right)^{-1} \mathbf{\Gamma}_s \end{bmatrix} \begin{Bmatrix} \mathbf{z}_m \\ \tau \end{Bmatrix} = \begin{Bmatrix} \mathbf{0} \\ \mathbf{0} \end{Bmatrix} \tag{4-27}$$

Resolving τ from the second line of Eq. (4-27) and substituting it into the first line, one obtains

$$\left[\mathbf{\Lambda}_m^p + \mathbf{\Gamma}_m \left(\mathbf{\Gamma}_s^T \left(\mathbf{\Lambda}_s^p\right)^{-1} \mathbf{\Gamma}_s\right)^{-1} \mathbf{\Gamma}_m^T\right] \{\mathbf{z}_m\} = \bar{\lambda}\{\mathbf{z}_m\} \tag{4-28}$$

The final standard form of the eigenequation is thus expressed as

$$\boldsymbol{\Psi}\{\mathbf{z}_m\} = \bar{\lambda}\{\mathbf{z}_m\} \tag{4-29}$$

where $\boldsymbol{\Psi} = \boldsymbol{\Lambda}_m^p + \boldsymbol{\Gamma}_m \left(\boldsymbol{\Gamma}_s^T \left(\boldsymbol{\Lambda}_s^p \right)^{-1} \boldsymbol{\Gamma}_s \right)^{-1} \boldsymbol{\Gamma}_m^T$, $\boldsymbol{\Gamma}_s^T \left(\boldsymbol{\Lambda}_s^p \right)^{-1} \boldsymbol{\Gamma}_s = \mathbf{C}\boldsymbol{\Phi}_s^p \left(\boldsymbol{\Lambda}_s^p \right)^{-1} \left[\boldsymbol{\Phi}_s^p \right]^T \mathbf{C}^T$.

$\boldsymbol{\Phi}_s^p \left(\boldsymbol{\Lambda}_s^p \right)^{-1} \left[\boldsymbol{\Phi}_s^p \right]^T$ is regarded as the *first-order residual flexibility*, which can be acquired as

$$\begin{aligned}
&\boldsymbol{\Phi}_s^p \left(\boldsymbol{\Lambda}_s^p \right)^{-1} \left[\boldsymbol{\Phi}_s^p \right]^T \\
&= \begin{bmatrix} \boldsymbol{\Phi}_s^{(1)} & \mathbf{0} & \cdots & \mathbf{0} \\ \mathbf{0} & \boldsymbol{\Phi}_s^{(2)} & \cdots & \mathbf{0} \\ \vdots & \vdots & \ddots & \vdots \\ \mathbf{0} & \mathbf{0} & \cdots & \boldsymbol{\Phi}_s^{(N_S)} \end{bmatrix} \begin{bmatrix} \left(\boldsymbol{\Lambda}_s^{(1)} \right)^{-1} & \mathbf{0} & \cdots & \mathbf{0} \\ \mathbf{0} & \left(\boldsymbol{\Lambda}_s^{(2)} \right)^{-1} & \cdots & \mathbf{0} \\ \vdots & \vdots & \ddots & \vdots \\ \mathbf{0} & \mathbf{0} & \cdots & \left(\boldsymbol{\Lambda}_s^{(N_S)} \right)^{-1} \end{bmatrix} \begin{bmatrix} \left[\boldsymbol{\Phi}_s^{(1)} \right]^T & \mathbf{0} & \cdots & \mathbf{0} \\ \mathbf{0} & \left[\boldsymbol{\Phi}_s^{(2)} \right]^T & \cdots & \mathbf{0} \\ \vdots & \vdots & \ddots & \vdots \\ \mathbf{0} & \mathbf{0} & \cdots & \left[\boldsymbol{\Phi}_s^{(N_S)} \right]^T \end{bmatrix} \\
&= \begin{bmatrix} \boldsymbol{\Phi}_s^{(1)} \left(\boldsymbol{\Lambda}_s^{(1)} \right)^{-1} \left[\boldsymbol{\Phi}_s^{(1)} \right]^T & \mathbf{0} & \cdots & \mathbf{0} \\ \mathbf{0} & \boldsymbol{\Phi}_s^{(2)} \left(\boldsymbol{\Lambda}_s^{(2)} \right)^{-1} \left[\boldsymbol{\Phi}_s^{(2)} \right]^T & \cdots & \mathbf{0} \\ \vdots & \vdots & \ddots & \vdots \\ \mathbf{0} & \mathbf{0} & \cdots & \boldsymbol{\Phi}_s^{(N_S)} \left(\boldsymbol{\Lambda}_s^{(N_S)} \right)^{-1} \left[\boldsymbol{\Phi}_s^{(N_S)} \right]^T \end{bmatrix}
\end{aligned} \tag{4-30}$$

Therefore, the primitive form of the first-order residual flexibility can be constructed from the stiffness matrices and the master modes of substructures as

$$\begin{aligned}
&\boldsymbol{\Phi}_s^p \left(\boldsymbol{\Lambda}_s^p \right)^{-1} \left[\boldsymbol{\Phi}_s^p \right]^T \\
&= \mathrm{Diag}\left[\left(\left(\mathbf{K}^{(1)} \right)^{-1} - \boldsymbol{\Phi}_m^{(1)} \left(\boldsymbol{\Lambda}_m^{(1)} \right)^{-1} \left[\boldsymbol{\Phi}_m^{(1)} \right]^T \right), \ldots, \left(\left(\mathbf{K}^{(N_S)} \right)^{-1} - \boldsymbol{\Phi}_m^{(N_S)} \left(\boldsymbol{\Lambda}_m^{(N_S)} \right)^{-1} \left[\boldsymbol{\Phi}_m^{(N_S)} \right]^T \right) \right]
\end{aligned} \tag{4-31}$$

If the *j*th substructure is free after partition, the rigid body components should be included to construct the residual flexibility matrix. Calculation of the residual flexibility matrix for a free substructure can be found in Appendix D.

Subsequently, the reduced eigenequation (Eq. (4-29)) can be solved with the standard

Subspace Iteration or Lanczos method. The expanded eigenvectors of the global structure can be recovered by

$$\bar{\boldsymbol{\Phi}} = \boldsymbol{\Phi}_m^p \mathbf{z}_m \tag{4-32}$$

where $\{\mathbf{z}_m\}$ can be viewed as the mode participation factor while the master eigenvectors of the substructures act as the modal space. Finally, the eigenvectors of the global structure $\boldsymbol{\Phi}$ can be directly obtained after discarding the identical values at the interface points in $\bar{\boldsymbol{\Phi}}$.

In this section, the eigensolutions of the global structure is represented by a few master modes of the substructures, while the contribution of the slave modes is compensated by the first-order residual flexibility matrix. In consequence, the eigenequation is reduced to the size of $N_m^p \times N_m^p$, which is much smaller than the original one ($N^P \times N^P$). This substructuring method is entitled as **F**irst order **R**esidual **F**lexibility based **S**ubstructuring (FRFS) method.

4.3.2 Error Quantification

In the FRFS method, the approximation is introduced by replacing $\left(\boldsymbol{\Lambda}_s^p - \bar{\lambda}\mathbf{I}\right)^{-1}$ with $\left(\boldsymbol{\Lambda}_s^p\right)^{-1}$. Consequently, the error due to this approximation is

$$Error = \left(\boldsymbol{\Lambda}_s^p - \bar{\lambda}\mathbf{I}\right)^{-1} - \left(\boldsymbol{\Lambda}_s^p\right)^{-1} = \begin{bmatrix} \frac{1}{\left(\boldsymbol{\Lambda}_s^p\right)_1 - \bar{\lambda}} - \frac{1}{\left(\boldsymbol{\Lambda}_s^p\right)_1} & & \\ & \ddots & \\ & & \frac{1}{\left(\boldsymbol{\Lambda}_s^p\right)_{N_s^p} - \bar{\lambda}} - \frac{1}{\left(\boldsymbol{\Lambda}_s^p\right)_{N_s^p}} \end{bmatrix}$$

$$= \begin{bmatrix} \dfrac{\bar{\lambda}}{\left(\left(\boldsymbol{\Lambda}_s^p\right)_1 - \bar{\lambda}\right)\left(\boldsymbol{\Lambda}_s^p\right)_1} & & \\ & \ddots & \\ & & \dfrac{\bar{\lambda}}{\left(\left(\boldsymbol{\Lambda}_s^p\right)_{N_s^p} - \bar{\lambda}\right)\left(\boldsymbol{\Lambda}_s^p\right)_{N_s^p}} \end{bmatrix} = \mathrm{Diag}\left(\frac{\bar{\lambda}}{\left(\left(\boldsymbol{\Lambda}_s^p\right)_i - \bar{\lambda}\right)\left(\boldsymbol{\Lambda}_s^p\right)_i} \right) \tag{4-33}$$

And the relative error is

$$\textit{Relative error} = \mathrm{Diag}\left(\frac{\dfrac{\bar{\lambda}}{\left(\left(\boldsymbol{\Lambda}_s^p\right)_i - \bar{\lambda}\right)\left(\boldsymbol{\Lambda}_s^p\right)_i}}{\dfrac{1}{\left(\boldsymbol{\Lambda}_s^p\right)_i - \bar{\lambda}}} \right) = \mathrm{Diag}\left(\frac{\bar{\lambda}}{\left(\boldsymbol{\Lambda}_s^p\right)_i} \right) \tag{4-34}$$

$$(\, i = 1, 2, \ldots, \ N_s^p \,)$$

It means that the largest relative error is determined by $\dfrac{\bar{\lambda}}{\min\left(\boldsymbol{\Lambda}_s^p\right)}$. If the required eigenvalues $\bar{\lambda}$ are much smaller than the minimum value of $\boldsymbol{\Lambda}_s^p$, the error introduced will be insignificant. Therefore, the minimum eigenvalue of the substructures controls the accuracy of the FRFS method. In practice, the substructures have larger natural frequencies than the global structure has. The number of the master modes in the substructures is usually suggested to be 2 ~ 3 times the modes required for a large-scale structure to ensure $\bar{\lambda}$ is much smaller than $\min\left(\boldsymbol{\Lambda}_s^p\right)$. If the eigenvalues of interest become large, the results may be not always accurate enough using the FRFS method. In this case, the second item of Taylor expansion (Eq. (4-26)) should be retained, which result in the second-order residual flexibility substructuring method as described in the next section.

4.4 Second-order Residual Flexibility Based Modal Truncation

4.4.1 Method Description

If the first two items of the Taylor expansion in Eq. (4-26) are retained, Eq. (4-27) becomes

$$\begin{bmatrix} \mathbf{\Lambda}_m^p - \bar{\lambda}\mathbf{I} & -\mathbf{\Gamma}_m \\ -\mathbf{\Gamma}_m^T & -\left(\mathbf{\Gamma}_s^T\left(\mathbf{\Lambda}_s^p\right)^{-1}\mathbf{\Gamma}_s + \bar{\lambda}\mathbf{\Gamma}_s^T\left(\mathbf{\Lambda}_s^p\right)^{-2}\mathbf{\Gamma}_s\right) \end{bmatrix} \begin{Bmatrix} \mathbf{z}_m \\ \tau \end{Bmatrix} = \begin{Bmatrix} \mathbf{0} \\ \mathbf{0} \end{Bmatrix} \tag{4-35}$$

After arranging Eq. (4-35), the standard form of the eigenequation can be expressed as

$$\begin{bmatrix} \mathbf{\Lambda}_m^p & -\mathbf{\Gamma}_m \\ -\mathbf{\Gamma}_m^T & -\mathbf{\Gamma}_s^T\left(\mathbf{\Lambda}_s^p\right)^{-1}\mathbf{\Gamma}_s \end{bmatrix} \begin{Bmatrix} \mathbf{z}_m \\ \tau \end{Bmatrix} = \bar{\lambda} \begin{bmatrix} \mathbf{I} & \mathbf{0} \\ \mathbf{0} & \mathbf{\Gamma}_s^T\left(\mathbf{\Lambda}_s^p\right)^{-2}\mathbf{\Gamma}_s \end{bmatrix} \begin{Bmatrix} \mathbf{z}_m \\ \tau \end{Bmatrix} \tag{4-36}$$

where

$$\begin{cases} \mathbf{\Gamma}_s^T\left(\mathbf{\Lambda}_s^p\right)^{-1}\mathbf{\Gamma}_s = \mathbf{C}\mathbf{\Phi}_s^p\left(\mathbf{\Lambda}_s^p\right)^{-1}\left[\mathbf{\Phi}_s^p\right]^T\mathbf{C}^T \\ \mathbf{\Gamma}_s^T\left(\mathbf{\Lambda}_s^p\right)^{-2}\mathbf{\Gamma}_s = \mathbf{C}\mathbf{\Phi}_s^p\left(\mathbf{\Lambda}_s^p\right)^{-2}\left[\mathbf{\Phi}_s^p\right]^T\mathbf{C}^T \end{cases} \tag{4-37}$$

$\mathbf{\Phi}_s^p\left(\mathbf{\Lambda}_s^p\right)^{-2}\left[\mathbf{\Phi}_s^p\right]^T$ is the *second-order residual flexibility*. The primitive form of the second-order residual flexibility can also be obtained by the diagonal assembly of the system matrices and master modes of the substructures as

$$\mathbf{\Phi}_s^p\left(\mathbf{\Lambda}_s^p\right)^{-2}\left[\mathbf{\Phi}_s^p\right]^T = \text{Diag}\left[\left(\left(\mathbf{K}^{(1)}\right)^{-1}\mathbf{M}^{(1)}\left(\mathbf{K}^{(1)}\right)^{-1} - \mathbf{\Phi}_m^{(1)}\left(\mathbf{\Lambda}_m^{(1)}\right)^{-2}\left[\mathbf{\Phi}_m^{(1)}\right]^{\mathrm{T}}\right),\ldots,\left(\left(\mathbf{K}^{(N_S)}\right)^{-1}\mathbf{M}^{(N_S)}\left(\mathbf{K}^{(N_S)}\right)^{-1} - \mathbf{\Phi}_m^{(N_S)}\left(\mathbf{\Lambda}_m^{(N_S)}\right)^{-2}\left[\mathbf{\Phi}_m^{(N_S)}\right]^{\mathrm{T}}\right)\right] \tag{4-38}$$

Calculation of the second-order residual flexibility is given in the Appendix D. With both the first- and second- order residual flexibility, the eigensolutions of the global structure are obtained similarly to the FRFS method.

As compared with the FRFS procedure introduced previously, this **S**econd-order **R**esidual **F**lexibility based **S**ubstructuring method (SRFS) will achieve much more accurate results as it includes the contribution of the second item in the Taylor expansion. However, this high precision is achieved at the cost of computational load in terms of two aspects:

i) The SRFS method spends some additional effort to calculate the second-order residual flexibility matrix $\boldsymbol{\Phi}_s^p \left(\boldsymbol{\Lambda}_s^p\right)^{-2} \left[\boldsymbol{\Phi}_s^p\right]^T$.

ii) The size of the eigenequation in the SRFS method (Eq. (4-36)), which contains the 'misfit' displacements at the interface points, is a little larger than that in the FRFS method.

4.4.2 Error Quantification

Similar to the FRFS method, the error in the SRFS method is introduced by the truncation of Taylor expansion, which is evaluated as

$$\textit{Error}=\left(\boldsymbol{\Lambda}_s^p-\bar{\lambda}\mathbf{I}\right)^{-1}-\left(\boldsymbol{\Lambda}_s^p\right)^{-1}-\bar{\lambda}\left(\boldsymbol{\Lambda}_s^p\right)^{-2}=\mathrm{Diag}\left(\frac{1}{\left(\boldsymbol{\Lambda}_s^p\right)_i-\bar{\lambda}}-\frac{1}{\left(\boldsymbol{\Lambda}_s^p\right)_i}-\frac{\bar{\lambda}}{\left(\boldsymbol{\Lambda}_s^p\right)_i^2}\right)$$

$$=\mathrm{Diag}\left(\frac{\left(\boldsymbol{\Lambda}_s^p\right)_i^2-\left(\left(\boldsymbol{\Lambda}_s^p\right)_i-\bar{\lambda}\right)\left(\boldsymbol{\Lambda}_s^p\right)_i-\bar{\lambda}\left(\left(\boldsymbol{\Lambda}_s^p\right)_i-\bar{\lambda}\right)}{\left(\left(\boldsymbol{\Lambda}_s^p\right)_i-\bar{\lambda}\right)\left(\boldsymbol{\Lambda}_s^p\right)_i^2}\right)=\mathrm{Diag}\left(\frac{\bar{\lambda}^2}{\left(\left(\boldsymbol{\Lambda}_s^p\right)_i-\bar{\lambda}\mathbf{I}\right)\left(\boldsymbol{\Lambda}_s^p\right)_i^2}\right) \tag{4-39}$$

$$\textit{Relative error}=\mathrm{Diag}\left(\frac{\dfrac{\bar{\lambda}^2}{\left(\left(\boldsymbol{\Lambda}_s^p\right)_i-\bar{\lambda}\right)\left(\boldsymbol{\Lambda}_s^p\right)_i^2}}{\dfrac{1}{\left(\boldsymbol{\Lambda}_s^p\right)_i-\bar{\lambda}}}\right)=\mathrm{Diag}\left(\left(\frac{\bar{\lambda}}{\left(\boldsymbol{\Lambda}_s^p\right)_i}\right)^2\right) \tag{4-40}$$

$$(\ i=1,\ 2,\ \ldots,\ \ N_s^p\ )$$

Therefore, the relative error in the SRFS method is dependent on $\left(\frac{\bar{\lambda}}{\min\left(\mathbf{\Lambda}_s^p\right)}\right)^2$. The minimum value of $\mathbf{\Lambda}_s^p$ controls the accuracy of the SRFS method, similar to the FRFS method. Because $\bar{\lambda}$ is usually much smaller than the values in $\left(\mathbf{\Lambda}_s^p\right)$, the SRFS method is more accurate than the FRFS method. This will be demonstrated in the following numerical examples.

4.5 Case Studies

4.5.1 Three-span Frame Structure

The three-span frame structure described in Chapter 3 is used here to demonstrate the procedure and accuracy of the substructuring method in calculation of eigensolutions.

For comparison, the frame is analyzed with five approaches to extract the first 20 eigensolutions of the global structure. First, the entire structure is analyzed with the conventional Lanczos method on the global structure. In the second approach, the frame is analyzed by the original Kron's substructuring method, in which the complete eigensolutions of all substructures are calculated to assemble the primitive matrices. The primitive matrices $\mathbf{\Lambda}^p$ and $\mathbf{\Phi}^p$ have the size of 432×432 and are solved with the standard Lanczos eigensolver. Because the contribution of the complete modes in each substructure is considered and there is no approximation during the whole process, the obtained eigensolutions can be regarded as accurate.

In the third approach, the first 50 modes of each substructure are retained to assemble the global structure, while the residual high modes are discarded directly without any

compensation. The eigenequation has the size of 150×150.

Afterwards, the frame is analyzed by the proposed FRFS method. The first 50 modes in each substructure are chosen as 'master', while the higher modes are compensated by the first-order residual flexibility. The procedure consists of the following steps.

1) Divide the global structure into three substructures. Each substructure is regarded as an independent structure, and the nodes and elements are labeled individually.
2) Obtain the first 50 eigensolutions of the three substructures, and calculate the first-order residual flexibility of each substructure.
3) Assemble the primitive form of the master eigensolutions $\mathbf{\Lambda}_m^p$ and $\mathbf{\Phi}_m^p$ with the master modes of the three substructures. $\mathbf{\Lambda}_m^p$ and $\mathbf{\Phi}_m^p$ have the size of 150×150 and 150×432, respectively.
4) Establish the connection matrix **C**. Eight interface points (each has 3 DOFs) result in 24 connections to assemble the global structure. Consequently, the connection matrix has the size of 24×432.
5) Form the matrix $\mathbf{\Psi}$ of order 150×150 in Eq. (4-29), and solve the reduced eigenequation with the standard Lanczos method to calculate the first 20 eigenpairs ($\bar{\lambda}$ and $\mathbf{z}_m$).
6) Calculate the expanded eigenvectors with $\bar{\mathbf{\Phi}} = \mathbf{\Phi}_m^p \mathbf{z}_m$ and recover the eigenvectors of the global structure by discarding the identical coordinates in the expanded eigenvectors $\bar{\mathbf{\Phi}}$.

Finally, the frame is analyzed with the SRFS method. Likewise, the first 50 modes in each substructure are chosen as the master modes. The process is similar to the FRFS method except Step 5, where the eigenequation (Eq. (4-36)) contains the 'misfit'

displacement and has the size of 174×174.

The first 20 frequencies of the global structure are obtained from the above-mentioned five approaches and listed in Table 4-1 for comparison. In this table, ‘Lanczos’, ‘Original’, ‘Original-Partial’, ‘FRFS’ and ‘SRFS’ denote the aforementioned five methods respectively. The second line of Table 4-1 gives the computation time (in second) consumed by the central processing unit (CPU) in obtaining the first 20 eigensolutions of the global structure with the corresponding methods on a personal computer (PC) with 1.86 GHz Intel Core 2 Duo processor and 2 GB memory.

In the Table 4-1, two indices are utilized to evaluate the accuracy of the eigenvector accuracy obtained with different approaches. The first index is the MAC value, indicating the similarity of two sets of mode shapes as

$$MAC\left(\{\phi_i\},\{\tilde{\phi}_i\}\right)=\frac{\left|\{\phi_i\}^T\{\tilde{\phi}_i\}\right|^2}{\left(\{\phi_i\}^T\{\phi_i\}\right)\left(\{\tilde{\phi}_i\}^T\{\tilde{\phi}_i\}\right)} \tag{4-41}$$

where $\{\phi_i\}$ is the *i*th eigenvector obtained from the Lanczos method on the global structure, and is taken as the accurate for reference. $\{\tilde{\phi}_i\}$ represents the *i*th eigenvector by the other four substructuring methods. An MAC value of identity implies that the two vectors are identical, whereas a value of 0 indicates that the two vectors are perpendicular.

Table 4-1: Frequencies and Modal Shapes of the Frame Structure Obtained with Different Methods

	Lanczos	Original	Original-Partial		FRFS				SRFS			
CPU time (second)	0.1703	0.5640	0.1671		0.1978				0.2413			
Mode index	Freq. (Hz)	Freq. (Hz)	Freq. (Hz)	Relative error	Freq. (Hz)	Relative error	Mode shape error		Freq. (Hz)	Relative error	Mode shape error	
							(1-MAC)	Difference Norm			(1-MAC)	Difference Norm
1	1.7843	1.7843	1.7898	0.341%	1.7843	0.000%	0.000%	0.000%	1.7843	0.000%	0.000%	0.000%
2	5.5365	5.5365	5.5495	0.539%	5.5365	0.000%	0.000%	0.000%	5.5365	0.000%	0.000%	0.000%
3	9.8198	9.8198	9.7959	0.582%	9.8199	0.001%	0.003%	0.006%	9.8198	0.000%	0.003%	0.005%
4	14.6864	14.6864	14.5231	0.415%	14.6865	0.001%	0.002%	0.003%	14.6864	0.000%	0.002%	0.002%
5	16.6188	16.6188	18.8166	13.396%	16.6223	0.034%	0.081%	0.000%	16.6188	0.000%	0.081%	0.000%
6	18.8074	18.8074	19.8156	5.997%	18.8122	0.060%	0.130%	0.018%	18.8075	0.001%	0.130%	0.021%
7	20.1977	20.1977	21.1509	7.214%	20.1979	0.003%	0.006%	0.018%	20.1977	0.000%	0.006%	0.018%
8	22.6170	22.6170	25.0778	12.328%	22.6235	0.111%	0.236%	0.029%	22.6172	0.002%	0.236%	0.028%
9	25.4704	25.4704	25.4569	2.184%	25.4753	0.040%	0.099%	0.085%	25.4705	0.001%	0.094%	0.040%
10	26.1799	26.1799	27.0610	6.533%	26.1808	0.018%	0.058%	0.019%	26.1799	0.000%	0.044%	0.011%
11	28.0818	28.0818	27.6134	3.494%	28.0839	0.008%	0.016%	0.062%	28.0818	0.000%	0.015%	0.062%
12	29.7843	29.7843	28.5257	1.047%	29.7877	0.017%	0.043%	0.109%	29.7843	0.000%	0.043%	0.108%
13	30.9747	30.9747	29.8720	1.632%	30.9789	0.032%	0.069%	0.141%	30.9748	0.001%	0.068%	0.139%
14	31.4907	31.4907	30.1980	0.303%	31.4924	0.004%	0.009%	0.020%	31.4907	0.000%	0.009%	0.019%
15	32.3470	32.3470	30.8539	0.410%	32.3492	0.006%	0.007%	0.047%	32.3470	0.000%	0.007%	0.046%
16	32.3574	32.3574	31.0906	0.635%	32.3604	0.012%	0.023%	0.047%	32.3574	0.000%	0.023%	0.039%
17	33.5952	33.5952	32.0649	0.379%	33.5979	0.007%	0.019%	0.067%	33.5952	0.000%	0.018%	0.066%
18	33.8409	33.8409	32.3354	0.693%	33.8432	0.014%	0.034%	0.039%	33.8409	0.000%	0.033%	0.033%
19	34.4871	34.4871	33.0881	0.760%	34.4924	0.015%	0.037%	0.085%	34.4873	0.001%	0.034%	0.084%
20	34.5654	34.5654	33.1796	1.036%	34.5690	0.025%	0.051%	0.048%	34.5657	0.001%	0.048%	0.041%

Difference Norm, the second index, is applied to evaluate the relative error of mode shapes as

$$Difference \quad Norm = \frac{norm\left(\{\phi_i\} - \{\tilde{\phi}_i\}\right)}{norm\left(\{\phi_i\}\right)} \tag{4-42}$$

From Table 4-1, one can find that,

1) As compared with the global Lanczos method, the original Kron's substructuring method takes much longer time.
2) Discarding the slave mode directly without compensation introduces a significant error. Since the substructures are connected based on the principle of virtual work, completely discarding the energy contribution of the higher modes results in error.
3) Using the proposed substructuring method in which the higher modes are taken into consideration via residual flexibility, the accuracy of the eigenvalues is improved significantly. For example, the relative errors of the first 20 frequencies are less than 0.1% with the FRFS method, and less than 0.002% with the SRFS method. The accuracy is sufficient for usual engineering applications. As compared with the traditional Kron's substructuring method, the proposed method reduces the computational loads significantly.
4) The SRFS method achieves a higher precision, but costs a little more computation time and memory than the FRFS method.
5) The proposed method can achieve not only high precision eigenvalues but also good eigenvector results.
6) The proposed substructuring method takes a little longer time than the global Lanczos method. This is because the analyses of each substructure, especially calculation of the residual flexibility, costs a lot of computation effort. These

interim results will be re-used in calculation of the eigensensitivity, which will be introduced in the next chapter. If the proposed substructuring method is applied to model updating or damage identification, the calculation of eigensolutions and sensitivity matrix are required for the concerned substructures only. Besides, the eigenequation size of the proposed method is much smaller than that of the global Lanczos method and the original Kron's substructuring method, as listed in Table 4-2. This is an attractive merit for model updating process, which will be demonstrated in the subsequent chapters.

Table 4-2: Size of the Eigenequation with Various Methods

	Lanczos method	Original Kron's method	FRFS	SRFS
Sub 1		153×153	50×50	50×50
Sub 2		165×165	50×50	50×50
Sub 3		142×142	50×50	50×50
Global structure	408×408	432×432	150×150	174×174

This example indicates that the proposed substructuring method can reduce the computation load significantly while remain a high precision. Although the accuracy of the FRFS method is not as good as that of the SRFS method, it can satisfy most of the engineering applications and cost much less computational resource. Therefore, the FRFS method might be preferable in practice. In the next example, only the FRFS method will be utilized.

4.5.2 The Balla Balla River Bridge

The analytical model of the Balla Balla River Bridge described in Chapter 3 is adopted to demonstrate the computational efficiency of the substructuring method in

calculation of eigensolutions. In addition, the influence of the master modes and the division formation of the substructures on the computation accuracy and efficiency are investigated.

The global structure is divided into five substructures respectively at 10 m, 20 m, 30 m and 40 m along the longitudinal direction as shown in Figure 4-1. The detailed information of the five substructures is listed in Table 4-3.

Table 4-3: Division Formation with Five Substructures

Index of substructures	Sub 1	Sub 2	Sub 3	Sub 4	Sub 5
Geometric range (m)*	0~10	10~20	20~30	30~40	40~54
No. of elements	187	182	132	182	224
No. of nodes	205	212	161	212	251
No. of DOFs	1095	1260	966	1260	1371
No. of interface nodes	23	23	23	23	

Note:* in longitudinal direction.

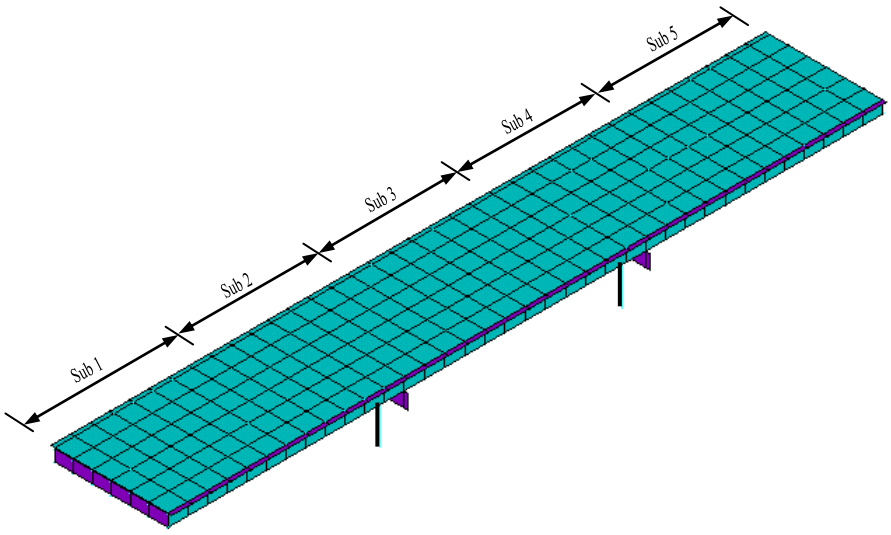

Figure 4-1: FE Model of the Balla Balla River Bridge with Five Substructures

Table 4-4: Frequencies of the Balla Balla Bridge with Different Master Modes

	Exact	Original	40 master modes		60 master modes		90 master modes	
CPU time (second)	8.0253	238.8509	10.3725		10.9643		13.0231	
Mode index	Frequency (Hz)	Frequency (Hz)	Frequency (Hz)	Relative error	Frequency (Hz)	Relative error	Frequency (Hz)	Relative error
1	5.8232	5.8232	5.8288	0.097%	5.8281	0.084%	5.8269	0.063%
2	5.9998	5.9998	6.0028	0.051%	6.0028	0.051%	6.0028	0.051%
3	6.0007	6.0007	6.0038	0.052%	6.0038	0.051%	6.0037	0.051%
4	6.2635	6.2635	6.2691	0.089%	6.2677	0.066%	6.2669	0.053%
5	6.8621	6.8621	6.8656	0.051%	6.8655	0.051%	6.8655	0.051%
6	6.8987	6.8987	6.9023	0.052%	6.9023	0.052%	6.9022	0.051%
7	6.9975	6.9975	7.0034	0.084%	7.0022	0.067%	7.0012	0.052%
8	7.7391	7.7391	7.7465	0.095%	7.7449	0.075%	7.7432	0.053%
9	8.6063	8.6063	8.6142	0.092%	8.6128	0.075%	8.6109	0.053%
10	8.7145	8.7145	8.7205	0.069%	8.7197	0.059%	8.7191	0.052%
11	9.4460	9.4460	9.4535	0.079%	9.4525	0.068%	9.4510	0.053%
12	10.9814	10.9814	10.9870	0.051%	10.9870	0.051%	10.9870	0.051%
13	10.9816	10.9816	10.9872	0.051%	10.9872	0.051%	10.9872	0.051%
14	12.1302	12.1302	12.1511	0.172%	12.1417	0.094%	12.1375	0.059%
15	13.0048	13.0048	13.0227	0.137%	13.0167	0.091%	13.0122	0.057%
16	13.2693	13.2693	13.2868	0.132%	13.2810	0.088%	13.2767	0.056%
17	14.9312	14.9312	14.9431	0.080%	14.9421	0.073%	14.9399	0.058%
18	15.8194	15.8194	15.8880	0.434%	15.8610	0.263%	15.8337	0.090%
19	16.9266	16.9266	16.9515	0.147%	16.9463	0.116%	16.9370	0.062%
20	17.5480	17.5480	17.6043	0.321%	17.5646	0.095%	17.5602	0.070%

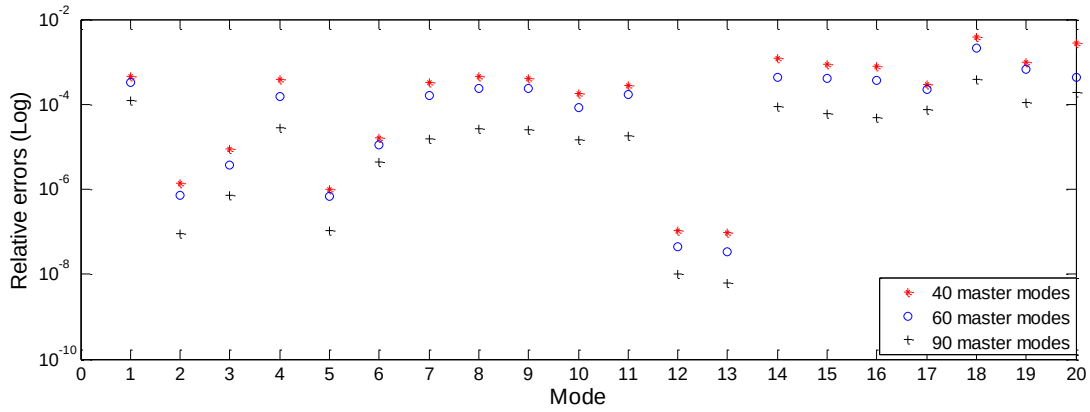

Figure 4-2: Accuracy of Frequencies with Different Master Modes

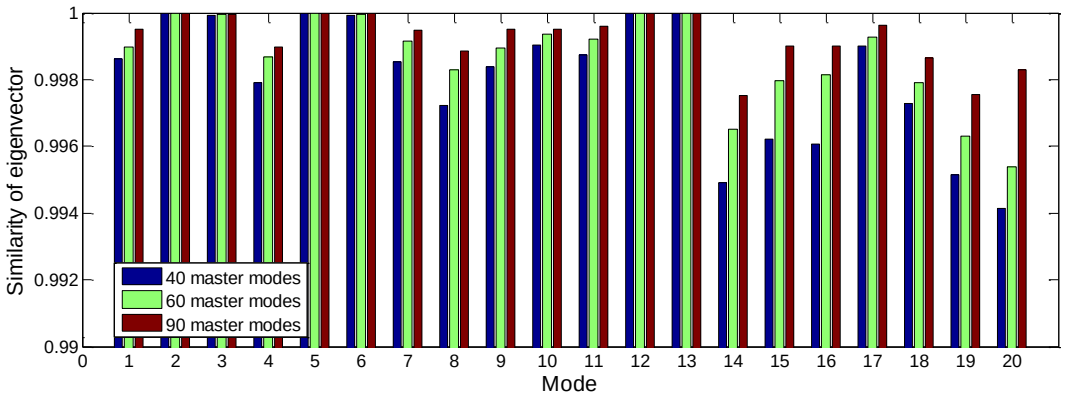

Figure 4-3: Accuracy of Eigenvectors with Different Master Modes

In this example, only the FRFS method is utilized, and the first 40 modes in each substructure are chosen as the master modes. The first 20 eigensolutions of the global structure are calculated and the frequencies are listed in Table 4-4, together with the relative errors compared with the exact results using the global Lanczos method.

The computational accuracy is certainly influenced by the master modes retained in each substructure. To investigate the effect of the number of master modes on the computational accuracy, 40 modes, 60 modes and 90 modes in each substructure are chosen as 'master', respectively. The obtained 20 eigensolutions and the corresponding errors are listed in Table 4-4. The second line of Table 4-4 gives the CPU time to calculate the eigensolutions using the different master modes. The

relative errors of the frequencies and the MAC values of the eigenvectors are compared in Figure 4-2 and Figure 4-3, respectively.

It is apparent that the accuracy of the frequencies and eigenvectors is improved when more master modes are included in each substructure, especially for the higher modes. At the same time, the computation time increases as more master modes are included.

The number of master modes required in each substructure depends on the accuracy requirement. Based on the error analysis described previously, one should make the minimum value of $\mathbf{\Lambda}_s^p$ as large as possible. Sturm's Sequence check (Bathe 1982) can be employed to determine the number of eigenvalues that smaller than a specified value, i.e., all the smallest eigenvalue modes among all substructures are selected as master modes.

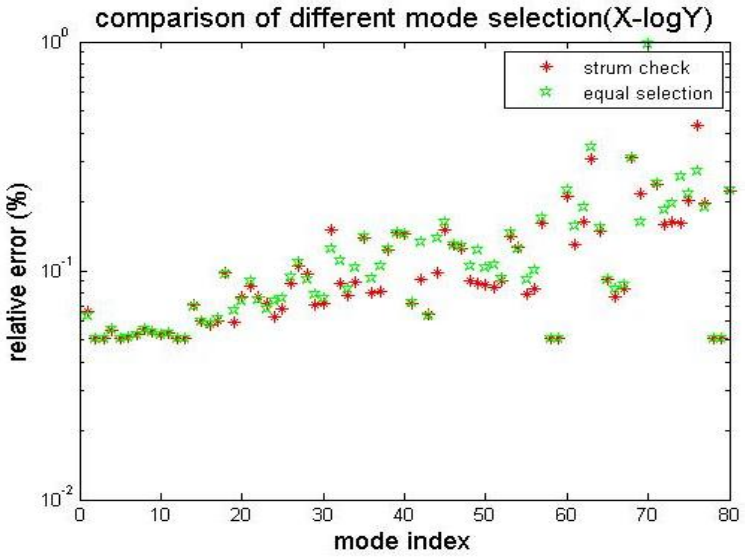

Figure 4-4: Computation Accuracy Using Different Selection of Master Modes

In this study, 940000 are selected as the boundary value for the Sturm's Sequence check. Accordingly, there are 61, 87, 76, 92, 84 master modes in the five

substructures, respectively. The relative errors of equally selecting 80 master modes in each substructure and using Sturm's Sequence check are compared in Figure 4-4. Figure 4-4 reports that selecting master modes with Sturm's Sequence check has a slightly better result than that of equally selecting them from each substructure. For the lower eigenmodes, there is almost no discrepancy among the two selecting strategy. In the case that the substructures are similarly divided, equally selecting master modes from each substructure is a convenient and realistic preference.

On the other hand, division formation of the substructures also affects the accuracy and efficiency. From a practical point of view, one should reduce the interface joints for a smaller transformation matrix **C**. In this regard, dividing a building across the columns is better than through the slabs, and dividing a bridge across the slab is better than across the piers.

To investigate the influence of the division formation of the substructures, the bridge is approximately averaged into 3, 5, 8, 11 substructures respectively along the longitudinal direction. The detailed information for the substructures with these division formations are given in Tables 4-5 ~ 4-7. For different division formations, the master modes are selected in two manners.

Table 4-5: Division Formation with Three Substructures

Index of substructures	Sub 1	Sub 2	Sub 3
Geometric range (m)*	0~16.5	16.5~34.5	34.5~54
No. of elements	275	292	340
No. of nodes	394	327	371
No. of interface nodes	23	23	

Note:* in longitudinal direction.

Table 4-6: Division Formation with Eight Substructures

Substructure Index	Sub 1	Sub 2	Sub 3	Sub 4	Sub 5	Sub 6	Sub 7	Sub 8
Geometric range (m)*	0~7	7~14	14~21	21~27	27~34	35~41	41~47	47~54
No. of elements	143	110	116	88	110	116	88	136
No. of nodes	159	138	143	115	138	143	115	159
No. of interface nodes	23	23	23	23	23	23	23	

Note:* in longitudinal direction.

Table 4-7: Division Formation with 11 Substructures

Substructure Index	Sub 1	Sub 2	Sub 3	Sub 4	Sub 5	Sub 6	Sub 7	Sub 8	Sub 9	Sub 10	Sub 11
Geometric range (m)	0~5	5~10	10~15	15~20	20~25	25~30	30~35	35~40	40~45	45~50	50~54
No. of elements	99	88	66	116	66	66	66	116	66	66	99
No. of nodes	113	115	92	143	92	92	92	143	92	92	113
No. of interface nodes	23	23	23	23	23	23	23	23	23	23	

Note:* in longitudinal direction.

In the first scheme, the first 80 modes in each substructure are chosen as master modes. The master modes in each substructure and the size of the reduced eigenequation are listed in Table 4-8, together with the corresponding CPU time in calculation of the first 40 eigensolutions of the global structure. The relative errors of the frequencies are compared in Figure 4-5.

It can be found that, except dividing the global structure into 3 substructures, other three division formations achieve similar accuracy, and more substructures result in a

slightly better accuracy.

The division formations of three substructures and 11 substructures cost more computation time than that of the five substructures and eight substructures as listed in Table 4-8. If a structure is divided into a small quantity of substructures, the independent substructure has a large amount of elements and nodes. Correspondingly, calculation of the eigensolutions and the residual flexibility matrix of each substructure will cost more CPU resource. On the other hand, when the global structure is divided into a large quantity of substructures, many substructures need to be analyzed. In addition, the global eigenequation has a larger size. Comparison of these four division formations shows that dividing the global structure into much excessive substructures or too few ones are both inefficient. In this example, dividing the global structure into five substructures can not only reach the high precision but also save the computational resource.

In the second scheme, the total number of master modes is selected around 400 as listed in Table 4-8. In this case, the reduced eigenequation will have similar size for different division formations, but the divided substructures have distinct master modes. The CPU time cost in calculation of the first 40 eigensolutions of the global structure with these four division formations are listed in Table 4-8, and the relative errors of the frequencies are compared in Figure 4-6.

Figure 4-6 shows that, if the total number of the master modes among all substructures is similar, the division with more substructures results in lower precision. This is because it has less master modes in each substructure, and thus $\min\left(\mathbf{\Lambda}_s^p\right)$ decreases. In contrast, the division with fewer substructures achieves a higher precision, since it includes more master modes in each substructure. However, the latter costs much CPU time in calculating the eigensolutions and the residual flexibility matrix for the large-size substructures. Furthermore, when applying the

substructuring method in model updating, the calculation of the sensitivity matrix in each substructure will be heavier, and the substructuring technology may lose its promising advantages. In practice, a few trials may be helpful to determine the optimized number of substructures before model updating is employed.

Table 4-8: The Matrix Size and Computation Time with Different Division Formations

No. substructures		3	5	8	11
Scheme 1	No. of master modes in each substructure	80	80	80	80
	Size of the global eigenequation	240	400	640	880
	CPU time (second)	20.8	12.8	16.7	26.1
Scheme 2	No. of master modes in each substructure	133	80	50	37
	Size of the global eigenequation	399	400	400	407
	CPU time (second)	24.9	12.8	13.4	22.7

The advantages of the present substructuring method in model updating can be also found from the eigenequation size. If the bridge is divided into 5 substructures, the eigenequation size can be heavily reduced with the proposed FRFS method as listed in Table 4-9. This is helpful for model updating process, in which the eigenequation is repeatedly constructed and solved.

Table 4-9: The Size of Eigenequation with Various Master Modes

	Lanczos	40 master modes	60 master modes	90 master modes
Each substructure		40×40	60×60	90×90
Global structure	5400×5400	200×200	300×300	450×450

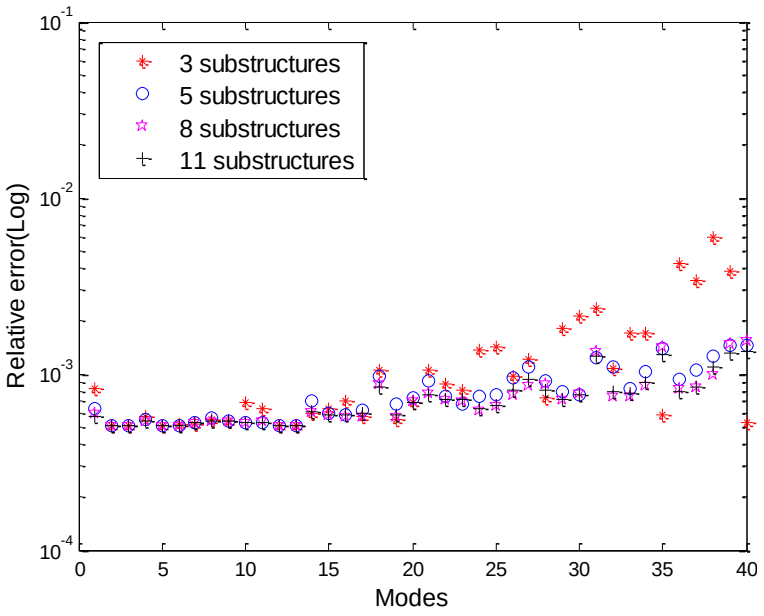

Figure 4-5: Relative Errors of Frequencies with Various Substructure Division Formations (Scheme 1)

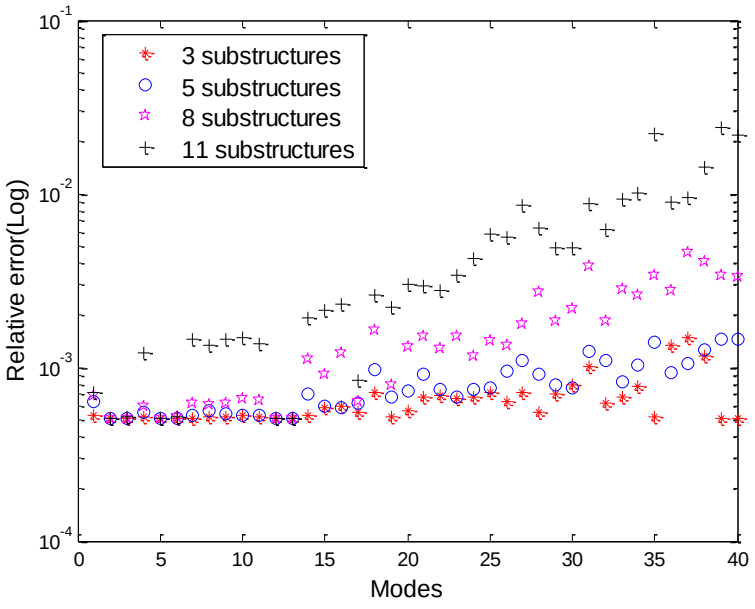

Figure 4-6: Relative Errors of Frequencies with Various Substructure Division Formations (Scheme 2)

4.6 Summary

A substructuring method is proposed in this chapter to calculate some lowest eigensolutions of large-scale structures. A modal truncation approximation is developed to reduce the computational load of the original Kron's substructuring method. With the compensation of the residual flexibility, only a few eigensolutions

of the substructures are retained to assemble the global structure, while the higher modes are compensated with the first-order residual flexibility and second-order residual flexibility, respectively. The utilization of the second-order residual flexibility achieves much better results than that of the first-order residual flexibility, whereas increases the computation effort. The division formation needs to trade off the number of the substructures and the number of master modes in each substructure. Divisions with much excessive or insufficient number of substructures are both undesirable.

CHAPTER FIVE

EIGENSENSITIVITY WITH SUBSTRUCTURING METHOD

5.1 Introduction

Methods for computing the derivatives of eigenvalues and eigenvectors with respect to elemental parameters (eigensensitivity) have been studied by many researchers in the past thirty years. In model updating, the eigensensitivity is usually used to estimate the most sensitive design parameters that contribute to the discrepancy of the analytical model and practical testing, and thus accelerate the convergence of the optimization process. The cost of calculating the eigensensitivity is always the dominant contributor to the total cost in many optimization procedures. As many practical engineering structures today are large-scale in nature, efficient computation of the eigensensitivity with respect to various design parameters is a key requirement in the model updating analysis. The substructuring technology can be a promising solution to accelerate the calculation of eigensensitivity for a large-scale structure. With the substructuring concept, the substructures are analyzed independently and then be assembled to obtain the properties of the global structure by imposing constraints at the interfaces of the adjacent substructures. To calculate the eigensensitivity with respect to one parameter, the substructural derivative matrices are required in only one substructure while those in other substructures are zeros. The substructural derivative matrices are then assembled to acquire the eigensensitivity of the global structure. Since the substructure has a much smaller size than the entire structure, the computation efficiency can be improved.

In this chapter, the eigensensitivity is calculated based on the reduced eigenequation

of the substructuring method proposed in Chapter 4. The first-order derivatives of eigensolutions are formulated firstly, followed by the second-order derivatives and the general high-order derivatives.

5.2 First-order Eigensolution Derivatives with Substructuring Method

5.2.1 Eigenvalue Derivatives

The reduced eigenequation (Eq. (4-29)) is rewritten for the *i*th mode as

$$\left(\mathbf{\Psi}-\bar{\lambda}_i\mathbf{I}\right)\{\mathbf{z}_i\}=\mathbf{0}$$

$$\mathbf{\Psi}=\mathbf{\Lambda}_m^p+\mathbf{\Gamma}_m\left(\mathbf{\Gamma}_s^T\left(\mathbf{\Lambda}_s^p\right)^{-1}\mathbf{\Gamma}_s\right)^{-1}\mathbf{\Gamma}_m^T \tag{5-1}$$

The eigenvalue $\bar{\lambda}_i$ and eigenvector $\{\mathbf{z}_i\}$ have been solved in Chapter 4. Eq. (5-1) is differentiated with respect to a designed parameter *r* as follows.

$$\left(\mathbf{\Psi}-\bar{\lambda}_i\mathbf{I}\right)\left\{\frac{\partial\mathbf{z}_i}{\partial r}\right\}+\frac{\partial\left(\mathbf{\Psi}-\bar{\lambda}_i\mathbf{I}\right)}{\partial r}\{\mathbf{z}_i\}=\{\mathbf{0}\} \tag{5-2}$$

Here *r* is an elemental parameter of the global structure, for example bending rigidity.

Pre-multiplying $\{\mathbf{z}_i\}^T$ on both sides of Eq. (5-2) gives the following.

$$\{\mathbf{z}_i\}^T\left(\mathbf{\Psi}-\bar{\lambda}_i\mathbf{I}\right)\left\{\frac{\partial\mathbf{z}_i}{\partial r}\right\}+\{\mathbf{z}_i\}^T\frac{\partial\left(\mathbf{\Psi}-\bar{\lambda}_i\mathbf{I}\right)}{\partial r}\{\mathbf{z}_i\}=0 \tag{5-3}$$

Due to the symmetry of $\left(\mathbf{\Psi}-\bar{\lambda}_i\mathbf{I}\right)$, the first item on the left-hand side of Eq. (5-3) is zero. By arranging Eq. (5-3), the derivative of eigenvalue $\bar{\lambda}_i$ with respect to the designed parameter *r* is

$$\frac{\partial\bar{\lambda}_i}{\partial r}=\{\mathbf{z}_i\}^T\frac{\partial\mathbf{\Psi}}{\partial r}\{\mathbf{z}_i\} \tag{5-4}$$

where

$$\frac{\partial \boldsymbol{\Psi}}{\partial r} = \frac{\partial \left[\boldsymbol{\Lambda}_m^p + \boldsymbol{\Gamma}_m \left(\boldsymbol{\Gamma}_s^T \left(\boldsymbol{\Lambda}_s^p \right)^{-1} \boldsymbol{\Gamma}_s \right)^{-1} \boldsymbol{\Gamma}_m^T \right]}{\partial r}$$

$$= \frac{\partial \boldsymbol{\Lambda}_m^p}{\partial r} + \frac{\partial \boldsymbol{\Gamma}_m}{\partial r} \left(\boldsymbol{\Gamma}_s^T \left(\boldsymbol{\Lambda}_s^p \right)^{-1} \boldsymbol{\Gamma}_s \right)^{-1} \boldsymbol{\Gamma}_m^T + \boldsymbol{\Gamma}_m \frac{\partial \left[\left(\boldsymbol{\Gamma}_s^T \left(\boldsymbol{\Lambda}_s^p \right)^{-1} \boldsymbol{\Gamma}_s \right)^{-1} \right]}{\partial r} \boldsymbol{\Gamma}_m^T + \boldsymbol{\Gamma}_m \left(\boldsymbol{\Gamma}_s^T \left(\boldsymbol{\Lambda}_s^p \right)^{-1} \boldsymbol{\Gamma}_s \right)^{-1} \frac{\partial \boldsymbol{\Gamma}_m^T}{\partial r} \tag{5-5}$$

In Eq. (5-5), $\frac{\partial \boldsymbol{\Lambda}_m^p}{\partial r}$ is the diagonal assembly of the eigenvalue derivatives of the master modes of the substructures, $\frac{\partial \boldsymbol{\Gamma}_m}{\partial r} = \frac{\partial \left[\boldsymbol{\Phi}_m^p \right]^T}{\partial r} \mathbf{C}^T$ is associated with the diagonal assembly of the master eigenvector derivatives of the substructures, and $\frac{\partial \left[\left(\boldsymbol{\Gamma}_s^T \left(\boldsymbol{\Lambda}_s^p \right)^{-1} \boldsymbol{\Gamma}_s \right)^{-1} \right]}{\partial r}$ is associated with the derivative matrices of the first-order residual flexibility of the substructures and can be obtained from the derivative of master modes as

$$\frac{\partial \left(\boldsymbol{\Gamma}_s^T \left(\boldsymbol{\Lambda}_s^p \right)^{-1} \boldsymbol{\Gamma}_s \right)^{-1}}{\partial r} = -\left(\boldsymbol{\Gamma}_s^T \left(\boldsymbol{\Lambda}_s^p \right)^{-1} \boldsymbol{\Gamma}_s \right)^{-1} \frac{\partial \left(\boldsymbol{\Gamma}_s^T \left(\boldsymbol{\Lambda}_s^p \right)^{-1} \boldsymbol{\Gamma}_s \right)}{\partial r} \left(\boldsymbol{\Gamma}_s^T \left(\boldsymbol{\Lambda}_s^p \right)^{-1} \boldsymbol{\Gamma}_s \right)^{-1} \tag{5-6}$$

where

$$\frac{\partial \left(\boldsymbol{\Gamma}_s^T \left(\boldsymbol{\Lambda}_s^p \right)^{-1} \boldsymbol{\Gamma}_s \right)}{\partial r} = \mathbf{C} \frac{\partial \left(\boldsymbol{\Phi}_s^p \left(\boldsymbol{\Lambda}_s^p \right)^{-1} \left[\boldsymbol{\Phi}_s^p \right]^T \right)}{\partial r} \mathbf{C}^T = \mathbf{C} \times \mathrm{Diag} \left[\frac{\partial \left(\left(\mathbf{K}^{(j)} \right)^{-1} - \boldsymbol{\Phi}_m^{(j)} \left(\boldsymbol{\Lambda}_m^{(j)} \right)^{-1} \left[\boldsymbol{\Phi}_m^{(j)} \right]^T \right)}{\partial r} \right] \times \mathbf{C}^T \tag{5-7}$$

As the substructures are independent, the derivative matrices of the eigenvalues, the eigenvectors, and the residual flexibility are calculated only in a particular substructure (for example, the *r*th substructure) that contains the elemental parameter *r*. These quantities in the other substructures are zero, i.e.,

$$\frac{\partial \boldsymbol{\Lambda}_m^p}{\partial r} = \begin{bmatrix} \mathbf{0} & \mathbf{0} & \mathbf{0} \\ \mathbf{0} & \frac{\partial \boldsymbol{\Lambda}_m^{(r)}}{\partial r} & \mathbf{0} \\ \mathbf{0} & \mathbf{0} & \mathbf{0} \end{bmatrix}, \quad \frac{\partial \boldsymbol{\Phi}_m^p}{\partial r} = \begin{bmatrix} \mathbf{0} & \mathbf{0} & \mathbf{0} \\ \mathbf{0} & \frac{\partial \boldsymbol{\Phi}_m^{(r)}}{\partial r} & \mathbf{0} \\ \mathbf{0} & \mathbf{0} & \mathbf{0} \end{bmatrix},$$

$$\frac{\partial \boldsymbol{\Phi}_s^p \left(\boldsymbol{\Lambda}_s^p\right)^{-1} \left[\boldsymbol{\Phi}_s^p\right]^T}{\partial r} = \begin{bmatrix} \mathbf{0} & \mathbf{0} & \mathbf{0} \\ \mathbf{0} & \dfrac{\partial \boldsymbol{\Phi}_s^{(r)} \left(\boldsymbol{\Lambda}_s^{(r)}\right)^{-1} \left[\boldsymbol{\Phi}_s^{(r)}\right]^T}{\partial r} & \mathbf{0} \\ \mathbf{0} & \mathbf{0} & \mathbf{0} \end{bmatrix} \tag{5-8}$$

By treating the *r*th substructure as an independent structure, the eigenvalue derivatives and eigenvector derivatives can be obtained using traditional global methods, such as Nelson's method (Nelson 1976). The detailed procedure in calculation of the residual flexibility matrix and its first-order derivative can be found in the Appendix E.

It can be found that, the eigenvalue derivatives of the global structure with respect to the elemental parameter rely solely on the particular substructure (the *r*th substructure), not on the other substructures. As the substructures are always smaller in size than the global structure, computational efficiency is improved. This merits significant advantage when applied to the iterative model updating methods. The substructuring method requires only the modified substructures to be re-analyzed, leaving the other substructures untouched.

5.2.2 Eigenvector Derivatives

As the *i*th eigenvector of the global structure can be recovered by

$$\bar{\boldsymbol{\Phi}}_i = \boldsymbol{\Phi}_m^p \left\{\mathbf{z}_i\right\} \tag{5-9}$$

the eigenvector derivative of the *i*th mode to the structural parameter *r* can be differentiated as

$$\frac{\partial \bar{\boldsymbol{\Phi}}_i}{\partial r} = \frac{\partial \boldsymbol{\Phi}_m^p}{\partial r} \left\{\mathbf{z}_i\right\} + \boldsymbol{\Phi}_m^p \left\{\frac{\partial \mathbf{z}_i}{\partial r}\right\} \tag{5-10}$$

where $\boldsymbol{\Phi}_m^p$ represents the eigenvectors of the master modes in the substructures, $\frac{\partial \boldsymbol{\Phi}_m^p}{\partial r}$ the associated eigenvector derivatives of the master modes of the *r*th

substructure, and $\{\mathbf{z}_i\}$ the eigenvector of the reduced eigenequation. Once $\left\{\frac{\partial \mathbf{z}_i}{\partial r}\right\}$ is available, the eigenvector derivative of the *i*th mode of the global structure can be obtained.

Similar to Nelson's method, $\left\{\frac{\partial \mathbf{z}_i}{\partial r}\right\}$ is separated into the sum of a particular part and a homogeneous part as

$$\left\{\frac{\partial \mathbf{z}_i}{\partial r}\right\} = \{\mathbf{v}_i\} + c_i \{\mathbf{z}_i\} \tag{5-11}$$

where c_i is a participation factor. Substituting Eq. (5-11) into Eq. (5-2) gives the following.

$$\left(\mathbf{\Psi} - \bar{\lambda}_i \mathbf{I}\right)\left(\{\mathbf{v}_i\} + c_i \{\mathbf{z}_i\}\right) = -\frac{\partial\left(\mathbf{\Psi} - \bar{\lambda}_i \mathbf{I}\right)}{\partial r}\{\mathbf{z}_i\} \tag{5-12}$$

Given that $\left(\mathbf{\Psi} - \bar{\lambda}_i \mathbf{I}\right)\{\mathbf{z}_i\} = \{\mathbf{0}\}$, Eq. (5-12) can be simplified to

$$\left(\mathbf{\Psi} - \bar{\lambda}_i \mathbf{I}\right)\{\mathbf{v}_i\} = \{\mathbf{Y}_i\} \tag{5-13}$$

where

$$\{\mathbf{Y}_i\} = -\frac{\partial\left(\mathbf{\Psi} - \bar{\lambda}_i \mathbf{I}\right)}{\partial r}\{\mathbf{z}_i\}$$

All of the items in $\mathbf{\Psi}$ and $\{\mathbf{Y}_i\}$ were obtained during the calculation of the eigenvalue derivatives presented in the previous section.

If there are no repeated frequencies, the reduced system matrix $\mathbf{\Psi}$ takes size N_m^p and rank (N_m^p -1). To solve Eq. (5-13), the *k*th row and column of $\mathbf{\Psi}$ and *k*th item of $\{\mathbf{Y}_i\}$ are set to zero. The full rank equation is

$$\begin{bmatrix} \mathbf{\Psi}_{11} & \mathbf{0} & \mathbf{\Psi}_{13} \\ \mathbf{0} & 1 & \mathbf{0} \\ \mathbf{\Psi}_{31} & \mathbf{0} & \mathbf{\Psi}_{33} \end{bmatrix} \begin{Bmatrix} \mathbf{v}_{i1} \\ \mathbf{v}_{ik} \\ \mathbf{v}_{i3} \end{Bmatrix} = \begin{Bmatrix} \mathbf{Y}_{i1} \\ 0 \\ \mathbf{Y}_{i3} \end{Bmatrix} \tag{5-14}$$

where the pivot, *k*, is chosen at the maximum entry in $\{\mathbf{z}_i\}$. In consequence, the vector $\{\mathbf{v}_i\}$ can be solved from Eq. (5-14).

The solution of c_i requires the orthogonal condition of the eigenvector

$$\{\mathbf{z}_i\}^T \{\mathbf{z}_i\} = 1 \tag{5-15}$$

Differentiating Eq. (5-15) with respect to *r* gives

$$\frac{\partial \{\mathbf{z}_i\}^T}{\partial r} \{\mathbf{z}_i\} + \{\mathbf{z}_i\}^T \frac{\partial \{\mathbf{z}_i\}}{\partial r} = 0 \tag{5-16}$$

Substituting Eq. (5-11) into Eq. (5-16) results in

$$\left(\{\mathbf{v}_i\}^T + c_i \{\mathbf{z}_i\}^T\right)\{\mathbf{z}_i\} + \{\mathbf{z}_i\}^T \left(\{\mathbf{v}_i\} + c_i \{\mathbf{z}_i\}\right) = 0 \tag{5-17}$$

Participation factor c_i is thus obtained as

$$c_i = -\frac{1}{2}\left(\{\mathbf{v}_i\}^T \{\mathbf{z}_i\} + \{\mathbf{z}_i\}^T \{\mathbf{v}_i\}\right) \tag{5-18}$$

Finally, the first-order derivative of $\{\mathbf{z}_i\}$ with respect to the structural parameter *r* is

$$\left\{\frac{\partial \mathbf{z}_i}{\partial r}\right\} = \{\mathbf{v}_i\} - \frac{1}{2}\left(\{\mathbf{v}_i\}^T \{\mathbf{z}_i\} + \{\mathbf{z}_i\}^T \{\mathbf{v}_i\}\right)\{\mathbf{z}_i\} \tag{5-19}$$

As far as Eq. (5-10) is concerned, the eigenvector derivatives of the global structure can be regarded as the combination of the eigenvectors $\mathbf{\Phi}_m^p$ and eigenvector derivatives $\frac{\partial \mathbf{\Phi}_m^p}{\partial r}$ of the substructures, and $\left\{\frac{\partial \mathbf{z}_i}{\partial r}\right\}$ and $\mathbf{z}$ act as the weights. Similar to the calculation of the eigenvalue derivatives, that of the eigenvector derivatives of the global structure is equivalent to analyzing the *r*th substructure and a reduced eigenequation. This is a significant merit of the substructuring method, since calculation of eigensensitivity consumes dominant computation resource in usual model updating process. The procedures and advantages of the proposed substructuring method are demonstrated through two numerical examples in the following.

5.2.3 Case Studies

1) The Three-span Frame Structure

The three-span frame with three substructures described in Chapter 3, serves to illustrate the procedure of calculating the eigensensitivity using the proposed substructuring method. The influence of the master modes on the computational accuracy is also investigated.

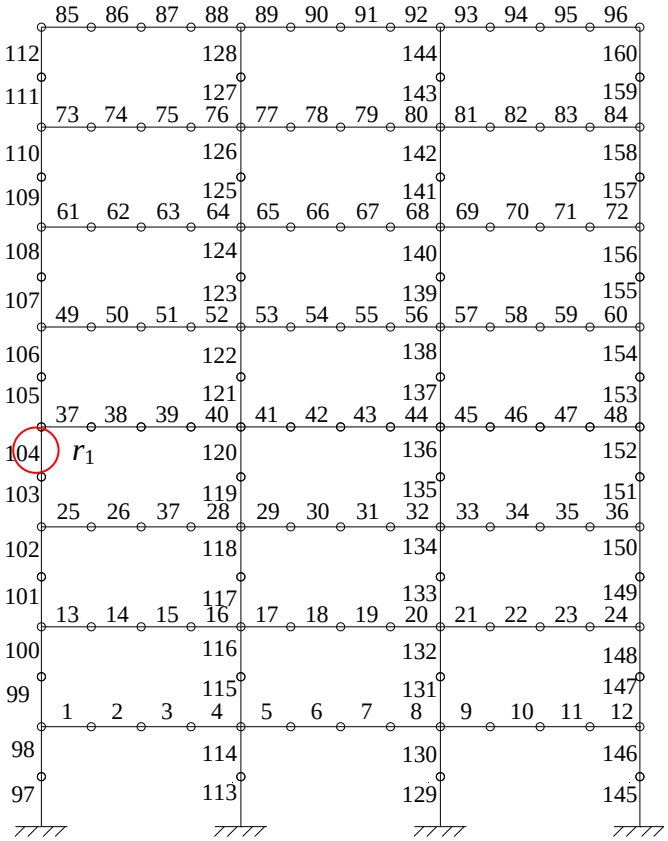

Figure 5-1: The Three-span Frame and the Designated Parameter r_1

Without losing generality, the Young's modulus of one element in Substructure 2 is arbitrarily chosen as the design parameter and denoted as r_1 in Figure 5-1. The first 30 modes of each substructure are chosen as the master modes to calculate the eigensensitivity of the first 10 modes of the global structure with respect to r_1, which can be achieved with the proposed substructuring method as follows.

(1) Calculate the eigensolutions of each substructure: $\mathbf{\Lambda}_m^{(1)}$, $\mathbf{\Lambda}_m^{(2)}$, $\mathbf{\Lambda}_m^{(3)}$, $\mathbf{\Phi}_m^{(1)}$, $\mathbf{\Phi}_m^{(2)}$, and $\mathbf{\Phi}_m^{(3)}$ (m = 1, 2, …, 30), obtain the eigensolutions of the global structure with the reduced eigenequation Eq. (5-1) as $\bar{\lambda}_i$ and $\{\mathbf{z}_i\}$, and recover the eigenvector of the global structure through $\bar{\mathbf{\Phi}}_i = \mathbf{\Phi}_m^p \{\mathbf{z}_i\}$ (i = 1, 2, …, 10).

(2) Compute the eigenvalue and eigenvector derivatives of the first 30 modes of Substructure 2 with respect to parameter r_1: $\frac{\partial \mathbf{\Lambda}_m^{(2)}}{\partial r_1}, \frac{\partial \mathbf{\Phi}_m^{(2)}}{\partial r_1}$, and calculate the derivative of the residual flexibility with respect to r_1: $\frac{\partial \left(\mathbf{\Phi}_s^{(2)} \left(\mathbf{\Lambda}_s^{(2)} \right)^{-1} \left[\mathbf{\Phi}_s^{(2)} \right]^T \right)}{\partial r_1}$.

Since Substructure 2 is free after partition, the rigid body modes are taken into account to calculate the derivative of the residual flexibility matrix as described in Appendix E.

(3) Set the derivatives of the eigensolutions and residual flexibility of the other two substructures to zeros: $\frac{\partial \mathbf{\Lambda}_m^{(j)}}{\partial r_1} = [\mathbf{0}]$, $\frac{\partial \mathbf{\Phi}_m^{(j)}}{\partial r_1} = [\mathbf{0}]$, $\frac{\partial \left(\mathbf{\Phi}_s^{(j)} \left(\mathbf{\Lambda}_s^{(j)} \right)^{-1} \left[\mathbf{\Phi}_s^{(j)} \right]^T \right)}{\partial r_1} = [\mathbf{0}]$, ($j$ = 1, 3), and then construct the primitive form of the derivative matrices as

$$\frac{\partial \left[\mathbf{\Lambda}_m^p \right]}{\partial r_1} = \begin{bmatrix} \mathbf{0} & \mathbf{0} & \mathbf{0} \\ \mathbf{0} & \frac{\partial \mathbf{\Lambda}_m^{(2)}}{\partial r_1} & \mathbf{0} \\ \mathbf{0} & \mathbf{0} & \mathbf{0} \end{bmatrix}, \quad \frac{\partial \left[\mathbf{\Phi}_m^p \right]}{\partial r_1} = \begin{bmatrix} \mathbf{0} & \mathbf{0} & \mathbf{0} \\ \mathbf{0} & \frac{\partial \mathbf{\Phi}_m^{(2)}}{\partial r_1} & \mathbf{0} \\ \mathbf{0} & \mathbf{0} & \mathbf{0} \end{bmatrix},$$

$$\frac{\partial \left[\left(\mathbf{\Phi}_s^p \left(\mathbf{\Lambda}_s^p \right)^{-1} \left[\mathbf{\Phi}_s^p \right]^T \right) \right]}{\partial r_1} = \begin{bmatrix} \mathbf{0} & \mathbf{0} & \mathbf{0} \\ \mathbf{0} & \frac{\partial \left(\mathbf{\Phi}_s^{(2)} \left(\mathbf{\Lambda}_s^{(2)} \right)^{-1} \left[\mathbf{\Phi}_s^{(2)} \right]^T \right)}{\partial r_1} & \mathbf{0} \\ \mathbf{0} & \mathbf{0} & \mathbf{0} \end{bmatrix}.$$

(4) Obtain the first-order eigenvalue derivatives of the global structure: $\frac{\partial \bar{\lambda}_i}{\partial r_1}$ (i = 1, 2, …, 10), using Eq. (5-4).

(5) Calculate the first-order derivatives of $\{\mathbf{z}_i\}$ with respect to parameter r_1: $\left\{\frac{\partial \mathbf{z}_i}{\partial r_1}\right\}$, using Eq. (5-19).

(6) Form the eigenvector derivatives of the global structure with respect to parameter r_1 using Eq. (5-10) and then eliminate the identical values of $\frac{\partial \bar{\mathbf{\Phi}}_i}{\partial r}$ at the interfaces of the substructures.

To verify the accuracy of the proposed substructuring method in calculation of the eigensensitivity, the traditional Nelson's method is employed to calculate the eigensensitivity of the global structure directly, that is, without division into individual substructures. The results from the proposed substructuring method and the global method are compared in Table 5-1. The relative errors of the eigenvalue derivatives are less than 3%, which is sufficient for most practical engineering applications.

Following MAC, the similarity of the eigenvector derivatives obtained with the global method and the proposed substructuring method is denoted as the Correlation of Eigenvector Derivatives (COED), and is given by

$$\mathrm{COED}\left(\left\{\frac{\partial \phi_i}{\partial r_1}\right\},\left\{\frac{\partial \tilde{\phi}_i}{\partial r_1}\right\}\right)=\frac{\left|\left\{\frac{\partial \phi_i}{\partial r_1}\right\}^T\left\{\frac{\partial \tilde{\phi}_i}{\partial r_1}\right\}\right|^2}{\left(\left\{\frac{\partial \phi_i}{\partial r_1}\right\}^T\left\{\frac{\partial \phi_i}{\partial r_1}\right\}\right)\left(\left\{\frac{\partial \tilde{\phi}_i}{\partial r_1}\right\}^T\left\{\frac{\partial \tilde{\phi}_i}{\partial r_1}\right\}\right)} \tag{5-20}$$

where $\left\{\frac{\partial \phi_i}{\partial r_1}\right\}$ represents the eigenvector derivative obtained with the global method, and $\left\{\frac{\partial \tilde{\phi}_i}{\partial r_1}\right\}$ that with the substructuring method. In this example, the COED values for most modes are above 0.99 as shown in Table 5-1, which indicates that the proposed method can achieve good accuracy eigenvector derivative calculation.

Table 5-1: Comparison of Eigensensitivity with Respect to r_1

Mode	Eigenvalue derivatives			Correlation of eigenvector derivatives (COED)
	Nelson's method	Substructuring method	Difference (%)	
1	0.876	0.876	0.00%	0.999
2	3.621	3.622	0.02%	0.999
3	3.431	3.433	0.07%	0.992
4	49.478	49.567	0.18%	0.997
5	72.918	73.650	1.00%	0.997
6	292.125	294.986	0.98%	0.995
7	219.068	220.354	0.59%	0.999
8	742.183	756.540	1.93%	0.995
9	675.675	689.697	2.08%	0.987
10	526.273	535.207	1.70%	0.981

The master modes retained in the substructures undoubtedly affect the accuracy of the calculated eigensensitivity. Herein, 10 master modes and 50 master modes are additionally employed for each substructure to calculate the eigensensitivity. Figure 5-2 reports the relative errors of the eigenvalue derivatives using 10, 30 and 50 master modes, respectively. The accuracy of eigenvector derivatives are compared in Figure 5-3 in terms of COED values. It can be found that, as expected, the use of more master modes improves the accuracy of the eigensolution derivatives, especially for the higher modes. The master modes retained in each substructure are usually 2~3 times that of the interest modes of the global structure. Too few master modes may result in undesirable results. Retaining 50 master modes in each substructure slightly improves the results from 30 master modes in terms of accuracy, while consumes more computation time. The computational efficiency of the proposed method will be investigated using a relatively large structure in the next section.

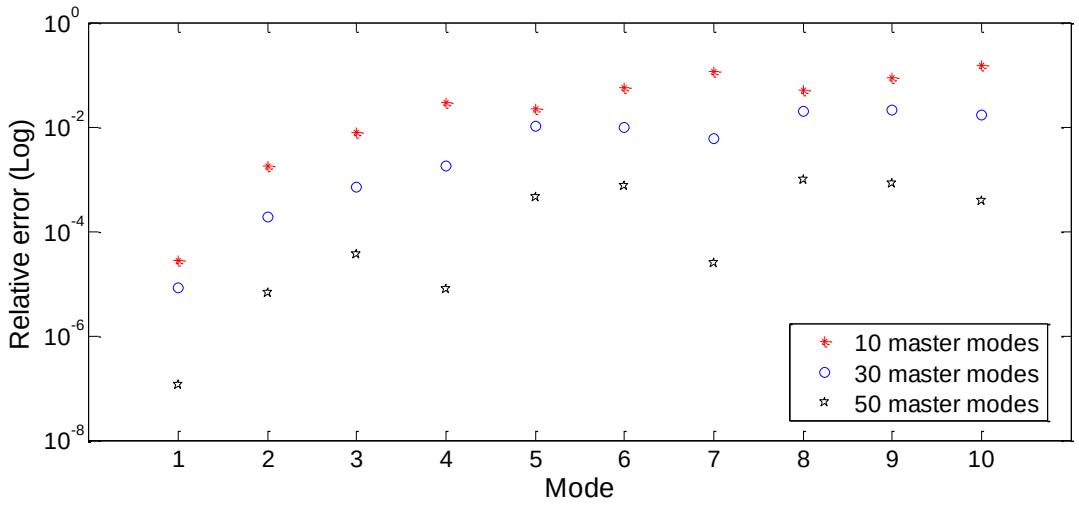

Figure 5-2: Accuracy of the Eigenvalue Derivatives with Different Master Modes

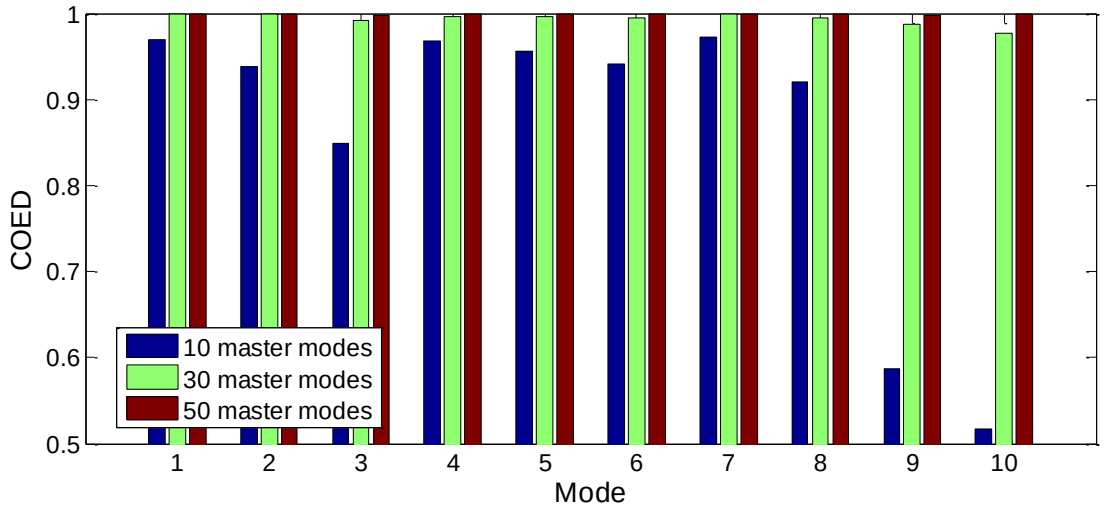

Figure 5-3: Accuracy of the Eigenvector Derivatives with Different Master Modes

2) The Balla Balla River Bridge

The Balla Balla River Bridge with 11 substructures as shown in Figure 5-4 is employed to investigate the accuracy and efficiency of the present substructuring method for eigensensitivity. Details of these 11 substructures are provided in Table 4-7. 50 master modes are retained in each substructure to assemble the global structure.

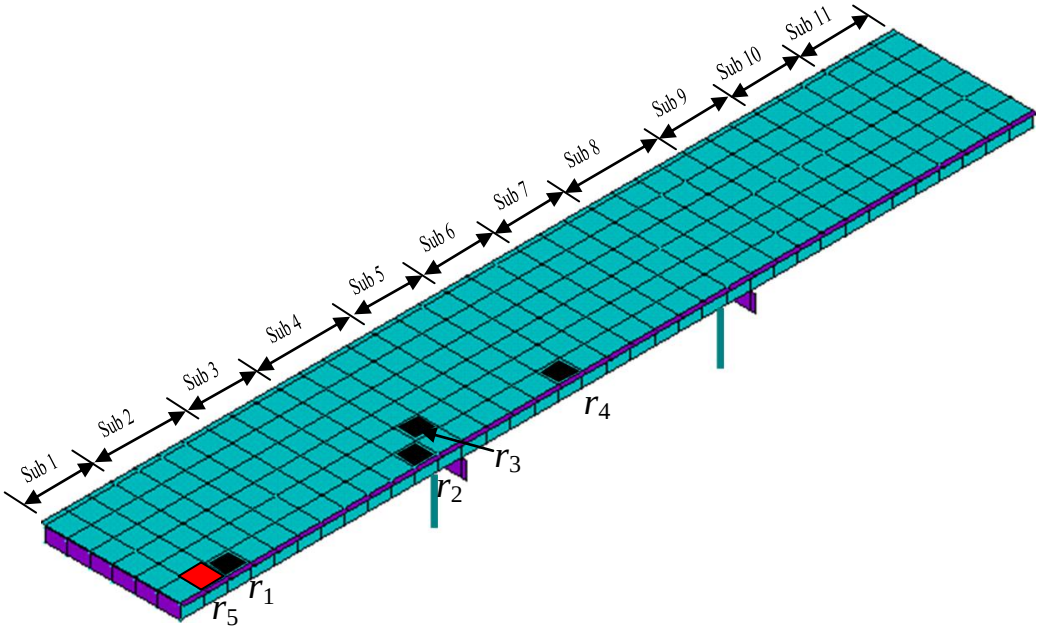

Figure 5-4: FE Model of the Balla Balla River Bridge and the Designated Parameters

The designed elemental parameters refer to the Young's moduli of the four shell elements denoted as r_1~r_4 in Figure 5-4. The elemental parameters are intentionally located in different substructures, within both the free substructures and fixed substructures. Using the proposed substructuring method, the eigensensitivities of the first 20 modes of the global structure with respect to the four elemental parameters are calculated and shown in Table 5-2. Those eigensensitivities with the global method are directly calculated using the traditional Nelson's method for comparison purpose. It can be seen from the table that, when the global structure is divided into 11 substructures and the first 50 modes are retained as the master modes in each, most of errors of the first 20 eigenvalue derivatives are less than 0.1%, and the COED values are greater than 0.99, which is acceptable in most engineering applications, such as model updating.

Table 5-2: Eigensensitivity with Respect to the Four Designed Structural Parameters

	r_1				r_2				r_3				r_4			
	Eigenvalue derivatives				Eigenvalue derivatives				Eigenvalue derivatives				Eigenvalue derivatives			
Mode	Global method (10^{-2})	Present method (10^{-2})	Relative error (%)	COED	Global method (10^{-2})	Present method (10^{-2})	Relative error (%)	COED	Global method (10^{-2})	Present method (10^{-2})	Relative error (%)	COED	Global method (10^{-2})	Present method (10^{-2})	Relative error (%)	COED
1	121.13	121.24	0.09%	0.989	223.79	223.99	0.09%	0.995	188.36	188.20	0.10%	0.997	378.76	378.89	0.03%	0.998
2	0.67	0.67	0.00%	1.000	0.18	0.18	0.00%	1.000	0.05	0.05	0.00%	1.000	0.02	0.02	0.00%	1.000
3	2.43	2.43	0.00%	1.000	7.35	7.34	0.14%	1.000	5.85	5.84	0.11%	1.000	6.91	6.89	0.28%	1.000
4	120.99	121.02	0.03%	0.973	329.45	329.46	0.00%	0.990	247.13	247.21	0.03%	0.997	374.17	373.96	0.06%	0.998
5	0.16	0.16	0.00%	0.997	0.48	0.48	0.00%	0.999	0.33	0.33	0.00%	0.999	0.37	0.37	0.00%	0.999
6	5.19	5.20	0.26%	0.995	9.17	9.19	0.26%	0.999	5.43	5.43	0.00%	0.999	14.31	14.33	0.14%	0.999
7	241.73	241.75	0.01%	0.960	140.42	140.44	0.02%	0.992	39.40	39.38	0.05%	0.997	4.21	4.20	0.26%	0.998
8	112.24	112.26	0.02%	0.976	468.14	468.18	0.02%	0.995	155.04	155.04	0.00%	0.999	1193.00	1194.77	0.15%	0.999
9	321.56	321.59	0.01%	0.990	566.79	566.83	0.01%	0.999	121.18	121.08	0.08%	0.999	8.72	8.73	0.13%	0.999
10	140.96	141.00	0.02%	0.997	23.86	23.84	0.09%	0.999	43.89	43.89	0.00%	0.999	559.87	559.77	0.02%	0.999
11	151.98	152.01	0.02%	0.969	73.59	73.62	0.03%	0.995	66.51	66.51	0.00%	0.999	314.84	314.73	0.03%	0.999
12	0.05	0.05	0.00%	1.000	0.06	0.06	0.00%	1.000	0.03	0.03	0.00%	1.000	0.00	0.00	0.00%	1.000
13	0.03	0.03	0.00%	1.000	0.05	0.05	0.00%	1.000	0.02	0.02	0.00%	1.000	0.18	0.18	0.00%	1.000
14	238.87	239.01	0.06%	0.993	179.95	179.80	0.22%	0.992	241.79	241.09	0.03%	0.996	754.21	745.73	1.12%	0.990
15	805.96	805.98	0.00%	0.998	874.12	873.25	0.10%	0.998	1090.01	1088.32	0.02%	0.998	76.32	76.66	0.39%	0.997
16	566.15	567.23	0.19%	0.998	760.02	760.64	0.08%	0.998	894.03	898.99	0.05%	0.999	227.23	226.81	0.02%	0.998
17	48.60	48.57	0.06%	0.970	678.54	677.02	0.22%	0.954	572.98	573.61	0.11%	0.948	4.78	4.74	0.82%	0.984
18	611.82	611.41	0.06%	0.979	1498.32	1496.84	0.11%	0.963	655.92	639.04	2.57%	0.969	1277.09	1281.57	0.36%	0.971
19	589.08	590.99	0.32%	0.984	11.90	11.77	1.06%	0.976	41.22	41.49	0.66%	0.997	170.75	169.89	0.51%	0.986
20	649.76	651.47	0.26%	0.987	792.71	790.86	0.29%	0.993	1265.73	1260.49	0.45%	0.996	3364.71	3360.68	0.16%	0.982

Table 5-3: Division Formation with 15 Substructures

Substructure Index	Sub 1	Sub 2	Sub 3	Sub 4	Sub 5	Sub 6	Sub 7	Sub 8	Sub 9	Sub 10	Sub 11	Sub 12	Sub 13	Sub 14	Sub 15
Geometric range (m)*	0~3	3~ 7.5	7.5~ 10.5	10.5~ 13.5	13.5~ 16.5	16.5~ 19.5	19.5~ 22.5	22.5~ 27	27~ 30	30~ 34.5	34.5~ 37.5	37.5~ 40.5	40.5~ 45	45~ 49.5	49.5~ 54
No. of elements	77	66	44	44	44	72	44	66	44	66	72	44	66	66	92
No. of nodes	90	92	69	69	69	97	69	92	69	92	97	69	92	92	113
No. of interface nodes	23	23	23	23	23	23	23	23	23	23	23	23	23	23	23

Note:* in longitudinal direction.

Here, the computational efficiency is evaluated in terms of the computation time in calculation of the eigensensitivities with respect to the four designed elemental parameters. The computational efficiency is affected by the division formation of the substructures. To investigate the effects of the division formation, the bridge is also divided into 5, 8, and 15 substructures, respectively. Details of the different division formations are provided in Table 4-3, Table 4-6, and Table 5-3.

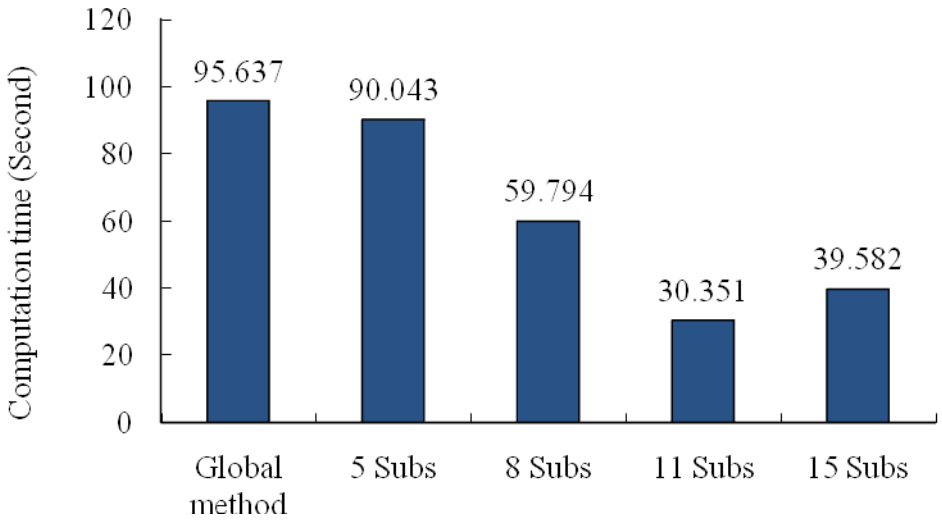

Figure 5-5: Computation Time with Different Division Formations

Selection of different master modes for the four division formations results in different levels of precision. Therefore, the relative errors of the first 20 eigenvalue derivatives of the global structure are set to less than 3% as compared with the conventional global method. Based on this criterion, 80 master modes are required in each substructure with the division formation of five substructures, 60 master modes in eight substructures, 50 master modes in 11 substructures, and 50 master modes in 15 substructures. The computation time required for the eigensensitivity calculation using the conventional global method and the proposed substructuring method with the four division schemes is compared in Figure 5-5, from which the following can be observed.

(1) Relative to the traditional global method, the proposed substructuring method reduces the computation time because only a particular substructure and the reduced eigenequation need to analyze when forming the eigensensitivity of the global structure.

(2) The computational efficiency of the proposed method is heavily dependent on the substructure division. For example, dividing the global structure into five or eight substructures requires greater computational time than does dividing it into 11 because large substructures take longer to handle than smaller ones. However, dividing it into 15 substructures is less efficient than dividing it into 11 because an excessive number of substructures lead to a large connection matrix **C** and large primitive matrices of the substructures, which renders the transformations among these matrices more computationally expensive. This phenomenon has also been observed in calculation of the eigensolutions in Chapter 4. The trade-off between the number of substructures and the size of each deserves caution, and the division formation can be tested prior to applying the proposed method to a model updating process.

5.3 High-Order Eigensolution Derivatives

The first-order eigensensitivities are usually calculated by researchers, and they are

estimated in previous sections with substructuring manner. The second- and high-order derivatives of the eigenpairs are particularly important to the case when large variations in design parameters exist or the natural frequencies are closely spaced. For the case of large changes in design parameters, the linear approximation inherent in the use of first-order derivatives may be inadequate for the sensitivity-based model updating, and the high-order derivatives need to be taken account. The eigensensitivity with repeated or close eigenvalues usually requires the second-order derivatives, or even high-order derivatives.

Due to the symmetric property and simple form of the reduced eigenequation (Eq. (5-1)), it is easy to derive the high-order derivatives of the eigensolutions by directly re-differentiating this reduced eigenequation. In this section, the second-order eigenvalue and eigenvector derivatives are formulated with the substructuring method, which can be easily extended to the high-order eigensensitivity.

5.3.1 Eigenvalue Derivative

Without losing generality, Eq. (5-1) is differentiated with respect to two design variables r_j and r_k as

$$\frac{\partial^2\left(\mathbf{\Psi}-\bar{\lambda}_i\mathbf{I}\right)}{\partial r_j \partial r_k}\left\{\mathbf{z}_i\right\}+\frac{\partial\left(\mathbf{\Psi}-\bar{\lambda}_i\mathbf{I}\right)}{\partial r_j}\frac{\partial\left\{\mathbf{z}_i\right\}}{\partial r_k}+\frac{\partial\left(\mathbf{\Psi}-\bar{\lambda}_i\mathbf{I}\right)}{\partial r_k}\frac{\partial\left\{\mathbf{z}_i\right\}}{\partial r_j}+\left(\mathbf{\Psi}-\bar{\lambda}_i\mathbf{I}\right)\frac{\partial^2\left\{\mathbf{z}_i\right\}}{\partial r_j \partial r_k}=\mathbf{0} \quad (5\text{-}21)$$

Premultiplying $\left\{\mathbf{z}_i^T\right\}$ on both sides of Eq. (5-21) gives the second-order eigenvalue derivative

$$\frac{\partial^2\bar{\lambda}_i}{\partial r_j \partial r_k}=\left\{\mathbf{z}_i^T\right\}\frac{\partial^2\mathbf{\Psi}}{\partial r_j \partial r_k}\left\{\mathbf{z}_i\right\}+\left\{\mathbf{z}_i^T\right\}\frac{\partial\left(\mathbf{\Psi}-\bar{\lambda}_i\mathbf{I}\right)}{\partial r_j}\frac{\partial\left\{\mathbf{z}_i\right\}}{\partial r_k}+\left\{\mathbf{z}_i^T\right\}\frac{\partial\left(\mathbf{\Psi}-\bar{\lambda}_i\mathbf{I}\right)}{\partial r_k}\frac{\partial\left\{\mathbf{z}_i\right\}}{\partial r_j} \quad (5\text{-}22)$$

In Eq. (5-22), the second-order eigenvalue derivative comprises two parts: the component of the second-order derivative $\frac{\partial^2\mathbf{\Psi}}{\partial r_j \partial r_k}$, and the multiplication of the first-order derivative matrix. The latter could be obtained from the previous section,

while the former $\frac{\partial^2 \boldsymbol{\Psi}}{\partial r_j \partial r_k}$ is calculated as follows.

$\frac{\partial^2 \boldsymbol{\Psi}}{\partial r_j \partial r_k}$ is contributed by the second-order eigenvalue derivatives, eigenvector derivatives and residual flexibility derivatives of the substructures as

$$\frac{\partial^2 \boldsymbol{\Psi}}{\partial r_j \partial r_k} = \frac{\partial^2 \left[\boldsymbol{\Lambda}_m^p + \boldsymbol{\Gamma}_m \left(\boldsymbol{\Gamma}_s^T \left(\boldsymbol{\Lambda}_s^p \right)^{-1} \boldsymbol{\Gamma}_s \right)^{-1} \boldsymbol{\Gamma}_m^T \right]}{\partial r_j \partial r_k} = \frac{\partial^2 \boldsymbol{\Lambda}_m^p}{\partial r_j \partial r_k} + \frac{\partial^2 \left(\boldsymbol{\Gamma}_m \left(\boldsymbol{\Gamma}_s^T \left(\boldsymbol{\Lambda}_s^p \right)^{-1} \boldsymbol{\Gamma}_s \right)^{-1} \boldsymbol{\Gamma}_m^T \right)}{\partial r_j \partial r_k} \tag{5-23}$$

Concerning Eq. (5-5), the second-order derivative of $\boldsymbol{\Gamma}_m \left(\boldsymbol{\Gamma}_s^T \left(\boldsymbol{\Lambda}_s^p \right)^{-1} \boldsymbol{\Gamma}_s \right)^{-1} \boldsymbol{\Gamma}_m^T$ gives

$$\begin{aligned} &\frac{\partial^2 \left(\boldsymbol{\Gamma}_m \left(\boldsymbol{\Gamma}_s^T \left(\boldsymbol{\Lambda}_s^p \right)^{-1} \boldsymbol{\Gamma}_s \right)^{-1} \boldsymbol{\Gamma}_m^T \right)}{\partial r_j \partial r_k} \\ &= \left[\boldsymbol{\Gamma}_m \frac{\partial^2 \left[\left(\boldsymbol{\Gamma}_s^T \left(\boldsymbol{\Lambda}_s^p \right)^{-1} \boldsymbol{\Gamma}_s \right)^{-1} \right]}{\partial r_j \partial r_k} \boldsymbol{\Gamma}_m^T + 2 \boldsymbol{\Gamma}_m \frac{\partial \left[\left(\boldsymbol{\Gamma}_s^T \left(\boldsymbol{\Lambda}_s^p \right)^{-1} \boldsymbol{\Gamma}_s \right)^{-1} \right]}{\partial r_j} \frac{\partial \boldsymbol{\Gamma}_m^T}{\partial r_k} \right] \\ &+ 2 \left[\frac{\boldsymbol{\Gamma}_m}{\partial r_k} \left(\boldsymbol{\Gamma}_s^T \left(\boldsymbol{\Lambda}_s^p \right)^{-1} \boldsymbol{\Gamma}_s \right)^{-1} \frac{\partial \boldsymbol{\Gamma}_m^T}{\partial r_j} + \boldsymbol{\Gamma}_m \frac{\partial \left(\boldsymbol{\Gamma}_s^T \left(\boldsymbol{\Lambda}_s^p \right)^{-1} \boldsymbol{\Gamma}_s \right)^{-1}}{\partial r_k} \frac{\partial \boldsymbol{\Gamma}_m^T}{\partial r_j} + \boldsymbol{\Gamma}_m \left(\boldsymbol{\Gamma}_s^T \left(\boldsymbol{\Lambda}_s^p \right)^{-1} \boldsymbol{\Gamma}_s \right)^{-1} \frac{\partial^2 \boldsymbol{\Gamma}_m^T}{\partial r_j \partial r_k} \right] \end{aligned} \tag{5-24}$$

In Eq. (5-24), the second-order derivative matrix of the inversion of the residual flexibility is given by

$$\begin{aligned} &\frac{\partial \left[\left(\boldsymbol{\Gamma}_s^T \left(\boldsymbol{\Lambda}_s^p \right)^{-1} \boldsymbol{\Gamma}_s \right)^{-1} \right]}{\partial r_j \partial r_k} = - \left(\boldsymbol{\Gamma}_s^T \left(\boldsymbol{\Lambda}_s^p \right)^{-1} \boldsymbol{\Gamma}_s \right)^{-2} \frac{\partial \left(\left(\mathbf{K}^p \right)^{-1} - \boldsymbol{\Phi}_m^p \left(\boldsymbol{\Lambda}_m^p \right)^{-1} \left[\boldsymbol{\Phi}_m^p \right]^T \right)}{\partial r_j \partial r_k} \\ &+ 2 \left(\boldsymbol{\Gamma}_s^T \left(\boldsymbol{\Lambda}_s^p \right)^{-1} \boldsymbol{\Gamma}_s \right)^{-3} \frac{\partial \left(\boldsymbol{\Gamma}_s^T \left(\boldsymbol{\Lambda}_s^p \right)^{-1} \boldsymbol{\Gamma}_s \right)}{\partial r_j} \frac{\partial \left(\boldsymbol{\Gamma}_s^T \left(\boldsymbol{\Lambda}_s^p \right)^{-1} \boldsymbol{\Gamma}_s \right)}{\partial r_k} \end{aligned} \tag{5-25}$$

where $\frac{\partial\left(\boldsymbol{\Phi}_m^p\left(\boldsymbol{\Lambda}_m^p\right)^{-1}\left[\boldsymbol{\Phi}_m^p\right]^T\right)}{\partial r_j \partial r_k}$ can be obtained from the derivatives of the master modes of the substructures as

$$\frac{\partial\left(\boldsymbol{\Phi}_m^p\left(\boldsymbol{\Lambda}_m^p\right)^{-1}\left[\boldsymbol{\Phi}_m^p\right]^T\right)}{\partial r_j \partial r_k}$$

$$= -\boldsymbol{\Phi}_m^p\left(\boldsymbol{\Lambda}_m^p\right)^{-1}\frac{\partial^2\boldsymbol{\Lambda}_m^p}{\partial r_j \partial r_k}\left(\boldsymbol{\Lambda}_m^p\right)^{-1}\left[\boldsymbol{\Phi}_m^p\right]^T - 2\boldsymbol{\Phi}_m^p\left(\boldsymbol{\Lambda}_m^p\right)^{-1}\frac{\partial\boldsymbol{\Lambda}_m^p}{\partial r_j}\frac{\partial\left(\boldsymbol{\Lambda}_m^p\right)^{-1}}{\partial r_k}\left[\boldsymbol{\Phi}_m^p\right]^T - 2\boldsymbol{\Phi}_m^p\left(\boldsymbol{\Lambda}_m^p\right)^{-1}\frac{\partial\boldsymbol{\Lambda}_m^p}{\partial r_j}\left(\boldsymbol{\Lambda}_m^p\right)^{-1}\frac{\partial\left[\boldsymbol{\Phi}_m^p\right]^T}{\partial r_k}$$

$$+2\left[\frac{\boldsymbol{\Phi}_m^p}{\partial r_k}\left(\boldsymbol{\Lambda}_m^p\right)^{-1}\frac{\partial\left[\boldsymbol{\Phi}_m^p\right]^T}{\partial r_j} + \boldsymbol{\Phi}_m^p\frac{\partial\left(\boldsymbol{\Lambda}_m^p\right)^{-1}}{\partial r_k}\frac{\partial\left[\boldsymbol{\Phi}_m^p\right]^T}{\partial r_j} + \boldsymbol{\Phi}_m^p\left(\boldsymbol{\Lambda}_m^p\right)^{-1}\frac{\partial^2\left[\boldsymbol{\Phi}_m^p\right]^T}{\partial r_j \partial r_k}\right] \qquad (5\text{-}26)$$

It is seen that, the derivative matrix $\frac{\partial^2\boldsymbol{\Psi}}{\partial r_j \partial r_k}$ is contributed by two kinds of derivative matrices. The first group is the second-order derivative matrices of the substructures, such as $\frac{\partial^2\boldsymbol{\Lambda}_m^p}{\partial r_j \partial r_k}$, $\frac{\partial^2\boldsymbol{\Gamma}_m^T}{\partial r_j \partial r_k}$ and $\frac{\partial^2\left[\left(\boldsymbol{\Gamma}_s^T\left(\boldsymbol{\Lambda}_s^p\right)^{-1}\boldsymbol{\Gamma}_s\right)^{-1}\right]}{\partial r_j \partial r_k}$. The second group is the multiplication of the first-order derivative matrices, for example, the multiplication of $\frac{\partial\left[\left(\boldsymbol{\Gamma}_s^T\left(\boldsymbol{\Lambda}_s^p\right)^{-1}\boldsymbol{\Gamma}_s\right)^{-1}\right]}{\partial r_j}$ and $\frac{\partial\boldsymbol{\Gamma}_m^T}{\partial r_k}$, and the multiplication involved $\frac{\partial\boldsymbol{\Gamma}_m^T}{\partial r_j}$ and $\frac{\partial\boldsymbol{\Gamma}_m^T}{\partial r_k}$.

In the former group, $\frac{\partial^2\boldsymbol{\Lambda}_m^p}{\partial r_j \partial r_k}$, $\frac{\partial^2\boldsymbol{\Gamma}_m^T}{\partial r_j \partial r_k}$ are respectively the second-order eigenvalue derivatives and eigenvector derivatives of the master modes in substructures, and $\frac{\partial^2\left[\left(\boldsymbol{\Gamma}_s^T\left(\boldsymbol{\Lambda}_s^p\right)^{-1}\boldsymbol{\Gamma}_s\right)^{-1}\right]}{\partial r_j \partial r_k}$ are associated with the second-order derivatives of the

substructural residual flexibility. If r_j and r_k are located in the same substructure (for example, the rth substructure), the three items are calculated for the rth substructure solely, while those corresponding to the other substructures are zero, i.e.,

$$\frac{\partial^2 \mathbf{\Lambda}_m^p}{\partial r_j \partial r_k} = \begin{bmatrix} \mathbf{0} & \mathbf{0} & \mathbf{0} \\ \mathbf{0} & \dfrac{\partial^2 \mathbf{\Lambda}_m^{(r)}}{\partial r_j \partial r_k} & \mathbf{0} \\ \mathbf{0} & \mathbf{0} & \mathbf{0} \end{bmatrix}, \quad \frac{\partial^2 \mathbf{\Gamma}_m^T}{\partial r_j \partial r_k} = \mathbf{C} \frac{\partial^2 \mathbf{\Phi}_m^p}{\partial r_j \partial r_k} = \mathbf{C} \begin{bmatrix} \mathbf{0} & \mathbf{0} & \mathbf{0} \\ \mathbf{0} & \dfrac{\partial^2 \mathbf{\Phi}_m^{(r)}}{\partial r_j \partial r_k} & \mathbf{0} \\ \mathbf{0} & \mathbf{0} & \mathbf{0} \end{bmatrix},$$

$$\frac{\partial^2 \left(\mathbf{\Gamma}_s^T \left(\mathbf{\Lambda}_s^p \right)^{-1} \mathbf{\Gamma}_s \right)}{\partial r_j \partial r_k} = \mathbf{C} \frac{\partial^2 \left(\mathbf{\Phi}_s^p \left(\mathbf{\Lambda}_s^p \right)^{-1} \left[\mathbf{\Phi}_s^p \right]^T \right)}{\partial r_j \partial r_k} \mathbf{C}^T = \mathbf{C} \begin{bmatrix} \mathbf{0} & \mathbf{0} & \mathbf{0} \\ \mathbf{0} & \dfrac{\partial^2 \left(\mathbf{\Phi}_s^{(r)} \left(\mathbf{\Lambda}_s^{(r)} \right)^{-1} \left[\mathbf{\Phi}_s^{(r)} \right]^T \right)}{\partial r_j \partial r_k} & \mathbf{0} \\ \mathbf{0} & \mathbf{0} & \mathbf{0} \end{bmatrix} \mathbf{C} \tag{5-27}$$

In case that r_j and r_k are located in different substructures, the second-order derivative matrices $\dfrac{\partial^2 \mathbf{\Lambda}_m^p}{\partial r_j \partial r_k}$, $\dfrac{\partial^2 \mathbf{\Gamma}_m^T}{\partial r_j \partial r_k}$ and $\dfrac{\partial^2 \left(\mathbf{\Gamma}_s^T \left(\mathbf{\Lambda}_s^p \right)^{-1} \mathbf{\Gamma}_s \right)}{\partial r_j \partial r_k}$ are zero-matrix.

In the latter group, the primitive form of the first-order derivative matrices of the residual flexibility and eigenvectors: $\dfrac{\partial \left(\mathbf{\Gamma}_s^T \left(\mathbf{\Lambda}_s^p \right)^{-1} \mathbf{\Gamma}_s \right)}{\partial r_j}$ and $\dfrac{\partial \mathbf{\Gamma}_m^T}{\partial r_k}$, are diagonal assembly of the derivative matrices of the substructures. They are non-zeros only in the sub-block corresponding to the substructures which include the parameters r_j or r_k as stated in Section 5.2. Therefore, if r_j and r_k are located in different substructures, the multiplication of them gives zero-matrix as well.

To conclude, if the designed variables r_j and r_k are located in different substructures, all items in $\dfrac{\partial^2 \mathbf{\Psi}}{\partial r_j \partial r_k}$ are zeros, i.e.,

$$\frac{\partial^2 \boldsymbol{\Psi}}{\partial r_j \partial r_k} = \frac{\partial^2 \boldsymbol{\Lambda}_m^p}{\partial r_j \partial r_k} + \frac{\partial^2 \left[\boldsymbol{\Gamma}_m \left(\boldsymbol{\Gamma}_s^T \left(\boldsymbol{\Lambda}_s^p \right)^{-1} \boldsymbol{\Gamma}_s \right)^{-1} \boldsymbol{\Gamma}_m^T \right]}{\partial r_j \partial r_k} = \mathbf{0} \tag{5-28}$$

In this case, the second-order derivative of the eigenvalue is simplified into

$$\begin{aligned} \frac{\partial^2 \bar{\lambda}_i}{\partial r_j \partial r_k} &= \left\{ \mathbf{z}_i^T \right\} \frac{\partial^2 \boldsymbol{\Psi}}{\partial r_j \partial r_k} \left\{ \mathbf{z}_i \right\} + \left\{ \mathbf{z}_i^T \right\} \frac{\partial \left(\boldsymbol{\Psi} - \bar{\lambda}_i \right)}{\partial r_j} \frac{\partial \left\{ \mathbf{z}_i \right\}}{\partial r_k} + \left\{ \mathbf{z}_i^T \right\} \frac{\partial \left(\boldsymbol{\Psi} - \bar{\lambda}_i \right)}{\partial r_k} \frac{\partial \left\{ \mathbf{z}_i \right\}}{\partial r_j} \\ &= 2 \left\{ \mathbf{z}_i \right\}^T \frac{\partial \left(\boldsymbol{\Psi} - \bar{\lambda}_i \right)}{\partial r_j} \frac{\partial \left\{ \mathbf{z}_i \right\}}{\partial r_k} \end{aligned} \tag{5-29}$$

If the design variables r_j and r_k are located in the same substructure (for example the rth substructure). Items $\frac{\partial^2 \boldsymbol{\Lambda}_m^p}{\partial r_j \partial r_k}$, $\frac{\partial^2 \boldsymbol{\Gamma}_m^T}{\partial r_j \partial r_k}$ and $\frac{\partial^2 \left(\boldsymbol{\Gamma}_s^T \left(\boldsymbol{\Lambda}_s^p \right)^{-1} \boldsymbol{\Gamma}_s \right)}{\partial r_j \partial r_k}$ are assembled using the derivative matrices of the rth substructure solely. $\frac{\partial^2 \boldsymbol{\Lambda}_m^p}{\partial r_j \partial r_k}$ and $\frac{\partial \boldsymbol{\Gamma}_m^T}{\partial r_j \partial r_k}$ can be calculated with the traditional method addressed in Appendix B, by treating the rth substructure as an independent structure. Subsequently, $\frac{\partial^2 \boldsymbol{\Psi}}{\partial r_j \partial r_k}$ can be formed by the second-order derivative matrices and the multiplication of the first-order derivative matrices within the rth substructure.

In the proposed substructuring method, the second-order eigenvalue derivative can be expressed by the first-order derivative matrices of the substructural eigensolutions and residual flexibility, if the two parameters r_j and r_k are located in different substructures. In case that the two parameters r_j and r_k are located in the same substructure, the first- and second-order derivative matrices of the master eigensolutions and residual flexibility of only one substructure are required.

5.3.2 Eigenvector Derivative

The ith eigenvector of the global structure can be recovered by

$$\bar{\boldsymbol{\Phi}}_i = \boldsymbol{\Phi}_m^p \{\mathbf{z}_i\} \tag{5-30}$$

The second-order eigenvector derivative of the *i*th mode with respect to the two parameters r_j and r_k is acquired as

$$\frac{\partial^2 \bar{\boldsymbol{\Phi}}_i}{\partial r_j \partial r_k} = \frac{\partial^2 \boldsymbol{\Phi}_m^p}{\partial r_j \partial r_k}\{\mathbf{z}_i\} + \frac{\partial \boldsymbol{\Phi}_m^p}{\partial r_j}\frac{\partial \{\mathbf{z}_i\}}{\partial r_k} + \frac{\partial \boldsymbol{\Phi}_m^p}{\partial r_k}\frac{\partial \{\mathbf{z}_i\}}{\partial r_j} + \boldsymbol{\Phi}_m^p \frac{\partial^2 \{\mathbf{z}_i\}}{\partial r_j \partial r_k} \tag{5-31}$$

All items are available based on the previous analysis, except $\frac{\partial^2 \mathbf{z}_i}{\partial r_j \partial r_k}$.

The double-differentiated eigenequation (Eq. (5-21)) is rewritten as

$$\left(\boldsymbol{\Psi} - \bar{\lambda}_i \mathbf{I}\right)\frac{\partial^2 \{\mathbf{z}_i\}}{\partial r_j \partial r_k} = \left\{\mathbf{Y}_{i(j,k)}\right\} \tag{5-32}$$

where

$$\left\{\mathbf{Y}_{i(j,k)}\right\} = \frac{\partial^2 \left(\boldsymbol{\Psi} - \bar{\lambda}_i \mathbf{I}\right)}{\partial r_j \partial r_k}\{\mathbf{z}_i\} + \frac{\partial \left(\boldsymbol{\Psi} - \bar{\lambda}_i \mathbf{I}\right)}{\partial r_j}\frac{\partial \{\mathbf{z}_i\}}{\partial r_k} + \frac{\partial \left(\boldsymbol{\Psi} - \bar{\lambda}_i \mathbf{I}\right)}{\partial r_k}\frac{\partial \{\mathbf{z}_i\}}{\partial r_j} \tag{5-33}$$

$\left\{\mathbf{Y}_{i(j,k)}\right\}$ can be obtained directly using the interim results when calculating the eigenvalue derivatives.

As before, $\frac{\partial^2 \{\mathbf{z}_i\}}{\partial r_j \partial r_k}$ is expressed as the sum of a particular part and a homogeneous part as

$$\frac{\partial^2 \{\mathbf{z}_i\}}{\partial r_j \partial r_k} = \left\{\mathbf{v}_{i(j,k)}\right\} + c_{i(j,k)}\{\mathbf{z}_i\} \tag{5-34}$$

where $\left\{\mathbf{v}_{i(j,k)}\right\}$ is not unique but may be calculated by substituting Eq. (5-34) into Eq. (5-32) as

$$\left(\boldsymbol{\Psi} - \bar{\lambda}_i \mathbf{I}\right)\left\{\mathbf{v}_{i(j,k)}\right\} = \left\{\mathbf{Y}_{i(j,k)}\right\} \tag{5-35}$$

The following orthogonality property is satisfied

$$\{\mathbf{z}_i\}^T \{\mathbf{z}_i\} = 1 \tag{5-36}$$

Differentiating Eq. (5-36) with respect to r_j and r_k , and substituting Eq. (5-34) into it gives

$$2\left(\frac{\partial\{\mathbf{z}_i\}^T}{\partial r_k}\frac{\partial\{\mathbf{z}_i\}}{\partial r_j}+\{\mathbf{z}_i\}^T\left(\{\mathbf{v}_{i(j,k)}\}+c_{i(j,k)}\{\mathbf{z}_i\}\right)\right)=0$$

The participation factor $c_{i(j,k)}$ is obtained as

$$c_{i(j,k)}=-\frac{\partial\{\mathbf{z}_i\}^T}{\partial r_k}\frac{\partial\{\mathbf{z}_i\}}{\partial r_j}-\{\mathbf{z}_i\}^T\{\mathbf{v}_{i(j,k)}\} \tag{5-37}$$

Given $\{\mathbf{v}_{i(j,k)}\}$ and $c_{i(j,k)}$, the second-order eigenvector derivative can be recovered from Eq. (5-31) and Eq. (5-34). It is seen that, the second-order eigenvector derivative is obtained by solving the reduced eigenequation solely. As the calculation of eigenvector derivatives usually consumes dominant computation resource in the common global method, this substructuring method improves the computational efficiency significantly, which will be demonstrated by a numerical example.

Using similar procedures, the high-order eigensensitivity can be derived with this substructuring method easily, by further differentiating the eigenequation Eq. (5-21). They are not addressed here.

5.3.3 Case Study

The Balla Balla River Bridge (Figure 5-4) is also employed to illustrate the accuracy and efficiency of the proposed substructuring method in calculation of the second-order eigensensitivity.

The second-order eigensensitivities with respect to the parameter pairs (r_5, r_5), (r_5, r_1), and (r_5, r_2) shown in Figure 5-4 are calculated. First, the second-order eigenvalue and eigenvector derivatives of the first 20 modes are calculated using the global method addressed in Appendix B, and are regarded as the accurate results for comparison. Afterwards, they are calculated by the proposed substructuring method. The global

structure is divided into 11 substructures and each retains the first 50 modes as master. The second-order eigensensitivities using the present substructuring method are compared with the exact results in Table 5-4.

In this table, the second-order eigensolution derivatives with respect to the parameter pair (r_5, r_5) represent the case that the two elemental parameters are identical. The eigensolution derivatives with respect to (r_5, r_1) gives the results with respect to two different parameters in the same substructure, while parameter pair of (r_5, r_2) the case that the two parameters in different substructures. Table 5-4 demonstrates that the relative differences in the second-order eigenvalue derivatives using the proposed substructuring method and the global method are less than 3% for most modes.

Following the previous first-order eigenvector derivative, the accuracy of the second-order eigenvector derivative is denoted by COED as well, and is given by

$$\mathrm{COED}\left(\left\{\frac{\partial^2\phi_i}{\partial r_j\partial r_k}\right\},\left\{\frac{\partial^2\tilde{\phi}_i}{\partial r_j\partial r_k}\right\}\right)=\frac{\left|\left\{\frac{\partial^2\phi_i}{\partial r_j\partial r_k}\right\}^T\left\{\frac{\partial^2\tilde{\phi}_i}{\partial r_j\partial r_k}\right\}\right|^2}{\left(\left\{\frac{\partial^2\phi_i}{\partial r_j\partial r_k}\right\}^T\left\{\frac{\partial^2\phi_i}{\partial r_j\partial r_k}\right\}\right)\left(\left\{\frac{\partial^2\tilde{\phi}_i}{\partial r_j\partial r_k}\right\}^T\left\{\frac{\partial^2\tilde{\phi}_i}{\partial r_j\partial r_k}\right\}\right)} \qquad (5\text{-}38)$$

where $\left\{\frac{\partial^2\phi_i}{\partial r_j\partial r_k}\right\}$ represents the second-order eigenvector derivative from the global method, and $\left\{\frac{\partial^2\tilde{\phi}_i}{\partial r_j\partial r_k}\right\}$ from the substructuring method. Table 5-4 reports the COED values of most modes are above 0.95, indicating a good accuracy of the second-order eigenvector derivatives.

Table 5-4: Comparison of Second-order Eigenvalue Derivatives and Eigenvector Derivatives

Mode	$\frac{\partial^2\lambda}{\partial r_5\partial r_5}$, $\frac{\partial^2\{\phi\}}{\partial r_5\partial r_5}$				$\frac{\partial^2\lambda}{\partial r_5\partial r_1}$, $\frac{\partial^2\{\phi\}}{\partial r_5\partial r_1}$				$\frac{\partial^2\lambda}{\partial r_5\partial r_2}$, $\frac{\partial^2\{\phi\}}{\partial r_5\partial r_2}$			
	Eigenvalue derivative			COED	Eigenvalue derivative			COED	Eigenvalue derivative			COED
	Global method	Substructuring method	Relative error (%)		Global method	Substructuring method	Relative error (%)		Global method	Substructuring method	Relative error (%)	
1	-0.7010	-0.7012	0.03%	0.998	-0.0730	-0.0729	0.12%	0.996	-0.0295	-0.0296	0.21%	0.996
2	-0.0016	-0.0016	0.00%	0.999	0.0001	0.0001	0.00%	0.998	-0.0003	-0.0003	0.00%	0.993
3	-0.0030	-0.0031	0.66%	0.990	0.0008	0.0008	0.00%	0.983	0.0003	0.0003	0.00%	0.995
4	-0.1537	-0.1536	0.02%	0.985	0.0339	0.0340	0.29%	0.995	0.0036	0.0035	1.07%	0.990
5	-0.0008	-0.0008	0.00%	0.992	-0.0001	-0.0001	0.00%	0.994	0.0000	0.0000	0.00%	0.988
6	-0.0258	-0.0259	0.23%	0.992	-0.0025	-0.0025	0.00%	0.991	-0.0012	-0.0012	0.00%	0.994
7	-0.4020	-0.4022	0.05%	0.981	0.0938	0.0937	0.12%	0.986	0.0231	0.0230	0.55%	0.982
8	-0.0643	-0.0643	0.00%	0.987	0.0014	0.0014	0.00%	0.986	-0.0010	-0.0010	0.00%	0.985
9	-0.2160	-0.2168	0.36%	0.996	0.0161	0.0159	1.42%	0.985	-0.0062	-0.0065	4.90%	0.982
10	-0.1997	-0.1999	0.10%	0.974	0.0610	0.0609	0.16%	0.986	0.0502	0.0502	0.00%	0.992
11	-0.1860	-0.1864	0.22%	0.988	-0.0063	-0.0062	0.03%	0.985	0.0051	0.0053	3.22%	0.978
12	-0.0002	-0.0002	0.00%	0.981	0.0000	0.0000	0.00%	0.974	0.0000	0.0000	0.00%	0.969
13	-0.0001	-0.0001	0.00%	0.993	0.0000	0.0000	0.00%	0.970	0.0000	0.0000	0.00%	0.975
14	-1.1484	-1.1497	0.11%	0.991	-0.2129	-0.2139	0.48%	0.971	-0.1031	-0.1037	0.59%	0.985
15	-3.9496	-3.9901	1.03%	0.985	-0.7531	-0.7539	0.11%	0.980	-0.3398	-0.3401	0.08%	0.985
16	-2.4723	-2.4320	1.63%	0.986	-0.2371	-0.2343	1.17%	0.973	0.0102	0.0105	2.74%	0.987
17	-0.5327	-0.5337	0.20%	0.982	0.0462	0.0455	1.34%	0.977	-0.0066	-0.0065	1.67%	0.990
18	-4.9578	-4.9587	0.02%	0.977	-0.6186	-0.6166	0.32%	0.981	-0.1997	-0.1996	0.07%	0.980
19	-0.9347	-0.9247	1.07%	0.985	0.1271	0.1231	3.16%	0.983	-0.0093	-0.0094	1.15%	0.979
20	-1.3160	-1.3274	0.86%	0.988	-0.5541	-0.5642	1.82%	0.975	-0.3337	-0.3346	0.27%	0.974

The computational efficiency of the substructuring method is evaluated in terms of the computation time to calculate the second-order eigensensitivities with respect to the slab elements in the first substructure and all of the slab elements. That is, the first elemental parameters r_j are designated to the Young's moduli of the 24 slab element in the first substructure, and the second elemental parameters r_k are the Young's moduli of all 288 slab elements across the whole structure. Among the 288 parameters of r_k, 24 parameters are located in the first substructure, and the remainders are in the other substructures as listed in Table 5-5.

It is noted that, computation time cost by the second-order eigensensitivity encompasses those in calculation of the first-order eigensensitivity for both the global method and the substructuring method. The computation time is shown in Table 5-5. The global method totally takes up 13,427 seconds to calculate the second-order eigensensitivities with respect to the 24 parameters r_j and the 288 parameters r_k, whereas the substructuring method takes 3,594 seconds. In particular, if parameters r_j and parameters r_k are both located in the first substructure, calculating the second-order eigensensitivities with respect to the 24 parameters of r_j and 24 parameters of r_k takes 434.4 seconds. In the case that parameters r_j and r_k are located in different substructures, for example the parameters r_j are located in first substructure and the parameters r_k are located in the third, five, six, seven or nine substructure (The third, five, six, seven and nine substructures have 24 parameters r_k as well, and they have similar size with the first substructure), calculating the second-order eigensensitivity costs about 280 seconds. As expected, the parameters r_j and r_k located in the same substructure takes longer time than they are in different substructures, since the former requires the item $\frac{\partial^2 \boldsymbol{\Psi}}{\partial r_j \partial r_k}$ which is zero in the latter.

Similar to the calculation of the first-order eigensensitivity, the number of the master modes and the division formation of the substructures affect the computational accuracy and efficiency, which deserves several trials before application.

Table 5-5: Computation Time of the Global and Substructuring Methods

	Global method	Substructuring method										
		Location of parameter r_k										
		Sub 1	Sub 2	Sub 3	Sub 4	Sub 5	Sub 6	Sub 7	Sub 8	Sub 9	Sub 10	Sub 11
No. of elements	288	24	32	24	32	24	24	24	32	24	32	16
Time (Second)	13427	434.4	382.3	286.3	398.7	286.7	283.6	283.0	390.3	282.9	377.6	188.8
		3594										

5.4 Summary

In the first part of this chapter, the first-order eigenvalue derivatives and eigenvector derivatives are derived based on the reduced eigenequation of the improved substructuring method developed in Chapter 4. The eigensensitivity formula of a global structure is assembled from the eigensensitivity matrices of a particular substructure and the derivative matrix of a reduced eigenequation by emulating Nelson's method. Two numerical examples demonstrate that the proposed method can achieve a good degree of accuracy when proper master modes are retained. The division formation of the substructures also affects the accuracy. A trade-off needs to be made between the number of substructures and the size of each. Retaining more master modes in the substructures can achieve better accuracy, but result in greater computational expense.

In the second part, the second-order eigensensitivity with respect to two parameters is derived by further differentiating the reduced eigenequation. If the two parameters are located in different substructures, the first-order derivative matrices of two substructures that contain the two parameters are calculated to assemble the second-order sensitivity matrix of the global structure. In the case that the two parameters are in the same substructure, the second-order derivative matrices are solely required in the focused substructure. The high accuracy and efficiency of the substructuring method for the second-order eigensensitivity are illustrated with a

bridge structure. This substructuring method can be generalized to calculate the high-order eigensensitivity, by further differentiating the reduced eigenequation. The high-order eigensensitivity of the global structure are determined by the derivative matrix of particular substructures that contain the designated parameters. The substructuring method in calculation of eigensensitivity will be applied to model updating process in the following chapter.

CHAPTER SIX

SUBSTRUCTURING-BASED MODEL UPDATING

6.1 Introduction

Due to the uncertainties in geometry, material properties and boundary conditions, the dynamic responses of a structure predicted from a highly idealized numerical model usually differ from the practical measurements. An effective and efficient model updating is necessary to obtain a more accurate FE model to be used for various purposes.

Model updating methods are usually classified into one-step methods and iterative methods (Brownjohn *et al.* 2001). The one-step methods directly reconstruct the stiffness matrix and mass matrix of the analytical model, while the iterative methods modify the physical parameters of the FE model repeatedly to minimize the discrepancy between the analytical and experimental modal properties. The latter approach allows for the physical interpretation of the predicted parameters and the preservation of the symmetry, positive-definiteness and sparseness in the updated matrices. As a result, the iterative model updating method is adopted in this research. In the iterative model updating methods, the eigensolutions are required to construct the objective function, while the eigensensitivities serve to indicate the searching direction in each optimization step (Bakir *et al.* 2007).

The objective function combining the modal properties of the frequencies and mode shapes is usually denoted as

$$J(r)=\sum_i W_{\lambda i}^2\left[\frac{\lambda_i\left(\{r\}\right)^A-\lambda_i{}^E}{\lambda_i{}^E}\right]^2+\sum_i W_{\phi i}^2\sum_j\left[\frac{\phi_{ji}\left(\{r\}\right)^A-\phi_{ji}{}^E}{\max\left\{\phi_i{}^E\right\}}\right]^2 \quad (6\text{-}1)$$

In Eq. (6-1), the eigenvalue and the maximum value of the associated mode shape are scaled to unity for the *i*th mode; $\lambda_i{}^E$ represents the *i*th experimental eigenvalue which is the square of natural frequency, and $\phi_{ji}{}^E$ is the associated mode shape at the *j*th point; $\lambda_i{}^A$ and $\phi_{ji}{}^A$ denote the *i*th eigenvalue and mode shape of the analytical FE model, which are expressed as the function of the uncertain physical parameters $\{r\}$, and $W_{\lambda i}$ and $W_{\phi i}$ are the weight coefficients considering the different accuracy of the measured frequencies and mode shapes (Brownjohn *et al*. 2001; Bakir *et al*. 2007).

The objective function is minimized by adjusting continuously the parameters $\{r\}$ of the analytical model through optimization searching techniques. To find the optimal searching direction, the derivative matrices of the eigenvalues and mode shapes with respect to parameter *r* can be formulated as

$$\left[S_\lambda(r)\right]=\frac{\partial\lambda(r)}{\partial r},\ \left[S_\phi(r)\right]=\frac{\partial\phi(r)}{\partial r} \quad (6\text{-}2)$$

Using the substructuring approach, the eigenvalues, mode shapes, and their sensitivity matrices are calculated by the methods developed in Chapter 4 and Chapter 5.

The elemental stiffness reduction factor (SRF), p_i, is employed to indicate the change ratio of the updated parameter to the initial value before updating

$$p_i=\frac{\Delta r_i}{r_i}=\frac{r_i^U-r_i^O}{r_i^O} \quad (6\text{-}3)$$

where i = 1, 2, ..., m is the uncertain parameters. The superscript '*O*' represents the original parameters before updating and the superscript '*U*' represents the updated

values after updating. A negative SRF indicates that the updated parameter is weaker than the original one and a positive SRF indicates that the updated parameter is stronger.

The lower and upper bounds are imposed during the updating procedure. For different purposes, the bounds differ. For example, in updating an initial model in the undamaged state, the bounds are set to

$$-0.5 < p_i \leq 0.5 \qquad (6\text{-}4)$$

In the damage detection, the damaged elements are usually assumed to be weaker than the undamaged state. Consequently, the bounds are set to

$$-1 < p_i \leq 0 \qquad (6\text{-}5)$$

A negative SRF indicates the location of the damage and the magnitude quantifies the damage severity.

6.2 The Numerical Three-span Frame Structure

The three-span frame structure described in Chapter 3 is utilized here to demonstrate the effectiveness of the proposed substructuring-based model updating process. The 'experimental' frequencies and mode shapes are generated with Lanczos method on the global structure, by intentionally introducing a discrepancy on the bending rigidity of some elements. Three scenarios are considered as listed in Table 6-1.

Table 6-1: Simulated Discrepancy in the Elements

	Case 0	Case 1	Case 2
Assumed discrepancy of bending rigidity	No discrepancy	Element 147(-30%) Element 148(-30%)	Element 147(-30%) Element 148(-30%) Element 139(-20%) Element 140(-20%)

It is assumed that the first 10 modes are available, and the measurements are obtained at the points and directions denoted in Figure 6-1. The mode shapes have been

normalized to the mass matrix. The objective function is the discrepancies of both the frequencies and mode shapes between the experimental and analytical model. The weight coefficients are set to 1.0 for the frequencies and 0.1 for the mode shapes (Brownjohn *et al*. 2001; Bakir *et al*. 2007).

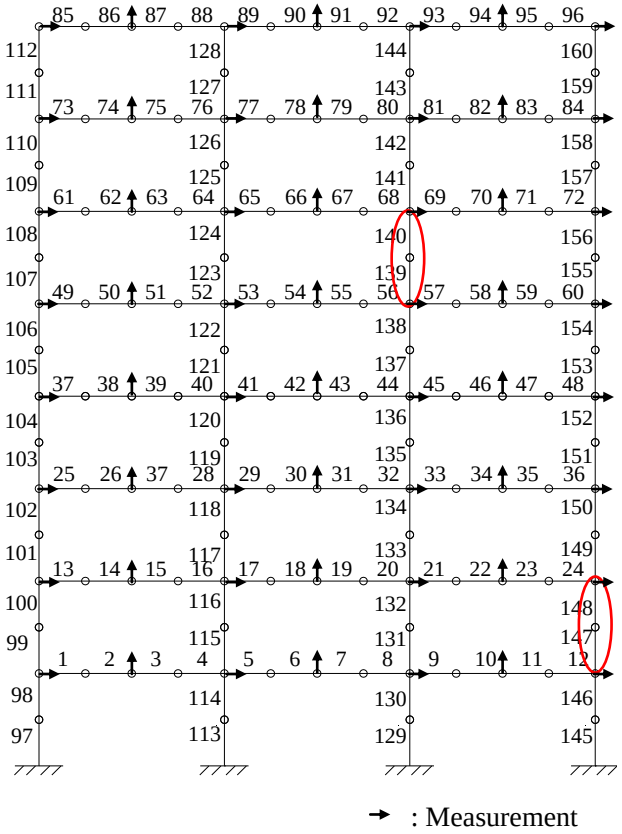

Figure 6-1: Measured DOFs and Simulated Damaged Elements of the Three-Span Frame Structure (Unit: m)

In each iteration, the eigensolutions and the eigensensitivities are calculated with the FRFS method proposed in Chapter 4 and Chapter 5. The frame is disassembled into three substructures (N_S = 3) at 8 nodes (Figure 3-3). Using the substructuring method, the first 30 modes are retained as master modes in each substructure to calculate the first 10 eigensolutions and eigensensitivities of the full-DOF global structure. The eigenmodes and eigensensitivities at the measured points are then singled out to match the 'experimental' modal data for model updating purpose. The bending rigidity of all column elements is assumed to be uncertain parameters. Accordingly, there are 64 updating parameters in total.

The optimization is processed with the trust-region method provided by the Matlab Optimization Toolbox (Zhang 2003; Bakir *et al.* 2007). The algorithm can automatically select the steps and the searching directions according to the objective function and the provided eigensensitivity matrices. The model updating process stops when the pre-defined tolerance of the objective function or the maximum number of iterations is reached.

The FRFS method introduces some slight errors in calculation of the eigensolutions and eigensensitivities, which is regarded as methodology error (Xia 2002). This methodology error is first investigated by generating the experimental data without introducing any discrepancy on the elemental parameters, as denoted Case 0 in Table 6-1. The analytical eigensolutions are calculated using the substructuring method and are compared with the experimental modal data which is generated using the traditional global method in Table 6-2. Some minor differences are found in Table 6-2, as expected. To investigate the influence of these slight differences on model updating results, model updating is conducted to find out the change in the elemental bending rigidity due to the methodology error. The identified relative change in the bending rigidity before and after updating is shown in Figure 6-2(a). It verifies that the methodology error in calculation of the eigensolutions and eigensensitivities has a negligible effect on the model updating results.

The experimental modal data is then generated by introducing certain known discrepancies in the bending rigidity of some elements, which are given in Table 6-1. In Case 1, the bending rigidity of a column in the first substructure is reduced by 30%. The frequencies and model shapes before and after updating are compared in Table 6-3, which demonstrates that the analytical modal data closely match the simulated experimental data after updating. The identified change in the elemental parameters is plotted in Figure 6-2(b), which coincides with the assumed one.

Table 6-2: Frequencies and Mode Shapes of the Frame with the Proposed Substructuring Method (Case 0)

Modes	Experimental frequencies (Hz)	Analytical frequencies (Hz)	Diff. (%)	MAC
1	1.7843	1.7843	0.000%	1.0000
2	5.5365	5.5365	0.000%	1.0000
3	9.8198	9.8199	0.001%	0.9999
4	14.6864	14.6867	0.002%	0.9999
5	16.6188	16.6485	0.179%	0.9967
6	18.8074	18.8420	0.184%	0.9958
7	20.1977	20.1983	0.003%	0.9999
8	22.6170	22.6690	0.230%	0.9949
9	25.4704	25.5241	0.211%	0.9941
10	26.1799	26.1862	0.024%	0.9986

Without losing generality, the elements located in different substructures are assumed to have some known discrepancy as well. In Case 2, the bending rigidity of two columns, which are located in different substructures, is reduced by 30% and 20%, respectively. The frequencies and mode shapes before and after updating are compared in Table 6-4, and the identified change in bending rigidity is shown in Figure 6-2(c). After updating, the frequencies and mode shapes of the analytical model reproduce the simulated experimental modal data accurately, and the identified change in the elemental parameters agrees with the assumed one very well.

Both Case 1 and Case 2 verify that, using the proposed substructuring method, the location and severity of the assumed discrepancy in elemental parameters can be successfully identified after updating. The proposed substructuring method is effective to be applied in model updating process. It again proves that the influence of the errors due to FRFS method is insignificant, when proper size of the master modes is retained. One can improve the accuracy of the eigensolutions and eigensensitivities by including more master modes in the substructures as demonstrated in Chapter 4 and Chapter 5.

Table 6-3: Frequencies and Mode Shapes of the Frame Structure Before and After Updating (Case 1)

Modes	Experimental frequencies (Hz)	Before updating			After updating		
		Analytical frequencies (Hz)	Diff. (%)	MAC	Analytical frequencies (Hz)	Diff. (%)	MAC
1	1.7800	1.7843	0.24%	1.0000	1.7803	0.01%	1.0000
2	5.5263	5.5365	0.18%	1.0000	5.5274	0.02%	1.0000
3	9.8055	9.8199	0.15%	0.9999	9.8048	0.01%	1.0000
4	14.6566	14.6867	0.21%	0.9998	14.6572	0.00%	1.0000
5	16.5682	16.6485	0.49%	0.9934	16.5633	0.03%	1.0000
6	18.6379	18.8420	1.10%	0.9897	18.6339	0.02%	1.0000
7	20.1435	20.1983	0.27%	0.9995	20.1453	0.01%	1.0000
8	22.2818	22.6690	1.74%	0.9838	22.2844	0.01%	1.0000
9	25.2257	25.5241	1.18%	0.9791	25.2280	0.01%	0.9999
10	26.0476	26.1862	0.53%	0.9934	26.0457	0.01%	1.0000

Table 6-4: Frequencies and Mode Shapes of the Frame Structure Before and After Updating (Case 2)

Modes	Experimental frequencies (Hz)	Before updating			After updating		
		Analytical frequencies (Hz)	Diff. (%)	MAC	Analytical frequencies (Hz)	Diff. (%)	MAC
1	1.7783	1.7843	0.34%	1.0000	1.7786	0.02%	1.0000
2	5.5089	5.5365	0.50%	1.0000	5.5100	0.02%	1.0000
3	9.7976	9.8199	0.23%	0.9998	9.7971	0.01%	1.0000
4	14.6183	14.6867	0.47%	0.9997	14.6243	0.04%	1.0000
5	16.5153	16.6485	0.81%	0.9927	16.5212	0.04%	1.0000
6	18.6042	18.8420	1.28%	0.9875	18.6008	0.02%	1.0000
7	20.0675	20.1983	0.65%	0.9987	20.0755	0.04%	1.0000
8	22.2570	22.6690	1.85%	0.9816	22.2602	0.01%	1.0000
9	25.1976	25.5241	1.30%	0.9775	25.1877	0.04%	0.9999
10	26.0313	26.1862	0.60%	0.9936	26.0383	0.03%	0.9999

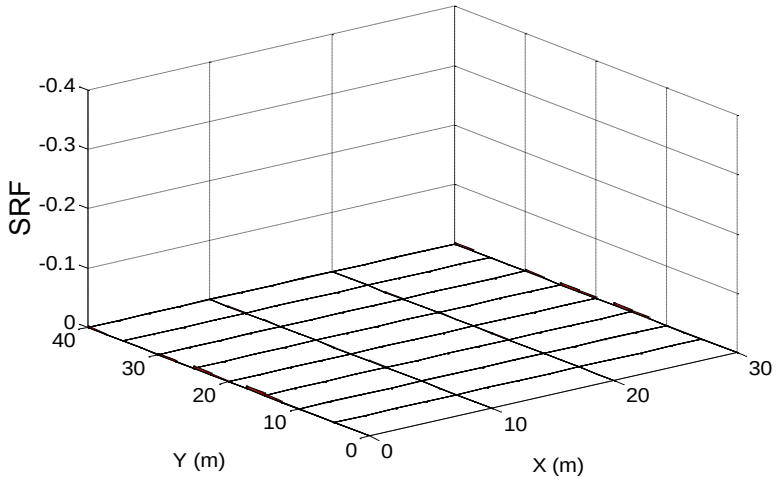

(a) Case 0

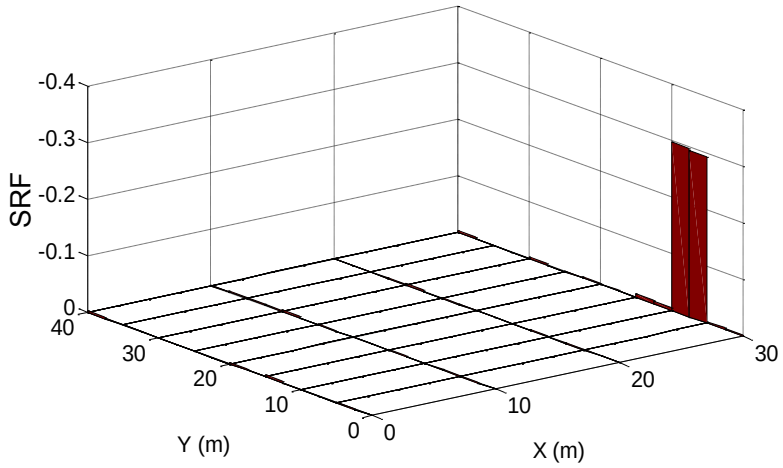

(b) Case 1

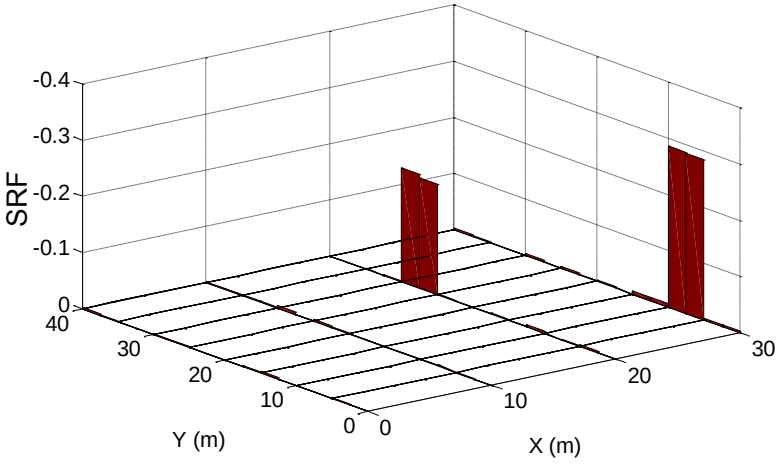

(c) Case 2

Figure 6-2: Location and Severity of Elemental Stiffness Reduction for Different Damage Configurations

6.3 The Experimental Frame Structure

In this section, the substructuring-based model updating approach is applied to the laboratory-tested frame structure. The frame structure is first updated using the measured modal data in the undamaged state, and the refined model is subsequently used for damage identification. The experimental set-ups and the results are provided in Chapter 3.

The frame is modelled by 44 nodes and 45 two-dimensional elements as shown in Figure 6-3, and each element is 100 mm in length. In experimental testing, the accelerometers are arranged at the nodes to measure the translational vibration.

The Young's moduli of all 45 elements are updated, with the initial values setting to 2×10^{11} Pa. The analytical model is separated into three substructures, as shown in Figure 6-3. Accordingly, three are 17 updating parameters in the first substructure, 15 in the second and 13 in the third. The first 30 modes in each substructure are chosen as the master modes to calculate the first 25 eigensolutions and eigensensitivities of the global structure. It is noted that in the range of 0 ~ 400Hz only 14 modes were measured in the experiment and some modes may be missed. The eigensolutions are calculated using the FRFS method proposed in Chapter 4 and the eigensensitivity are calculated employing the substructuring method proposed in Chapter 5. Concerning this relatively small structure, inclusion of 30 master modes in each substructure can provide sufficient accurate results since an independent substructure has about 50 eigenmodes in total.

Using the eigensolutions and eigensensitivities calculated with the substructirng method, the analytical model is tuned to match the 14 frequencies and mode shapes measured in the experiment (Figure 3-19) through an optimization process. The

weight coefficients are set to 1.0 for the frequencies and 0.1 for the mode shapes. The frequencies and MAC values of mode shapes before and after updating are compared with the measured data in Table 6-5, which reveals that the updated model is better at representing the real frame structure. Figure 6-4 reports the SRF values of the three substructures after updating. It is noted that the change in bending rigidity of all elements are less than 10%.

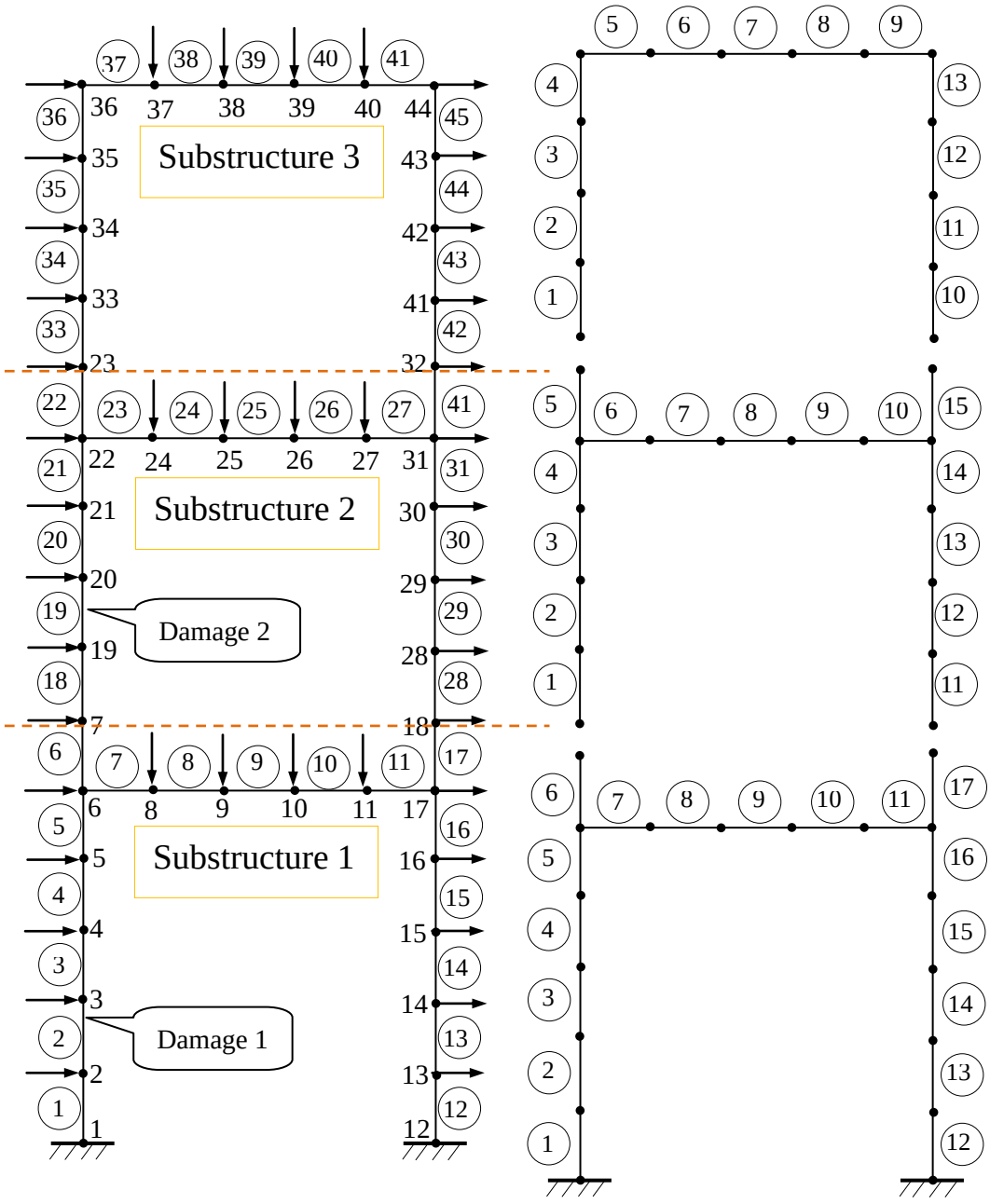

Figure 6-3: Analytical Model of the Laboratory Frame Structure and the Updating Substructures

Afterwards, the model improved in the undamaged state is used for damage identification. Two damage configurations were introduced artificially. The mass loss due to the cuts is ignored in the analytical model. In the first damage configuration, the cut is located in the first substructure. In consequence, only the 17 elemental parameters in Substructure 1 are adjusted to ensure the analytical modal data match the measured modal data, whereas Substructure 2 and Substructure 3 are used directly without change. As before, the first 30 modes are retained in each substructure to calculate the first 25 eigensolutions and eigensensitivities of the global structure, which are compared with the 14 eigenmodes measured in the experiment through the optimization process. In each iteration, only the first substructure is re-analyzed, and is then assembled together with the second and third substructures that remain unchanged through the whole process to calculate the eigensolutions of global structure. The substructural eigensensitivity matrices with respect to the 17 parameters are calculated for the first substructure solely whereas those in the second and third substructures are zero-matrix. The substructural eigensensitivity matrices are then assembled to obtain the eigensensitivity of the global structure.

The identified SRF values are shown in Figure 6-5, and the frequencies and mode shapes before and after updating are compared in Table 6-6. It is seen that, Element 2 has an obvious reduction in stiffness, which agrees with the location of the cut in the experiment. Other undamaged elements are incorrectly identified with small SRFs, which may due to the measurement noise, methodology errors and modelling errors.

It should be noted that the magnitude of SRF indicates the damage severity of the element. Here Element 2 has an SRF of about 20%. This, however, represents the overall equivalent reduction in the elemental bending rigidity due to the local cut with 60% decrease in width. It is difficult to use one single global parameter to quantify the local damage.

In the second damage configuration, the two cuts are located in the first and second substructures, respectively. Consequently, the first and second substructures are updated, while the third substructure remains unchanged. The SRF values are demonstrated in Figure 6-6. The frequencies and mode shapes after updating match better with the measured ones than those before updating as compared in Table 6-7.

In Figure 6-6, Element 2 in the first substructure and Element 2 in the second substructure are found with significant SRFs. The identified locations coincide with the cuts in the experiment. The SRF of Element 2 in the first storey is about -23%, similar to that identified in the first damage configuration, because the cut is unchanged in the two damage configurations.

Table 6-5: Frequencies and Mode Shapes Before and After Updating (Undamaged State)

Mode	Analytical modes	Measured frequency (Hz)	Before updating			After updating		
			Frequency (Hz)	Diff. (%)	MAC	Frequency (Hz)	Diff. (%)	MAC
1	1	3.12	3.16	1.27%	0.993	3.11	-0.22%	0.997
2	2	9.11	9.23	1.27%	0.976	9.15	0.45%	0.997
3	3	14.34	14.04	-2.13%	0.989	14.32	-0.20%	0.998
4	4	52.46	50.42	-3.88%	0.981	52.51	0.09%	0.989
5	5	58.18	56.51	-2.87%	0.980	58.50	0.55%	0.988
6	6	66.80	64.34	-3.68%	0.871	66.86	0.09%	0.972
7	7	71.65	70.80	-1.18%	0.928	71.49	-0.23%	0.994
8	8	82.14	82.51	0.45%	0.877	82.13	-0.01%	0.938
9	9	82.87	80.98	-2.29%	0.885	83.36	0.59%	0.989
10	16	200.13	211.12	5.49%	0.919	204.83	2.35%	0.963
11	17	222.36	215.91	-2.90%	0.920	218.88	-1.56%	0.984
12	18	226.55	220.37	-2.73%	0.913	225.15	-0.62%	0.965
13	19	236.58	230.60	-2.53%	0.905	235.49	-0.46%	0.975
14	22	383.33	395.44	3.16%	0.903	385.19	0.48%	0.964
average				2.56%	0.932		0.56%	0.980

[a] Average of absolute value.

Table 6-6: Frequencies and Mode Shapes Before and After Updating (Damaged State 1)

Mode	Analytical modes	Measured frequency (Hz)	Before updating			After updating		
			Frequency (Hz)	Diff. (%)	MAC	Frequency (Hz)	Diff. (%)	MAC
1	1	3.11	3.11	0.00%	0.991	3.11	-0.00%	0.992
2	2	9.09	9.15	0.65%	0.994	9.12	0.27%	0.996
3	3	14.34	14.32	-0.17%	0.993	14.32	-0.13%	0.996
4	4	52.24	52.51	0.51%	0.998	52.42	0.34%	0.994
5	5	57.72	58.50	1.34%	0.982	58.08	0.62%	0.983
6	6	66.73	66.86	0.20%	0.973	66.65	-0.11%	0.983
7	7	71.28	71.49	0.29%	0.989	71.15	-0.18%	0.990
8	8	81.60	82.13	0.65%	0.872	81.90	0.37%	0.939
9	9	82.19	83.36	1.43%	0.870	82.07	-0.14%	0.945
10	16	199.70	204.83	2.57%	0.934	201.02	0.66%	0.952
11	17	220.93	218.88	-0.93%	0.876	221.51	0.26%	0.944
12	18	224.97	225.15	0.08%	0.854	224.92	-0.02%	0.932
13	19	234.78	235.49	0.30%	0.954	235.18	0.17%	0.953
14	22	382.50	385.19	0.70%	0.927	381.05	-0.38%	0.967
Average				0.71%	0.943		0.27%	0.969

[a] Average of absolute value.

Table 6-7: Frequencies and Mode Shapes Before and After Updating (Damaged State 2)

Mode	Analytical modes	Measured frequency (Hz)	Before updating			After updating		
			Frequency (Hz)	Diff. (%)	MAC	Frequency (Hz)	Diff. (%)	MAC
1	1	3.11	3.11	0.00%	0.996	3.11	0.00%	0.995
2	2	9.09	9.15	0.68%	0.994	9.09	-0.07%	0.995
3	3	14.33	14.32	-0.13%	0.993	14.26	-0.53%	0.996
4	4	51.88	52.51	1.20%	0.989	52.32	0.84%	0.990
5	5	57.41	58.50	1.90%	0.946	57.04	-0.64%	0.973
6	6	66.48	66.86	0.57%	0.906	66.40	-0.13%	0.972
7	7	70.73	71.49	1.08%	0.954	70.47	-0.37%	0.970
8	8	80.99	82.13	1.41%	0.862	81.64	0.80%	0.946
9	9	81.98	83.36	1.69%	0.850	82.08	0.13%	0.944
10	16	199.11	204.83	2.87%	0.928	200.78	0.84%	0.972
11	17	220.03	218.88	-0.52%	0.925	219.36	-0.31%	0.972
12	18	224.14	225.15	0.45%	0.872	224.42	0.12%	0.959
13	19	233.50	235.49	0.85%	0.904	233.97	0.20%	0.948
14	22	376.49	385.19	2.31%	0.911	378.78	0.61%	0.961
Average				1.14%	0.931		0.41%	0.971

[a] Average of absolute value.

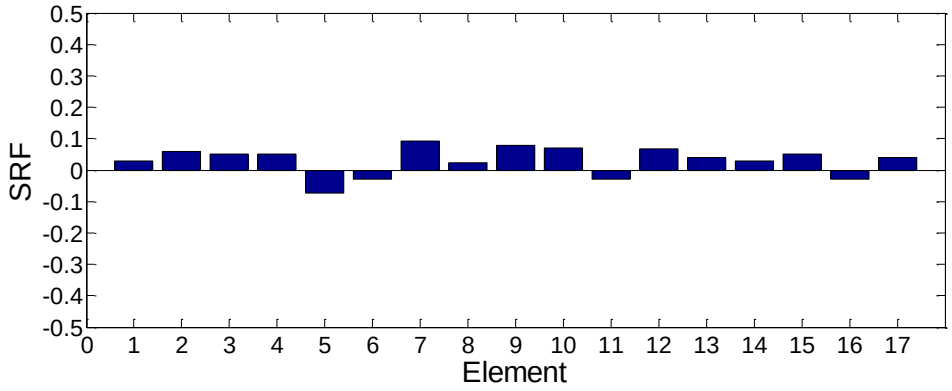

(a) First Substructure

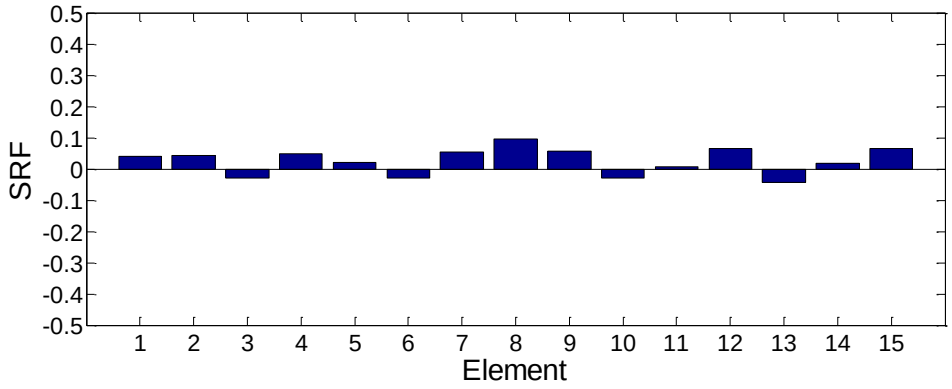

(b) Second Substructure

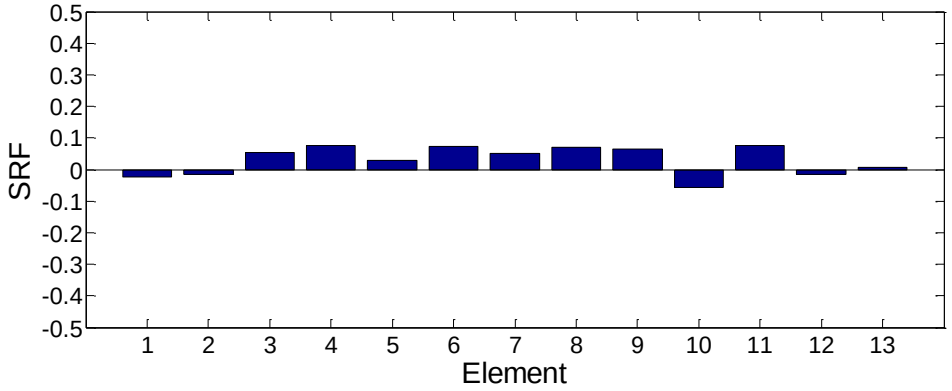

(c) Third Substructure

Figure 6-4: SRF Values of the Three Substructures in the Undamaged State

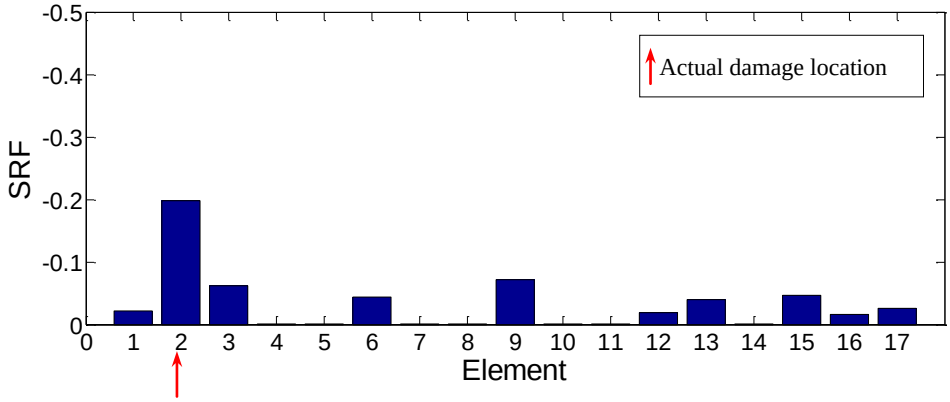

Figure 6-5: SRF Values of the First Damage Configuration (First Substructure)

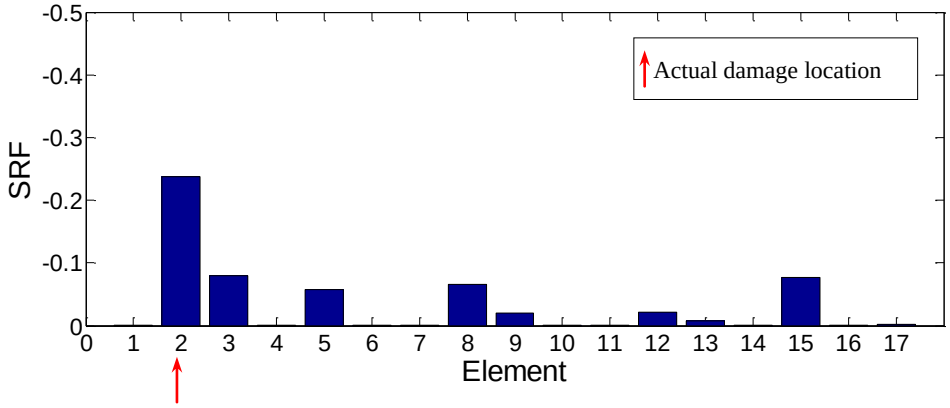

(a) First Substructure

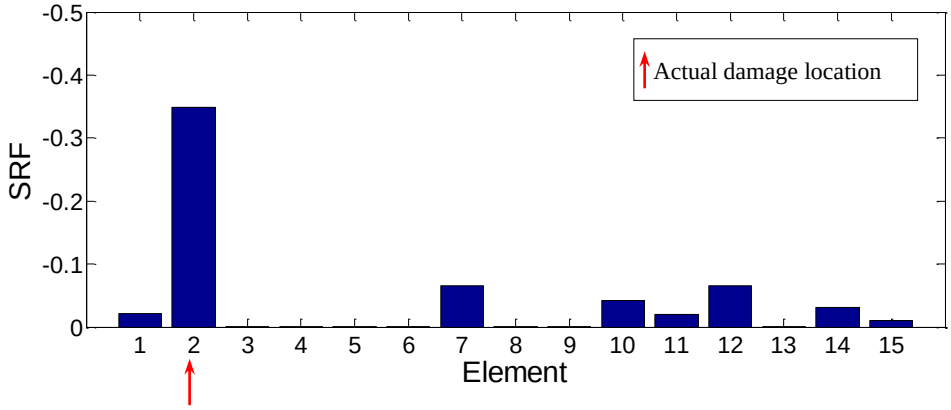

(b) Second Substructure

Figure 6-6: SRF Values of the Second Damage Configuration

The SRF of Element 2 in the second substructure is identified to have -35%. The reduction ratio is larger than the damage that in the first substructure, although the two cuts have the same depth and width. This is because the cuts are at different locations of the elements. In particular, the cut in the first substructure is 80 mm away from the bottom of the element while that in the second substructure is 50 mm away from the bottom of the element. The SRF value represents the overall equivalent reduction in the elemental stiffness due to the local cut. A cut in different location of an element has different effect on the equivalent stiffness reduction of that element. Nevertheless, the present method can locate damage correctly.

6.4 The Balla Balla River Bridge

The Balla Balla River Bridge is employed here, to illustrate the feasibility and computational efficiency of the proposed substructuring method in real structures. A field vibration test was conducted to extract the first 10 natural frequencies and mode shapes at 133 points on the bridge deck (Xia *et al.* 2008). An FE model based on design drawings was established. Here the analytical model will be updated using both the traditional global method and the proposed substructuring method to investigate the effectiveness and efficiency of the substructuring method in practical model updating.

There are 1289 physical parameters selected as updating candidates, which include the Young's modulus (E) of diaphragms, girders, slabs, and the axial rigidty (EA) and bending rigidity (EI_{xx}, EI_{yy}) of the shear connectors. The objective function in this example combines the differences in the frequencies and mode shapes between the experimental data and the analytical model. The weight coefficients are set to be 0.1 for the mode shapes and 1.0 for the frequencies.

Using the traditional model updating method, the eigensolutions and

eigensensitivities are calculated based on the system matrices of the global structure employing the Lanczos method and the Nelson's method. The first 30 global eigenmodes are extracted from the FE model to match the 10 experimental modes. The model updating process is terminated after 69 iterations, which costs about 86.16 hours on an ordinary personal computer and one iteration takes about 1.26 hours. The convergence process in terms of the norm of the objective function is demonstrated in Figure 6-7. The updating details and results can be found in Xia *et al*. (2008).

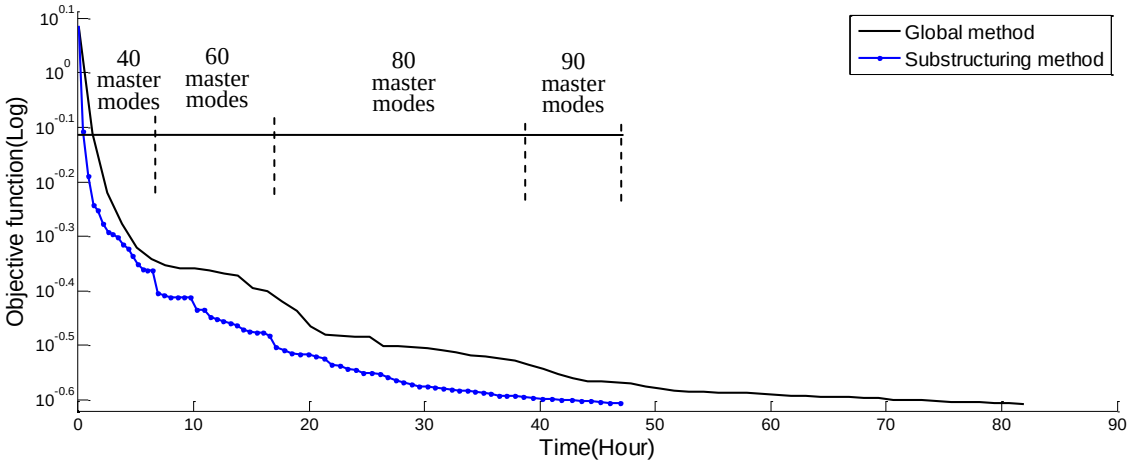

Figure 6-7: Convergence of the Model Updating Process with the Substructuring Method and the Global Method

Afterwards, the substructuring method is employed to calculate the eigensolutions and eigensensitivities of the global structure for model updating. The optimization algorithm, updating parameters, and convergence criterion are the same as those used in the previous traditional model updating. In Chapter 5, it was proved that dividing the bridge structure into 11 substructures could achieve higher computational efficiency than other division formations in calculation of the eigensensitivity. Since the eigensensitivities usually consume dominant computation time in model updating process, the global structure is thus divided into 11 substructures along the longitudinal direction. Division of substructures can be referred to Figure 5-4 and Table 4-7.

As stated in Chapter 4 and Chapter 5, size of master modes retained in the substructures influences the accuracy of the eigensolutions and eigensensitivities, and thus affects the convergence of the model updating process. To balance the accuracy and efficiency, different number of master modes is retained in the substructures according to the progress of the model updating. At the beginning, the first 40 modes of each substructure are retained as master modes to calculate the first 30 eigensolutions and eigensensitivities of the global structure. The number of master modes retained in the substructures then increases gradually as the convergence slows down. At the final several steps, 90 modes are retained in each substructure to improve the accuracy of the eigensolutions and eigensensitivities. With this adaptive scheme, the substructuring-based model updating process is completed within 76 iterations and the convergence process is plotted in Figure 6-7. The computation time spent on different stages is listed in Table 6-8 and totals about 48.07 hours, which is about 56% of that using the global model updating.

Table 6-8: Computation Time and Number of Iterations with the Different Master Modes

	Global method	Substructuring method			
		40 master modes	60 master modes	80 master modes	90 master modes
Time for each iteration (Hour)	1.26	0.43	0.57	0.69	0.84
No. of iterations	69	16	18	31	11
Total for the updating process (Hour)	86.16	48.07			

The frequencies and mode shapes of the updated structure are compared with those values before updating as listed in Table 6-9. It is observed that the substructuring method can achieve similar results as the global method. In particular, the averaged

difference in frequencies between the updated model and the experimental measurement is less than 1%. The MAC values are improved from 0.85 to 0.93. Therefore, even for the practical structure with a large number of updating parameters, the proposed substructuring-based model updating method is computationally efficient and accurate.

Table 6-9: The Frequencies and Mode Shapes of the Bridge Before and After Updating

Mode	Measured Freq. (Hz)	Before updating			After updating					
					Global method			Substructuring method		
		Freq. (Hz)	Diff. (%)	MAC	Freq. (Hz)	Diff. (%)	MAC	Freq. (Hz)	Diff. (%)	MAC
1	6.76	6.26	-7.34%	0.93	6.53	-3.47%	0.95	6.55	-3.17%	0.95
2	7.95	7.74	-0.27%	0.96	7.93	-0.27%	0.99	7.92	-0.33%	0.99
3	10.06	8.71	-13.37%	0.71	10.02	-0.42%	0.94	10.02	-0.39%	0.94
4	10.75	12.13	12.84%	0.80	11.01	2.42%	0.89	11.03	2.60%	0.89
5	11.03	9.45	-14.36%	0.76	10.86	-1.56%	0.82	10.85	-1.60%	0.81
6	12.64	13.27	4.98%	0.85	12.58	-0.45%	0.97	12.59	-0.38%	0.96
7	14.71	17.55	19.29%	0.92	14.77	0.38%	0.90	14.78	0.45%	0.90
8	15.76	18.52	17.49%	0.88	15.77	0.06%	0.93	15.77	0.06%	0.94
9	16.39	18.74	14.35%	0.82	16.38	-0.07%	0.95	16.39	0.00%	0.95
10	20.18	24.91	23.42%	0.86	20.23	0.24%	0.92	20.28	0.50%	0.93
Averaged			12.77%	0.85		0.93%	0.93		0.95%	0.93

6.5 Summary

This chapter presents a substructuring-based model updating procedure, in which the eigensolutions and the eigensensitivities are calculated with the substructuring method presented in Chapter 4 and Chapter 5.

The effectiveness of the substructuring-based model updating method was verified by a numerical three-span frame structure. Although the substructuring method introduces some slight errors in calculating the eigensolutions and eigensensitivities,

their effects on the model updating are negligible.

Afterwards, the substructuring method is applied to update a laboratory-tested frame structure. With the refined model improved in the undamaged state, the substructuring-based model updating method can identify the artificial damages in the structure successfully by adjusting a part of the elemental parameters within one or more substructures.

Finally, application to a practical bridge demonstrates that the proposed substructuring-based method is more efficient in updating large-scale structures with a large number of design parameters than the global-based method, subject to the same accuracy.

A successful model updating process depends on many aspects, such as high-quality experimental data, a validated FE model, a proper optimization algorithm, and the experience of the analyst. In the proposed substructuring-based model updating process, special attention should be paid to the division formation of the substructures and the number of master modes retained in each substructure. One may try a few times to obtain the optimised number of substructures and number of master modes before updating.

CHAPTER SEVEN

AN ITERATIVE SUBSTRUCTURING METHOD FOR EIGENSOLUTION AND EIGENSENSITIVITY

7.1 Introduction

In the previous chapters, the master modes in the substructures are assembled to represent the eigensolutions and eigensensitivities of the global structure. The reduced eigenequation is obtained by approximating a non-linear item with the truncation of the Taylor expansion. Consequently, it results in some slight errors in the eigensolutions and associated eigensensitivities, which may not be desirable in some applications. For example, during an optimization process, accurate eigensolutions and eigensensitivities are required when the results are close to the optimum, as even small errors may lead to a wrong search direction thus hindering the convergence of solution. To achieve higher accuracy, one way is to include more master modes in the substructures, which results in two difficulties: first, extracting more master modes from the substructures may be computationally expensive, specifically when the individual substructures are large in size; second, including more master modes increases the size of the reduced eigenequation. These two difficulties may decrease the efficiency of the substructuring method.

In this chapter, a new iterative substructuring method is proposed to accurately obtain the eigensolutions and eigensensitivities of a structure. Similar to the FRFS and SRFS methods proposed in the previous chapters, only a few of the lowest modes are retained in each substructure, and a residual flexibility matrix serves to compensate the contribution of the higher modes. Nevertheless, using this new approach, the

higher modes contribute to the reduced eigenequation in an iterated form, from which the eigenvalues can be obtained accurately. The eigenvalue derivatives can also be derived based on this iterative eigenequation. The eigenvectors and the eigenvector derivatives can be calculated upon the reduced eigenequation directly without iteration.

Other than the FRFS and SRFS method by including more master modes, this iterative method achieves high accuracy with an iterative scheme using a few master modes. Therefore, the computation cost in extracting the master eigensolutions from the independent substructures is reduced. In addition, this method keeps the reduced eigenequation in small size. Upon convergence, the iterative scheme reproduces the eigensolutions and eigensensitivities of the original structure accurately.

7.2. Eigensolutions with the Iterative Substructuring Method

As described in Chapter 4, the eigenequation (Eq. (4-17)) of the original global structure is constructed as

$$\begin{bmatrix} \mathbf{\Lambda}^p - \bar{\lambda}\mathbf{I} & -\mathbf{\Gamma} \\ -\mathbf{\Gamma}^T & \mathbf{0} \end{bmatrix} \begin{Bmatrix} \mathbf{z} \\ \tau \end{Bmatrix} = \begin{Bmatrix} \mathbf{0} \\ \mathbf{0} \end{Bmatrix} \tag{7-1}$$

Dividing the eigenmodes of the substructures into the master and slave parts, the primitive eigenequation (Eq. (7-1)) is disassembled into

$$\begin{bmatrix} \mathbf{\Lambda}_m^p - \bar{\lambda}\mathbf{I} & \mathbf{0} & -\mathbf{\Gamma}_m \\ \mathbf{0} & \mathbf{\Lambda}_s^p - \bar{\lambda}\mathbf{I} & -\mathbf{\Gamma}_s \\ -\mathbf{\Gamma}_m^T & -\mathbf{\Gamma}_s^T & \mathbf{0} \end{bmatrix} \begin{Bmatrix} \mathbf{z}_m \\ \mathbf{z}_s \\ \tau \end{Bmatrix} = \begin{Bmatrix} \mathbf{0} \\ \mathbf{0} \\ \mathbf{0} \end{Bmatrix} \tag{7-2}$$

From the second line of Eq. (7-2), one has

$$\{\mathbf{z}_s\} = \left(\mathbf{\Lambda}_s^p - \bar{\lambda}\mathbf{I}\right)^{-1} \mathbf{\Gamma}_s \{\tau\} = \mathbf{t}\{\tau\} \tag{7-3}$$

which gives

$$\left(\mathbf{\Lambda}_s^p - \bar{\lambda}\mathbf{I}\right)^{-1} \mathbf{\Gamma}_s = \mathbf{t} \tag{7-4}$$

Eq. (7-4) can be re-written as

$$\mathbf{t} = \left(\mathbf{\Lambda}_s^p\right)^{-1} \mathbf{\Gamma}_s + \bar{\lambda}\left(\mathbf{\Lambda}_s^p\right)^{-1} \mathbf{t} \tag{7-5}$$

The complete eigenvector of the eigenequation (Eq. (7-2)) is therefore expressed as

$$\begin{Bmatrix} \mathbf{z}_m \\ \mathbf{z}_s \\ \tau \end{Bmatrix} = \begin{bmatrix} \mathbf{I} & \mathbf{0} \\ \mathbf{0} & \mathbf{t} \\ \mathbf{0} & \mathbf{I} \end{bmatrix} \begin{Bmatrix} \mathbf{z}_m \\ \tau \end{Bmatrix} = \mathbf{T}_1 \begin{Bmatrix} \mathbf{z}_m \\ \tau \end{Bmatrix} \tag{7-6}$$

Substituting Eq. (7-6) into Eq. (7-2) and pre-multiplying $\mathbf{T}_1$ on both sides of Eq. (7-2) reduces the eigenequation to

$$\begin{bmatrix} \mathbf{\Lambda}_m^p - \bar{\lambda}\mathbf{I}_m & -\mathbf{\Gamma}_m \\ -\mathbf{\Gamma}_m^T & -\mathbf{\Gamma}_s^T\mathbf{t} \end{bmatrix} \begin{Bmatrix} \mathbf{z}_m \\ \tau \end{Bmatrix} = \begin{Bmatrix} \mathbf{0} \\ \mathbf{0} \end{Bmatrix} \tag{7-7}$$

The second line of Eq. (7-7) gives

$$\{\tau\} = -\left(\mathbf{\Gamma}_s^T\mathbf{t}\right)^{-1} \mathbf{\Gamma}_m^T \mathbf{z}_m \tag{7-8}$$

Accordingly, the eigenvector of the reduced eigenequation (Eq. (7-7)) is expressed as

$$\begin{Bmatrix} \mathbf{z}_m \\ \tau \end{Bmatrix} = \begin{bmatrix} \mathbf{I} \\ -\left(\mathbf{\Gamma}_s^T\mathbf{t}\right)^{-1} \mathbf{\Gamma}_m^T \end{bmatrix} \mathbf{z}_m = \mathbf{T}_2 \mathbf{z}_m \tag{7-9}$$

Substituting Eq. (7-9) into Eq. (7-7) and pre-multiplying $\mathbf{T}_2$ on both sides of Eq. (7-7) gives

$$\left[\left(\mathbf{\Lambda}_m^p - \bar{\lambda}\mathbf{I}_m\right) + \mathbf{\Gamma}_m\left(\mathbf{\Gamma}_s^T\mathbf{t}\right)^{-1} \mathbf{\Gamma}_m^T\right]\{\mathbf{z}_m\} = \mathbf{0} \tag{7-10}$$

As $\mathbf{\Gamma}_s^T\mathbf{t} = \mathbf{C}\mathbf{\Phi}_s^p\mathbf{t}$ and $\mathbf{C}$ is a constant matrix, $\mathbf{\Phi}_s^p\mathbf{t}$ is required to solve the reduced eigenequation. Pre-multiplying $\mathbf{\Phi}_s^p$ on both sides of Eq. (7-5) gives

$$\xi = \mathbf{\Phi}_s^p\mathbf{t} = \mathbf{\Phi}_s^p\left(\mathbf{\Lambda}_s^p\right)^{-1}\left[\mathbf{\Phi}_s^p\right]^T \mathbf{C}^T + \bar{\lambda}\mathbf{\Phi}_s^p\left(\mathbf{\Lambda}_s^p\right)^{-1}\mathbf{t} \tag{7-11}$$

Due to the orthogonality $\left[\mathbf{\Phi}_s^p\right]^T \mathbf{M}^p\mathbf{\Phi}_s^p = \mathbf{I}_{N_s^p}$, it has

$$\begin{aligned} \xi = \mathbf{\Phi}_s^p\mathbf{t} &= \mathbf{\Phi}_s^p\left(\mathbf{\Lambda}_s^p\right)^{-1}\left[\mathbf{\Phi}_s^p\right]^T \mathbf{C}^T + \bar{\lambda}\mathbf{\Phi}_s^p\left(\mathbf{\Lambda}_s^p\right)^{-1}\left[\mathbf{\Phi}_s^p\right]^T \mathbf{M}^p\mathbf{\Phi}_s^p\mathbf{t} \\ &= \mathbf{G}^p\mathbf{C}^T + \bar{\lambda}\mathbf{G}^p\mathbf{M}^p\xi \end{aligned} \tag{7-12}$$

in which $\mathbf{G}^p = \boldsymbol{\Phi}_s^p \left(\boldsymbol{\Lambda}_s^p \right)^{-1} \left[\boldsymbol{\Phi}_s^p \right]^T$ is the primitive form of the residual flexibility and given by the diagonal assembly of the residual flexibility matrices of the independent substructures as

$$\boldsymbol{\Phi}_s^p \left(\boldsymbol{\Lambda}_s^p \right)^{-1} \left[\boldsymbol{\Phi}_s^p \right]^T = \begin{bmatrix} \left(\mathbf{K}^{(1)} \right)^{-1} - \boldsymbol{\Phi}_m^{(1)} \left(\boldsymbol{\Lambda}_m^{(1)} \right)^{-1} \left[\boldsymbol{\Phi}_m^{(1)} \right]^T & & \\ & \ddots & \\ & & \left(\mathbf{K}^{(N_S)} \right)^{-1} - \boldsymbol{\Phi}_m^{(N_S)} \left(\boldsymbol{\Lambda}_m^{(N_S)} \right)^{-1} \left[\boldsymbol{\Phi}_m^{(N_S)} \right]^T \end{bmatrix} \tag{7-13}$$

Finally, the reduced eigenequation Eq. (7-10) can be expressed in a simple form as

$$\left[\mathbf{K}_d \right] \left\{ \mathbf{z}_m \right\} = \bar{\lambda} \left\{ \mathbf{z}_m \right\} \tag{7-14}$$

where $\mathbf{K}_d = \left[\boldsymbol{\Lambda}_m^p + \boldsymbol{\Gamma}_m \left(\mathbf{C} \xi \right)^{-1} \boldsymbol{\Gamma}_m^T \right]$.

As ξ includes unknown $\bar{\lambda}$, an iterative process is required to solve Eq. (7-14). From Eq. (7-12), the iteration starts with $\xi^{[1]}$ as

$$\xi^{[1]} = \mathbf{G}^p \mathbf{C}^T \tag{7-15}$$

where the number in the square bracket indicates the iteration step. With the initial value $\xi^{[1]}$, the eigensolutions can be calculated simultaneously for all interested modes by

$$\left[\boldsymbol{\Lambda}_m^p + \boldsymbol{\Gamma}_m \left(\mathbf{C} \mathbf{G}^p \mathbf{C}^T \right)^{-1} \boldsymbol{\Gamma}_m^T \right] \left\{ \mathbf{z}_m^{[1]} \right\} = \bar{\lambda}^{[1]} \left\{ \mathbf{z}_m^{[1]} \right\} \tag{7-16}$$

From Eq. (7-12), the iteration formulae can be established ($k \geq 2$) as follows.

1) $\xi^{[k]} = \mathbf{G}^p \mathbf{C}^T + \bar{\lambda}^{[k-1]} \mathbf{G}^p \mathbf{M}^p \xi^{[k-1]}$. (7-17)

2) $\mathbf{K}_d^{[k]} = \boldsymbol{\Lambda}_m^p + \boldsymbol{\Gamma}_m \left(\mathbf{C} \xi^{[k]} \right)^{-1} \boldsymbol{\Gamma}_m^T$. (7-18)

3) Calculate the eigenvalue $\bar{\lambda}^{[k]}$ in the kth iteration by conventional eigensolvers

such as QR algorithm or the Cholesky factorization (Bathe 1982).

When the eigenvalue in the *k*th iteration reaches the required accuracy, the eigenequation $\mathbf{K}_d^{[k]}\mathbf{z}_m^{[k]} = \bar{\lambda}^{[k]}\mathbf{z}_m^{[k]}$ is solved to estimate both $\bar{\lambda}^{[k]}$ and $\mathbf{z}_m^{[k]}$. The eigenvector of the global structure is then recovered by calculating $\bar{\mathbf{\Phi}} = \mathbf{\Phi}_m^p \mathbf{z}_m^{[k]}$.

It is noted that, the initial eigenequation of Eq. (7-16) is equivalent to the FRFS method, and the second iteration is equivalent to the SRFS method proposed in Chapter 4.

In Eq. (7-17), $\xi^{[k]} = \mathbf{G}^p\mathbf{C}^T + \bar{\lambda}^{[k-1]}\mathbf{G}^p\mathbf{M}^p\xi^{[k-1]}$ is calculated at the substructure level. In other words, $\left(\xi^{(j)}\right)^{[k]} = \mathbf{G}^{(j)}\mathbf{C}^T + \bar{\lambda}^{[k-1]}\mathbf{G}^{(j)}\mathbf{M}^{(j)}\left(\xi^{(j)}\right)^{[k-1]}$ is calculated for the *j*th substructure (j=1, 2, …, N_S) independently, and then the individual substructures are assembled in the diagonal form.

Eq. (7-12) reveals that ξ depends on $\bar{\lambda}$, which varies for different modes. The iteration needs to be performed mode by mode. In practice, the eigensolutions of the lower modes generally converge faster than those of the higher modes.

During the iteration process, only the item ξ needs to be re-calculated, while other items, such as $\mathbf{\Lambda}_m^p$ and $\mathbf{\Gamma}_m$, remain unchanged. Furthermore, the reduced system matrix $\mathbf{K}_d$ is equal in size to the number of master modes of the substructures, and thus the iteration process does not require much additional computational power. This will be explained in more detail in the discussion of the numerical examples.

7.3. Eigensensitivities with the Iterative Substructuring Method

This section presents the method for deriving the first-order derivatives of the eigenvalues and eigenvectors with respect to an elemental parameter. As before, the elemental parameter is denoted by *r* in the *r*th substructure, which could be the bending rigidity or axial rigidity of an element.

The reduced eigenequation (Eq. (7-14)) can be rewritten for the *i*th mode as

$$\left[\left(\mathbf{\Lambda}_m^p - \bar{\lambda}_i \mathbf{I}_m\right) + \mathbf{\Gamma}_m \left(\mathbf{C}\xi\right)^{-1} \mathbf{\Gamma}_m^T\right]\left\{\mathbf{z}_i\right\} = \left\{\mathbf{0}\right\} \tag{7-19}$$

Eq. (7-19) is differentiated with respect to *r* as

$$\left[\left(\mathbf{\Lambda}_m^p - \bar{\lambda}_i \mathbf{I}_m\right) + \mathbf{\Gamma}_m \left(\mathbf{C}\xi\right)^{-1} \mathbf{\Gamma}_m^T\right]\frac{\partial\left\{\mathbf{z}_i\right\}}{\partial r} + \frac{\partial\left[\left(\mathbf{\Lambda}_m^p - \bar{\lambda}_i \mathbf{I}_m\right) + \mathbf{\Gamma}_m \left(\mathbf{C}\xi\right)^{-1} \mathbf{\Gamma}_m^T\right]}{\partial r}\left\{\mathbf{z}_i\right\} = \left\{\mathbf{0}\right\} \tag{7-20}$$

7.3.1 Eigenvalue Derivatives

Pre-multiplying $\left\{\mathbf{z}_i\right\}^T$ on both sides of Eq. (7-20) gives

$$\left\{\mathbf{z}_i\right\}^T\left[\left(\mathbf{\Lambda}_m^p - \bar{\lambda}_i \mathbf{I}_m\right) + \mathbf{\Gamma}_m \left(\mathbf{C}\xi\right)^{-1} \mathbf{\Gamma}_m^T\right]\frac{\partial\left\{\mathbf{z}_i\right\}}{\partial r} + \left\{\mathbf{z}_i\right\}^T\frac{\partial\left[\left(\mathbf{\Lambda}_m^p - \bar{\lambda}_i \mathbf{I}_m\right) + \mathbf{\Gamma}_m \left(\mathbf{C}\xi\right)^{-1} \mathbf{\Gamma}_m^T\right]}{\partial r}\left\{\mathbf{z}_i\right\} = \left\{\mathbf{0}\right\} \tag{7-21}$$

Given Eq. (7-19), Eq. (7-21) can be transformed into

$$\frac{\partial \bar{\lambda}_i}{\partial r} = \left\{\mathbf{z}_i\right\}^T\left[\frac{\partial \mathbf{\Lambda}_m^p}{\partial r} + \frac{\partial\left(\mathbf{\Gamma}_m \left(\mathbf{C}\xi\right)^{-1} \mathbf{\Gamma}_m^T\right)}{\partial r}\right]\left\{\mathbf{z}_i\right\} \tag{7-22}$$

in which

$$\frac{\partial\left(\mathbf{\Gamma}_m \left(\mathbf{C}\xi\right)^{-1} \mathbf{\Gamma}_m^T\right)}{\partial r} = \frac{\partial \mathbf{\Gamma}_m}{\partial r}\left(\mathbf{C}\xi\right)^{-1} \mathbf{\Gamma}_m^T - \mathbf{\Gamma}_m \left(\mathbf{C}\xi\right)^{-1}\frac{\partial\left(\mathbf{C}\xi\right)}{\partial r}\left(\mathbf{C}\xi\right)^{-1} \mathbf{\Gamma}_m^T + \mathbf{\Gamma}_m \left(\mathbf{C}\xi\right)^{-1}\frac{\partial \mathbf{\Gamma}_m^T}{\partial r}$$

$$\frac{\partial \boldsymbol{\Lambda}_m^p}{\partial r}=\begin{bmatrix}\mathbf{0} & \mathbf{0} & \mathbf{0}\\ \mathbf{0} & \dfrac{\partial \boldsymbol{\Lambda}_m^{(r)}}{\partial r} & \mathbf{0}\\ \mathbf{0} & \mathbf{0} & \mathbf{0}\end{bmatrix},\quad \frac{\partial \boldsymbol{\Gamma}_m^T}{\partial r}=\mathbf{C}\frac{\partial \boldsymbol{\Phi}_m^p}{\partial r}=\mathbf{C}\begin{bmatrix}\mathbf{0} & \mathbf{0} & \mathbf{0}\\ \mathbf{0} & \dfrac{\partial \boldsymbol{\Phi}_m^{(r)}}{\partial r} & \mathbf{0}\\ \mathbf{0} & \mathbf{0} & \mathbf{0}\end{bmatrix}$$

where $\boldsymbol{\Gamma}_m$, $\{\mathbf{z}_i\}$, and $(\mathbf{C}\xi)^{-1}$ were obtained during the calculation of the eigensolutions, $\frac{\partial \boldsymbol{\Lambda}_m^p}{\partial r}$ and $\frac{\partial \boldsymbol{\Gamma}_m^T}{\partial r}$ are associated with the eigensolution derivatives of the master modes of the substructures which are zeros except for those in the *r*th substructure, and $\frac{\partial \boldsymbol{\Lambda}_m^{(r)}}{\partial r}$ and $\frac{\partial \boldsymbol{\Phi}_m^{(r)}}{\partial r}$ can be calculated using traditional approaches such as Nelson's method by treating the *r*th substructure as an independent structure. $\frac{\partial(\mathbf{C}\xi)}{\partial r}$ is thus required to calculate the first-order derivatives of the eigenvalues.

According to Eq. (7-12), ξ is differentiated as

$$\frac{\partial \xi}{\partial r}=\frac{\partial \mathbf{G}^p}{\partial r}\mathbf{C}^T+\bar{\lambda}\left(\frac{\partial \mathbf{G}^p}{\partial r}\mathbf{M}^p\xi+\mathbf{G}^p\mathbf{M}^p\frac{\partial \xi}{\partial r}\right)+\frac{\partial \bar{\lambda}}{\partial r}\mathbf{G}^p\mathbf{M}^p\xi \qquad (7\text{-}23)$$

The derivative matrix of the first-order residual flexibility $\mathbf{G}^p$ with respect to parameter *r* can be represented by the derivative of the residual flexibility of the *r*th substructure as

$$\frac{\partial \mathbf{G}^p}{\partial r}=\begin{bmatrix}\mathbf{0} & \mathbf{0} & \mathbf{0}\\ \mathbf{0} & \dfrac{\partial \mathbf{G}^{(r)}}{\partial r} & \mathbf{0}\\ \mathbf{0} & \mathbf{0} & \mathbf{0}\end{bmatrix} \qquad (7\text{-}24)$$

where

$$\frac{\partial \mathbf{G}^{(r)}}{\partial r}=\frac{\partial\left(\left(\mathbf{K}^{(r)}\right)^{-1}-\boldsymbol{\Phi}_m^{(r)}\left(\boldsymbol{\Lambda}_m^{(r)}\right)^{-1}\left[\boldsymbol{\Phi}_m^{(r)}\right]^T\right)}{\partial r}=-\left(\mathbf{K}^{(r)}\right)^{-1}\frac{\partial\left(\mathbf{K}^{(r)}\right)}{\partial r}\left(\mathbf{K}^{(r)}\right)^{-1}-\frac{\partial\left(\boldsymbol{\Phi}_m^{(r)}\left(\boldsymbol{\Lambda}_m^{(r)}\right)^{-1}\left[\boldsymbol{\Phi}_m^{(r)}\right]^T\right)}{\partial r}$$

Iteration is required to achieve an accurate $\frac{\partial \xi}{\partial r}$. In the first round,

$\left(\frac{\partial \xi}{\partial r}\right)^{[1]} = \frac{\partial \mathbf{G}^p}{\partial r}\mathbf{C}^T$. Afterwards, $\frac{\partial \xi}{\partial r}$ in the *k*th iteration is expressed as

$$\left(\frac{\partial \xi}{\partial r}\right)^{[k]} = \frac{\partial \mathbf{G}^p}{\partial r}\mathbf{C}^T + \bar{\lambda}\left(\frac{\partial \mathbf{G}^p}{\partial r}\mathbf{M}^p\xi + \mathbf{G}^p\mathbf{M}^p\left(\frac{\partial \xi}{\partial r}\right)^{[k-1]}\right) + \left(\frac{\partial \bar{\lambda}}{\partial r}\right)^{[k-1]}\mathbf{G}^p\mathbf{M}^p\xi \quad (7\text{-}25)$$

and the eigenvalue derivative in the *k*th step is obtained as

$$\left(\frac{\partial \bar{\lambda}_i}{\partial r}\right)^{[k]} =$$

$$\{\mathbf{z}_i\}^T\left[\frac{\partial \mathbf{\Lambda}_m^p}{\partial r} + \frac{\partial \mathbf{\Gamma}_m}{\partial r}(\mathbf{C}\xi)^{-1}\mathbf{\Gamma}_m^T - \mathbf{\Gamma}_m(\mathbf{C}\xi)^{-1}\mathbf{C}\left(\frac{\partial \xi}{\partial r}\right)^{[k]}(\mathbf{C}\xi)^{-1}\mathbf{\Gamma}_m^T + \mathbf{\Gamma}_m(\mathbf{C}\xi)^{-1}\frac{\partial \mathbf{\Gamma}_m^T}{\partial r}\right]\{\mathbf{z}_i\} \quad (7\text{-}26)$$

The eigensensitivities can be calculated for all modes simultaneously in the initial iteration. Thereafter, the iteration is performed mode by mode. In each iteration, only $\frac{\partial \xi}{\partial r}$ needs to be re-calculated and the other items remain unchanged.

7.3.2 Eigenvector Derivatives

The *i*th eigenvector of the global structure can be recovered by calculating

$$\bar{\mathbf{\Phi}}_i = \mathbf{\Phi}_m^p\{\mathbf{z}_i\} \quad (7\text{-}27)$$

Differentiating Eq. (7-27) with respect to parameter *r* gives

$$\frac{\partial \bar{\mathbf{\Phi}}_i}{\partial r} = \frac{\partial \mathbf{\Phi}_m^p}{\partial r}\{\mathbf{z}_i\} + \mathbf{\Phi}_m^p\left\{\frac{\partial \mathbf{z}_i}{\partial r}\right\} \quad (7\text{-}28)$$

In Eq. (7-28), $\{\mathbf{z}_i\}$ and $\mathbf{\Phi}_m^p$ are already known, and $\frac{\partial \mathbf{\Phi}_m^p}{\partial r}$ are the eigenvector derivatives of the substructures, which are non-zero only for the *r*th substructure. $\left\{\frac{\partial \mathbf{z}_i}{\partial r}\right\}$ can be calculated directly from Eq. (7-20) by applying Nelson's method to the reduced eigenequation. The procedure is similar to that described in Section 5.2.2, which is not shown here for simplification. Therefore, calculation of the eigenvector

derivatives of the global structure does not need any iteration. This is a major advantage of the proposed approach, because calculation of the eigenvector derivatives usually costs a great deal more in computation time and resources than the calculation of the eigensolutions and eigenvalue derivatives. The computational accuracy and efficiency of the proposed method is investigated through two numerical examples in the following section.

7.4 Case Studies

7.4.1 The Three-span Frame Structure

The three-span frame structure with three substructures shown in Figure 7-1 is utilized here to verify the accuracy of the iterative substructuring method for calculating the eigensolutions and eigensensitivities.

The traditional Lanczos method is first employed to calculate the first 10 eigensolutions of the global structure. The results are treated as exact for comparison, and are listed in Table 7-1. The proposed iterative substructuring method is then utilized to calculate the first 10 eigensolutions of the global structure, by choosing the first 20 modes as the master modes in each substructure.

The convergence criterion is set to $Tol = 1 \times 10^{-6}$, which means that the iteration stops when the relative difference in the frequencies from two consecutive iterations is less than 10^{-6}. The convergence of the first 10 frequencies is listed in Table 7-1. The initial step in Table 7-1 denotes the results of the substructuring method without iteration, which is equivalent to the FRFS method presented in Chapter 4.

Table 7-1 shows that the frequencies in the absence of iteration are insufficiently accurate except for the lowest modes, when only 20 master modes are retained in

each substructure. With a few iterations, however, the predefined tolerance of 10^{-6} can be achieved for all modes. Table 7-1 also compares the MAC values of the eigenvectors obtained using the substructuring method with those using the global method. The results show that the MAC values of the eigenvectors are about 0.99 in the initial step, but are improved to greater than 0.999 after a few iterations.

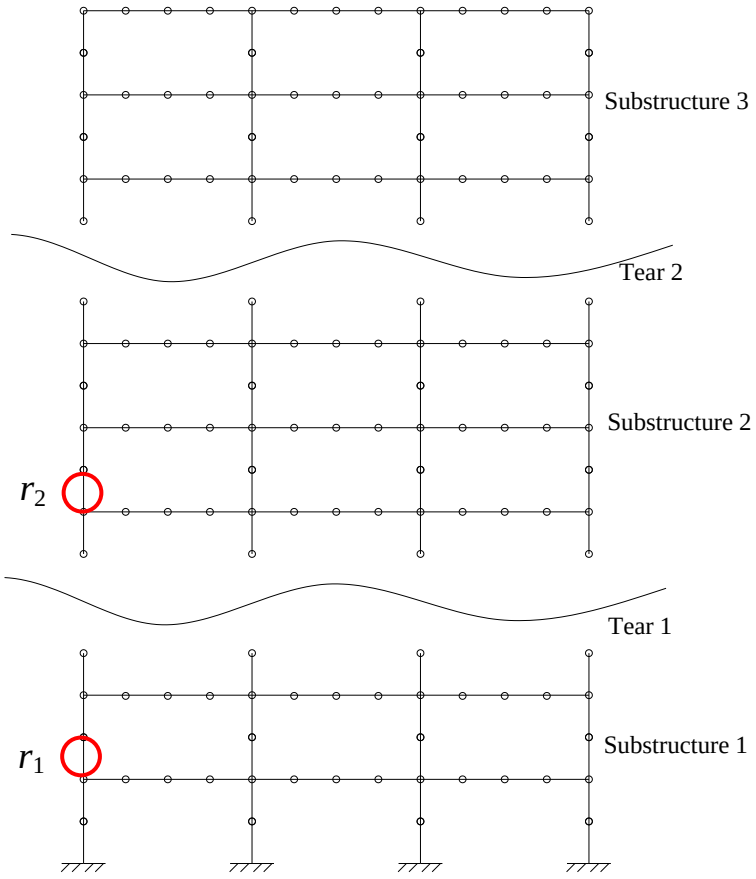

Figure 7-1: Substructures of the Frame Structure

Table 7-1: Convergence of the Natural Frequencies of the Frame Structure

Iteration	Natural frequencies (Hz)									
	1	2	3	4	5	6	7	8	9	10
1	1.784275	5.537789	9.821755	14.703893	16.659498	18.895124	20.219286	22.755837	25.636194	26.306896
2	1.784265	5.536539	9.819860	14.687199	16.619370	18.810203	20.198991	22.622879	25.477829	26.197063
3	1.784265	5.536531	9.819823	14.686449	16.618857	18.807554	20.197700	22.617502	25.471004	26.180333
4		5.536530	9.819822	14.686413	16.618847	18.807393	20.197692	22.617051	25.470426	26.179965
5				14.686411	16.618844	18.807380	20.197691	22.617043	25.470418	26.179903
6						18.807379		22.617036	25.470416	26.179893
7										26.179891
Global method (Exact)	1.784265	5.536529	9.819822	14.686408	16.618843	18.807372	20.197690	22.617033	25.470405	26.179880
Relative error	8.19E-08	2.09E-07	8.14E-08	1.78E-07	4.64E-08	3.86E-07	7.35E-08	1.40E-07	4.39E-07	4.09E-07
MAC (Initial step)	0.9999	0.9990	0.9995	0.9933	0.9945	0.9951	0.9974	0.9941	0.9919	0.9936
MAC (Iterative scheme)	1.0000	1.0000	1.0000	1.0000	0.9999	0.9994	0.9999	0.9998	0.9999	0.9997

Table 7-2: Convergence of the Eigenvalue Derivatives with Respect to Parameter r_1

Iteration	Eigenvalue derivative with respect to r_1									
	1	2	3	4	5	6	7	8	9	10
1	2.889566	25.885745	78.778372	169.073194	77.206903	319.175632	291.612678	809.410739	733.017479	429.545360
2	2.889565	25.885211	78.423707	168.926074	76.883478	313.653135	286.556056	796.980672	715.498553	429.101623
3	2.889564	25.885055	78.422759	168.892020	76.880538	313.311088	286.486862	795.869119	714.101445	428.126404
4		25.885043	78.422694	168.889373	76.880283	313.286574	286.478940	795.750097	713.963480	427.836827
5				168.889206	76.880270	313.284245	286.478034	795.732809	713.945252	427.816851
6						313.284000	286.477813	795.732174	713.942276	427.816473
7									713.941645	
Global method (Exact)	2.889564	25.884992	78.422680	168.889156	76.879949	313.281242	286.477777	795.729988	713.940620	427.815117
Relative error	9.40E-08	1.97E-06	1.81E-07	3.01E-07	4.17E-06	8.81E-06	1.25E-07	2.75E-06	1.44E-06	3.17E-06

Table 7-3: Eigensensitivity of the Frame Structure with Respect to Parameter r_2

Mode	Global method	Substructuring method without iterations			Substructuring method with iterations		
	Eigenvalue derivative	Eigenvalue derivative	Relative error	Eigenvector derivative (COED)	Eigenvalue derivative	Relative error	Eigenvector derivative (COED)
1	0.876335	0.876339	3.95E-06	1.000	0.876335	0.00E+00	1.000
2	3.635904	3.636177	7.52E-05	0.999	3.635905	1.48E-07	1.000
3	3.442241	3.443368	3.27E-04	0.988	3.442242	1.59E-07	0.999
4	49.031834	49.038606	1.38E-04	0.999	49.031836	5.07E-08	0.999
5	72.316067	72.037396	3.85E-03	0.997	72.315913	2.13E-06	0.999
6	292.043804	295.245299	1.10E-02	0.996	292.044391	2.01E-06	0.998
7	215.692368	216.031321	1.57E-03	0.999	215.692429	2.83E-07	1.000
8	748.426540	765.470734	2.28E-02	0.995	748.427627	1.45E-06	0.999
9	671.580079	686.289966	2.19E-02	0.984	671.584254	6.22E-06	0.999
10	528.853542	538.692678	1.86E-02	0.980	528.854851	2.48E-06	0.998

The first 10 eigenvalue derivatives and eigenvector derivatives of the global structure with respect to r_1 (see Figure 7-1) are then calculated. The convergence process of the eigenvalue derivatives is detailed in Table 7-2, where the global method refers to Nelson's method at the global structural level and can be treated as exact. It can be observed that the eigenvalue derivatives achieve high precision in just a few runs. It should be noted that the precision of the eigenvalue derivatives depends on the eigensolutions ($\bar{\lambda}$ and $\bar{\mathbf{\Phi}}$), $\frac{\partial \xi}{\partial r}$, and ξ. It is reasonable that the eigenvalue derivatives are usually not as accurate as the eigenvalues.

Without loss of generality, the eigensensitivities with respect to the parameter r_2, which is located in the second substructure of Figure 7-1, are calculated. In Table 7-3, the eigensensitivities obtained from the three approaches (the global method, the substructuring method without iteration, and the substructuring method with iteration) are compared. The similarity of the eigenvector derivatives obtained using the global method and the proposed substructuring method is denoted by the value of COED given in Eq. (5-20). Table 7-3 again shows that the proposed iterative approach improves the accuracy of eigensensitivities significantly.

7.4.2 The Guangzhou New Television Tower

The Guangzhou New TV Tower (described in Chapter 3) is utilized here to investigate the computation efficiency of the iterative substructuring method in calculation of the eigensolutions and eigensensitivities of a large-scale structure. The FE analytical model (Figure 3-5(b)) of the structure includes 8,738 three-dimensional elements, 3,671 nodes, and 21,690 DOFs in total. The global structure is divided into 10 substructures along the vertical direction as shown in Figure 3-5(c). The nodes and elements included in each substructure are listed in Table 3-1. Using the proposed

substructuring method, the first 20 modes are retained as the master modes in each substructure to calculate the first 10 eigensolutions and eigensensitivities of the global structure. Again, the convergence criterion is set to $Tol = 1\times10^{-6}$. To evaluate the accuracy of the results and the computational efficiency of the proposed method, global methods without substructuring are also employed for comparison and the results are treated as exact. Lanczos method is employed as the global method to calculate the eigensolutions, and Nelson's method is employed as the global method to calculate the eigensensitivities. The detailed algorithms of the Lanczos method and the Nelson's method are respectively presented in the Appendix A and Appendix B.

Figure 7-2 illustrates the relative errors of the frequencies using the iterative substructuring method in each iteration, as compared with the exact ones using the global method. Figure 7-3 shows the relative errors of the eigenvalue derivatives with respect to a randomly selected elemental parameter. For clarity, only the first and the tenth modes are plotted in Figure 7-2 and Figure 7-3. The two figures show that the first natural frequency and eigenvalue derivative have a high accuracy at the initial step, whereas those of mode 10 have relatively larger error, as expected. After a few iterations, the accuracy of the tenth mode is improved significantly.

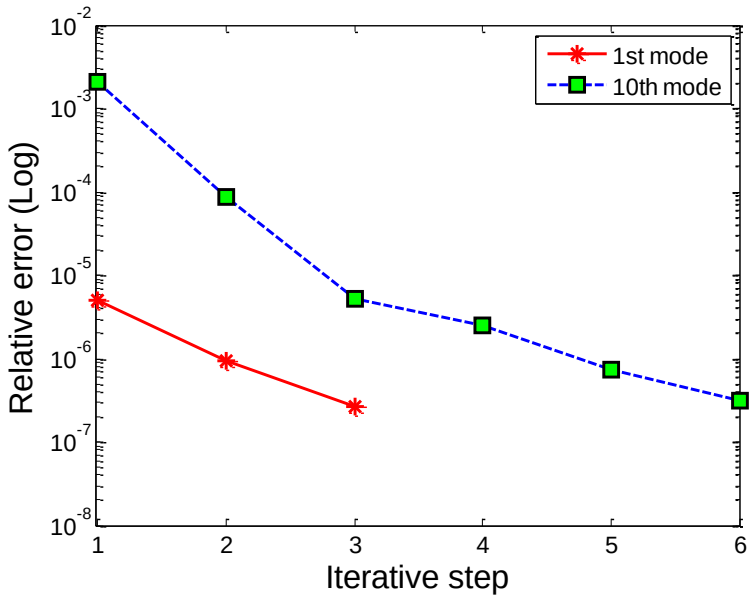

Figure 7-2: Convergence of the Frequencies

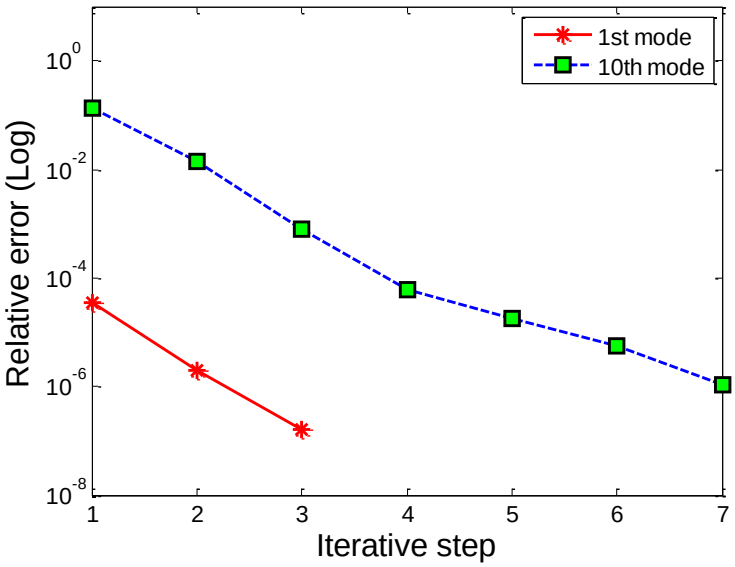

Figure 7-3: Convergence of the Eigenvalue Derivatives

The computation time cost of calculating the first 10 eigensolutions and the eigensensitivities is presented in Table 7-4. The global method takes 11.6 seconds to calculate the first 10 eigensolutions of the global structure. Using the iterative substructuring method, the initial step takes about 34.7 seconds and each subsequent iteration adds about 3.0 seconds. In total, 32 iterations are required to satisfy the predefined accuracy, which takes about 131.0 seconds. Although the iterative substructuring method takes longer than the global method for eigensolutions, it contributes to the calculation of the eigensensitivities, which is the more time-consuming process.

In Table 7-4, the global method takes about 197.6 seconds to calculate the first 10 eigensensitivities with respect to one parameter. The proposed substructuring method takes about 13.2 seconds to perform the initialization step, and each subsequent iteration adds just 2.6 seconds to the computation time. Moreover, the calculation of the eigenvector derivatives, which usually takes up the majority of the computation time in the global eigensensitivity method, takes only 0.8 seconds using the present substructuring method. This is because the eigenvector is calculated based on the

reduced eigenequation, which has the size of 200 × 200 and is much smaller than that of the global structure (21,690 × 21,690). In this case study, 39 iterations are required to achieve the predefined accuracy for the eigensensitivities of the 10 modes, which takes about 115.4 seconds in total. This improvement in computational efficiency is significant when applied to a practical model updating process, as actual structures always include a large number of uncertain parameters. For example, in this TV Tower structure, the columns of the steel outer tube are composed of 1,104 three-dimensional beam elements. If the 1,104 elements are chosen as updated candidates, the global method requires 51.9 hours to calculate the eigensensitivities of the first 10 modes, whereas the iterative substructuring method requires only 32.4 hours. Given the time needed to calculate the eigensensitivities, the time spent in deriving the eigensolutions is negligible.

The substructuring method also reduces the computational memory required. For example, the global method needs to handle the global stiffness and mass matrices, which are 21,690 × 21,690 in size. Even if the matrices are sparse, up to 2,151 MB of memory is needed to acquire the eigensolutions and eigensensitivities. However, with the substructuring method, only 10 substructures are handled, each of a size of about 2,200 × 2,200 and a half-bandwidth of about 600. Furthermore, the reduced eigenequation is only 200 × 200 in size, upon which the iteration is performed. The substructuring method thus requires only 338 MB of computer memory to estimate the eigensolutions and eigensensitivities as listed in Table 7-4. These findings indicate that the proposed substructuring method will be very useful for large-size structures.

Table 7-4: Comparison of Computation Time and Storage Memory Required by the Substructuring and Global Methods

	CPU time (Second)								Memory (MB)
	Eigensolution				Eigensensitivity				
	Eigenvalue		Eigenvector	Total	Eigenvalue derivative		Eigenvector derivative	Total	
	Initialization	Iteration			Initialization	Iteration			
Substructuring method	34.7	3.0×32	0.3	**131.0**	13.2	2.6×39	0.8	**115.4**	**338**
Global method				**11.6**	1.8		195.8	**197.6**	**2151**
FRFS method (500 master modes)	416.6		6.7	**423.3**	209.6 (207.2+2.4)		16.8	**226.4**	**304**

It should be noted that, although using only a few master modes can achieve highly accurate eigensolutions and eigensensitivities with the iterative scheme, the number of master modes retained is usually 2 ~ 3 times of the interested modes in the global structure. Neither decreasing the master modes, nor increasing the master modes is always helpful for the computation efficiency. If more master modes are retained in each substructure, the iterations might converge to the predefined tolerance in fewer steps. But analysis of the master modes in each substructure consumes more computation time, and the size of the reduced eigenequation is enlarged. As the master modes become huge, the computation effort saved by the reduced steps might not compensate the cost on the analysis of master modes in the substructures. On the other hand, retaining too few master modes may hinder the convergence of the iteration scheme, although this may reduce the endeavor in extracting the master modes from the substructures. Similar to the previous study, the division formation of the substructures and the master modes that are retained in each substructure both affect the convergence and accuracy. Dividing a structure into either an excessive or an insufficient number of substructures is undesirable. The division formations thus need to trade off between the number of substructures and the number of master modes in each substructure.

In Chapter 4 and Chapter 5, more master modes are included to improve the computation accuracy of the eigensolutions and eigensensitivities in FRFS method. Although inclusion of more master modes can also improve the accuracy of the results using the FRFS method, the cost of computation time for this precision improvement is luxurious. To demonstrate this, the master modes retained in each substructure are increased from 50 to 500 gradually. The computation accuracy and computation time for the first 10 eigensolutions and eigensensitivities with respect to the number of master modes are illustrated in Figure 7-4 and Figure 7-5. For clarity, only the first mode and the tenth mode are plotted.

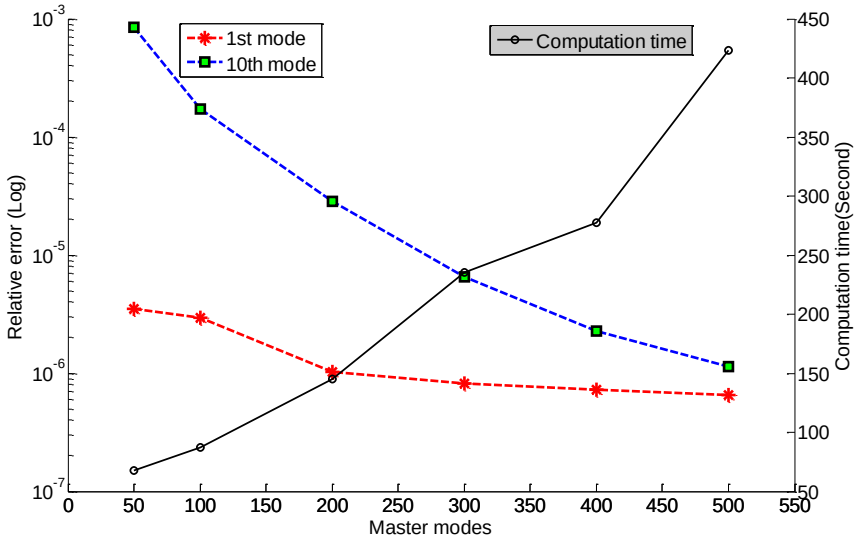

Figure 7-4: Accuracy and Computation Time of Eigensolutions with Respect to the Number of Master Modes

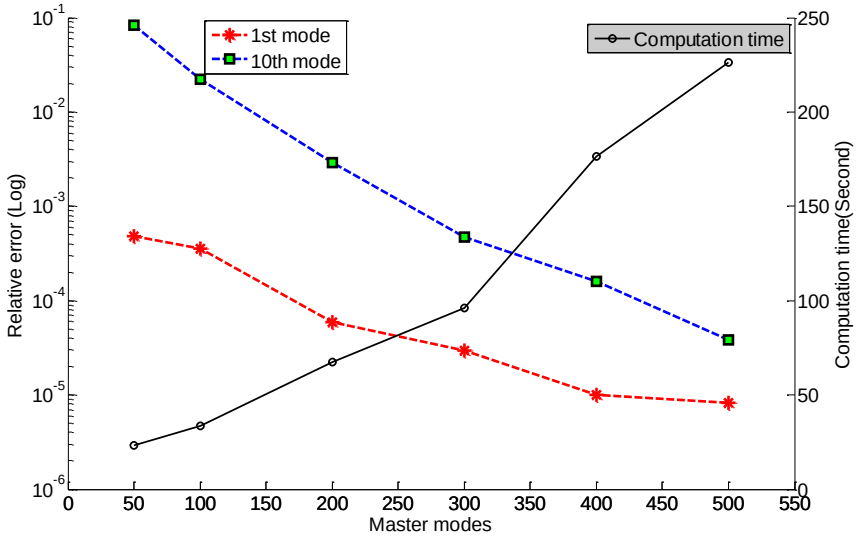

Figure 7-5 Accuracy and Computation Time of Eigensensitivities with Respect to the Number of Master Modes

Figure 7-4 and Figure 7-5 reveal that, to achieve the accuracy with the relative error of 10^{-6}, at least 500 master modes need to be retained in the substructures for the FRFS method. It implies that, 500 master modes need to be extracted from each substructure. In addition, the resulting reduced eigenequation has the size of 5000$\times$ 5000. It is noted that, inclusion of more master modes improves the accuracy slightly, but increases the computation time heavily. In this regard, the FRFS method is not

efficient to acquire highly accurate eigensolutions and eigensensitivities.

The consumed computation time and memory for the FRFS method and the iterative method are compared in Table 7-4, both satisfying the tolerance of 10^{-6}. It can be found that, comparing with the FRFS method, the iterative substructuring method requires a little more computer memory, since it has to retain some interim results for iteration. However, the iterative method takes much shorter computation time, mainly due to two reasons: 1) the iterative method needs to extract only 20 master modes of the 10 independent substructures, other than 500 master modes required by the FRFS method; 2) the reduced eigenequation of the iterative method takes the size of 200×200, which is much smaller than that of the FRFS method in size of 5000×5000. In this example, the FRFS method needs about 416.6 seconds to extract the 500 master eigenmodes and residual flexibility matrix from the each independent substructures, and 6.7 seconds to solve the eigenequation in size of 5000×5000. The FRFS method consumes 207.2 seconds to compute the eigensolution derivatives for the 500 master modes, 2.4 seconds to assemble the eigenvalue derivatives and 16.8 seconds to solve the derivative of the reduced eigenequation, which takes much longer time than the proposed iterative method. Based on the above observation, the iterative method is preferable to the FRFS method, when the high-accuracy eigensolutions and eigensensitivities are required.

The shortcoming of the iterative substructuring method is that the eigensolutions and eigensensitivities are computed one by one rather than all required are calculated simultaneously. Since the lowest eigenpairs converge very fast, the present method is effective when a few lowest eigenpairs are required as it is a usual case in practice. When more modes need to be computed, the efficiency may decrease. The developed method that handles all eigensolutions and eigensensitivities simultaneously deserves future research.

7.5 Model Updating with the Iterative Substructuring Method

The substructuring method is preferable in model updating because only one or more substructures instead of the large-size global structure are involved in the repeatedly estimation of eigensolutions and eigensensitivities. The iterative substructuring method can achieve high accuracy in calculation of eigensolutions and eigensensitivities which is competitive with the conventional global method, and can save much computation time and storage memory. Therefore, it is promising to be applied in model updating process.

Application of the substructuring method in model updating is first advantageous in assembling the system matrices, which is required in each iteration. Taking the TV tower structure as an example, the global method spends 122.16 seconds to re-assemble the stiffness and mass matrices for each iteration of model updating (Table 7-5), while the substructuring method only costs about 11 seconds to assemble the system matrices for the 10 substructures. Since the assembly of system matrices is required repeatedly during model updating process, this saving is prominent. Moreover, because much smaller matrices are involved in computation, the substructuring method also saves the computer memory.

Table 7-5: Computation Time in Assembling the System Matrix

	Global method	Substructuring method
Size of system matrix	21690×21690	2200×2200
Time in assembly of system matrix (second)	122.16	1.10×10

The substructuring method is also advantageous in calculation of eigensolutions and eigensensitivities for model updating purpose. This will be demonstrated by a model updating procedure simulated on the TV tower structure. The 'experimental' frequencies and mode shapes are generated with the Lanczos method on the global structure, by intentionally reducing the bending rigidity of the 48 column elements of the outer tube in the second substructure by 20%. All elements of the outer tube in the second substructure are chosen as the updating parameters, and accordingly, there are 144 updating candidates in total. It is assumed that the first 10 modes are available, and the measurements are obtained at the translational directions of nodes. The mode shapes have been normalized to the mass matrix. The objective function combines the differences in the frequencies and mode shapes between the generated 'experimental' data and the analytical model. The weight coefficients are set to 0.1 for the mode shapes and 1.0 for the frequencies.

Three model updating approaches are employed for comparison. First, the traditional global method is applied, that is, the first 10 eigensolutions are calculated with the Lanczos method, and the associated eigensensitivities are calculated with the Nelson's method. Figure 7-6 reports the optimization process before the norm of objective function is less than 2×10^{-7}. Since the experimental eigenmodes are generated numerically without considering the noise, the updated frequencies and mode shapes recover the experimental counterparts exactly as listed in Table 7-6. The global method takes about 76.24 hours to achieve the convergence criterion through 15 iterations. Each iteration takes about 5.43 hours.

Second, the iterative substructuring method presented in this chapter is utilized to calculate the eigensolutions and eigensensitivities for the model updating process. The first 20 eigenmodes are retained as master modes in each substructure to extract the first 10 modes of the global structure. The iteration in searching the eigensolutions

stops when the relative difference in the frequencies from two consecutive iterations is less than 10^{-6}, and the iteration of eigensensitivities terminates when the relative difference in the eigenvalue derivatives from two consecutive iterations is less than 10^{-6}. Using the eigensolutions and eigensensitivities calculated with the iterative substructuring method, the optimization process is demonstrated in Figure 7-6. The iterative substructuring method can achieve competitive accurate results as the exact global method in each step, and it also takes 15 iterations to achieve the predefined convergence criterion. The whole procedure lasts 50.87 hours, and each iteration takes about 3.62 hours. The computation time is about 66.7% of that using the traditional global method. The updated frequencies and mode shapes are listed in Table 7-7, and they match the experimental ones very well. It can be observed that, the frequencies and MAC values of mode shapes in this table are quite similar to those in Table 7-6 for both before updating and after updating, which again proves that the iterative substructuring method can achieve high accuracy in eigensolutions and eigensensitivities.

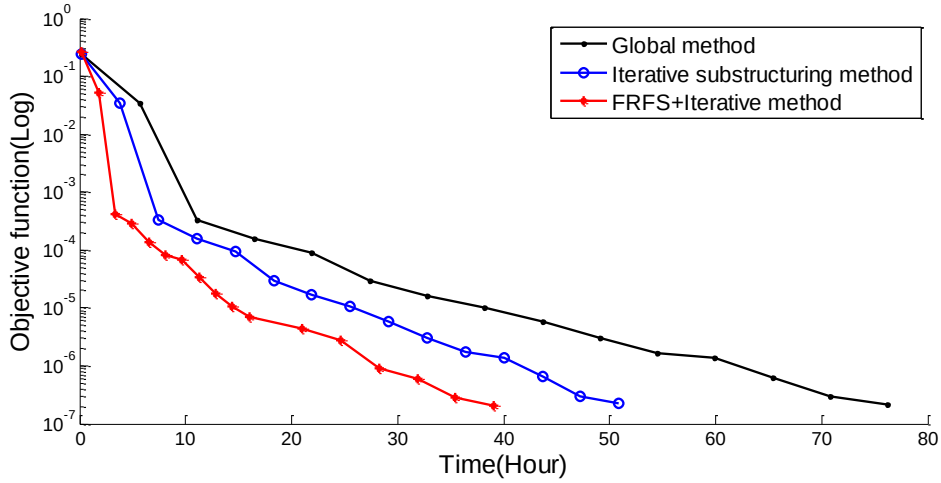

Figure 7-6: Model Updating Process with Three Methods

Table 7-6: Frequencies and Model Shapes Before and After Updating with the Global Method

Mode	Measured Frequency (Hz)	Before updating			After updating		
		Frequency (Hz)	Difference (%)	MAC	Frequency (Hz)	Difference (%)	MAC
1	0.111	0.112	0.76%	1.0000	0.111	0.00%	1.0000
2	0.162	0.163	0.95%	1.0000	0.162	0.00%	1.0000
3	0.344	0.344	0.09%	0.9999	0.344	0.00%	1.0000
4	0.373	0.376	0.84%	0.9990	0.373	0.00%	0.9999
5	0.406	0.406	0.11%	0.9999	0.406	0.00%	1.0000
6	0.429	0.431	0.32%	0.9997	0.429	0.00%	1.0000
7	0.493	0.496	0.71%	0.9994	0.493	0.00%	1.0000
8	0.694	0.697	0.42%	0.9998	0.694	0.00%	1.0000
9	0.817	0.818	0.13%	0.9999	0.817	0.00%	1.0000
10	0.868	0.869	0.14%	0.9995	0.868	0.00%	1.0000

Table 7-7: Frequencies and Model Shapes Before and After Updating with the Iterative Substructuring Method

Mode	Measured Frequency (Hz)	Before updating			After updating		
		Frequency (Hz)	Difference (%)	MAC	Frequency (Hz)	Difference (%)	MAC
1	0.111	0.112	0.76%	1.0000	0.111	0.00%	1.0000
2	0.162	0.163	0.95%	1.0000	0.162	0.00%	1.0000
3	0.344	0.344	0.09%	0.9999	0.344	0.00%	1.0000
4	0.373	0.376	0.84%	0.9991	0.373	0.00%	0.9999
5	0.406	0.406	0.11%	0.9999	0.406	0.00%	1.0000
6	0.429	0.431	0.32%	0.9997	0.429	0.00%	1.0000
7	0.493	0.496	0.71%	0.9994	0.493	0.00%	0.9999
8	0.694	0.697	0.42%	0.9998	0.694	0.00%	1.0000
9	0.817	0.818	0.13%	0.9998	0.817	0.00%	1.0000
10	0.868	0.869	0.14%	0.9993	0.868	0.00%	1.0000

Table 7-8: Frequencies and Model Shapes Before and After Updating with Combination of the FRFS Method and the Iterative Substructuring Method

Mode	Measured Frequency (Hz)	Before updating			After updating		
		Frequency (Hz)	Difference (%)	MAC	Frequency (Hz)	Difference (%)	MAC
1	0.111	0.112	0.76%	0.9999	0.111	0.00%	1.0000
2	0.162	0.163	0.95%	0.9999	0.162	0.00%	1.0000
3	0.344	0.345	0.15%	0.9989	0.344	0.00%	0.9999
4	0.373	0.376	0.88%	0.9988	0.373	0.00%	0.9999
5	0.406	0.406	0.12%	0.9998	0.406	0.00%	1.0000
6	0.429	0.431	0.35%	0.9995	0.429	0.00%	0.9999
7	0.493	0.496	0.79%	0.9987	0.493	0.00%	1.0000
8	0.694	0.698	0.58%	0.9982	0.694	0.00%	1.0000
9	0.817	0.820	0.31%	0.9991	0.817	0.00%	0.9999
10	0.868	0.870	0.23%	0.9985	0.868	0.00%	1.0000

Finally, the FRFS method and the iterative substructuring are combined to be used in the model updating process, according to the optimization procedure. The FRFS method is computationally efficient in calculation of the eigensolutions and eigensensitivities with lower accuracy, whereas it is not competitive in obtaining the highly accurate eigensolutions and eigensensitivities, as compared with the iterative substructuring method. In the first 11 iterations, the FRFS method is adopted to calculate the first 10 eigensolutions and eigensensitivities, using the first 30 modes in each substructure. When the updated parameters approach to the optimized solutions, the convergence process is sensitive to the methodology error of the FRFS method. In the last few steps, the iterative substructuring method is adopted with 20 master modes retained in each substructure. The whole process converges within 17 iterations. The updated frequencies and mode shapes are listed Table 7-8. The FRFS method takes about 1.58 hours for each iteration, while the iterative method requires 3.62 hours. The whole procedure consumes 39.18 hours as shown in Figure 7-6. In Table 7-8, the frequencies and mode shapes before updating are a little different from those of the former two cases in Table 7-6 and Table 7-7, because the FRFS method inherently involves some errors in calculation of eigensolutions. This methodology

error may mask the real discrepancy of the analytical model and experimental data, thus hinder the convergence of optimization. That's why the highly accurate method needs to be used in the last steps of model updating. The combination of the FRFS method and the iterative method can achieve highly accurate results efficiently for model updating process.

7.6 Summary

This chapter proposes a new iterative substructuring method to calculate the accurate eigensolutions and eigensensitivities for large-size structures. The method retains the contribution of the higher modes using the residual flexibility matrix in an iterative form. Consequently, it can predict the eigensolutions and eigensensitivities accurately in just a few iterations. The iterative process is mainly performed on two items (ξ and $\frac{\partial \xi}{\partial r}$) at the substructure level, which adds only a small amount of extra computation time. The method is thus computationally efficient, especially for large structural systems.

Other than the substructuring methods proposed in previous chapters which improve the accuracy by enlarging the number of the retained master modes, this iterative substructuring method can achieve high accuracy using only few master modes by an iterative scheme upon a reduced eigenequation. Since the high accuracy is achieved without enlarging the size of the master modes retained in the substructures, the computation effort in analyzing the independent substructures is saved. Subsequently, the proposed method can keep the reduced eigenequation in small size, based on which the iteration is performed.

Application of the method to two examples demonstrates its ability to predict the eigensolutions and eigensensitivities with a high level of accuracy. The lower modes

converge faster than the higher modes, as expected. As compared with the global method, the present method may require more computation time to calculate the eigensolutions, but makes significant savings in the time needed to compute the eigensensitivities. As the calculation of eigensensitivities usually takes up much more computation time, this method shows promise for use in the sensitivity-based model updating process. Furthermore, it not only improves on computational efficiency, but also saves on computer storage memory.

The FRFS method described in previous chapters and the present iterative substructuring method are compared in this chapter. The former method is efficient with relatively lower accuracy. To achieve high accuracy, the FRFS method requires more effort extracting a large amount of master modes from the substructures, and hence handling a large-size eigenequation. The latter method, which is proposed in this chapter, improves the accuracy by an iterative scheme using only few master modes, and it keeps the reduced eigenequation in small size. Comparison of the two methods based upon the TV tower structure demonstrates that, if highly accurate eigensolutions and eigensensitivities are required, the iterative substructuring method is preferable. Combination of the FRFS method and iterative method in model updating process are beneficial to achieve both high accuracy and efficiency.

CHAPTER EIGHT

MODEL UPDATING USING SUBSTRUCTURAL MODAL DATA

8.1 Introduction

In the substructuring-based model updating approach described in previous chapters, the substructural eigensolutions and their derivatives of the independent substructures are assembled to recover the eigensolutions and eigensensitivities of the global structure. The eigenproperties of the global structure are then compared with those measured through model updating procedure.

In the approach described in this chapter, the substructural flexibility matrices are instead extracted from the measured global modal data. Consequently, the substructures are treated as independent structures and are updated using the common global model updating process. In each iteration, the eigensolutions of the substructures are compared with the extracted substructural flexibility matrices.

8.2 Extraction of the Substructural Flexibility Matrices

To explain the specific details of the new substructuring approach, the global structure with N DOFs is divided into Substructure A and Substructure B by N_B interface DOFs as illustrated in Figure 8-1.

The global structure before partition comprises three parts: the inner part of Substructure A $\left(\Pi_g^{(A)}\right)_I$, the inner part of Substructure B $\left(\Pi_g^{(B)}\right)_I$, and the interface area $\left(\Pi_g\right)_B$ shared by Substructure A and Substructure B.

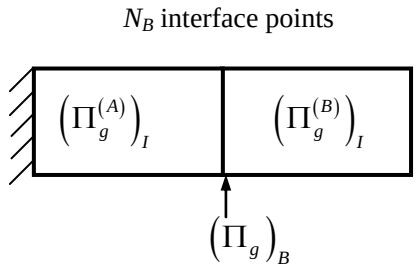

(a) Global Structure

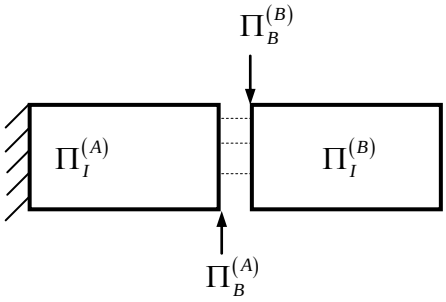

(b) Divided Substructures

Figure 8-1: Configuration of a Structure with Two Substructures

After partition, Substructure *A* is composed of two parts: the inner part $\Pi_I^{(A)}$ and the interface boundary $\Pi_B^{(A)}$. Likewise, Substructure *B* comprises an inner part $\Pi_I^{(B)}$ and an interface boundary $\Pi_B^{(B)}$. The superscripts '*A*' and '*B*' in bracket respectively represent the variables belong to Substructure *A* and Substructure *B*. The subscripts '*I*' and '*B*' hereinafter indicate the inner part and the interface boundary, respectively. The subscript '*g*' represents the variables in the original global structure before disassembly.

The DOFs of the four domains $\Pi_I^{(A)}$, $\Pi_B^{(A)}$, $\Pi_I^{(B)}$, and $\Pi_B^{(B)}$ take the size of $N_I^{(A)}$, $N_B^{(A)}$, $N_I^{(B)}$ and $N_I^{(B)}$, respectively, which satisfy

$$N^{(A)} = N_B^{(A)} + N_I^{(A)}$$

$$N^{(B)} = N_B^{(B)} + N_I^{(B)}$$

$$N_B^{(A)} = N_B^{(B)} = N_B$$

$$N = N_I^{(A)} + N_I^{(B)} + N_B$$

$$N^P = N_I^{(A)} + N_B^{(A)} + N_I^{(B)} + N_B^{(B)} \tag{8-1}$$

where N^P denotes the DOFs of all the substructures.

The stiffness and flexibility matrices of Substructure *A* and Substructure *B* are

$$\mathbf{K}^{(A)} = \begin{bmatrix} \mathbf{K}_{II}^{(A)} & \mathbf{K}_{IB}^{(A)} \\ \mathbf{K}_{BI}^{(A)} & \mathbf{K}_{BB}^{(A)} \end{bmatrix}, \quad \mathbf{F}^{(A)} = \begin{bmatrix} \mathbf{F}_{II}^{(A)} & \mathbf{F}_{IB}^{(A)} \\ \mathbf{F}_{BI}^{(A)} & \mathbf{F}_{BB}^{(A)} \end{bmatrix}$$

$$\mathbf{K}^{(B)} = \begin{bmatrix} \mathbf{K}_{II}^{(B)} & \mathbf{K}_{IB}^{(B)} \\ \mathbf{K}_{BI}^{(B)} & \mathbf{K}_{BB}^{(B)} \end{bmatrix}, \quad \mathbf{F}^{(B)} = \begin{bmatrix} \mathbf{F}_{II}^{(B)} & \mathbf{F}_{IB}^{(B)} \\ \mathbf{F}_{BI}^{(B)} & \mathbf{F}_{BB}^{(B)} \end{bmatrix} \tag{8-2}$$

The stiffness and flexibility matrices of the independent substructures are assembled in the following primitive form:

$$\mathbf{K}^p = \begin{bmatrix} \mathbf{K}_{II}^{(A)} & \mathbf{K}_{IB}^{(A)} & & \\ \mathbf{K}_{BI}^{(A)} & \mathbf{K}_{BB}^{(A)} & & \\ & & \mathbf{K}_{BB}^{(B)} & \mathbf{K}_{BI}^{(B)} \\ & & \mathbf{K}_{IB}^{(B)} & \mathbf{K}_{II}^{(B)} \end{bmatrix}, \quad \mathbf{F}^p = \begin{bmatrix} \mathbf{F}_{II}^{(A)} & \mathbf{F}_{IB}^{(A)} & & \\ \mathbf{F}_{BI}^{(A)} & \mathbf{F}_{BB}^{(A)} & & \\ & & \mathbf{F}_{BB}^{(B)} & \mathbf{F}_{BI}^{(B)} \\ & & \mathbf{F}_{IB}^{(B)} & \mathbf{F}_{II}^{(B)} \end{bmatrix} \tag{8-3}$$

Let $\{x_g\}$ denote the nodal displacement vector of the global structure and $\{f_g\}$ the external force vector. The primitive forms of the substructural displacements and forces are

$$\left\{x^p\right\} = \begin{Bmatrix} x_I^{(A)} \\ x_B^{(A)} \\ x_B^{(B)} \\ x_I^{(B)} \end{Bmatrix}, \quad \left\{f^p\right\} = \begin{Bmatrix} f_I^{(A)} \\ f_B^{(A)} \\ f_B^{(B)} \\ f_I^{(B)} \end{Bmatrix} \tag{8-4}$$

The size of the vectors $\left\{x^p\right\}$ and $\left\{f^p\right\}$ is $N^P \times 1$. They are associated with the global displacement vector and force as

$$\left\{x^p\right\} = \mathbf{L}^p \left\{x_g\right\} \tag{8-5}$$

$$\left[\mathbf{L}^p\right]^T \left\{f^p\right\} = \left\{f_g\right\} \tag{8-6}$$

where $\mathbf{L}^p$ is the geometric operator with a size of $N^P \times N$ and is determined by the geometric relation between the substructures and the global structure. For example, if the *j*th DOF of the global structure corresponds to the *i*th DOF in the separated substructures, then $\mathbf{L}_{ij}^p = 1$. Accordingly, Eq. (8-5) is expanded as

$$\begin{Bmatrix} x_I^{(A)} \\ x_B^{(A)} \\ x_B^{(B)} \\ x_I^{(B)} \end{Bmatrix} = \begin{bmatrix} \mathbf{L}_I^{(A)} & \mathbf{0} & \mathbf{0} \\ \mathbf{0} & \mathbf{L}_B^{(A)} & \mathbf{0} \\ \mathbf{0} & \mathbf{L}_B^{(B)} & \mathbf{0} \\ \mathbf{0} & \mathbf{0} & \mathbf{L}_I^{(B)} \end{bmatrix} \begin{Bmatrix} \left(x_g^{(A)}\right)_I \\ \left(x_g\right)_B \\ \left(x_g^{(B)}\right)_I \end{Bmatrix} \tag{8-7}$$

and Eq. (8-6) is expanded as

$$\begin{bmatrix} \left[\mathbf{L}_I^{(A)}\right]^T & \mathbf{0} & \mathbf{0} & \mathbf{0} \\ \mathbf{0} & \left[\mathbf{L}_B^{(A)}\right]^T & \left[\mathbf{L}_B^{(B)}\right]^T & \mathbf{0} \\ \mathbf{0} & \mathbf{0} & \mathbf{0} & \left[\mathbf{L}_I^{(A)}\right]^T \end{bmatrix} \begin{Bmatrix} f_I^{(A)} \\ f_B^{(A)} \\ f_B^{(B)} \\ f_I^{(B)} \end{Bmatrix} = \begin{Bmatrix} \left(f_g^{(A)}\right)_I \\ \left(f_g\right)_B \\ \left(f_g^{(B)}\right)_I \end{Bmatrix} \tag{8-8}$$

The structural equilibrium satisfies

$$\left(\left[\mathbf{L}^p\right]^T \mathbf{K}^p \mathbf{L}^p\right)\left\{x_g\right\} = \left[\mathbf{L}^p\right]^T \mathbf{K}^p \left\{x^p\right\} = \left[\mathbf{L}^p\right]^T \left\{f^p\right\} = \left\{f_g\right\} = \mathbf{K}_g \left\{x_g\right\} \tag{8-9}$$

In consequence, the global stiffness matrix and the primitive form of the substructural stiffness matrices have the relation

$$\left[\mathbf{L}^p\right]^T \mathbf{K}^p \mathbf{L}^p = \mathbf{K}_g \tag{8-10}$$

The displacement of a substructure can be written as a superposition of its deformational and rigid body motions. The displacement vector of Substructure *A* is composed of

$$\left\{x^{(A)}\right\} = \left\{x_d^{(A)}\right\} + \left\{x_R^{(A)}\right\} = \mathbf{F}^{(A)} \left\{f^{(A)}\right\} + \mathbf{R}^{(A)} \left\{\alpha^{(A)}\right\} \tag{8-11}$$

Likewise, the displacement vector of Substructure *B* can be expressed as

$$\left\{x^{(B)}\right\} = \left\{x_d^{(B)}\right\} + \left\{x_R^{(B)}\right\} = \mathbf{F}^{(B)} \left\{f^{(B)}\right\} + \mathbf{R}^{(B)} \left\{\alpha^{(B)}\right\} \tag{8-12}$$

where $\mathbf{F}^{(A)}$ and $\mathbf{F}^{(B)}$ are the substructural flexibility matrices, $\left\{f^{(A)}\right\}$ and $\left\{f^{(B)}\right\}$

are the forces imposed on Substructure *A* and Substructure *B*, respectively, $\mathbf{R}^{(A)}$ and $\mathbf{R}^{(B)}$ are the orthogonal rigid body modes of the two substructures, and $\left\{\alpha^{(A)}\right\}$ and $\left\{\alpha^{(B)}\right\}$ act as the modal participation factors of $\mathbf{R}^{(A)}$ and $\mathbf{R}^{(B)}$.

Eq. (8-11) and Eq. (8-12) give the primitive displacement vector in the form of

$$\left\{x^p\right\}=\begin{Bmatrix}x^{(A)}\\x^{(B)}\end{Bmatrix}=\begin{bmatrix}\mathbf{F}^{(A)} & \\ & \mathbf{F}^{(B)}\end{bmatrix}\begin{Bmatrix}f^{(A)}\\f^{(B)}\end{Bmatrix}+\begin{bmatrix}\mathbf{R}^{(A)} & \\ & \mathbf{R}^{(B)}\end{bmatrix}\begin{Bmatrix}\alpha^{(A)}\\\alpha^{(B)}\end{Bmatrix} \tag{8-13}$$

i.e.,

$$\left\{x^p\right\}=\mathbf{F}^p\left\{f^p\right\}+\mathbf{R}^p\left\{\alpha^p\right\} \tag{8-14}$$

Without losing generality, Substructure *A* is a fixed structure after partition and Substructure *B* is a free structure. Therefore, the rigid body components of Substructure *A* vanish and $\mathbf{R}^{(A)}=\mathbf{0}$ in this example. Theoretically, the flexibility matrix of a free structure does not exist. The flexibility matrix described in this chapter denotes the contributions made by the deformational motions and does not include those made by the rigid body motions. Appendix C describes the flexibility matrix of a free substructure in detail.

For Substructure *B*, $\mathbf{R}^{(B)}$ satisfies the substructural static force equilibrium (Alvin and Park 1999)

$$\left[\mathbf{R}^{(B)}\right]^T\left\{f^{(B)}\right\}=\{\mathbf{0}\} \tag{8-15}$$

In general, the primitive matrices of the rigid body modes and the forces in the substructures satisfy the force equilibrium compatibility equation

$$\left[\mathbf{R}^p\right]^T\left\{f^p\right\}=\{\mathbf{0}\} \tag{8-16}$$

As an independent structure, a substructure is loaded by the external force and the connecting force from the adjacent substructures. The forces exerted on Substructure *A* and Substructure *B* are respectively composed of

$$\left\{ f^{(A)} \right\} = \left\{ f_g^{(A)} \right\} + \{\tau\} \tag{8-17}$$

$$\left\{ f^{(B)} \right\} = \left\{ f_g^{(B)} \right\} - \{\tau\} \tag{8-18}$$

where $\left\{ f_g^{(A)} \right\}$ and $\left\{ f_g^{(B)} \right\}$ represent the external forces applied to Substructure *A* and Substructure *B*, respectively, and $\{\tau\}$, the Lagrange multiplier, represents the connecting force along the boundaries of the substructures.

In consequence, the primitive form of the substructural forces $\left\{ f^p \right\}$ is expressed as the superposition of the external and interface forces

$$\left\{ f^p \right\} = \left(\left[\mathbf{L}^p \right]^T \right)^+ \left\{ f_g \right\} + \mathbf{C}\{\tau\} = \left\{ \tilde{f}_g \right\} + \mathbf{C}\{\tau\} \tag{8-19}$$

where $\left\{ \tilde{f}_g \right\} = \left(\left[\mathbf{L}^p \right]^T \right)^+ \left\{ f_g \right\} = \tilde{\mathbf{L}}^p \left\{ f_g \right\}$, $\tilde{\mathbf{L}}^p = \left(\left[\mathbf{L}^p \right]^T \right)^+$ is the generalized inverse of $\left[\mathbf{L}^p \right]^T$ and matrix **C** implicitly defines the general connection between Substructure *A* and Substructure *B* as formulated in Chapter 4. From the physical point of view, the null-space of matrix **C** bears the displacement compatibility (Sehmi 1989)

$$\mathbf{C}^T \left\{ x^p \right\} = \{\mathbf{0}\} \tag{8-20}$$

i.e.,

$$\begin{bmatrix} \mathbf{0} & \mathbf{I} & -\mathbf{I} & \mathbf{0} \end{bmatrix} \begin{Bmatrix} x_I^{(A)} \\ x_B^{(A)} \\ x_B^{(B)} \\ x_I^{(B)} \end{Bmatrix} = \{\mathbf{0}\} \tag{8-21}$$

Substitution of Eq. (8-19) into Eq. (8-14) gives

$$\left\{ x^p \right\} = \mathbf{F}^p \left\{ f^p \right\} + \mathbf{R}^p \left\{ \alpha^p \right\} = \mathbf{F}^p \left(\left\{ \tilde{f}_g \right\} + \mathbf{C}\{\tau\} \right) + \mathbf{R}^p \left\{ \alpha^p \right\} \tag{8-22}$$

As for Eq. (8-5), the global displacement can be expressed by the substructural variables as

$$\left\{ x_g \right\} = \left[\mathbf{L}^p \right]^+ \left\{ x^p \right\} = \left[\tilde{\mathbf{L}}^p \right]^T \mathbf{F}^p \left(\left\{ \tilde{f}_g \right\} + \mathbf{C}\{\tau\} \right) + \left[\tilde{\mathbf{L}}^p \right]^T \mathbf{R}^p \left\{ \alpha^p \right\} \tag{8-23}$$

If the two variables $\{\tau\}$ and $\left\{ \alpha^p \right\}$ are known, the global displacement $\left\{ x_g \right\}$ and

the external force $\{f_g\}$ can be related by the substructural flexibility matrix $\mathbf{F}^p$, taking the place of the global flexibility matrix $\mathbf{F}_g$.

The force compatibility Eq. (8-16) and the displacement compatibility Eq. (8-20) are employed to solve the two variables $\{\tau\}$ and $\{\alpha^p\}$. Substitution of Eq. (8-19) into Eq. (8-16) yields

$$\left[\mathbf{R}^p\right]^T\left(\{\tilde{f}_g\}+\mathbf{C}\{\tau\}\right)=0 \tag{8-24}$$

Substituting Eq. (8-22) into Eq. (8-20) leads to

$$\mathbf{C}^T\left(\mathbf{F}^p\left(\{\tilde{f}_g\}+\mathbf{C}\{\tau\}\right)+\mathbf{R}^p\{\alpha^p\}\right)=\{\mathbf{0}\} \tag{8-25}$$

From Eq. (8-25), $\{\tau\}$ is expressed as

$$\{\tau\}=-\mathbf{F}_C^{-1}\left(\mathbf{C}^T\mathbf{F}^p\{\tilde{f}_g\}+\mathbf{R}_C\{\alpha^p\}\right) \tag{8-26}$$

where

$$\mathbf{F}_C=\mathbf{C}^T\mathbf{F}^p\mathbf{C},\ \ \mathbf{R}_C=\mathbf{C}^T\mathbf{R}^p \tag{8-27}$$

Substitution of Eq. (8-26) into Eq. (8-24) gives

$$\{\alpha^p\}=\mathbf{K}_R^{-1}\left(\left[\mathbf{R}^p\right]^T-\mathbf{R}_C^T\mathbf{F}_C^{-1}\mathbf{C}^T\mathbf{F}^p\right)\{\tilde{f}_g\} \tag{8-28}$$

where $\mathbf{K}_R=\mathbf{R}_C^T\mathbf{F}_C^{-1}\mathbf{R}_C$.

Substituting Eq. (8-28) into Eq. (8-26), $\{\tau\}$ is solved as

$$\{\tau\}=-\mathbf{F}_C^{-1}\mathbf{C}^T\mathbf{F}^p\{\tilde{f}_g\}+\mathbf{F}_C^{-1}\mathbf{R}_C\mathbf{K}_R^{-1}\left(\mathbf{R}_C^T\mathbf{F}_C^{-1}\mathbf{C}^T\mathbf{F}^p-\mathbf{R}^T\right)\{\tilde{f}_g\} \tag{8-29}$$

As long as $\{\tau\}$ and $\{\alpha^p\}$ are solved, Eq. (8-23) is expressed as

$$\begin{aligned}\{x_g\}&=\left[\tilde{\mathbf{L}}^p\right]^T\left(\mathbf{F}^p-\mathbf{F}^p\mathbf{K}_C\mathbf{F}^p+\mathbf{F}^p\mathbf{K}_C\mathbf{F}_R\mathbf{K}_C\mathbf{F}^p-\mathbf{F}^p\mathbf{K}_C\mathbf{F}_R-\mathbf{F}_R\mathbf{K}_C\mathbf{F}^p-\mathbf{F}^p\mathbf{H}\mathbf{F}^p+\mathbf{F}_R\right)\{\tilde{f}_g\}\\&=\left[\tilde{\mathbf{L}}^p\right]^T\left(\mathbf{F}^p-\mathbf{F}^p\mathbf{H}\mathbf{F}^p-\mathbf{F}^p\mathbf{K}_C\mathbf{F}_R-\mathbf{F}_R^T\mathbf{K}_C^T\mathbf{F}^p+\mathbf{F}_R\right)\tilde{\mathbf{L}}^p\{f_g\}\end{aligned} \tag{8-30}$$

in which

$$\mathbf{H}=\mathbf{K}_C-\mathbf{K}_C\mathbf{F}_R\mathbf{K}_C,\mathbf{K}_C=\mathbf{C}\mathbf{F}_C^{-1}\mathbf{C}^T,$$

$$\mathbf{F}_R = \mathbf{R}^p \left(\left[\mathbf{R}^p \right]^T \mathbf{K}_C \mathbf{R}^p \right)^{-1} \left[\mathbf{R}^p \right]^T \tag{8-31}$$

The displacement $\{x_g\}$ and force $\{f_g\}$ of the global structure are basically related to the global flexibility matrix as

$$\{x_g\} = \mathbf{F}_g \{f_g\} \tag{8-32}$$

Concerning Eq. (8-30) and Eq. (8-32), the global flexibility matrix is related to the substructural flexibility matrix by

$$\mathbf{F}_g = \left[\tilde{\mathbf{L}}^p \right]^T \left(\mathbf{F}^p - \mathbf{F}^p \mathbf{K}_C \mathbf{F}_R - \mathbf{F}_R^T \mathbf{K}_C^T \mathbf{F}^p - \mathbf{F}^p \mathbf{H} \mathbf{F}^p + \mathbf{F}_R \right) \tilde{\mathbf{L}}^p \tag{8-33}$$

which is rearranged as

$$\mathbf{L}^p \mathbf{F}_g \left[\mathbf{L}^p \right]^T = \mathbf{F}^p - \mathbf{F}^p \mathbf{K}_C \mathbf{F}_R - \mathbf{F}_R^T \mathbf{K}_C^T \mathbf{F}^p - \mathbf{F}^p \mathbf{H} \mathbf{F}^p + \mathbf{F}_R \tag{8-34}$$

In Eq. (8-34), the substructural flexibility matrix $\mathbf{F}^p$ contributes to the global flexibility matrix $\mathbf{F}_g$ in a complicated manner. It is difficult to express $\mathbf{F}^p$ in terms of $\mathbf{F}_g$ in an explicit form. An iterative scheme is required to obtain the substructural flexibility matrix $\mathbf{F}^p$ as follows.

1) The global flexibility matrix with size N is expanded to the dimension of N^P by the geometric operator $\mathbf{L}^p$

$$\bar{\mathbf{F}}_g = \mathbf{L}^p \mathbf{F}_g \left[\mathbf{L}^p \right]^T \tag{8-35}$$

Consequently, the items of the global flexibility matrix are rearranged according to the order of the DOFs in the separated substructures *A* and *B*.

2) The initial substructural flexibility matrix $\mathbf{F}^p$ is estimated from the diagonal sub-block of the global flexibility matrix $\bar{\mathbf{F}}_g$ corresponding to Substructure *A* and Substructure *B*, i.e.,

$$\left[\mathbf{F}^p \right]^{[0]} = \begin{bmatrix} \bar{\mathbf{F}}_g \left(1 : N^{(A)} \quad 1 : N^{(A)} \right) & \\ & \bar{\mathbf{F}}_g \left(\left(N^{(A)} + 1 \right) : N^P \quad \left(N^{(A)} + 1 \right) : N^P \right) \end{bmatrix} \tag{8-36}$$

3) The substructural flexibility matrix is extracted in an iterated form based on Eq.

(8-34). The *k*th iteration (*k* = 1, 2, …) has

$$\left[\mathbf{F}^{p}\right]^{[k]} = \bar{\mathbf{F}}_{g} + \left[\mathbf{F}^{p}\right]^{[k-1]} \mathbf{K}_{C}^{[k-1]} \mathbf{F}_{R}^{[k-1]} + \left[\mathbf{F}_{R}^{[k-1]}\right]^{T} \left[\mathbf{K}_{C}^{[k-1]}\right]^{T} \left[\mathbf{F}^{p}\right]^{[k-1]} + \left[\mathbf{F}^{p}\right]^{[k-1]} \mathbf{H}^{[k-1]} \left[\mathbf{F}^{p}\right]^{[k-1]} - \mathbf{F}_{R}^{[k-1]} \tag{8-37}$$

4) The diagonal sub-blocks of $\left[\mathbf{F}^{p}\right]^{[k]}$ corresponding to Substructure *A* and Substructure *B* are retained to keep the block-diagonal property of $\left[\mathbf{F}^{p}\right]^{[k]}$, i.e.,

$$\left[\mathbf{F}^{p}\right]^{[k]} = \begin{bmatrix} \left[\mathbf{F}^{p}\right]^{[k]}\left(1:N^{(A)} \quad 1:N^{(A)}\right) & \mathbf{0} \\ \mathbf{0} & \left[\mathbf{F}^{p}\right]^{[k]}\left(\left(N^{(A)}+1\right):N^{P} \quad \left(N^{(A)}+1\right):N^{P}\right) \end{bmatrix} \tag{8-38}$$

As Substructure *B* is free, the extracted substructural flexibility matrix should be orthogonal to the rigid-body modes. This can be achieved by multiplying a projector as

$$\mathbf{F}^{(B)} = \mathbf{P}^{(B)} \mathbf{F}^{(B)} \mathbf{P}^{(B)} \tag{8-39}$$

Appendix C gives the formulation of the projector $\mathbf{P}^{(B)}$, which is obtained from the rigid body modes as

$$\mathbf{P}^{(B)} = \mathbf{I} - \mathbf{R}^{(B)} \left[\mathbf{R}^{(B)}\right]^{T} \tag{8-40}$$

8.3 Extraction of the Substructural Flexibility Matrices in the Reduced DOFs

In practice, it is difficult to measure the target structure at all DOFs. Reduction of the full model to the desired DOFs is required.

The force compatibility Eq. (8-24) and the displacement compatibility Eq. (8-25) are disassembled according to the master DOFs and the slave DOFs as

$$\begin{bmatrix} \mathbf{R}_{a}^{p} \\ \mathbf{R}_{b}^{p} \end{bmatrix}^{T} \left(\begin{Bmatrix} \left\{\tilde{f}_{g}\right\}_{a} \\ \left\{\tilde{f}_{g}\right\}_{b} \end{Bmatrix} + \begin{bmatrix} \mathbf{C}_{a} \\ \mathbf{C}_{b} \end{bmatrix} \{\tau\} \right) = \mathbf{0} \tag{8-41}$$

$$\begin{bmatrix}\mathbf{C}_a\\ \mathbf{C}_b\end{bmatrix}^T\left(\begin{bmatrix}\mathbf{F}_{aa}^p & \mathbf{F}_{ab}^p\\ \mathbf{F}_{ba}^p & \mathbf{F}_{bb}^p\end{bmatrix}\left(\begin{Bmatrix}\{\tilde{f}_g\}_a\\ \{\tilde{f}_g\}_b\end{Bmatrix}+\begin{bmatrix}\mathbf{C}_a\\ \mathbf{C}_b\end{bmatrix}\{\tau\}\right)+\begin{bmatrix}\mathbf{R}_a^p\\ \mathbf{R}_b^p\end{bmatrix}\{\alpha^p\}\right)=\mathbf{0} \qquad (8\text{-}42)$$

where the subscript '*a*' represents the rows or columns corresponding to the measured DOFs, which are usually denoted as the master DOFs, and the subscript '*b*' represents those of the slave DOFs.

$\{\tau\}$ is solved from Eq. (8-42) as

$$\{\tau\}=-\left(\begin{bmatrix}\mathbf{C}_a\\ \mathbf{C}_b\end{bmatrix}^T\begin{bmatrix}\mathbf{F}_{aa}^p & \mathbf{F}_{ab}^p\\ \mathbf{F}_{ba}^p & \mathbf{F}_{bb}^p\end{bmatrix}\begin{bmatrix}\mathbf{C}_a\\ \mathbf{C}_b\end{bmatrix}\right)^{-1}\left(\begin{bmatrix}\mathbf{C}_a\\ \mathbf{C}_b\end{bmatrix}^T\begin{bmatrix}\mathbf{F}_{aa}^p & \mathbf{F}_{ab}^p\\ \mathbf{F}_{ba}^p & \mathbf{F}_{bb}^p\end{bmatrix}\begin{Bmatrix}\{\tilde{f}_g\}_a\\ \{\tilde{f}_g\}_b\end{Bmatrix}+\begin{bmatrix}\mathbf{C}_a\\ \mathbf{C}_b\end{bmatrix}^T\begin{bmatrix}\mathbf{R}_a^p\\ \mathbf{R}_b^p\end{bmatrix}\{\alpha^p\}\right) \qquad (8\text{-}43)$$

If the external forces are imposed on the master DOFs and the interface DOFs are always selected as the master DOFs, i.e., $\{\tilde{f}_g\}_b=\mathbf{0}$, $\mathbf{C}_b=\mathbf{0}$ and $\{\tilde{f}_g\}_a=\left(\left[\mathbf{L}_{aa}^p\right]^T\right)^+\{f_g\}_a=\tilde{\mathbf{L}}_{aa}^p\{f_g\}_a$, then Eq. (8-43) is equivalent to

$$\{\tau\}=-\mathbf{F}_{Ca}^{-1}\left(\mathbf{C}_a^T\mathbf{F}_{aa}^p\{\tilde{f}_g\}_a+\mathbf{C}_a^T\mathbf{R}_a^p\{\alpha^p\}\right) \qquad (8\text{-}44)$$

where $\mathbf{F}_{Ca}=\mathbf{C}_a^T\mathbf{F}_{aa}\mathbf{C}_a$.

Substituting Eq. (8-44) into Eq. (8-41) leads to

$$\left[\mathbf{R}_a^p\right]^T\{\tilde{f}_g\}_a-\left[\mathbf{R}_a^p\right]^T\mathbf{C}_a\mathbf{F}_{Ca}^{-1}\mathbf{C}_a^T\mathbf{F}_{aa}^p\{\tilde{f}_g\}_a-\left[\mathbf{R}_a^p\right]^T\mathbf{C}_a\mathbf{F}_{Ca}^{-1}\mathbf{C}_a^T\mathbf{R}_a^p\{\alpha^p\}=0 \qquad (8\text{-}45)$$

From Eq. (8-45), $\{\alpha^p\}$ can be solved as

$$\{\alpha^p\}=\mathbf{K}_{Ra}^{-1}\left(\left[\mathbf{R}_a^p\right]^T-\left[\mathbf{R}_a^p\right]^T\mathbf{C}_a\mathbf{F}_{Ca}^{-1}\mathbf{C}_a^T\mathbf{F}_{aa}^p\right)\{\tilde{f}_g\}_a \qquad (8\text{-}46)$$

and $\{\tau\}$ is therefore solved from Eq. (8-44) as

$$\{\tau\}=-\mathbf{F}_{Ca}^{-1}\mathbf{C}_a^T\mathbf{F}_{aa}^p\{\tilde{f}_g\}_a+\mathbf{F}_{Ca}^{-1}\mathbf{C}_a^T\mathbf{R}_a^p\mathbf{K}_{Ra}^{-1}\left(\left[\mathbf{R}_a^p\right]^T\mathbf{K}_{Ca}\mathbf{F}_{aa}^p-\left[\mathbf{R}_a^p\right]^T\right)\{\tilde{f}_g\}_a \qquad (8\text{-}47)$$

where $\mathbf{K}_{Ca}=\mathbf{C}_a\mathbf{F}_{Ca}^{-1}\mathbf{C}_a^T$, and $\mathbf{K}_{Ra}=\left[\mathbf{R}_a^p\right]^T\mathbf{K}_{Ca}\mathbf{R}_a^p=\left[\mathbf{R}_a^p\right]^T\mathbf{C}_a\mathbf{F}_{Ca}^{-1}\mathbf{C}_a^T\mathbf{R}_a^p$.

The displacement vector in Eq. (8-23) is partitioned according to the master and slave

DOFs as

$$\begin{Bmatrix} \{x_g\}_a \\ \{x_g\}_b \end{Bmatrix} = \begin{bmatrix} \tilde{\mathbf{L}}_{aa}^p & \\ & \tilde{\mathbf{L}}_{bb}^p \end{bmatrix}^T \begin{bmatrix} \mathbf{F}_{aa}^p & \mathbf{F}_{ab}^p \\ \mathbf{F}_{ba}^p & \mathbf{F}_{bb}^p \end{bmatrix} \left(\begin{Bmatrix} \{\tilde{f}_g\}_a \\ \{\tilde{f}_g\}_b \end{Bmatrix} + \begin{bmatrix} \mathbf{C}_a \\ \mathbf{C}_b \end{bmatrix} \{\tau\} \right) + \begin{bmatrix} \tilde{\mathbf{L}}_{aa}^p & \\ & \tilde{\mathbf{L}}_{bb}^p \end{bmatrix}^T \begin{bmatrix} \mathbf{R}_a^p \\ \mathbf{R}_b^p \end{bmatrix} \{\alpha^p\} \tag{8-48}$$

The displacements at the master DOFs are expressed as

$$\{x_g\}_a = \left[\tilde{\mathbf{L}}_{aa}^p\right]^T \mathbf{F}_{aa}^p \left(\{\tilde{f}_g\}_a + \mathbf{C}_a \{\tau\} \right) + \mathbf{R}_a^p \{\alpha^p\} \tag{8-49}$$

Given the solution of $\{\alpha^p\}$ in Eq. (8-46) and that of $\{\tau\}$ in Eq. (8-47), the displacement vector (Eq. (8-49)) of the global structure is thereby expressed as

$$\begin{aligned} \{x_g\}_a = \left[\tilde{\mathbf{L}}_{aa}^p\right]^T \Big(& \mathbf{F}_{aa}^p - \mathbf{F}_{aa}^p \mathbf{K}_{Ca} \mathbf{F}_{aa}^p + \mathbf{F}_{aa}^p \mathbf{K}_{Ca} \mathbf{F}_{Ra} \mathbf{K}_{Ca} \mathbf{F}_{aa}^p \\ & - \mathbf{F}_{aa}^p \mathbf{K}_{Ca} \mathbf{R}_a \mathbf{K}_{Ra}^{-1} \left[\mathbf{R}_a^p\right]^T - \mathbf{R}_a^p \mathbf{K}_{Ra}^{-1} \left[\mathbf{R}_a^p\right]^T \mathbf{K}_{Ca} \mathbf{F}_{aa}^p + \mathbf{R}_a^p \mathbf{K}_{Ra}^{-1} \left[\mathbf{R}_a^p\right]^T \Big) \tilde{\mathbf{L}}_{aa}^p \{f_g\}_a \end{aligned} \tag{8-50}$$

In the global structure, the displacements and external forces are related by the global flexibility as

$$x_g = \begin{Bmatrix} \{x_g\}_a \\ \{x_g\}_b \end{Bmatrix} = \begin{bmatrix} (\mathbf{F}_g)_{aa} & (\mathbf{F}_g)_{ab} \\ (\mathbf{F}_g)_{ba} & (\mathbf{F}_g)_{bb} \end{bmatrix} \begin{Bmatrix} \{f_g\}_a \\ \{f_g\}_b \end{Bmatrix} \tag{8-51}$$

Basically, the flexibility matrix corresponding to the master DOFs is defined as the displacement response due to a unit force applied at the master DOFs, whereas the forces at other DOFs are zero, i.e., $\{f_g\}_b = \mathbf{0}$. Therefore, the displacements at the master DOFs relate to the external forces by

$$\{x_g\}_a = (\mathbf{F}_g)_{aa} \{f_g\}_a \tag{8-52}$$

Concerning Eq. (8-50) and Eq. (8-52), the substructural flexibility matrix and global flexibility matrix at the master DOFs are related by

$$\begin{aligned} \mathbf{L}_{aa}^p (\mathbf{F}_g)_{aa} \left[\mathbf{L}_{aa}^p\right]^T = & \mathbf{F}_{aa}^p - \mathbf{F}_{aa}^p \mathbf{K}_{Ca} \mathbf{F}_{aa}^p + \mathbf{F}_{aa}^p \mathbf{K}_{Ca} \mathbf{F}_{Ra} \mathbf{K}_{Ca} \mathbf{F}_{aa}^p \\ & - \mathbf{F}_{aa}^p \mathbf{K}_{Ca} \mathbf{R}_a \mathbf{K}_{Ra}^{-1} \left[\mathbf{R}_a^p\right]^T - \mathbf{R}_a^p \mathbf{K}_{Ra}^{-1} \left[\mathbf{R}_a^p\right]^T \mathbf{K}_{Ca} \mathbf{F}_{aa}^p + \mathbf{R}_a^p \mathbf{K}_{Ra}^{-1} \left[\mathbf{R}_a^p\right]^T \end{aligned} \tag{8-53}$$

i.e.,

$$\mathbf{L}_{aa}^{p}\left(\mathbf{F}_{g}\right)_{aa}\left[\mathbf{L}_{aa}^{p}\right]^{T}=\mathbf{F}_{aa}^{p}-\mathbf{F}_{aa}^{p}\mathbf{H}_{aa}\mathbf{F}_{aa}^{p}-\mathbf{F}_{aa}^{p}\mathbf{K}_{Ca}\mathbf{F}_{Ra}-\mathbf{F}_{Ra}\mathbf{K}_{Ca}\mathbf{F}_{aa}^{p}+\mathbf{F}_{Ra} \quad (8\text{-}54)$$

where $\mathbf{F}_{Ra}=\mathbf{R}_{a}\mathbf{K}_{Ra}^{-1}\left[\mathbf{R}_{a}^{p}\right]^{T}$ and $\mathbf{H}_{aa}=\mathbf{K}_{Ca}-\mathbf{K}_{Ca}\mathbf{F}_{Ra}\mathbf{K}_{Ca}$. Similar to the procedure described in Section 8.2, the substructural flexibility matrix can be obtained using an iterative scheme. For a free substructure, the substructural flexibility matrix obtained needs to be normalized with the condensed projector $\mathbf{P}_R$ detailed in Appendix C.

In some instances, the uncertain parameters are localized within a substructure. It is preferable to extract only the substructural properties of that substructure to save on computational resources and experimental instruments. In consequence, the substructure of interest is chosen as the master DOFs and the other parts are the slave DOFs.

For example, Substructure *A* is known and Substructure *B* needs to be determined from the experimental global flexibility matrix. As regards Figure 8-1(a), the master DOFs of the global structure are selected as those in the domain $a\in\left(\left(\Pi_{g}^{(B)}\right)_{I}\bigcup\left(\Pi_{g}\right)_{B}\right)$. After partition, the master DOFs include the area $a\in\left(\Pi_{B}^{(A)}\bigcup\Pi_{B}^{(B)}\bigcup\Pi_{I}^{(B)}\right)$ of Figure 8-1(b), while the slave DOFs include $\Pi_{I}^{(A)}$.

Given the analytical model of Substructure *A*, the substructural flexibility matrix of Substructure *B* can be extracted according to the following procedure.

1) The global flexibility matrix $\left(\mathbf{F}_{g}\right)_{aa}^{E}$ is obtained from the measurement at the master DOFs $a\in\left(\left(\Pi_{g}^{(B)}\right)_{I}\bigcup\left(\Pi_{g}\right)_{B}\right)$. $\left(\mathbf{F}_{g}\right)_{aa}^{E}$ has the size of $N_a=N_I^{(B)}+N_B$. Superscript '*E*' denotes the variables from the experiment and Superscript '*A*' represents the variables of the analytical model.
2) The global flexibility matrix $\left(\mathbf{F}_{g}\right)_{aa}^{E}$ is expanded to $\left(\bar{\mathbf{F}}_{g}\right)_{aa}^{E}$ by the geometric operator $\mathbf{L}_{aa}^{p}$:

$$\left(\bar{\mathbf{F}}_g\right)_{aa}^{E} = \mathbf{L}_{aa}^{p}\left(\mathbf{F}_g\right)_{aa}^{E}\left[\mathbf{L}_{aa}^{p}\right]^{T} \tag{8-55}$$

where $\left(\bar{\mathbf{F}}_g\right)_{aa}^{E}$ takes the size of $N_a^P = N_B^{(A)} + N_I^{(B)} + N_B^{(B)}$.

3) The initial $\left[\mathbf{F}_{aa}^{p}\right]^{[0]}$ includes two parts: the substructural flexibility matrix of Substructure *A* at the boundary DOFs $\left(\mathbf{F}_B^{(A)}\right)^A$ and the global flexibility matrix corresponding to the points in Substructure *B*:

$$\left[\mathbf{F}_{aa}^{p}\right]^{[0]} = \begin{bmatrix} \mathbf{F}_B^{(A)} & \\ & \mathbf{F}^{(B)} \end{bmatrix} = \begin{bmatrix} \left(\mathbf{F}_B^{(A)}\right)^A & \\ & \left(\bar{\mathbf{F}}_g^{(B)}\right)^E \end{bmatrix} \tag{8-56}$$

where $\left(\mathbf{F}_B^{(A)}\right)^A$ takes the size of $N_B^{(A)}$, and $\left(\bar{\mathbf{F}}_g^{(B)}\right)^E$ takes the size of $N^{(B)}$ and is given by

$$\left(\bar{\mathbf{F}}_g^{(B)}\right)^E = \left(\bar{\mathbf{F}}_g\right)_{aa}^{E}\left(\left(N_B^{(A)}+1\right):N_a^P \quad \left(N_B^{(A)}+1\right):N_a^P\right) \tag{8-57}$$

4) Based on Eq. (8-54), the substructural flexibility matrix is extracted using an iterative scheme. In the *k*th iteration,

$$\left[\mathbf{F}_{aa}^{p}\right]^{[k]} = \left(\bar{\mathbf{F}}_g\right)_{aa}^{E} + \left[\mathbf{F}_{aa}^{p}\right]^{[k-1]}\mathbf{H}_{aa}^{[k-1]}\left[\mathbf{F}_{aa}^{p}\right]^{[k-1]} + \left[\mathbf{F}_{aa}^{p}\right]^{[k-1]}\mathbf{K}_{Ca}^{[k-1]}\mathbf{F}_{Ra}^{[k-1]} + \mathbf{F}_{Ra}^{[k-1]}\mathbf{K}_{Ca}^{[k-1]}\left[\mathbf{F}_{aa}^{p}\right]^{[k-1]} - \mathbf{F}_{Ra}^{[k-1]} \tag{8-58}$$

5) To keep the block-diagonal property of the substructural flexibility matrices, the sub-block of $\left[\mathbf{F}_{aa}^{p}\right]^{[k]}$ corresponding to Substructure *B* is used in the next iteration. The part corresponding to the boundary of Substructure *A* is filled with those from the analytical model of Substructure *A*:

$$\left[\mathbf{F}_{aa}^{p}\right]^{[k]} = \begin{bmatrix} \left(\mathbf{F}_B^{(A)}\right)^A & \\ & \left[\mathbf{F}^{(B)}\right]^{[k]} \end{bmatrix} \tag{8-59}$$

where $\left[\mathbf{F}^{(B)}\right]^{[k]} = \left[\mathbf{F}_{aa}^{p}\right]^{[k]}\left(\left(N_B^{(A)}+1\right):N_a^P \quad \left(N_B^{(A)}+1\right):N_a^P\right)$.

The projector $\mathbf{P}_R^{(B)}$ as described in Appendix C is subsequently constructed to normalize the $\left[\mathbf{F}^{(B)}\right]^{[k]}$ obtained to be used for model updating.

In practice, it is more convenient to construct the flexibility matrix or stiffness matrix

by using dynamic testing rather than static testing. Dynamic testing can extract basically the same modal information as the static measurement, but with less excitation and more economic process. The flexibility matrix can be assembled using a few of the lowest modes with sufficient accuracy (Duan *et al.* 2005). Pandey and Biswas (1994) showed that the flexibility matrix estimated from just the first two measured modes of a structure was accurate enough for damage condition assessment. Many researchers (Wu and Law 2004; Jaishi and Ren 2006; Perera and Ruiz 2008) have confirmed that the flexibility matrix is more sensitive to a local change in a structure than are other modal data such as frequencies and mode shapes.

The flexibility matrix determined through dynamic testing is usually denoted as modal flexibility, to which the mass-normalized deformational modes $\boldsymbol{\Phi}_d^E \left(\boldsymbol{\Lambda}_d^E\right)^{-1} \left[\boldsymbol{\Phi}_d^E\right]^T$ contribute. The mass-normalized deformational modes can be obtained in an experiment when one sensor-actuator pair exists (Alvin and Park 1994). In the present substructuring method, a projector associated with the mass-normalized mode shapes is constructed as described in Appendix C to ensure that the substructural flexibility matrix extracted is mass-normalized and is orthogonal to the rigid body modes.

It is noted that the interface DOFs should always be selected as the master DOFs. This is the limitation of the present substructuring method. The unmeasured components of the interface nodes can be estimated using either the analytical model or the curve fitting approach (Ng'andu *et al.* 1995). Future work is needed to overcome this shortcoming (Koh and Shankar 2003).

8.4 The Spring-mass Example

For a statically indeterminate structure, the iterative procedure described in Sections 8.2 and 8.3 is followed to extract the substructural flexibility matrices. For a

determinate structure, the substructural flexibility matrices can be obtained directly without iteration. The 6-DOF spring-mass model introduced in Chapter 3 is used to demonstrate this rule.

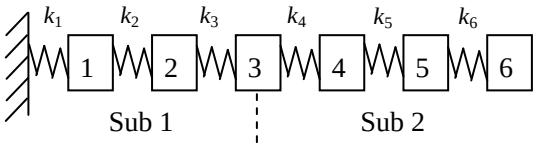

Figure 8-2: The Spring-mass Model with Six DOFs

The frequencies f^E and mode shapes $\mathbf{\Phi}^E$ of the global structure (Figure 8-2) are

$$\mathbf{\Lambda}^E = \left(2\pi f^E\right)^2 = \text{Diag}\left(\left[0.4198 \quad 4.9812 \quad 13.8865 \quad 23.4349 \quad 33.7875 \quad 43.4901\right]\right)$$

$$\mathbf{\Phi}^E = \begin{bmatrix} 0.1208 & 0.3639 & 0.2840 & 0.8735 & -0.0842 & 0.0458 \\ 0.2366 & 0.5466 & 0.1736 & -0.3001 & 0.1161 & -0.1077 \\ 0.3325 & 0.1847 & -0.4190 & -0.0673 & -0.4682 & 0.6753 \\ 0.3735 & -0.0422 & -0.4244 & 0.1279 & 0.0306 & -0.4017 \\ 0.3988 & -0.2481 & 0.1595 & 0.0234 & 0.4260 & 0.2682 \\ 0.4073 & -0.3304 & 0.5219 & -0.1360 & -0.6180 & -0.2284 \end{bmatrix} \quad (8\text{-}60)$$

As a result, the flexibility matrix of the global structure $\mathbf{F}_g^E$ is determined as

$$\mathbf{F}_g^E = \mathbf{\Phi}^E \left(\mathbf{\Lambda}^E\right)^{-1} \left[\mathbf{\Phi}^E\right]^T = \begin{bmatrix} 0.1 & 0.1 & 0.1 & 0.1 & 0.1 & 0.1 \\ 0.1 & 0.2 & 0.2 & 0.2 & 0.2 & 0.2 \\ 0.1 & 0.2 & 0.3 & 0.3 & 0.3 & 0.3 \\ 0.1 & 0.2 & 0.3 & 0.35 & 0.35 & 0.35 \\ 0.1 & 0.2 & 0.3 & 0.35 & 0.4 & 0.4 \\ 0.1 & 0.2 & 0.3 & 0.35 & 0.4 & 0.45 \end{bmatrix} \quad (8\text{-}61)$$

The global flexibility matrix corresponding to the first substructure is

$$\left(\mathbf{F}_g\right)_{aa}^E = \mathbf{F}_g^E\left(1\!:\!3 \quad 1\!:\!3\right) = \begin{bmatrix} 0.1 & 0.1 & 0.1 \\ 0.1 & 0.2 & 0.2 \\ 0.1 & 0.2 & 0.3 \end{bmatrix} \quad (8\text{-}62)$$

Because the first substructure is fixed-free, its substructural flexibility matrix can be obtained directly as

$$\left(\mathbf{F}^{(1)}\right)^{E} = \left(\mathbf{F}_{g}\right)_{aa}^{E} = \begin{bmatrix} 0.1 & 0.1 & 0.1 \\ 0.1 & 0.2 & 0.2 \\ 0.1 & 0.2 & 0.3 \end{bmatrix} \tag{8-63}$$

The global flexibility matrix corresponding to the second substructure is

$$\left(\mathbf{F}_{g}\right)_{aa}^{E} = \mathbf{F}_{g}^{E}\left(3{:}6 \quad 3{:}6\right) = \begin{bmatrix} 0.3 & 0.3 & 0.3 & 0.3 \\ 0.3 & 0.35 & 0.35 & 0.35 \\ 0.3 & 0.35 & 0.4 & 0.4 \\ 0.3 & 0.35 & 0.4 & 0.45 \end{bmatrix} \tag{8-64}$$

Given that the second substructure is free-free, the mass-normalized rigid body modes and projector are constructed according to Appendix C as

$$\mathbf{R}^{(2)} = \begin{bmatrix} 0.4082 \\ 0.4082 \\ 0.4082 \\ 0.4082 \end{bmatrix}, \quad \mathbf{P}^{(2)} = \begin{bmatrix} 0.8333 & -0.2357 & -0.2357 & -0.1667 \\ -0.2357 & 0.6667 & -0.3333 & -0.2357 \\ -0.2357 & -0.3333 & 0.6667 & -0.2357 \\ -0.1667 & -0.2357 & -0.2357 & 0.8333 \end{bmatrix} \tag{8-65}$$

The substructural flexibility matrix of the second substructure is therefore estimated with

$$\begin{aligned} \left(\mathbf{F}^{(2)}\right)^{E} &= \left(\mathbf{M}^{(2)}\right)^{-\frac{1}{2}} \mathbf{P}^{(2)} \left(\mathbf{M}^{(2)}\right)^{\frac{1}{2}} \left(\mathbf{F}_{g}\right)_{aa}^{E} \left(\mathbf{M}^{(2)}\right)^{\frac{1}{2}} \mathbf{P}^{(2)} \left(\mathbf{M}^{(2)}\right)^{-\frac{1}{2}} \\ &= \begin{bmatrix} 0.0486 & 0.0069 & -0.0181 & -0.0264 \\ 0.0069 & 0.0153 & -0.0097 & -0.0181 \\ -0.0181 & -0.0097 & 0.0153 & 0.0069 \\ -0.0264 & -0.0181 & 0.0069 & 0.0486 \end{bmatrix} \end{aligned} \tag{8-66}$$

In Chapter 3, the two substructures were analyzed independently, and the real substructural flexibility matrices of the independent substructures are

$$\left(\mathbf{F}^{(1)}\right)^{A} = \begin{bmatrix} 0.1 & 0.1 & 0.1 \\ 0.1 & 0.2 & 0.2 \\ 0.1 & 0.2 & 0.3 \end{bmatrix}, \quad \left(\mathbf{F}^{(2)}\right)^{A} = \begin{bmatrix} 0.0486 & 0.0069 & -0.0181 & -0.0264 \\ 0.0069 & 0.0153 & -0.0097 & -0.0181 \\ -0.0181 & -0.0097 & 0.0153 & 0.0069 \\ -0.0264 & -0.0181 & 0.0069 & 0.0486 \end{bmatrix} \tag{8-67}$$

The substructural flexibility matrices $\left(\mathbf{F}^{(1)}\right)^{E}$ and $\left(\mathbf{F}^{(2)}\right)^{E}$ extracted from the global modal data exactly reconstruct those calculated from the independent analytical models of the substructures $\left(\left(\mathbf{F}^{(1)}\right)^{A} \text{ and } \left(\mathbf{F}^{(2)}\right)^{A}\right)$ without iteration.

8.5 The Experimental Cantilever Beam

In this section, the proposed substructuring method is applied to the experimental cantilever beam structure. The detailed experimental set-up and modal data are provided in Chapter 3.

The beam is tested in five states: an undamaged state and four damaged scenarios. The mass loss due to the cuts is ignored in the analysis. The measured frequencies and mode shapes are employed to calculate the global mass-normalized flexibility as

$$\mathbf{F}_g^E = \mathbf{\Phi}^E \left(\mathbf{\Lambda}^E \right)^{-1} \left[\mathbf{\Phi}^E \right]^T \qquad (8\text{-}68)$$

The beam is measured in the vertical direction at the 10 points shown in Figure 8-3. Consequently, the global flexibility matrix takes the size of 10×10.

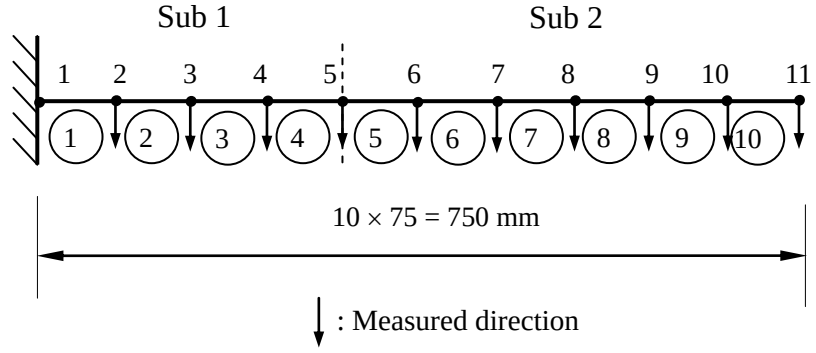

Figure 8-3: FE Model of the Cantilever Beam

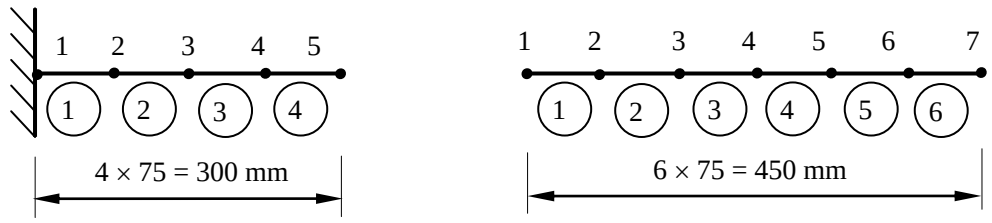

(a) The First Substructure (b) The Second Substructure

Figure 8-4: FE Model of the Partitioned Substructures

The beam is modeled using 10 two-dimensional beam elements and 11 nodes and is divided into two substructures at Node 5 as shown in Figure 8-3. After partition, the first substructure is fixed-free, while the second one is free-free. The sub-models of the two substructures are constructed independently as illustrated in Figure 8-4.

In all of the five states, the substructural flexibility matrices of the two substructures are extracted from the measured global modal data. The undamaged substructural flexibility matrices are used to update the two sub-models. Young's moduli of all elements are chosen as the updating parameters and are initially set to 2×10^{11} Pa. There are four updating parameters in the first substructure and six in the second. The refined sub-models of the two substructures are subsequently used for damage identification.

In each state, the two sub-models are tuned independently as follows.

1) Construct the projector $\mathbf{P}_R$ according to Appendix C. The condensed stiffness matrix $\mathbf{K}_R^{(2)}$, the condensed mass matrix $\mathbf{M}_R^{(2)}$, and the rigid body modes $\mathbf{R}_a^{(2)}$ are formed from the analytical model of the second substructure. The mass-normalized projector $\mathbf{P}_R^{(2)}$ is then constructed.

2) Extract the substructural flexibility matrices from the global flexibility matrix $\mathbf{F}_g^E$. The cantilever beam is a statically determinate structure and hence the substructural flexibility matrices can be extracted without iteration. The first substructural flexibility matrix is obtained directly from the corresponding rows and columns of the global flexibility matrix as

$$\left(\tilde{\mathbf{F}}_R^{(1)}\right)^E = \mathbf{F}_g^E\left(1{:}4 \quad 1{:}4\right) \tag{8-69}$$

The second substructural flexibility matrix is extracted from the global flexibility matrix

$$\mathbf{F}_g^{(2)} = \mathbf{F}_g^E\left(4{:}10 \quad 4{:}10\right)$$

and is normalized as

$$\left(\mathbf{P}_R^{(2)}\right)_1 = \left(\mathbf{M}_R^{(2)} \setminus \mathbf{M}_1^{(2)}\right)\mathbf{P}_R^{(2)}\mathbf{M}_2^{(2)}, \quad \left(\mathbf{P}_R^{(2)}\right)_2 = \left(\mathbf{P}_R^{(2)}\right)_1^T,$$

$$\left(\tilde{\mathbf{F}}_R^{(2)}\right)^E = \left(\mathbf{P}_R^{(2)}\right)_1 \mathbf{F}_g^{(2)} \left(\mathbf{P}_R^{(2)}\right)_2 \qquad (8\text{-}70)$$

where $\mathbf{M}_R^{(2)}$ is the condensed mass matrix of the second substructure and is decomposed by QR algorithm as $\mathbf{M}_R^{(2)} = \mathbf{M}_1^{(2)}\mathbf{M}_2^{(2)}$.

3) Update the two substructures independently. The substructures are treated as independent structures and are updated using the conventional global model updating method. For the first substructure, the substructural flexibility matrix $\left(\mathbf{F}^{(1)}\right)^A$ is calculated and condensed to the measured points $\left(\tilde{\mathbf{F}}_R^{(1)}\right)^A$ in each iteration to reproduce the extracted flexibility matrix $\left(\tilde{\mathbf{F}}_R^{(1)}\right)^E$. For the second substructure, the condensed substructural flexibility matrix $\left(\mathbf{F}_R^{(2)}\right)^A$ obtained from the analytical model needs to be normalized with the projector $\mathbf{P}_R^{(2)}$ by

$$\left(\tilde{\mathbf{F}}_R^{(2)}\right)^A = \left(\mathbf{P}_R^{(2)}\right)_1 \left(\mathbf{F}_R^{(2)}\right)^A \left(\mathbf{P}_R^{(2)}\right)_2 \qquad (8\text{-}71)$$

The second substructure is similarly updated as an independent structure so that $\left(\tilde{\mathbf{F}}_R^{(2)}\right)^A$ matches $\left(\tilde{\mathbf{F}}_R^{(2)}\right)^E$ throughout the optimization process.

The SRF values of the first substructure in the aforementioned five states are shown in Figure 8-5. Element 2 is found to have noticeable SRF values in the four damaged states (Cases 1 to 4), whereas the SRF values of the other elements are close to zero. The identified Element 2 coincides with the location of the artificial cut made in the experiment. As the depth of the cut increases progressively with d = 5 mm (Case 1), 10 mm (Case 2), and 15 mm (Case 3 and Case 4), the magnitude of SRF increase as expected. As explained in Chapter 6, the SRF value quantifies the overall equivalent change in the elemental parameter due to a local cut. As a result, Element 2 is believed to be damaged with the equivalent stiffness reductions of about 10% (Case 1), 14% (Case 2), and 22% (Case 3 and Case 4), respectively.

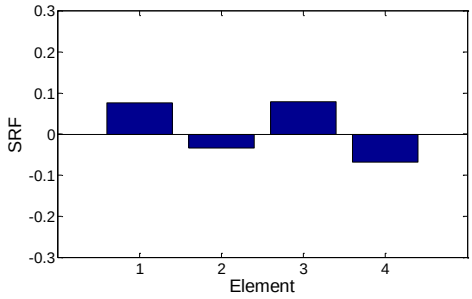

(a) Case 0 (No Damage)

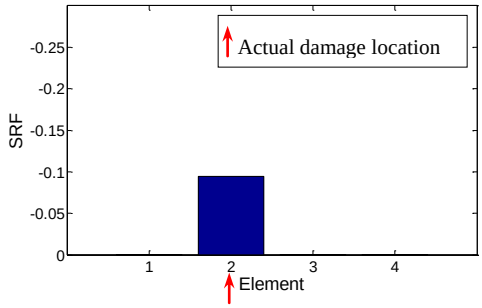

(b) Case 1

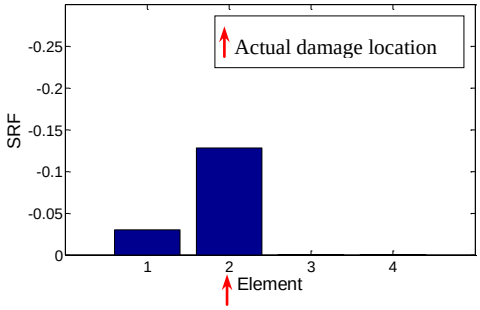

(c) Case 2

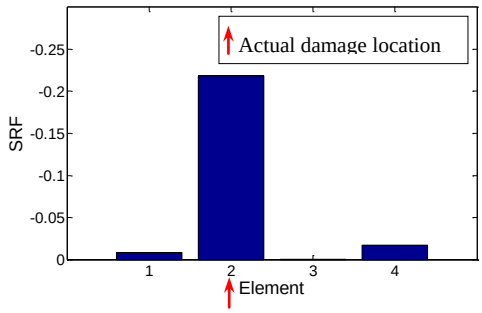

(d) Case 3

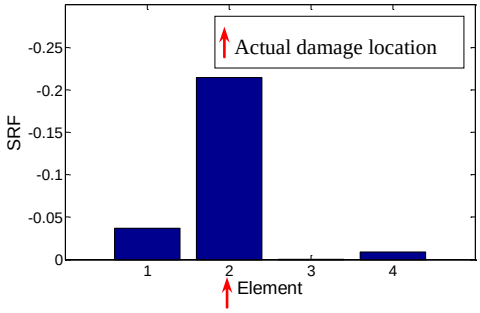

(e) Case 4

Figure 8-5: SRF Values of Substructure 1 in the Five States

The six elemental parameters of the second substructure are updated similarly in each of the five states. The SRF values are given in Figure 8-6.

In Cases 1 to 3, small SRF values are observed in some elements. No artificial cut was introduced within the second substructure in any of these three cases. The non-zero SRF values are due to the inevitable measurement noise and methodology errors. In Case 4, the SRF value of Element 3 (Element 7 of the global structure) is remarkably identified with -16%, as shown in Figure 8-6(e). This agrees with the location of the cut introduced in the experiment.

The updated parameters are then used in the global FE model to calculate the frequencies and mode shapes of the global structure and compare them with the measured ones, as listed in Tables 8-1 to 8-5. In all of the five states, the frequencies and mode shapes of the updated structure agree better with the measured ones than do those obtained before the model was updated.

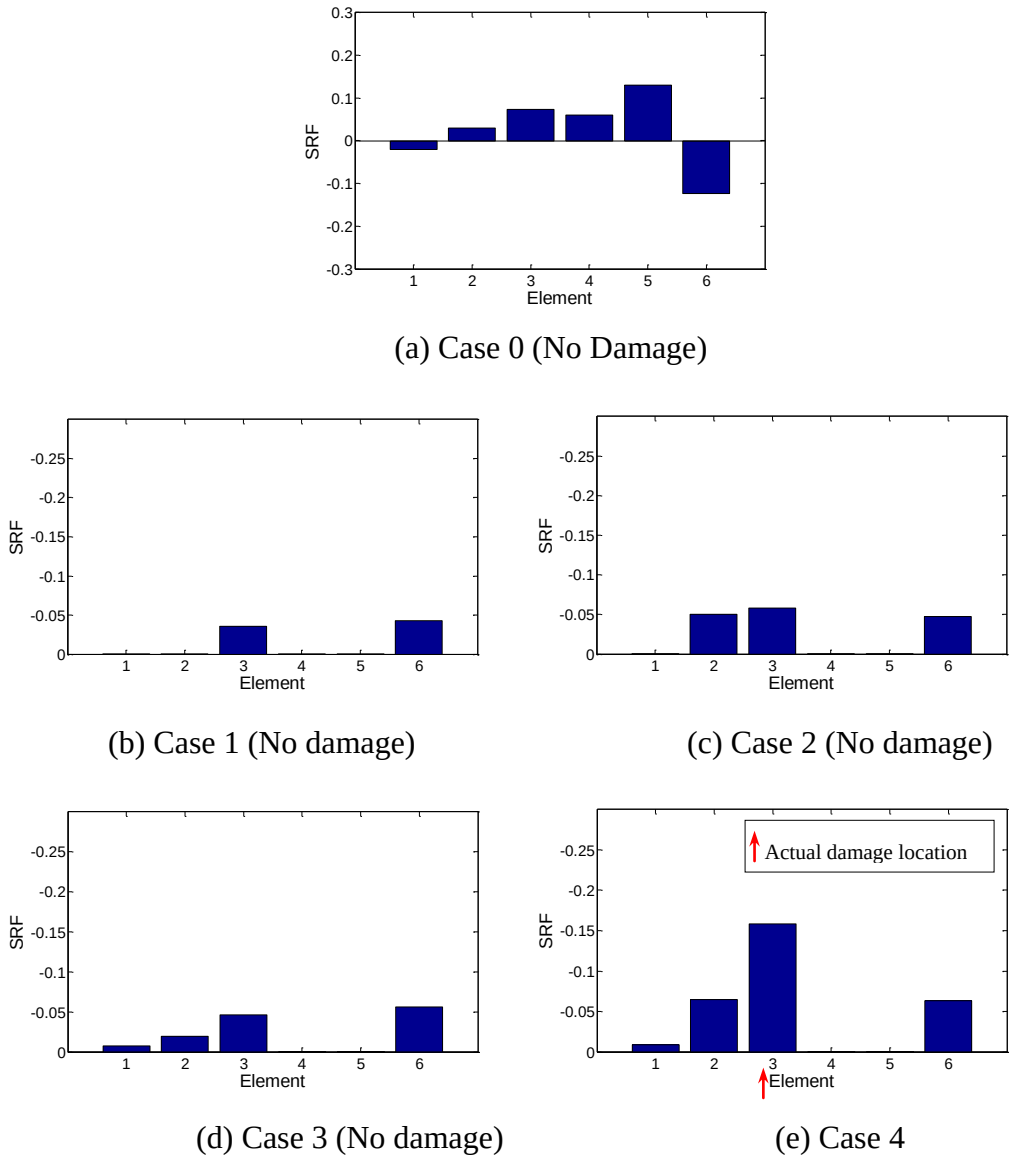

(a) Case 0 (No Damage)

(b) Case 1 (No damage)

(c) Case 2 (No damage)

(d) Case 3 (No damage)

(e) Case 4

Figure 8-6: SRF Values of Substructure 2 in the Five States

Table 8-1: Frequencies and Mode Shapes Before and After Updating (Case 0)

Modes	Experimental Frequency (Hz)	Before updating			After updating		
		Frequency (Hz)	Diff. (%)	MAC	Frequency (Hz)	Diff. (%)	MAC
1	3.50	3.47	-0.93%	0.9941	3.50	0.00%	0.9945
2	21.85	20.91	-4.29%	0.9975	21.85	0.00%	0.9982
3	60.29	57.60	-4.46%	0.9983	60.32	0.05%	0.9989
4	118.82	113.81	-4.21%	0.9985	118.63	-0.16%	0.9996
5	194.71	187.76	-3.57%	0.9958	192.82	-0.97%	0.9971
6	306.11	306.19	0.03%	0.9903	308.16	0.67%	0.9953
Average [a]			2.92%	0.9958		0.34%	0.9973

[a] Average of absolute value.

Table 8-2: Frequencies and Mode Shapes Before and After Updating (Case 1)

Modes	Experimental Frequency (Hz)	Before updating			After updating		
		Frequency (Hz)	Difference (%)	MAC	Frequency (Hz)	Difference (%)	MAC
1	3.44	3.50	1.94%	0.9921	3.45	0.45%	0.9929
2	21.85	21.85	0.00%	0.9980	21.84	-0.03%	0.9981
3	60.28	60.32	0.07%	0.9986	60.27	-0.02%	0.9983
4	118.68	118.63	-0.04%	0.9910	118.66	-0.02%	0.9957
5	193.71	192.82	-0.46%	0.9926	193.49	-0.12%	0.9950
6	304.32	308.16	1.26%	0.9891	306.02	0.56%	0.9987
Average [a]			0.63%	0.9935		0.20%	0.9965

[a] Average of absolute value.

Table 8-3: Frequencies and Mode Shapes Before and After Updating (Case 2)

Modes	Experimental Frequency (Hz)	Before updating			After updating		
		Frequency (Hz)	Difference (%)	MAC	Frequency (Hz)	Difference (%)	MAC
1	3.50	3.50	0.00%	0.9920	3.49	-0.22%	0.9926
2	21.52	21.85	1.54%	0.9970	21.58	0.27%	0.9960
3	59.58	60.32	1.24%	0.9973	59.61	0.04%	0.9927
4	117.40	118.63	1.05%	0.9822	117.00	-0.34%	0.9868
5	190.25	192.82	1.35%	0.9833	189.24	-0.53%	0.9865
6	299.23	308.16	2.98%	0.9271	300.65	0.47%	0.9568
Average [a]			1.38%	0.9798		0.31%	0.9852

[a] Average of absolute value.

Table 8-4: Frequencies and Mode Shapes Before and After Updating (Case 3)

Modes	Experimental Frequency (Hz)	Before updating			After updating		
		Frequency (Hz)	Difference (%)	MAC	Frequency (Hz)	Difference (%)	MAC
1	3.43	3.50	2.30%	0.9976	3.43	0.00%	0.9981
2	21.50	21.85	1.63%	0.9981	21.52	0.10%	0.9988
3	59.67	60.32	1.09%	0.9990	59.59	-0.13%	0.9966
4	116.82	118.63	1.56%	0.9881	116.47	-0.29%	0.9909
5	188.43	192.82	2.33%	0.9813	187.62	-0.43%	0.9946
6	295.67	308.16	4.22%	0.9601	296.93	0.43%	0.9822
Average [a]			2.19%	0.9873		0.24%	0.9935

[a] Average of absolute value.

Table 8-5: Frequencies and Mode Shapes Before and After Updating (Case 4)

Modes	Experimental Frequency (Hz)	Before updating			After updating		
		Frequency (Hz)	Difference (%)	MAC	Frequency (Hz)	Difference (%)	MAC
1	3.42	3.50	2.43%	0.9993	3.42	-0.08%	0.9992
2	21.20	21.85	3.05%	0.9968	21.24	0.19%	0.9978
3	59.00	60.32	2.23%	0.9936	58.93	-0.12%	0.9891
4	116.61	118.63	1.73%	0.9617	116.16	-0.39%	0.9717
5	187.29	192.82	2.95%	0.9714	186.92	-0.19%	0.9755
6	294.38	308.16	4.68%	0.9715	295.32	0.32%	0.9868
Average [a]			2.85%	0.9823		0.22%	0.9867

[a] Average of absolute value.

The beam is also updated according to the traditional global method using the same measurement data and updating parameters. The difference between the measured modal flexibility and the analytical modal flexibility is minimized by adjusting the 10 elemental stiffness parameters. The initial model is updated in the undamaged state and the refined model is then employed for damage identification. The SRF values identified in the five states are illustrated in Figure 8-7.

In Cases 1 to 4, the SRF values identified are consistent with those observed using the previous substructuring-based model updating method, and the results from both methods reveal the real locations and severity of the artificial cuts made in the

experiment. This again proves that the present substructuring method is effective in model updating and damage identification.

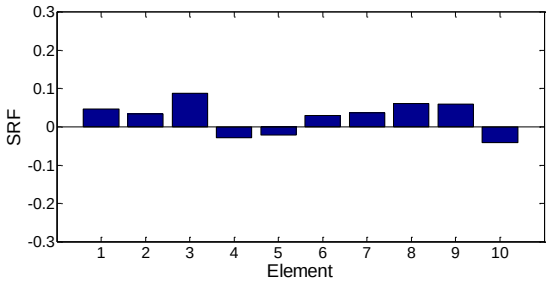

(a) Case 0 (No Damage)

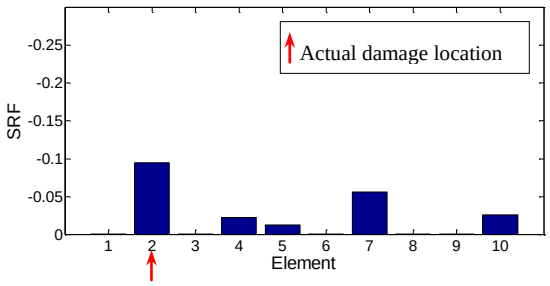

(b) Case 1

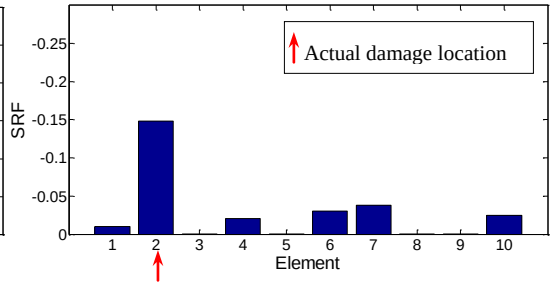

(c) Case 2

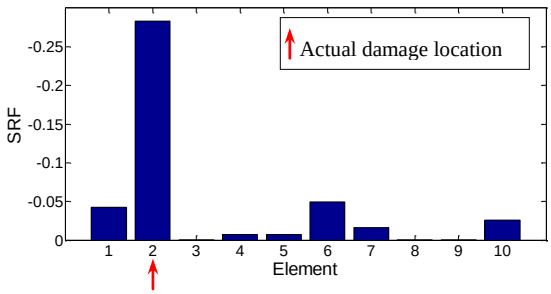

(d) Case 3

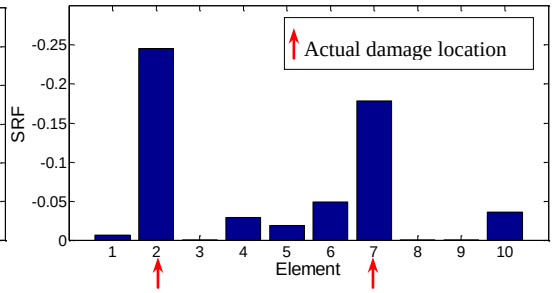

(e) Case 4

Figure 8-7: SRF Values of the Structure Using the Global Model Updating Method

8.6 The Experimental Frame Structure

The effectiveness of the substructuring method described in this chapter is examined further by using the portal frame, a statically indeterminate structure in which an iterative procedure is required to extract the substructural flexibility matrix from the global modal data. The accuracy of the extracted substructural flexibility matrix is first investigated via a numerical analysis. The substructuring-based model updating method is then applied to the laboratory-tested frame structure.

8.6.1 Numerical Analysis

The analytical model of the frame is composed of 44 nodes and 45 elements and is separated into three substructures as shown in Figure 8-8. In the numerical analysis, the substructural flexibility matrix of a substructure is extracted from the global modal data and compared with the real matrix obtained from the independent analytical model of the same substructure.

It is first necessary to extract the substructural flexibility matrix of the first substructure $\left(\tilde{\mathbf{F}}_R^{(1)}\right)^E$ from the global modal data, while the analytical sub-models of the second and third substructures are assumed to be known in advance. In this case, the frequencies and mode shapes corresponding to the first substructure are required to construct $\left(\mathbf{F}_g\right)_{aa}^E$, i.e., the global structure is measured at Nodes 1 to 18 in the directions illustrated in Figure 8-8.

The substructural flexibility matrix $\left(\tilde{\mathbf{F}}_R^{(1)}\right)^E$ is extracted using the global flexibility matrix $\left(\mathbf{F}_g\right)_{aa}^E$ by an iterative scheme. $\left(\tilde{\mathbf{F}}_R^{(1)}\right)^E$ is recorded in each iteration and compared with the actual flexibility matrix $\left(\tilde{\mathbf{F}}_R^{(1)}\right)^A$ calculated from the analytical sub-model of the first substructure.

$$Diff\left(\mathbf{F}\right) = \frac{norm\left(\left(\tilde{\mathbf{F}}_R^{(1)}\right)^E - \left(\tilde{\mathbf{F}}_R^{(1)}\right)^A\right)}{norm\left(\left(\tilde{\mathbf{F}}_R^{(1)}\right)^A\right)} \tag{8-72}$$

where $norm(\,)$ gives the Frobenius norm of a matrix hereinafter, and $Diff\left(\mathbf{F}\right)$ is employed here to assess the accuracy of the extracted flexibility matrix. The values of $Diff\left(\mathbf{F}\right)$ are less than $Tol = 1\times10^{-6}$ after 32 iterations, as illustrated in Figure 8-9. This indicates that the extracted substructural flexibility matrix $\left(\tilde{\mathbf{F}}_R^{(1)}\right)^E$ can accurately reproduce the actual flexibility matrix $\left(\tilde{\mathbf{F}}_R^{(1)}\right)^A$.

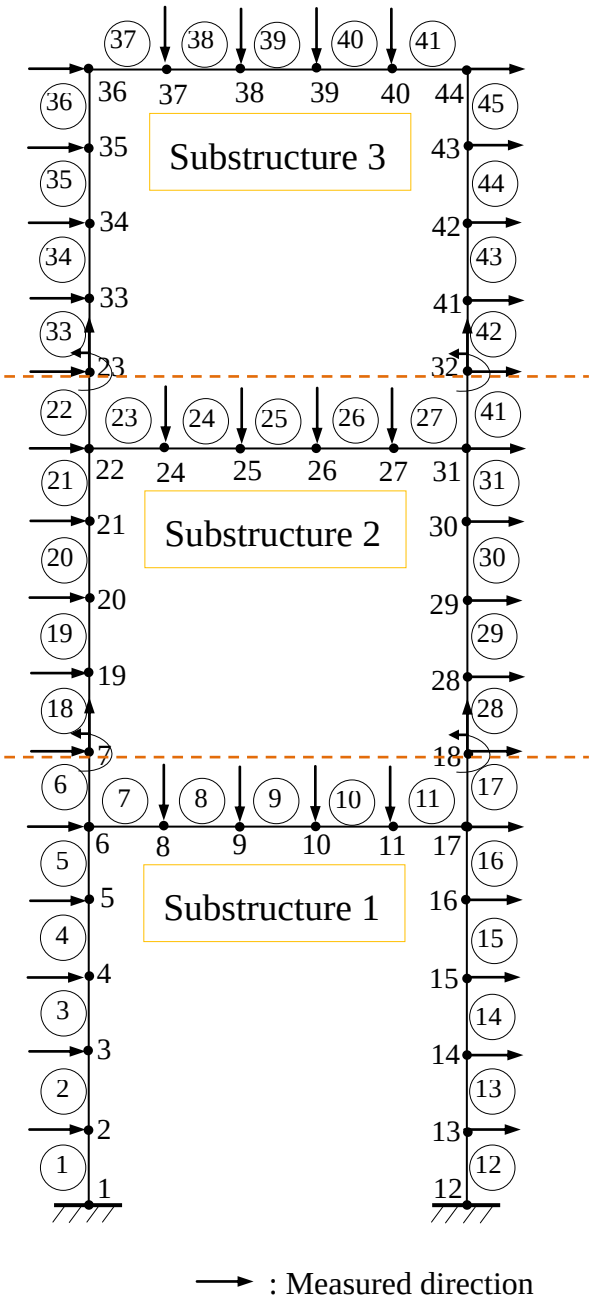

Figure 8-8: Configuration of the Frame Structure

Next, the substructural flexibility matrix of the second substructure is extracted from the global modal data, while the sub-models of the first and third substructures are assumed to be available. The global structure is measured at the second substructure to assemble $\left(\mathbf{F}_g\right)_{aa}^{E}$, including the measurements at Node 7 and Nodes 18 to 32.

The substructural flexibility matrix $\left(\mathbf{F}_R^{(2)}\right)^E$ is extracted from the global flexibility matrix $\left(\mathbf{F}_g\right)_{aa}^E$ by an iterative process. Because the second substructure is free after partition, $\left(\mathbf{F}_R^{(2)}\right)^E$ is normalized via $\left(\tilde{\mathbf{F}}_R^{(2)}\right)^E = \mathbf{P}_R^{(2)}\left(\mathbf{F}_R^{(2)}\right)^E \mathbf{P}_R^{(2)}$. For comparison, the real substructural flexibility matrix $\left(\mathbf{F}_R^{(2)}\right)^A$ is calculated from the analytical sub-model of the second substructure and is also normalized with $\left(\tilde{\mathbf{F}}_R^{(2)}\right)^A = \mathbf{P}_R^{(2)}\left(\mathbf{F}_R^{(2)}\right)^A \mathbf{P}_R^{(2)}$. The difference between $\left(\tilde{\mathbf{F}}_R^{(2)}\right)^E$ and $\left(\tilde{\mathbf{F}}_R^{(2)}\right)^A$ is calculated by Eq. (8-72) in each iteration. Setting the tolerance to $Tol=1\times10^{-6}$ again, the norm of difference is demonstrated in Figure 8-10.

Finally, the accuracy of the extracted substructural flexibility matrix of the third substructure is investigated. In this case, the sub-models of the first and second substructures are assumed to be known and the global structure is measured at the points corresponding to the third substructure, i.e., at Node 23 and Nodes 33 to 44.

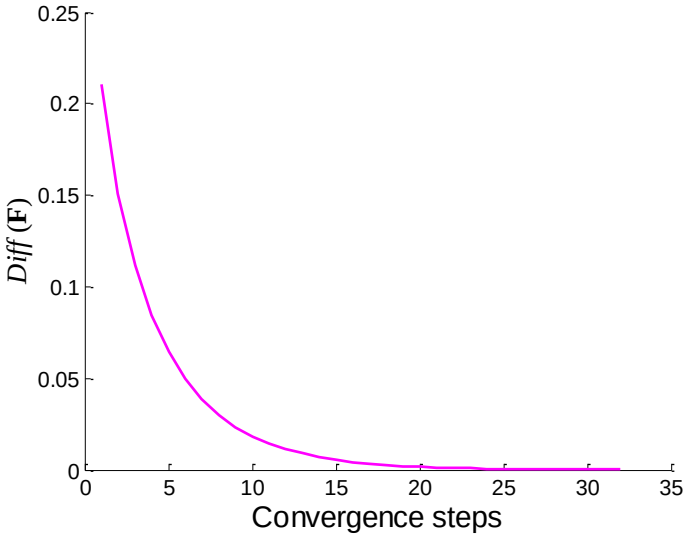

Figure 8-9: Convergence of the Substructural Flexibility Matrix of the First Substructure

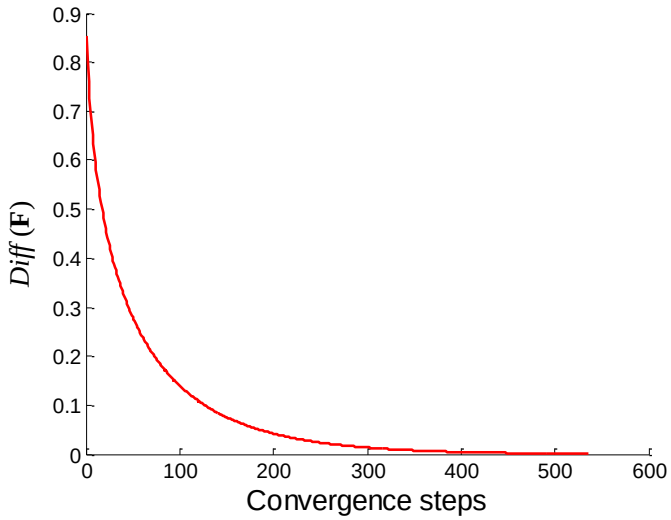

Figure 8-10: Convergence of the Substructural Flexibility Matrix of the Second Substructure

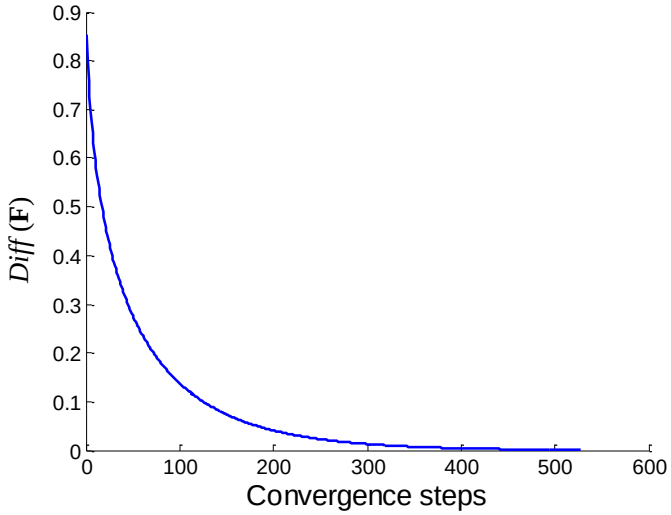

Figure 8-11: Convergence of the Substructural Flexibility Matrix of the Third Substructure

Similar to the previous steps, the normalized substructural flexibility matrix of the third substructure $\left(\tilde{\mathbf{F}}_R^{(3)}\right)^E$ is extracted in each iteration and compared with the normalized $\left(\tilde{\mathbf{F}}_R^{(3)}\right)^A$ calculated from the analytical sub-model. The value of *Diff* (**F**) in each iteration is illustrated in Figure 8-11 under the tolerance of $Tol = 1 \times 10^{-6}$.

Figures 8-9 to 8-11 reveal that the substructural flexibility matrices extracted from the

global modal data accurately reproduce the actual flexibility matrices of the independent substructures for all of the three substructures. The substructural flexibility matrix of the first substructure converges much more rapidly than do those of the other two substructures. It is noted that the first substructure is fixed, whereas the other two substructures are free after partition. The reason for this is not clear and merits further investigation.

8.6.2 Experimental Study

In consequence, this substructuring method is applied to the laboratory-tested frame structure. The test set-up and results are provided in Chapter 3. The global structure is also modeled using 45 two-dimensional beam elements and 44 nodes as shown in Figure 8-8. The analytical model is divided into three substructures as displayed in Figures 8-12 to 8-14. The substructural flexibility matrices of the three substructures are extracted from the measurement data in the undamaged states and are used as the basis for updating the three sub-models. The three refined sub-models are subsequently used for damage identification.

In the undamaged state, the mass-normalized flexibility matrix is obtained from the measured frequencies and mode shapes as

$$\mathbf{F}_g^E = \mathbf{\Phi}^E \left(\mathbf{\Lambda}^E \right)^{-1} \left[\mathbf{\Phi}^E \right]^T \qquad (8\text{-}73)$$

In the experiment, the interfaces at Node 7, Node 18, Node 23, and Node 32 are measured in the horizontal direction only. The unmeasured components (the Y direction and rotation) of the interfaces are estimated by the initial analytical model.

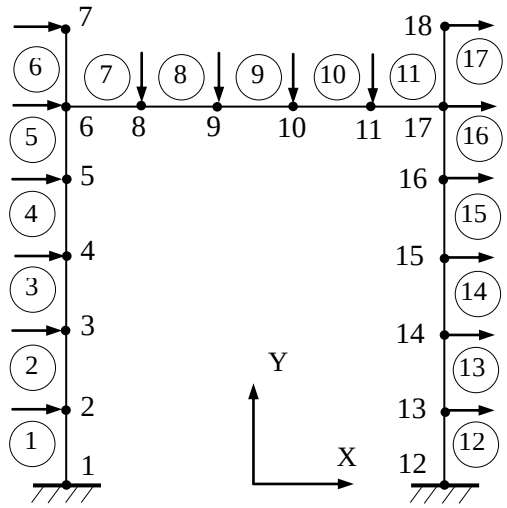

Figure 8-12: Analytical Model of the First Substructure

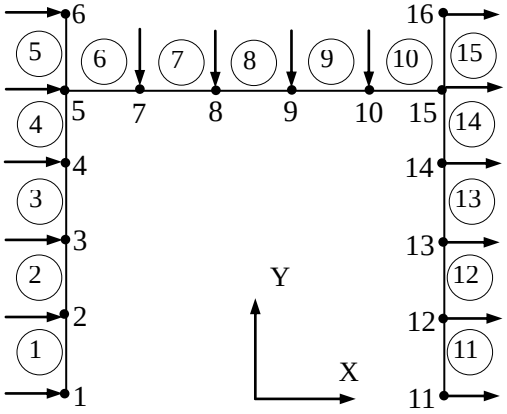

Figure 8-13: Analytical Model of the Second Substructure

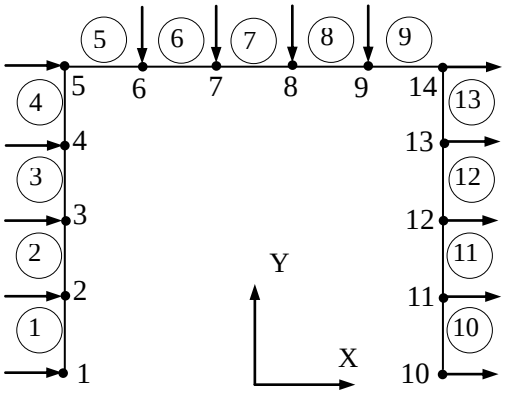

Figure 8-14: Analytical Model of the Third Substructure

Young's moduli of the 45 elements are updated in the undamaged state in which the initial values are set to 2×10^{11} Pa. Accordingly, there are 17 updating parameters in the first substructure, 15 in the second, and 13 in the third. The three sub-models are tuned according to the following procedure.

1) Construct the projector $\mathbf{P}_R$ for the second and third substructures. For the second substructure, the condensed stiffness matrix $\mathbf{K}_R^{(2)}$, the condensed mass matrix $\mathbf{M}_R^{(2)}$, and the rigid body modes $\mathbf{R}_a^{(2)}$ at the measured points are formed from the analytical model. The projector $\mathbf{P}_R^{(2)}$ is subsequently created according to Appendix C. $\mathbf{P}_R^{(3)}$ is similarly created for the third substructure.

2) Extract the substructural flexibility matrices from the measured global flexibility matrix $\mathbf{F}_g^E$. Following the procedure described in Section 8.2, use an iterative scheme to obtain the primitive matrix $\left(\mathbf{F}_R^p\right)^E$ from which the substructural flexibility matrices of the three substructures ($\mathbf{F}_R^{(1)}$, $\mathbf{F}_R^{(2)}$, and $\mathbf{F}_R^{(3)}$) are extracted simultaneously. The iterative procedure terminates when the relative difference in the Frobenius norm of the primitive flexibility matrix $\left(\mathbf{F}_R^p\right)^E$ from two consecutive iterations is less than $Tol=1\times10^{-6}$, i.e.,

$$Tol=\frac{norm\left(\left[\left(\mathbf{F}_R^p\right)^E\right]^{[k]}-\left[\left(\mathbf{F}_R^p\right)^E\right]^{[k-1]}\right)}{norm\left(\left[\left(\mathbf{F}_R^p\right)^E\right]^{[k]}\right)}\le10^{-6} \tag{8-74}$$

3) Normalize the extracted substructural flexibility matrices. For the second substructure, the normalized substructural flexibility matrix is obtained by

$$\mathbf{P}_1^{(2)}=\left(\mathbf{M}_R^{(2)}\setminus\mathbf{M}_1^{(2)}\right)\mathbf{P}_R^{(2)}\mathbf{M}_2^{(2)},\quad \mathbf{P}_2^{(2)}=\left[\mathbf{P}_1^{(2)}\right]^T=\mathbf{M}_2^{(2)}\mathbf{P}_R^{(2)}\left(\mathbf{M}_1^{(2)}/\mathbf{M}_R^{(2)}\right),$$
$$\left(\tilde{\mathbf{F}}_R^{(2)}\right)^E=\mathbf{P}_1^{(2)}\left(\mathbf{F}_R^{(2)}\right)^E\mathbf{P}_2^{(2)} \tag{8-75}$$

where $\mathbf{M}_R^{(2)}=\mathbf{M}_1^{(2)}\mathbf{M}_2^{(2)}$. The normalized substructural flexibility matrix of the third substructure $\tilde{\mathbf{F}}_R^{(3)}$ can be obtained in a similar way.

4) Update the analytical sub-models of the three substructures. The three substructures are treated as independent structures and are updated using the conventional global approach. Taking the second substructure as an example, the substructural flexibility matrix $\left(\mathbf{F}_R^{(2)}\right)^A$ corresponding to the measured DOFs is estimated by the analytical model in each iteration and is normalized with $\left(\tilde{\mathbf{F}}_R^{(2)}\right)^A = \mathbf{P}_1^{(2)}\left(\mathbf{F}_R^{(2)}\right)^A \mathbf{P}_2^{(2)}$. The 15 elemental parameters in the second substructure are adjusted to minimize the difference between the normalized $\left(\tilde{\mathbf{F}}_R^{(2)}\right)^A$ and $\left(\tilde{\mathbf{F}}_R^{(2)}\right)^E$, i.e., minimize $\Delta\mathbf{F} = norm\left(\left(\tilde{\mathbf{F}}_R^{(2)}\right)^E - \left(\tilde{\mathbf{F}}_R^{(2)}\right)^A\right)$. The sub-models of the first and third substructures are updated in a similar manner.

Figure 8-15 reports the SRF values of the three substructures after updating their respective sub-models according to the above procedure. The frequencies and MAC values of the mode shapes before and after updating are compared with their measured counterparts in Table 8-6, which shows that the updated model is better at representing the real structure.

In the next step, the refined sub-models of the three substructures are used for damage identification. In the first damage configuration, the 17 elemental parameters in the first substructure are adjusted, whereas the sub-models of the second and third substructures remain unchanged. In the experiment, only the first substructure, i.e., Nodes 1 to 18 of Figure 8-8, was measured. At the Node 7 and Node 18 interfaces, vibration in the X direction was measured and the unmeasured components (the Y direction and rotation) are estimated by the previously refined analytical model.

The substructural flexibility matrix $\left(\tilde{\mathbf{F}}_R^{(1)}\right)^E$ of the first substructure is extracted from the measured global flexibility matrix $\left(\mathbf{F}_g\right)_{aa}^E$ using the proposed iterative scheme. It is noted that the refined second and third substructures are combined into one substructure to assemble the primitive matrix $\mathbf{F}_{aa}^p$ in Eq. (8-56). This is because the

interface points need to be always selected as master DOFs. If the second and third substructures are integrated into one substructure, Node 23 and Node 32 need not be selected as master DOFs and their measurements are therefore saved. The iterative procedure terminates when the relative difference in the norm of the substructural flexibility matrix from two consecutive iterations is less than $Tol=1\times10^{-6}$, i.e.,

$$Tol=\frac{norm\left(\left[\left(\tilde{\mathbf{F}}_R^{(1)}\right)^E\right]^{[k]}-\left[\left(\tilde{\mathbf{F}}_R^{(1)}\right)^E\right]^{[k-1]}\right)}{norm\left(\left[\left(\tilde{\mathbf{F}}_R^{(1)}\right)^E\right]^{[k]}\right)}\le10^{-6} \qquad (8\text{-}76)$$

Similar to the approach taken for the undamaged state, the first substructure (Figure 8-12) is updated independently. Figure 8-16 shows the SRF values of the 17 elemental parameters after updating. It can be seen that the SRF of Element 2 is -23%, although small SRF values ranging from 0 to -10% exist in some other elements. The modal data of the updated model match their experimental counterparts reported in Table 8-7 more closely than the original data.

In the second damage configuration, two artificial cuts are located in different substructures. The frequencies and mode shapes measured in the first and second substructures are used to form the global flexibility matrix $\left(\mathbf{F}_g\right)_{aa}^E$. The normalized substructural flexibility matrices of the first substructure $\left(\tilde{\mathbf{F}}_R^{(1)}\right)^E$ and the second substructure $\left(\tilde{\mathbf{F}}_R^{(2)}\right)^E$ are extracted from $\left(\mathbf{F}_g\right)_{aa}^E$ simultaneously. The analytical sub-models of the first and second substructures are subsequently updated to recover $\left(\tilde{\mathbf{F}}_R^{(1)}\right)^E$ and $\left(\tilde{\mathbf{F}}_R^{(2)}\right)^E$, respectively.

Figure 8-17 (a) shows that after updating, the SRF value of Element 2 in the first substructure is about -20% and the SRF value of Element 2 in the second substructure (Element 19 of the global structure) is -25%. The figure also reports some negligible values for some of the other elements.

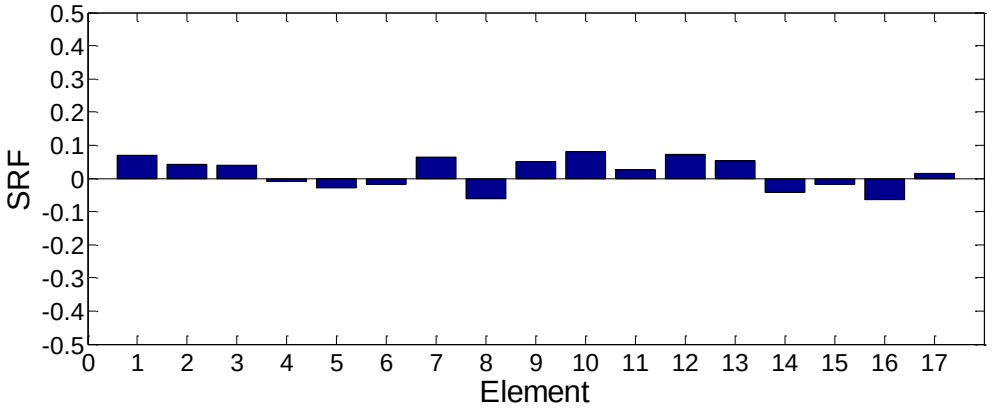

(a) First Substructure

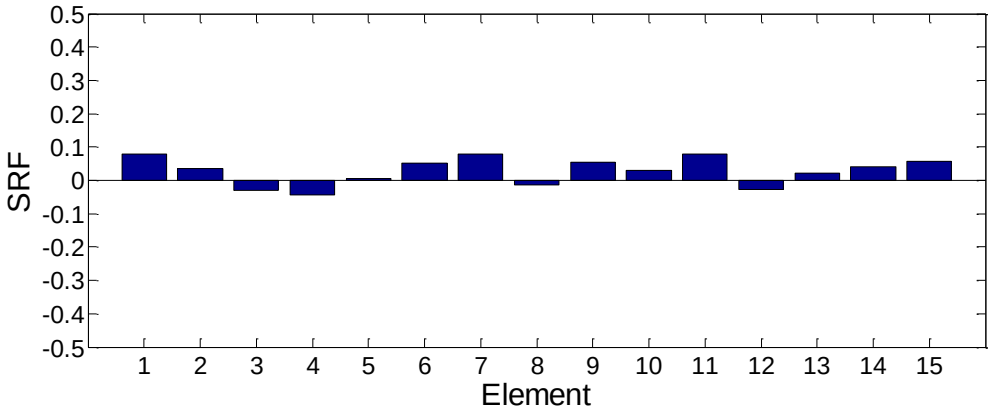

(b) Second Substructure

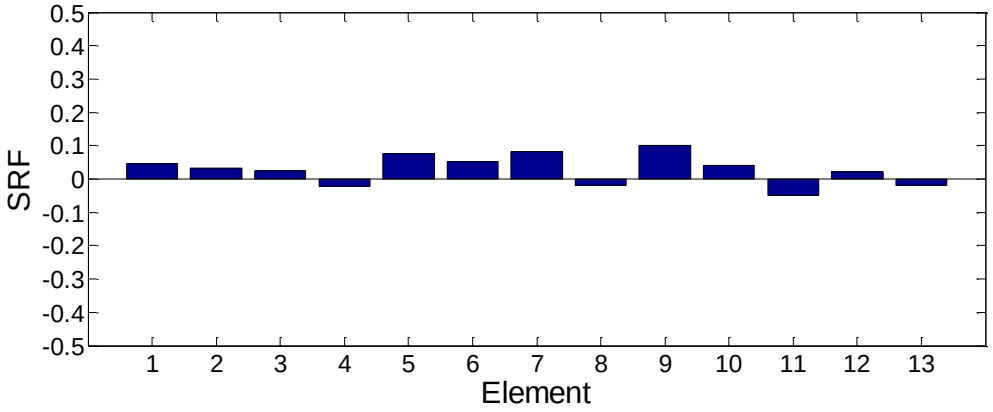

(c) Third Substructure

Figure 8-15: SRF Values of the Three Substructures in the Undamaged State

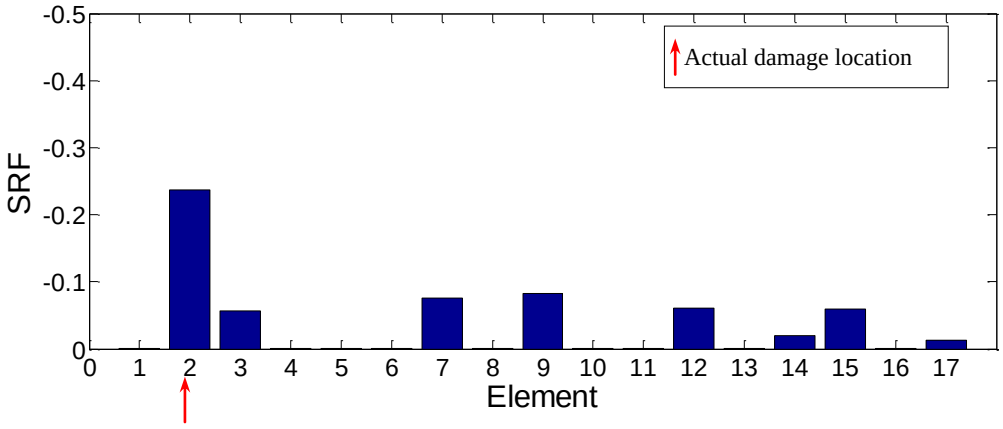

Figure 8-16: SRF Values of the First Damage Configuration (First Substructure)

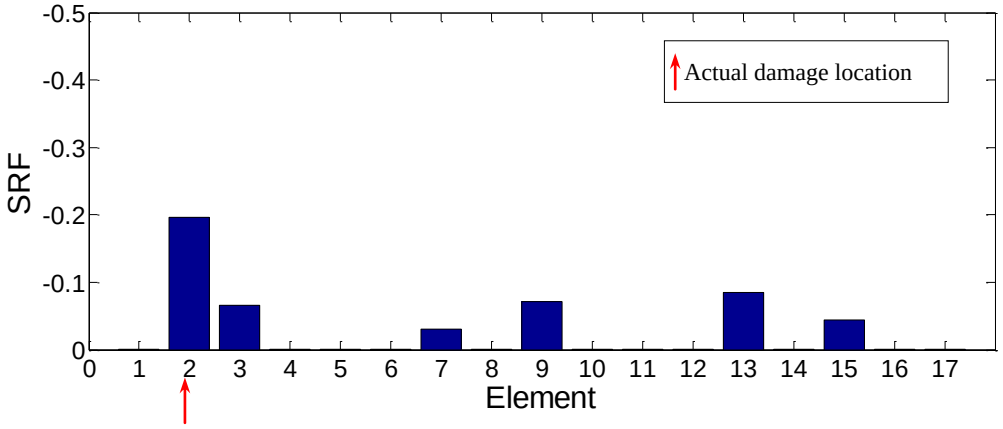

(a) First Substructure

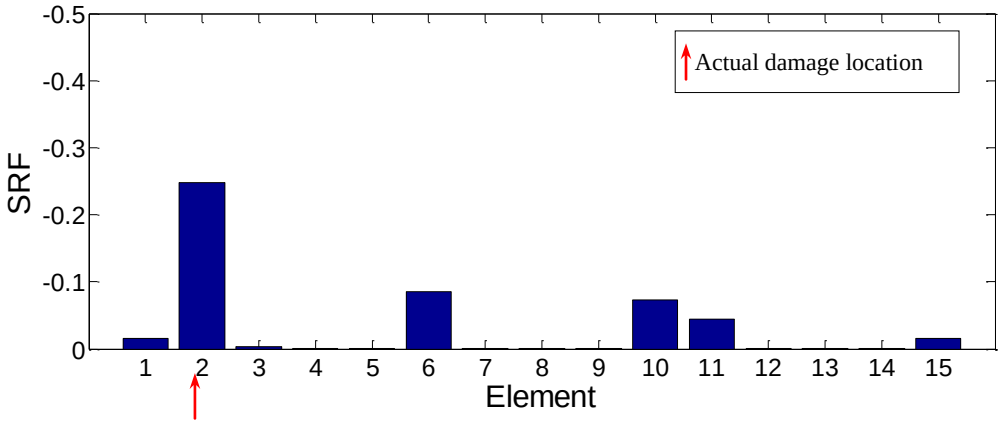

(b) Second Substructure

Figure 8-17: SRF Values of the Second Damage Configuration

Table 8-6: Frequencies and Mode Shapes Before and After Updating (Undamaged State)

Mode	Analytical mode	Measured frequency (Hz)	Before updating			After updating		
			Frequency (Hz)	Diff. (%)	MAC	Frequency (Hz)	Diff. (%)	MAC
1	1	3.12	3.16	1.27%	0.993	3.13	0.32%	0.997
2	2	9.11	9.23	1.27%	0.976	9.15	0.44%	0.996
3	3	14.34	14.04	-2.13%	0.989	14.40	0.39%	0.993
4	4	52.46	50.42	-3.88%	0.981	51.90	-1.07%	0.997
5	5	58.18	56.51	-2.87%	0.980	57.74	-0.75%	0.989
6	6	66.80	64.34	-3.68%	0.871	66.84	0.06%	0.951
7	7	71.65	70.80	-1.18%	0.928	72.00	0.49%	0.970
8	8	82.14	82.51	0.45%	0.877	81.78	-0.43%	0.933
9	9	82.87	80.98	-2.29%	0.885	82.41	-0.55%	0.975
10	16	200.13	211.12	5.49%	0.919	205.54	2.70%	0.957
11	17	222.36	215.91	-2.90%	0.920	224.62	1.02%	0.965
12	18	226.55	220.37	-2.73%	0.913	226.13	-0.18%	0.959
13	19	236.58	230.60	-2.53%	0.905	235.17	-0.60%	0.959
14	22	383.33	395.44	3.16%	0.903	389.95	1.73%	0.951
Average [a]				2.56%	0.932		0.77%	0.971

[a] Average of absolute value.

Table 8-7: Frequencies and Mode Shapes Before and After Updating (Damaged State 1)

Mode	Analytical mode	Measured frequency (Hz)	Before updating			After updating		
			Frequency (Hz)	Diff. (%)	MAC	Frequency (Hz)	Diff. (%)	MAC
1	1	3.11	3.13	0.62%	0.992	3.11	-0.10%	0.992
2	2	9.09	9.15	0.64%	0.996	9.18	0.94%	0.997
3	3	14.34	14.40	0.42%	0.997	14.14	-1.39%	0.997
4	4	52.24	51.90	-0.65%	0.986	52.26	0.04%	0.985
5	5	57.72	57.74	0.03%	0.991	57.85	0.22%	0.992
6	6	66.73	66.84	0.18%	0.916	66.76	0.05%	0.949
7	7	71.28	72.00	1.01%	0.970	71.13	-0.21%	0.980
8	8	81.60	81.78	0.22%	0.860	81.67	0.09%	0.919
9	9	82.19	82.41	0.28%	0.859	82.29	0.13%	0.917
10	16	199.70	205.54	2.93%	0.932	200.90	0.60%	0.944
11	17	220.93	224.62	1.67%	0.847	221.47	0.24%	0.915
12	18	224.97	226.13	0.52%	0.840	225.07	0.04%	0.927
13	19	234.78	235.17	0.16%	0.947	233.58	-0.51%	0.973
14	22	382.50	389.95	1.95%	0.926	387.54	1.32%	0.949
Average [a]				0.81%	0.933		0.42%	0.960

[a] Average of absolute value.

Table 8-8: Frequencies and Mode Shapes Before and After Updating (Damaged State 2)

Mode	Analytical mode	Measured frequency (Hz)	Before updating			After updating		
			Frequency (Hz)	Diff. (%)	MAC	Frequency (Hz)	Diff. (%)	MAC
1	1	3.11	3.13	0.77%	0.992	3.10	-0.36%	0.996
2	2	9.09	9.15	0.67%	0.996	9.11	0.21%	0.998
3	3	14.33	14.40	0.46%	0.997	14.29	-0.33%	0.997
4	4	51.88	51.90	0.04%	0.988	51.47	-0.80%	0.985
5	5	57.41	57.54	0.23%	0.989	57.56	0.27%	0.986
6	6	66.48	66.84	0.54%	0.924	65.84	-0.97%	0.938
7	7	70.73	72.00	1.80%	0.961	70.88	0.21%	0.978
8	8	80.99	81.78	0.98%	0.838	81.17	0.23%	0.933
9	9	81.98	82.41	0.54%	0.889	82.20	0.27%	0.916
10	16	199.11	205.54	3.23%	0.912	200.51	0.70%	0.933
11	17	220.03	224.62	2.08%	0.839	220.95	0.42%	0.922
12	18	224.14	226.13	0.89%	0.819	223.33	-0.36%	0.926
13	19	233.50	235.17	0.71%	0.934	230.65	-1.22%	0.952
14	22	376.49	389.95	3.58%	0.859	382.54	1.61%	0.941
Average [a]				1.18%	0.924		0.57%	0.957

[a] Average of absolute value.

In the two damage configurations, the damaged elements identified coincide with the locations of the artificial cuts made in the experiment and the equivalent reduction of elemental stiffness identified is consistent with that obtained in Chapter 6.

Both the substructuring method developed in Chapter 6 and the present substructuring method can be used successfully to identify the artificial cuts with consistent SRF values. The substructuring methods described correct only a part of the uncertain parameters at a time. This benefits the convergence of the optimization procedure. In particular, the substructuring method proposed in Chapter 6 re-analyzes one substructure in each iteration and then brings it together with the other unchanged substructures to obtain the modal properties of the global structure. Accordingly, the experimental measurement points are distributed across the whole structure to enable measurement of the global modal information. In the method described in this chapter, the experimental substructural flexibility matrix is extracted from the measured modal data. The sub-model of one substructure is updated directly without calculating

the eigenproperties of the global structure. As a result, the amount of computation work involved in optimization is reduced. Experimental measurements can also be concentrated on a local area.

In the final step, the frame is updated using the traditional global method based on the same measured modal data. Likewise, the difference in the flexibility matrices of the analytical model and the experimental measurements is chosen as the objective function used to adjust the 45 elemental parameters simultaneously. The initial model is first updated with the modal data measured in the undamaged state. The SRF values of the elemental parameters after updating are shown in Figure 8-18. The refined model is subsequently used for damage identification.

The SRF values from the two damage configurations are illustrated in Figure 8-19 and Figure 8-20, respectively. Element 2 is observed to have a clearly negative SRF value in both damage configurations. The SRF value of Element 19 is about -30% in the second damage configuration. These observations are consistent with those made for the two substructuring-based model updating methods described earlier (Figures 6-5 and 6-6, Figures 8-16 and 8-17).

The laboratory tested frame structure has been analyzed using three model updating methods ─ two substructuring-based model updating methods and the traditional global-based method ─ and the same set of experimental data. All three methods can be used successfully to locate artificial cuts and obtain consistent results on reductions in elemental stiffness, although there are some small discrepancies among them. This demonstrates that the two substructuring methods proposed in this thesis are effective in model updating and damage identification.

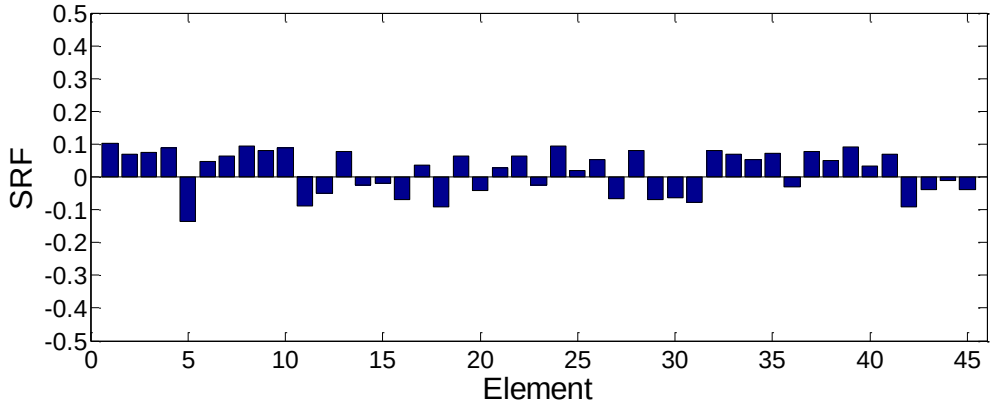

Figure 8-18: SRF Values of the Frame Structure in the Undamaged State (Global Method)

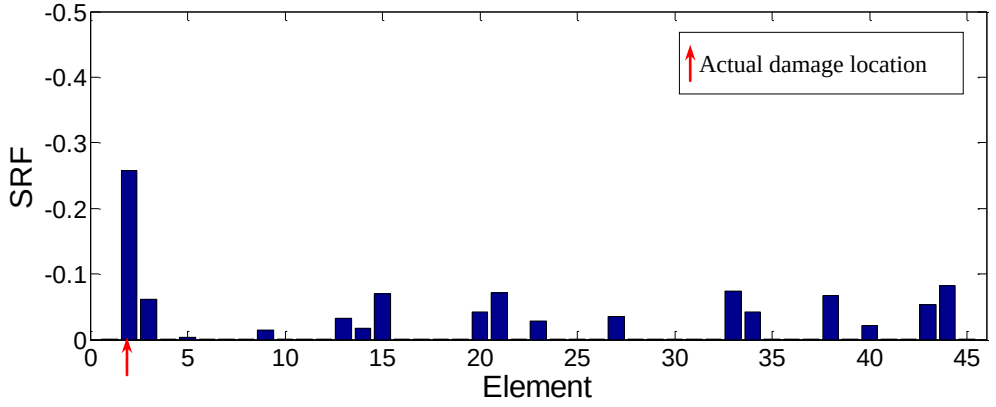

Figure 8-19: SRF Values of the First Damage Configuration (Global Method)

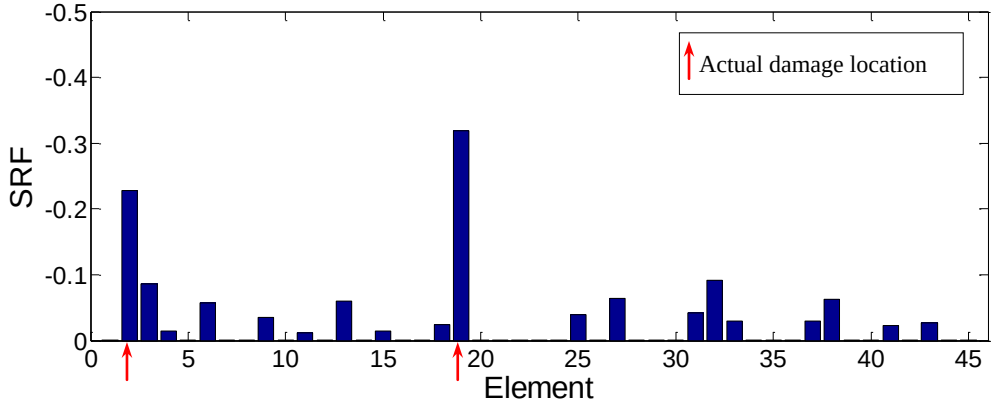

Figure 8-20: SRF Values of the Second Damage Configuration (Global Method)

8.7 Summary

In this chapter, a substructural flexibility matrix is extracted from global modal data under the constraints of force compatibility and displacement compatibility. The extracted substructural flexibility matrix is employed as a reference and the sub-model of the substructure is updated independently using the conventional global-based model updating approach. In consequence, the size of the analytical model and the uncertain parameters involved in model updating are reduced, which benefit the convergence of model updating.

As compared to the forward substructuring approach discussed in previous chapters, this inverse substructuring method is advantageous in two aspects: a) Only one substructure is independently involved in model updating without assembling the substructures. The inverse method is more efficient when conducting optimization process. b) The inverse method requires measuring the local area of a structure, to avoid the measurement of the entire structure.

Nevertheless, the inverse substructuring method requires a relatively complicated process to disassemble the global modal data into substructure level. The measurement noise can be accumulated or propagated. This inverse method can be possibly improved in the disassembly procedure in future work.

CHAPTER NINE

CONCLUSIONS AND FUTURE RESEARCH

9.1 Conclusions

Two substructuring-based model updating approaches are developed in this thesis: a forward approach and an inverse approach. In the forward approach, the eigensolutions and eigensensitivities of substructures are calculated and assembled to obtain the eigenproperties of the global structure, which are used to update the analytical model of the global structure. The second approach is an inverse scheme designed to extract the substructural flexibility matrix from the measured global modal data. The independent substructure is then updated to reproduce the extracted substructural flexibility matrix. Three numerical examples and three experimental structures are studied in detail to investigate the effectiveness and efficiency of the proposed substructuring-based model updating methods. The results and findings are summarized as follows.

A concise-form and efficient substructuring-based model updating method is developed on the basis of the forward substructuring approach.

1. Kron's substructuring method is developed by using a modal truncation technique to calculate the eigensolutions of the global structure in which the contribution of the complete eigenmodes of the substructures to the global structure is replaced by a few master modes and a residual flexibility matrix (the FRFS method or SRFS method). This improvement benefits computational efficiency in two respects: first, the computational work required in extracting the eigenmodes of the substructures is reduced; second, the assembled eigenequation is much smaller than that of the Kron's original substructuring method;

2. The FRFS method for eigensolutions is extended to calculate the associated first-order eigensensitivity. The eigensensitivity with respect to an elemental parameter of the global structure is recovered by the derivative matrix of a substructure contains the element and derivative of a reduced eigenequation, thus significantly reducing computational cost;

3. The procedure for calculating the second-order eigensensitivity with respect to two elemental parameters is developed using the FRFS method. The formula can be generalized to calculate the high-order eigensensitivity easily by further differentiating the reduced eigenequation. In a manner similar to that used for the first-order eigensensitivity, only substructures that include the elemental parameters are analyzed to recover the high-order eigensensitivity of the global structure;

4. The influences of master modes and the divisional formation of substructures on computational efficiency and accuracy are investigated, with extensive examples given. Retaining more master modes in the substructures can lead to better accuracy, but result in greater computational expense. To balance computational accuracy and efficiency, it is necessary to make a trade-off between the number of substructures and the size of each substructure;

5. The eigensolutions and eigensensitivities calculated using the FRFS method are successfully applied to the sensitivity-based model updating process. Errors made in calculating the eigensolutions and eigensensitivities have a negligible influence on the model updating results when appropriate master modes are retained in each substructure;

6. Although the inclusion of more master modes can improve the accuracy of the FRFS method, the computational effort required in extracting a large number of master modes makes it expensive to achieve highly accurate results. An iterative scheme is proposed for calculating accurate eigensolutions and eigensensitivities using only a few master modes. This iterative method is profitable when accurate

eigensolutions and eigensensitivities are required, such as in the final steps of model updating when the results are close to the optimum. A combination of the FRFS method and the iterative method can further improve computational efficiency in updating models of large-scale structures.

The inverse scheme proposed can be used to extract substructural flexibility matrices from global modal data and thereby directly update the model for an independent substructure.

1. The substructural flexibility matrices are extracted from the global flexibility matrix under the constraints of displacement compatibility and force compatibility. This substructuring approach employs dynamic modal flexibility rather than static flexibility. A projector is constructed to ensure that the extracted substructural flexibility matrix is normalized with respect to the mass matrix and is orthogonal to the rigid body modes. These improvements make the substructuring approach valuable in real large-scale structures;

2. A model condensation technique is utilized in this substructuring method. If parts of a structure are uncertain or damaged, only the local focused substructures need to be measured in the experiment. As a result, the requirement to measure the entire structure is avoided;

3. Under the proposed substructuring approach, because each substructure is updated independently to reproduce the extracted substructural flexibility, the amount of computation work involved in optimization is reduced. Moreover, the number of parameters that require updating in the substructures is significantly lower than the number of such parameters in the global structure, which further benefits the convergence of optimization.

9.2 Future Research

The substructuring methods developed in this thesis can be improved and extended in several respects to realize an automatic, robust, and generally applicable substructuring-based model updating procedure:

1. The automated selection of master modes and the divisional formation of substructures require further study to implement the substructuring-based model updating approach in real structures;

2. The iterative method (Chapter 7) proposed in this thesis calculates accurate eigensolutions and eigensensitivities mode by mode. It could be more efficient if all of the modes of interest were calculated simultaneously;

3. The present research developed a deterministic method without considering the modelling error and measurement noise. In practice, the measured vibration data and initial FE model inevitably contain uncertainties. The substructuring methods discussed in this thesis also introduce some slight errors during the disassembly and assembly procedures. The accumulation and propagation of these uncertainties deserve quantification.

4. The proposed substructuring method is potential to be applied to the in-construction health monitoring, where the analytical model can be updated at stages beginning from a substructure and progressively to more substructures until the whole structure, according to the different construction stage. The refined substructures in the previous stages can be kept unchanged in the later stages, and updating is performed solely on the new constructed component by treating it as another substructure. Additionally, for the in-service health monitoring, only the local area with high-probability of damage needs to be measured and updated by treating that area as an independent substructure.

APPENDIX A

BASIC METHODS IN CALCULATING EIGENSOLUTIONS OF LARGE-SCALE STRUCTURES

The classical eigenequation for a structure with *N* DOFs has the form of

$$\mathbf{K}\{\phi_i\} = \lambda_i \mathbf{M}\{\phi_i\} \tag{A-1}$$

where **K** and **M** are the $N \times N$ symmetric stiffness and mass matrices, respectively, and λ_i and $\{\phi_i\}$ represents the *i*th eigenvalue and the corresponding mode shape. The eigenvalue problem has been studied for centuries since the middle of last century. Special algorithms have been developed for large-scale problems, in which the Subspace Iteration Method and the Lanczos method are two powerful methods.

A.1 Subspace Iteration Method

Subspace iteration method extracts the partial solutions of a large-size eigenproblem by projecting them onto an approximated subspace to reduce the computational cost. As solving the complete eigensolutions is expensive and usually not necessary for the large-scale structures, the approximated solution in searching the lowest eigenpairs are favorable. Figure A-1 demonstrates the general procedure of Subspace Iteration method.

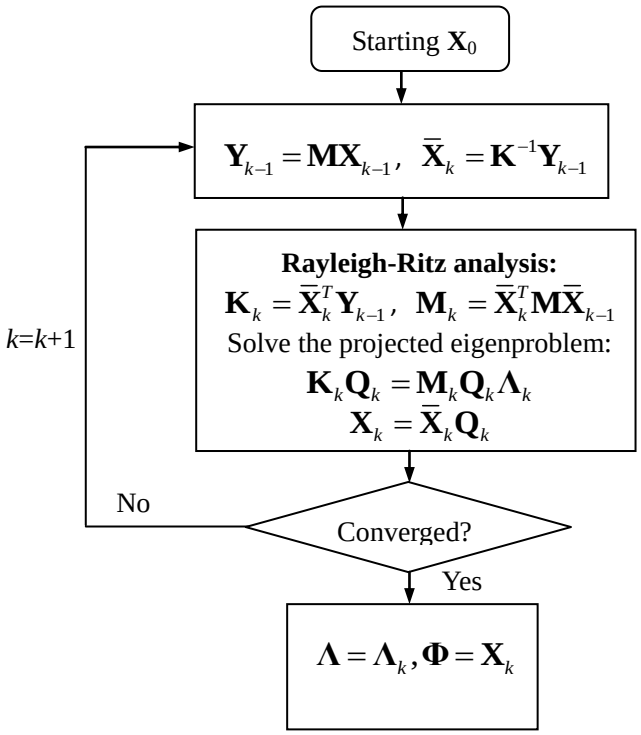

Figure A-1: Basic Subspace Iteration Method

A.2 Lanczos Method

The Lanczos algorithm was first proposed in 1950 for reducing a symmetric matrix to the tridiagonal form (Lanczos 1950). The Lanczos algorithm has been developed continuously as a powerful tool to extract a number of eigenvalues of a real symmetric matrix. The Lanczos algorithm involves the transformation of a generalized *N*-dimension eigenproblem into a standard tridiagonal matrix with smaller dimension *m* (Parlett 1987), as described in Figure A-2.

The Lanczos algorithm constructs an orthogonal basis for the *Krylov subspace* as

$$\mathbf{Q}_m = span\left(\{q_1\} \quad \left(\mathbf{K}^{-1}\mathbf{M}\right)\{q_1\} \quad \cdots \quad \left(\mathbf{K}^{-1}\mathbf{M}\right)^{m-1}\{q_1\}\right) = span\left(q_1 \quad q_2 \quad \cdots \quad q_m\right) \text{(A-2)}$$

$\{q_1\}$ is an arbitrary starting vector, and $\{q_j\}$ is a Lanczos vector orthogonal to the previous $\{q_{j-1}\}$ Lanczos vectors with respect to **M**, and *m* is the dimension of the Krylov subspace.

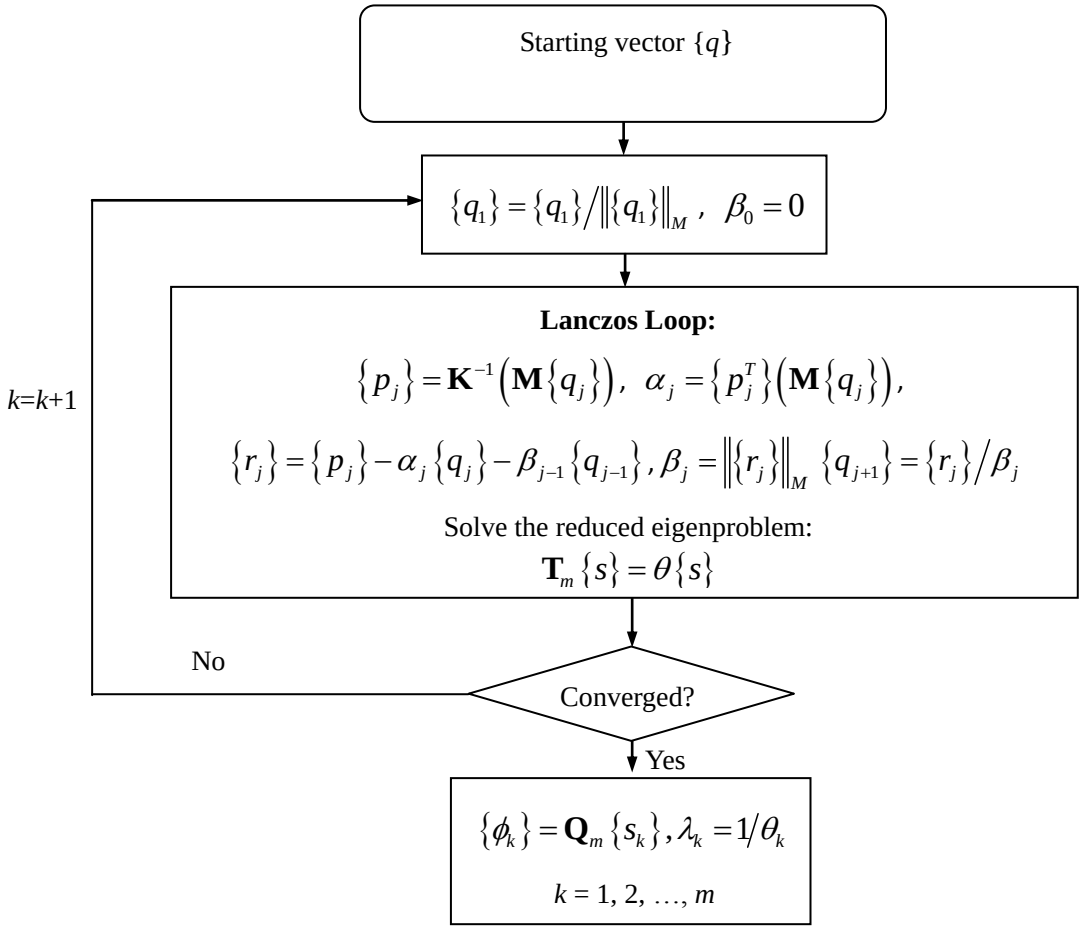

Figure A-2: Basic Lanczos Algorithm

The tridiagonal matrix in Figure A-2 is formulated by

$$\mathbf{T}_m = \begin{bmatrix} \alpha_1 & \beta_2 & & & \\ \beta_2 & \alpha_2 & \beta_3 & & \\ & \beta_3 & \ddots & \ddots & \\ & & \ddots & \ddots & \beta_m \\ & & & \beta_m & \alpha_m \end{bmatrix} \qquad \text{(A-3)}$$

Block version of Lanczos method is more powerful, which naturally produces a block tridiagonal matrix $\mathbf{T}_m$. As compared with the Subspace Iteration method, the Lanczos method is preferable to compute a large number of eigenpairs for very large sparse matrices (Nour-Omid *et al.* 1983).

APPENDIX B

BASIC METHODS IN CALCULATING EIGENSENSITIVITY

B.1 Eigenvalue Derivatives

Fox and Kapoor (1968) firstly derived the eigenvalue derivatives with respect to elemental parameters. By differentiating Eq. (A-1) with respect to an elemental parameter *r*, the eigenequation is expressed as

$$\left(\mathbf{K}-\lambda_i\mathbf{M}\right)\frac{\partial\{\phi_i\}}{\partial r}+\left(-\frac{\partial\lambda_i}{\partial r}\mathbf{M}-\lambda_i\frac{\partial\mathbf{M}}{\partial r}+\frac{\partial\mathbf{K}}{\partial r}\right)\{\phi_i\}=\{0\} \tag{B-1}$$

where i = 1, 2, …, m, and m is the number of interest modes. Pre-multiplying $\{\phi_i^T\}$ on both sides of Eq. (B-1) and noting $\{\phi_i\}^T\left(\mathbf{K}-\lambda_i\mathbf{M}\right)=\{\mathbf{0}\}$, the first-order eigenvalue derivative with respect to *r* is

$$\frac{\partial\lambda_i}{\partial r}=\{\phi_i\}^T\left(-\lambda_i\frac{\partial\mathbf{M}}{\partial r}+\frac{\partial\mathbf{K}}{\partial r}\right)\{\phi_i\} \tag{B-2}$$

The stiffness matrix **K** and mass matrix **M** are assembled by the contribution of all n elements in the discrete FE model. In particular,

$$\mathbf{K}=\sum_{j=1}^{n}\mathbf{K}_j=\sum_{j=1}^{n}\alpha_j\mathbf{K}_j^e,\quad \mathbf{M}=\sum_{j=1}^{n}\mathbf{M}_j=\sum_{j=1}^{n}\beta_j\mathbf{M}_j^e \tag{B-3}$$

where $\mathbf{K}_j$ and $\mathbf{M}_j$ are the j^{th} elemental stiffness matrix and elemental mass matrix, and α_j and β_j are respectively the ‘elemental stiffness parameter’ and ‘elemental mass parameter’. In case *r* is an elemental stiffness parameter, Eq. (B-2) is further simplified to

$$\frac{\partial\lambda_i}{\partial r_j}=\{\phi_i\}^T\mathbf{K}_j^e\{\phi_i\} \tag{B-4}$$

Likewise, if *r* is an elemental mass parameter, the eigenvalue derivative is formed as

$$\frac{\partial \lambda_i}{\partial r_j} = -\lambda_i \{\phi_i\}^T \mathbf{M}_j^e \{\phi_i\} \tag{B-5}$$

B.2 Eigenvector Derivatives

Eq. (B-1) is rewritten as

$$\mathbf{\Psi}_i \frac{\partial \{\phi_i\}}{\partial r} = \{\mathbf{Y}_{ir}\} \tag{B-6}$$

where

$$\{\mathbf{Y}_{ir}\} = \frac{\partial \lambda_i}{\partial r}\mathbf{M}\{\phi_i\} - \left(\frac{\partial \mathbf{K}}{\partial r} - \lambda_i \frac{\partial \mathbf{M}}{\partial r}\right)\{\phi_i\}$$

$$\mathbf{\Psi}_i = \mathbf{K} - \lambda_i \mathbf{M}$$

The eigenvector derivative $\frac{\partial \{\phi_i\}}{\partial r}$ can be achieved with modal method and Nelson's method, respectively.

B.2.1 Modal Method

In modal method, the eigenvector derivative is expressed as a linear combination of all eigenvectors $\mathbf{\Phi} = [\phi_1 \quad \phi_2 \quad \cdots \quad \phi_N]$, i.e.,

$$\frac{\partial \{\phi_i\}}{\partial r} = \sum_{j=1}^{N} \{\phi_j\} c_{ji} = \mathbf{\Phi}\{c_i\} \tag{B-7}$$

where $c_i = \{c_{1i} \quad c_{2i} \quad \cdots \quad c_{Ni}\}^T$ is the participation factors of the individual modes. Substituting Eq. (B-7) into Eq. (B-6) and pre-multiplying $\mathbf{\Phi}^T$ lead to

$$\mathbf{\Phi}^T (\mathbf{K} - \lambda_i \mathbf{M}) \mathbf{\Phi} \{c_i\} = \mathbf{\Phi}^T \{\mathbf{Y}_i\} \tag{B-8}$$

Noting $\mathbf{\Phi}^T \mathbf{M} \mathbf{\Phi} = \mathbf{I}$ and $\mathbf{\Phi}^T \mathbf{K} \mathbf{\Phi} = \mathbf{\Lambda}$, one has

$$(\mathbf{\Lambda} - \lambda_i \mathbf{I}) c_i = \mathbf{\Phi}^T \{\mathbf{Y}_i\} \tag{B-9}$$

This leads to the (N–1) equations of

$$(\lambda_j - \lambda_i) c_{ji} = \{\phi_j^T\} \{\mathbf{Y}_i\} \tag{B-10}$$

where j = 1, 2, …, N but $j \neq i$. Therefore, the coefficient of $\{c_i\}$ except c_{ii} can be

solved with

$$c_{ji} = \frac{\{\phi_j^T\}\{\mathbf{Y}_i\}}{\lambda_j - \lambda_i} \tag{B-11}$$

The coefficient c_{ii} can be solved from the mass orthogonal condition of the eigenvectors, which satisfies

$$\{\phi_i^T\}\mathbf{M}\{\phi_i\} = 1 \tag{B-12}$$

Eq. (B-12) is differentiated with respect to r as

$$2\{\phi_i^T\}\mathbf{M}\frac{\partial\{\phi_i\}}{\partial r} + \{\phi_i^T\}\frac{\partial\mathbf{M}}{\partial r}\{\phi_i\} = 0 \tag{B-13}$$

Due to the orthogonal property among the eigenvectors

$$\{\phi_i^T\}\mathbf{M}\mathbf{\Phi}\{c_i\} = \{\phi_i^T\}\mathbf{M}\left[\{\phi_1\} \quad \cdots \quad \{\phi_{i-1}\} \quad \{\phi_i\} \quad \{\phi_{i+1}\} \quad \cdots\right]\{c_i\} = \{c_i\} \tag{B-14}$$

Substitution of Eq. (B-7) into Eq. (B-13) thus gives the value of c_{ii} as

$$c_{ii} = -\frac{1}{2}\{\phi_i^T\}\frac{\partial\mathbf{M}}{\partial r}\{\phi_i\} \tag{B-15}$$

Eq. (B-7) indicates that the first-order derivative of the ith eigenvector requires all N eigenvectors to achieve the accurate results. Wang (1991) and Alvin (1997) developed the modified modal method to reduce the number of the required modes.

B.2.2 Nelson's Method

In Nelson's method, the ith eigenvector derivative is expressed with the sum of the particular and homogeneous vectors as

$$\frac{\partial\{\phi_i\}}{\partial r} = \{\mathbf{v}_i\} + c_i\{\phi_i\} \tag{B-16}$$

where c_i is a participation factor. Substituting Eq. (B-16) into Eq. (B-6) gives

$$\left(\mathbf{K} - \lambda_i\mathbf{M}\right)\{\mathbf{v}_i\} = \{\mathbf{Y}_i\} \tag{B-17}$$

Assuming that there are no repeated frequencies, then the rank of $\left(\mathbf{K} - \lambda_i\mathbf{M}\right)$ is (N–1). Setting the kth term of $\{\mathbf{v}_i\}$ to zero and eliminating the kth row and column of $\left(\mathbf{K} - \lambda_i\mathbf{M}\right)$ and kth term of $\{\mathbf{Y}_i\}$, the full-rank equation in solving $\{\mathbf{v}_i\}$ is established as

$$\begin{bmatrix} (\mathbf{K}-\lambda_i\mathbf{M})_{11} & 0 & (\mathbf{K}-\lambda_i\mathbf{M})_{13} \\ 0 & 1 & 0 \\ (\mathbf{K}-\lambda_i\mathbf{M})_{31} & 0 & (\mathbf{K}-\lambda_i\mathbf{M})_{33} \end{bmatrix} \begin{Bmatrix} \mathbf{v}_{i1} \\ \mathbf{v}_{ik} \\ \mathbf{v}_{i3} \end{Bmatrix} = \begin{Bmatrix} \mathbf{Y}_{i1} \\ 0 \\ \mathbf{Y}_{i3} \end{Bmatrix} \quad \text{(B-18)}$$

where k is chosen at the maximum value in $\{\phi_i\}$.

Substitution of Eq. (B-16) into the orthogonal condition in Eq. (B-13) leads to

$$2\{\phi_i^T\}\mathbf{M}\left(\{\mathbf{v}_i\}+c_i\{\phi_i\}\right)+\{\phi_i^T\}\frac{\partial\mathbf{M}}{\partial r}\{\phi_i\}=0 \quad \text{(B-19)}$$

Therefore, the participation factor c_i can be obtained as

$$c_i=-\{\phi_i^T\}\mathbf{M}\{\mathbf{v}_i\}-\frac{1}{2}\{\phi_i^T\}\frac{\partial\mathbf{M}}{\partial r}\{\phi_i\} \quad \text{(B-20)}$$

Given the vector $\{\mathbf{v}_i\}$ and the participation factor $\{c_i\}$, the eigenvector derivative $\frac{\partial\{\phi_i\}}{\partial r}$ can be achieved accurately.

B.3 High-order Eigensolution Derivatives

B.3.1 Second-order Eigensolution Derivatives

The second-order eigensolution derivatives can be achieved by differentiating Eq. (B-1) a second time. If the two parameters are denoted as r_j and r_k, respectively, the eigenequation is differentiated as

$$(\mathbf{K}-\lambda_i\mathbf{M})\frac{\partial^2\{\phi_i\}}{\partial r_j\partial r_k}+\frac{\partial(\mathbf{K}-\lambda_i\mathbf{M})}{\partial r_k}\frac{\partial\{\phi_i\}}{\partial r_j}+\frac{\partial(\mathbf{K}-\lambda_i\mathbf{M})}{\partial r_j}\frac{\partial\{\phi_i\}}{\partial r_k}+\frac{\partial^2(\mathbf{K}-\lambda_i\mathbf{M})}{\partial r_j\partial r_k}\{\phi_i\}=0 \quad \text{(B-21)}$$

Premultiplying $\{\phi_i^T\}$ on both side of Eq. (B-21) gives the second-order derivative of the ith eigenvalue

$$\frac{\partial^2\lambda_i}{\partial r_j\partial r_k}=\{\phi_i^T\}\frac{\partial(\mathbf{K}-\lambda_i\mathbf{M})}{\partial r_k}\frac{\partial\{\phi_i\}}{\partial r_j}+\{\phi_i^T\}\frac{\partial(\mathbf{K}-\lambda_i\mathbf{M})}{\partial r_j}\frac{\partial\{\phi_i\}}{\partial r_k}+\{\phi_i^T\}\left[\frac{\partial^2\mathbf{K}}{\partial r_j\partial r_k}-\lambda_i\frac{\partial^2\mathbf{M}}{\partial r_j\partial r_k}-\frac{\partial\lambda_i}{\partial r_j}\frac{\partial\mathbf{M}}{\partial r_k}-\frac{\partial\lambda_i}{\partial r_k}\frac{\partial\mathbf{M}}{\partial r_j}\right]\{\phi_i\} \quad \text{(B-22)}$$

Since the second-order derivatives of **K** and **M** with respect to r are zero, Eq. (B-22) is simplified to

$$\frac{\partial^2 \lambda_i}{\partial r_j \partial r_k} = \left\{\phi_i^T\right\} \frac{\partial \left(\mathbf{K} - \lambda_i \mathbf{M}\right)}{\partial r_k} \frac{\partial \left\{\phi_i\right\}}{\partial r_j} + \left\{\phi_i^T\right\} \frac{\partial \left(\mathbf{K} - \lambda_i \mathbf{M}\right)}{\partial r_j} \frac{\partial \left\{\phi_i\right\}}{\partial r_k} - \left\{\phi_i^T\right\} \left[\frac{\partial \lambda_i}{\partial r_j} \frac{\partial \mathbf{M}}{\partial r_k} + \frac{\partial \lambda_i}{\partial r_k} \frac{\partial \mathbf{M}}{\partial r_j} \right] \left\{\phi_i\right\} \tag{B-23}$$

The second-order eigenvector derivative is calculated based Eq. (B-21) as well, which is rewritten as

$$\mathbf{\Psi}_i \frac{\partial^2 \left\{\phi_i\right\}}{\partial r_j \partial r_k} = \mathbf{Y}_{i(j,k)} \tag{B-24}$$

and

$$\mathbf{\Psi}_i = \left(\mathbf{K} - \lambda_i \mathbf{M}\right)$$

$$\mathbf{Y}_{i(j,k)} = -\left(\frac{\partial \left(\mathbf{K} - \lambda_i \mathbf{M}\right)}{\partial r_k} \frac{\partial \left\{\phi_i\right\}}{\partial r_j} + \frac{\partial \left(\mathbf{K} - \lambda_i \mathbf{M}\right)}{\partial r_j} \frac{\partial \left\{\phi_i\right\}}{\partial r_k} + \frac{\partial^2 \left(\mathbf{K} - \lambda_i \mathbf{M}\right)}{\partial r_j \partial r_k} \left\{\phi_i\right\} \right)$$

As before, the second-order eigenvector derivative can be solved with both the modal method and the Nelson's method. Since the latter is utilized in this thesis, only the Nelson's method is addressed in the following. The second-order derivative of the *i*th eigenvector can be expressed as the sum of the particular and homogeneous solutions as

$$\frac{\partial^2 \left\{\phi_i\right\}}{\partial r_j \partial r_k} = \left\{\mathbf{v}_{i(j,k)}\right\} + c_{i(j,k)} \left\{\phi_i\right\} \tag{B-25}$$

where $\left\{\mathbf{v}_{i(j,k)}\right\}$ is not unique but could be calculated from

$$\mathbf{\Psi}_i \left\{\mathbf{v}_{i(j,k)}\right\} = \left\{\mathbf{Y}_{i(j,k)}\right\} \tag{B-26}$$

Equivalent to the expression of Eq. (B-18), the lines and columns of $\left\{\mathbf{v}_{i(j,k)}\right\}$, $\mathbf{\Psi}_i$ and $\left\{\mathbf{Y}_{i(j,k)}\right\}$ corresponding to the largest magnitude in the eigenvector is set to zero, thus a full-rank equation is formulated to uniquely determine the vector $\left\{\mathbf{v}_{i(j,k)}\right\}$.

The participation factor $c_{i(j,k)}$ is calculated from the second-order derivative of the

mass orthogonal condition of Eq. (B-12)

$$\left\{\phi_i^T\right\}\frac{\partial \mathbf{M}}{\partial r_j \partial r_k}\left\{\phi_i\right\}+2\left\{\phi_i^T\right\}\frac{\partial \mathbf{M}}{\partial r_j}\frac{\partial\left\{\phi_i\right\}}{\partial r_k}+2\left\{\phi_i^T\right\}\frac{\partial \mathbf{M}}{\partial r_k}\frac{\partial\left\{\phi_i\right\}}{\partial r_j}+2\frac{\partial\left\{\phi_i^T\right\}}{\partial r_k}\mathbf{M}\frac{\partial\left\{\phi_i\right\}}{\partial r_j}+2\left\{\phi_i^T\right\}\mathbf{M}\frac{\partial^2\left\{\phi_i\right\}}{\partial r_j \partial r_k}=\mathbf{0} \tag{B-27}$$

Substitution of Eq. (B-25) into Eq. (B-27) produces the following equation for the solution of the participation factor $c_{i(j,k)}$.

$$c_{i(j,k)}=-\left(\frac{1}{2}\left\{\phi_i^T\right\}\frac{\partial \mathbf{M}}{\partial r_j \partial r_k}\left\{\phi_i\right\}+\left\{\phi_i^T\right\}\frac{\partial \mathbf{M}}{\partial r_j}\frac{\partial\left\{\phi_i\right\}}{\partial r_k}+\left\{\phi_i^T\right\}\frac{\partial \mathbf{M}}{\partial r_k}\frac{\partial\left\{\phi_i\right\}}{\partial r_j}+\frac{\partial\left\{\phi_i^T\right\}}{\partial r_k}\mathbf{M}\frac{\partial\left\{\phi_i\right\}}{\partial r_j}+\left\{\phi_i^T\right\}\mathbf{M}\mathbf{v}_{i(j,k)}\right) \tag{B-28}$$

B.3.2 General High-order Eigensolution Derivatives

Calculation of the second-order eigensolution derivatives can be generalized to the higher-order eigensolution derivatives. The *h*th-order eigensolution derivative are achieved by differentiating the eigenequation (Eq. (B-1)) by *h* times with respect to the parameters $r_1, r_2, \ldots, r_h$ as

$$\left(\mathbf{K}-\lambda_i\mathbf{M}\right)\frac{\partial^h\left\{\phi_i\right\}}{\partial r_1 \partial r_2 \cdots \partial r_h}-\frac{\partial^h \lambda_i}{\partial r_1 \partial r_2 \cdots \partial r_h}\mathbf{M}\left\{\phi_i\right\}=\left\{\mathbf{Y}_{i(1,2,\ldots,h)}\right\} \tag{B-29}$$

where the vector $\left\{\mathbf{Y}_{i(1,2,\ldots,h)}\right\}$ contains terms involving the derivatives of order (*h*-1) and lower. Premultiplying $\left\{\phi_i^T\right\}$ on both side of Eq. (B-29) gives the *h*th-order derivative of the *i*th eigenvalue in form of

$$\frac{\partial^h \lambda_i}{\partial r_1 \partial r_2 \cdots \partial r_h}=-\left\{\mathbf{Y}_{i(1,2,\ldots,h)}\right\} \tag{B-30}$$

The *h*th-order eigenvector derivative can be obtained following the Eqs. (B-25) ~ (B-28). As before, the eigenvector derivative is expressed as the sum of a particular and a homogeneous part as

$$\frac{\partial^h\left\{\phi_i\right\}}{\partial r_1 \partial r_2 \cdots \partial r_h}=\left\{\mathbf{v}_{i(r_1,r_2,\ldots,r_h)}\right\}+c_{i(r_1,r_2,\ldots,r_h)}\left\{\phi_i\right\} \tag{B-31}$$

The unique $\left\{\mathbf{v}_{i(r_1,r_2,\ldots,r_h)}\right\}$ can be achieved using the equivalent method to Eq. (B-18)

and Eq. (B-26).

The participation factor $c_{i(r_1,r_2,\ldots,r_h)}$ can be obtained from the *h*th derivative of the mass orthogonal condition Eq. (B-12)

$$\left\{\phi_i^T\right\}\mathbf{M}\frac{\partial^h\left\{\phi_i\right\}}{\partial r_1\partial r_2\cdots\partial r_h}=d_{i(1,2,\ldots,h)} \tag{B-32}$$

where the scalar $d_{i(1,2,\ldots,h)}$ contains terms involving derivatives of order (*h*-1) and lower. Thereby the participation factor $c_{i(r_1,r_2,\ldots,r_h)}$ is achieved as

$$c_{i(1,2,\ldots,h)}=d_{i(1,2,\ldots,h)}-\left\{\phi_i^T\right\}\mathbf{M}\left\{\mathbf{v}_{i(1,2,\ldots,h)}\right\} \tag{B-33}$$

APPENDIX C

STIFFNESS AND MODAL FLEXIBILITY MATRICES OF FREE STRUCTURES

The substructuring methods require dividing the global structure into independent free or fixed substructures. As a free structure includes the rigid body components, its stiffness matrix is rank deficient and thus cannot be inversed to obtain the flexibility matrix as usual. It is noted that, the flexibility matrix of a free structure does not exist actually. The flexibility matrix of a free structure hereby is denoted as the modal flexibility matrix, which is contributed by the deformational eigenmodes as $\mathbf{\Phi}_d \mathbf{\Lambda}_d^{-1} \left[\mathbf{\Phi}_d\right]^T$.

In this section, the property of a free structure is addressed. The singular stiffness matrix is transformed into full-rank one, from the inversion of which the modal flexibility is acquired. The stiffness matrix can be obtained from the inversion of the transformed full-rank flexibility matrix in the same way. Afterwards, the transformation is generalized to the case of condensed model, since the flexibility or stiffness matrices are usually estimated at partial DOFs in practice.

C.1 Transformation of Stiffness and Modal Flexibility Matrices

The displacement $\{x\}$ of a free structure can be written as a superposition of the deformational and rigid body motions

$$\{x\} = \{x_d\} + \{x_r\} = \mathbf{\Phi}_d \{q\} + \mathbf{R}\{\alpha\} \qquad \text{(C-1)}$$

where $\{x_d\}$ is the the displacement due to the deformational motion, $\{x_r\}$ is the displacement due to the rigid body components, $\mathbf{\Phi}_d$ is the linear orthogonal

deformational modes satisfying $\boldsymbol{\Phi}_d^T\boldsymbol{\Phi}_d = \mathbf{I}$, $\mathbf{R}$ is the rigid body modes evaluated at the nodes and orthogonal as $\mathbf{R}^T\mathbf{R} = \mathbf{I}$, and $\{q\}$ and $\{\alpha\}$ are the corresponding participation factors.

According to Eq. (C-1), the displacement $\{x\}$ can be decoupled in the deformational space and rigid body space in Figure C-1.

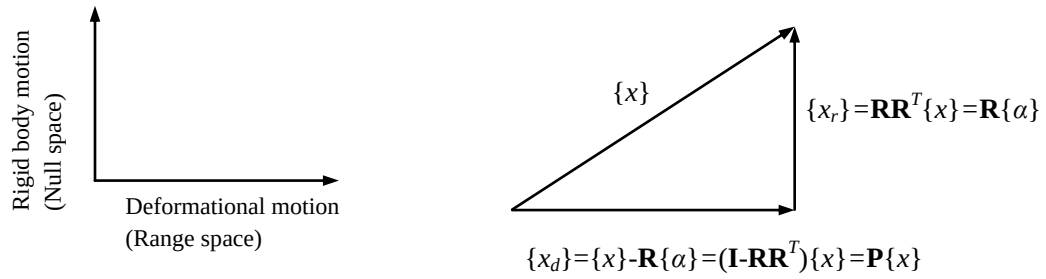

Figure C-1: Decoupling of Displacement of a Free Structure in Modal Space

The orthogonal projector associated with $\mathbf{R}$ can be constructed by

$$\mathbf{P} = \mathbf{I} - \mathbf{R}\left(\mathbf{R}^T\mathbf{R}\right)^{-1}\mathbf{R}^T = \mathbf{I} - \mathbf{R}\mathbf{R}^T \tag{C-2}$$

which has the properties

$$\mathbf{P}^2 = \mathbf{P}, \quad \mathbf{P}\mathbf{R} = \mathbf{R}^T\mathbf{P} = \mathbf{0} \tag{C-3}$$

In the modal space, the stiffness matrix $\mathbf{K}$ of a free structure has two kinds of eigenpairs:

1) N_r zero eigenvalues pertaining to the rigid body motions. The associated eigenvectors span the null space of $\mathbf{K}$, which contribute to the columns of $\mathbf{R}$.

2) $N_d = N\text{-}N_r$ nonzero eigenvalues λ_i (i=1, 2, …, N_d). The associated orthogonal deformational eigenvectors $\boldsymbol{\Phi}_d = \begin{bmatrix}\phi_1 & \phi_2 & \cdots & \phi_{N_d}\end{bmatrix}$ span the range space of $\mathbf{K}$, which satisfy $\mathbf{K}\{\phi_i\} = \lambda_i\{\phi_i\}$ and $\mathbf{R}\{\phi_i\} = \mathbf{0}$.

In usual sense, the stiffness matrix and flexibility matrix are composed by the deformational eigenmodes solely as

$$\mathbf{K} = \sum_{i=1}^{N_d} \lambda_i \phi_i \phi_i^T \ , \ \ \mathbf{F} = \sum_{i=1}^{N_d} \frac{1}{\lambda_i} \phi_i \phi_i^T \tag{C-4}$$

Mathematically, the stiffness matrix and the modal flexibility matrix formed with the deformational eigenmodes are singular and rank deficient for a free structure.

A generalized stiffness matrix and a generalized flexibility matrix are defined as follows, which include the contribution made by both the rigid body modes and deformational modes.

$$\bar{\mathbf{K}} = \mathbf{K} + \mathbf{R}\mathbf{R}^T = \sum_{i=1}^{N_d} \lambda_i \phi_i \phi_i^T + \mathbf{R}\mathbf{R}^T \ , \ \ \bar{\mathbf{F}} = \mathbf{F} + \mathbf{R}\mathbf{R}^T = \sum_{i=1}^{N_d} \frac{1}{\lambda_i} \phi_i \phi_i^T + \mathbf{R}\mathbf{R}^T \tag{C-5}$$

The eigenvectors of $\left(\mathbf{K} + \mathbf{R}\mathbf{R}^T\right)$ are identical to those of **K**, but only the eigenvalues of the rigid body modes are changed from 0 to 1.

The generalized stiffness matrix $\bar{\mathbf{K}}$ and flexibility matrix $\bar{\mathbf{F}}$ are full-rank, and can be transformed with each other by inversion of

$$\left(\mathbf{K} + \mathbf{R}\mathbf{R}^T\right)^{-1} = \left(\sum_{i=1}^{N_d} \lambda_i \phi_i \phi_i^T + \sum_{i=1}^{N_r} 1 \left(\phi_i \phi_i^T \right) \right)^{-1} = \left(\sum_{i=1}^{N_d+N_r} \lambda_i \phi_i \phi_i^T \right)^{-1} = \sum_{i=1}^{N_d+N_r} \frac{1}{\lambda_i} \phi_i \phi_i^T = \sum_{i=1}^{N_d} \frac{1}{\lambda_i} \phi_i \phi_i^T + \mathbf{R}\mathbf{R}^T = \mathbf{F} + \mathbf{R}\mathbf{R}^T \tag{C-6}$$

$$\left(\mathbf{F} + \mathbf{R}\mathbf{R}^T\right)^{-1} = \sum_{i=1}^{N_d} \lambda_i \phi_i \phi_i^T + \mathbf{R}\mathbf{R}^T = \mathbf{K} + \mathbf{R}\mathbf{R}^T \tag{C-7}$$

Accordingly, the stiffness matrix **K** and the modal flexibility matrix **F** can be easily acquired from the full-rank matrices, by subtracting the item $\mathbf{R}\mathbf{R}^T$ as following.

$$\mathbf{K} = \left(\mathbf{F} + \mathbf{R}\mathbf{R}^T\right)^{-1} - \mathbf{R}\mathbf{R}^T \tag{C-8}$$

$$\mathbf{F} = \left(\mathbf{K} + \mathbf{R}\mathbf{R}^T\right)^{-1} - \mathbf{R}\mathbf{R}^T \tag{C-9}$$

Alternatively, the stiffness matrix **K** and the modal flexibility matrix **F** can also be obtained by projecting the generalized matrices $\bar{\mathbf{K}}$ and $\bar{\mathbf{F}}$ onto the range space with projector **P**. The projector **P** is orthogonal to **R**, and can be formed by

$$\mathbf{P} = \mathbf{I} - \mathbf{R}\mathbf{R}^T = \mathbf{\Phi}_d \mathbf{\Phi}_d^T = \sum_{i=1}^{N_d} \phi_i \phi_i^T \tag{C-10}$$

which leads to

$$\mathbf{P}\left(\mathbf{K}+\mathbf{R}\mathbf{R}^T\right)=\left(\sum_{i=1}^{N_d}\phi_i\phi_i^T\right)\left(\sum_{i=1}^{N_d}\lambda_i\phi_i\phi_i^T+\mathbf{R}\mathbf{R}^T\right)=\sum_{i=1}^{N_d}\lambda_i\phi_i\phi_i^T+\sum_{i=1}^{N_d}\phi_i\phi_i^T\sum_{r=1}^{N_r}\phi_r\phi_r^T=\sum_{i=1}^{N_d}\lambda_i\phi_i\phi_i^T=\mathbf{K} \tag{C-11}$$

$$\mathbf{P}\left(\mathbf{F}+\mathbf{R}\mathbf{R}^T\right)=\left(\sum_{i=1}^{N_d}\phi_i\phi_i^T\right)\left(\sum_{i=1}^{N_d}\frac{1}{\lambda_i}\phi_i\phi_i^T+\mathbf{R}\mathbf{R}^T\right)=\sum_{i=1}^{N_d}\frac{1}{\lambda_i}\phi_i\phi_i^T=\mathbf{F} \tag{C-12}$$

The projector **P** can filter out the rigid body motions and leave only the deformational modes in the stiffness and flexibility matrices. To keep the symmetric property of the system matrices, the generalized stiffness and flexibility matrices is usually filtered as

$$\mathbf{F}=\mathbf{P}\bar{\mathbf{F}}\mathbf{P}=\mathbf{P}\left(\mathbf{K}+\mathbf{R}\mathbf{R}^T\right)^{-1}\mathbf{P} \tag{C-13}$$

$$\mathbf{K}=\mathbf{P}\bar{\mathbf{K}}\mathbf{P}=\mathbf{P}\left(\mathbf{F}+\mathbf{R}\mathbf{R}^T\right)^{-1}\mathbf{P} \tag{C-14}$$

To sum up, if the rank-deficient stiffness matrix **K** is obtainable as usual case, the modal flexibility matrix **F** can be obtained either by subtracting the rigid body modes from the inversion of the full-rank stiffness matrix $\bar{\mathbf{K}}$ or by multiplying a projector.

$$\mathbf{F}=\left(\mathbf{K}+\mathbf{R}\mathbf{R}^T\right)^{-1}-\mathbf{R}\mathbf{R}^T \tag{C-15}$$

$$\mathbf{F}=\mathbf{P}\left(\mathbf{K}+\mathbf{R}\mathbf{R}^T\right)^{-1}\mathbf{P} \tag{C-16}$$

With the former manner (Eq. (C-15)), the modal flexibility matrix **F** can be achieved from the rank-deficient stiffness matrix **K** by easily adding or subtracting the item $\mathbf{R}\mathbf{R}^T$ with high efficiency. This is adopted to calculate the residual flexibility and the associated derivative matrices for the free substructures in this thesis. However, sometimes the stiffness or flexibility matrices contain the rigid body motions in a random way, not exactly $\mathbf{R}\mathbf{R}^T$. As presented in Chapter 8, the substructural flexibility is extracted from the measured modal data. It is difficult to determine the participation coefficient of the rigid body motions. In that case, subtracting the item $\mathbf{R}\mathbf{R}^T$ from the given matrix may lead to an incorrect answer. Projecting the stiffness matrix or flexibility matrix onto the range space can always provide the desired matrices which are only contributed by the deformational modes, although it costs

additional computation time to construct the projector **P**.

Since the full-rank matrices $\bar{\mathbf{K}}$ and $\bar{\mathbf{F}}$ are dual inversion of each other, they are responsible to transfer the stiffness and modal flexibility matrices of the free structures.

C.2 Transformation of Mass-normalized Stiffness and Modal Flexibility Matrices

In practical dynamic testing, the mass-normalized eigenmodes are obtained if both the input and output are measured at one point. Accordingly, the achieved modal flexibility matrix is mass-normalized as well. In addition, the dynamic analysis in modal space is usually described by the eigenproblem in form of

$$\left(\mathbf{K}-\lambda\mathbf{M}\right)\mathbf{\Phi}=\mathbf{0} \tag{C-17}$$

As before, the eigenproblem has two kinds of eigenpairs, i.e., N_r zero eigenvalues associated with the rigid body modes **R**, and N_d nonzero eigenvalues associated with the deformational modes $\mathbf{\Phi}_d$. They satisfy the orthogonality condition

$$\mathbf{R}^T\mathbf{M}\mathbf{R}=\mathbf{I},\ \ \mathbf{\Phi}_d^T\mathbf{M}\mathbf{\Phi}_d=\mathbf{I},\ \ \mathbf{R}^T\mathbf{M}\mathbf{\Phi}_d=\mathbf{0} \tag{C-18}$$

The stiffness matrix **K** and modal flexibility **F** can be expanded by the mass-normalized modal modes as

$$\mathbf{K}=\sum_{i=1}^{N_d}\lambda_i\left(\mathbf{M}\phi_i\right)\left(\mathbf{M}\phi_i\right)^T \tag{C-19}$$

$$\bar{\mathbf{K}}=\mathbf{K}+\left(\mathbf{M}\mathbf{R}\right)\left(\mathbf{M}\mathbf{R}\right)^T=\sum_{i=1}^{N_d}\lambda_i\left(\mathbf{M}\phi_i\right)\left(\mathbf{M}\phi_i\right)^T+\left(\mathbf{M}\mathbf{R}\right)\left(\mathbf{M}\mathbf{R}\right)^T \tag{C-20}$$

$$\mathbf{F}=\sum_{i=1}^{N_d}\frac{1}{\lambda_i}\phi_i\phi_i^T \tag{C-21}$$

$$\bar{\mathbf{F}}=\mathbf{F}+\mathbf{R}\mathbf{R}^T=\sum_{i=1}^{N_d}\frac{1}{\lambda_i}\phi_i\phi_i^T+\mathbf{R}\mathbf{R}^T \tag{C-22}$$

Due to the relation

$$\left(\mathbf{K}+\left(\mathbf{MR}\right)\left(\mathbf{MR}\right)^{T}\right)\left(\mathbf{F}+\mathbf{RR}^{T}\right)=\mathbf{KF}+\left(\mathbf{MR}\right)\left(\mathbf{MR}\right)^{T}\mathbf{RR}^{T}=\boldsymbol{\Phi}_{d}^{T}\mathbf{M}\boldsymbol{\Phi}_{d}+\mathbf{R}^{T}\mathbf{MR}=\mathbf{I} \tag{C-23}$$

The generalized stiffness matrix $\bar{\mathbf{K}}$ and generalized flexibility matrix $\bar{\mathbf{F}}$ are dual inversion of each other

$$\left(\mathbf{K}+\left(\mathbf{MR}\right)\left(\mathbf{MR}\right)^{T}\right)^{-1}=\mathbf{F}+\mathbf{RR}^{T} \tag{C-24}$$

$$\left(\mathbf{F}+\mathbf{RR}^{T}\right)^{-1}=\mathbf{K}+\left(\mathbf{MR}\right)\left(\mathbf{MR}\right)^{T} \tag{C-25}$$

The generalized stiffness matrix $\bar{\mathbf{K}}$ leads to the eigenequation

$$\left(\left(\mathbf{K}+\left(\mathbf{MR}\right)\left(\mathbf{MR}\right)^{T}\right)-\lambda\mathbf{M}\right)\boldsymbol{\Phi}=\mathbf{0} \tag{C-26}$$

which has the identical eigenvectors to those of Eq. (C-17), and only the eigenvalues of the rigid body modes are changed from 0 to 1.

In this case, the projector **P** is constructed as

$$\mathbf{P}=\mathbf{I}-\left(\mathbf{M}^{\frac{1}{2}}\mathbf{R}\right)\left(\left(\mathbf{M}^{\frac{1}{2}}\mathbf{R}\right)^{T}\left(\mathbf{M}^{\frac{1}{2}}\mathbf{R}\right)\right)^{-1}\left(\mathbf{M}^{\frac{1}{2}}\mathbf{R}\right)^{T}=\mathbf{I}-\left(\mathbf{M}^{\frac{1}{2}}\mathbf{R}\right)\left(\mathbf{M}^{\frac{1}{2}}\mathbf{R}\right)^{T} \tag{C-27}$$

$$\mathbf{P}=\left(\mathbf{M}^{\frac{1}{2}}\boldsymbol{\Phi}_{d}\right)\left(\mathbf{M}^{\frac{1}{2}}\boldsymbol{\Phi}_{d}\right)^{T} \tag{C-28}$$

and satisfy

$$\mathbf{P}^{2}=\mathbf{P},\quad \mathbf{P}\left(\mathbf{M}^{\frac{1}{2}}\mathbf{R}\right)=\left(\mathbf{M}^{\frac{1}{2}}\mathbf{R}\right)^{T}\mathbf{P}=\mathbf{0} \tag{C-29}$$

The modal flexibility **F** and the stiffness matrix **K** can be acquired from the full-rank matrices with the help of projector **P** as

$$\mathbf{F}=\mathbf{M}^{-\frac{1}{2}}\mathbf{P}\mathbf{M}^{\frac{1}{2}}\left(\mathbf{K}+\left(\mathbf{MR}\right)\left(\mathbf{MR}\right)^{T}\right)^{-1}\mathbf{M}^{\frac{1}{2}}\mathbf{P}\mathbf{M}^{-\frac{1}{2}}$$

$$\mathbf{K}=\mathbf{M}^{\frac{1}{2}}\mathbf{P}\mathbf{M}^{-\frac{1}{2}}\left(\mathbf{F}+\mathbf{RR}^{T}\right)^{-1}\mathbf{M}^{-\frac{1}{2}}\mathbf{P}\mathbf{M}^{\frac{1}{2}} \tag{C-30}$$

If the mass matrix is unsymmetrical or invertible, **M** can be decomposed by QR

algorithm or Cholesky factorization. The mass matrix is decomposed by $\mathbf{M}=\mathbf{M}_1\mathbf{M}_2$, and the projector matrix **P** is constructed in the form of

$$\mathbf{P}=\mathbf{I}-\mathbf{M}_2\mathbf{R}\left[\mathbf{M}_1^T\mathbf{R}\right]^T \tag{C-31}$$

$$\mathbf{P}=\left(\mathbf{M}_2\boldsymbol{\Phi}_d\right)\left[\mathbf{M}_1^T\boldsymbol{\Phi}_d\right]^T$$

which satisfy

$$\mathbf{P}^2=\mathbf{P},\quad \mathbf{P}\left(\mathbf{M}_2\mathbf{R}\right)=\left[\mathbf{M}_1^T\mathbf{R}\right]^T\mathbf{P}=\mathbf{0} \tag{C-32}$$

Accordingly, the modal flexibility and stiffness matrices are projected onto the range space by

$$\mathbf{F}=\left(\mathbf{M}\setminus\mathbf{M}_1\right)\mathbf{P}\mathbf{M}_2\left(\mathbf{K}+\left(\mathbf{M}\mathbf{R}\right)\left(\mathbf{M}\mathbf{R}\right)^T\right)^{-1}\mathbf{M}_1\mathbf{P}\left(\mathbf{M}_2/\mathbf{M}\right)$$

$$\mathbf{K}=\mathbf{M}_1\mathbf{P}\left(\mathbf{M}_1\setminus\left(\mathbf{F}+\mathbf{R}\mathbf{R}^T\right)^{-1}/\mathbf{M}_2\right)\mathbf{P}\mathbf{M}_2 \tag{C-33}$$

C.3 Transformation of the Condensed Stiffness and Modal Flexibility Matrices

Practically, the stiffness or modal flexibility matrices are difficult to be estimated or measured on the full DOFs, it is necessary to construct the condensed stiffness and modal flexibility matrices for the free structure.

If the full-DOF model is divided into the master part and the slave part, the stiffness matrix and the modal flexibility matrix are condensed to the master DOFs by

$$\mathbf{K}_R=\mathbf{K}_{aa}-\mathbf{K}_{ab}\mathbf{K}_{bb}^{-1}\mathbf{K}_{ba} \tag{C-34}$$

$$\mathbf{F}_R=\mathbf{F}_{aa} \tag{C-35}$$

where the subscript '*a*' represents the master DOFs, while the subscript '*b*' represents the slave DOFs. Different from the condensation of stiffness matrix, reducing the full-DOF flexibility matrix to $\mathbf{F}_R$ is trivial and can be simply done by extracting the appropriate rows and columns of **F**. In addition, $\mathbf{K}_R$ is singular while $\mathbf{F}_R$ is usually nonsingular and well conditioned.

Concerning the full-DOF model described in the foregoing section, one can filter out the rigid body component from $\bar{\mathbf{K}}$ and $\bar{\mathbf{F}}$, either by subtracting the item $\mathbf{R}\mathbf{R}^T$ or by multiplying a projector **P**. Nevertheless, in the condensed model, the reduced rigid body modes $\mathbf{R}_a$ is not orthogonal to the condensed stiffness matrix $\mathbf{K}_R$ and flexibility matrix $\mathbf{F}_R$ any more. It is inappropriate to subtract the item $\mathbf{R}_a\mathbf{R}_a^T$ directly. An alternative is to construct a projector for the condensed matrix to filter out the rigid body component.

The projector is formed for the reduced model as

$$\mathbf{P}_R = \mathbf{I} - \mathbf{R}_a \left(\mathbf{R}_a^T \mathbf{R}_a \right)^{-1} \mathbf{R}_a^T \tag{C-36}$$

$\mathbf{R}_a$ is the rigid body modes at the master DOFs. The condensed stiffness matrix $\mathbf{K}_R$ and flexibility matrix $\mathbf{F}_R$ are not able to be related with $\mathbf{P}_R$ directly. An interim variable needs to be constructed. If denoting $\tilde{\mathbf{F}}_R = \mathbf{P}_R \mathbf{F}_R \mathbf{P}_R$, $\mathbf{K}_R$ and $\tilde{\mathbf{F}}_R$ have the relation

$$\mathbf{K}_R = \mathbf{P}_R \left(\tilde{\mathbf{F}}_R + \mathbf{R}_a \left(\mathbf{R}_a^T \mathbf{R}_a \right)^{-1} \mathbf{R}_a^T \right)^{-1} \mathbf{P}_R \tag{C-37}$$

$$\tilde{\mathbf{F}}_R = \mathbf{P}_R \left(\mathbf{K}_R + \mathbf{R}_a \left(\mathbf{R}_a^T \mathbf{R}_a \right)^{-1} \mathbf{R}_a^T \right)^{-1} \mathbf{P}_R \tag{C-38}$$

Eq. (C-38) indicates that, one can only obtain $\tilde{\mathbf{F}}_R$ on the space spanned by $\mathbf{P}_R$. The condensed stiffness matrix $\mathbf{K}_R$ and flexibility matrix $\mathbf{F}_R$ are both normalized to $\tilde{\mathbf{F}}_R$ by the condensed projector $\mathbf{P}_R$.

C.4 Transformation of Condensed Mass-normalized Stiffness and Modal Flexibility Matrices

If the mass-normalized eigenvectors are used in the condensed model, the dynamic condensation are employed (Xia and Lin 2004), which has the condensed

eigenequation

$$\mathbf{K}_R\boldsymbol{\Phi}_a = \lambda\mathbf{M}_R\boldsymbol{\Phi}_a \tag{C-39}$$

In Eq. (C-39), $\mathbf{K}_R = \mathbf{K}_{aa} - \mathbf{K}_{ab}\mathbf{K}_{bb}^{-1}\mathbf{K}_{ba}$ is the condensed stiffness matrix, while $\mathbf{M}_R$ is the dynamic condensed mass matrix obtained in an iterative way. Since $\mathbf{M}_R$ is usually unsymmetrical, it needs to be decomposed as $\mathbf{M}_R = \mathbf{M}_1\mathbf{M}_2$, and the condensed projector $\mathbf{P}_R$ is constructed as

$$\mathbf{P}_R = \mathbf{I} - \mathbf{M}_2\mathbf{R}_a\left[\mathbf{M}_1^T\mathbf{R}_a\right]^T \tag{C-40}$$

In this case, the interim flexibility is formulated as

$$\tilde{\mathbf{F}}_R = \left(\mathbf{M}_R \setminus \mathbf{M}_1\right)\mathbf{P}_R\mathbf{M}_2\mathbf{F}_R\mathbf{M}_1\mathbf{P}_R\left(\mathbf{M}_2 / \mathbf{M}_R\right) \tag{C-41}$$

$\mathbf{K}_R$ and $\tilde{\mathbf{F}}_R$ have the dual relationship

$$\mathbf{K}_R = \mathbf{M}_1\mathbf{P}_R\left(\mathbf{M}_1 \setminus \left(\tilde{\mathbf{F}}_R + \mathbf{R}_a\left(\mathbf{R}_a^T\mathbf{R}_a\right)^{-1}\mathbf{R}_a^T\right)^{-1} / \mathbf{M}_2\right)\mathbf{P}_R\mathbf{M}_2 \tag{C-42}$$

$$\tilde{\mathbf{F}}_R = \left(\mathbf{M}_R \setminus \mathbf{M}_1\right)\mathbf{P}_R\mathbf{M}_2\left(\mathbf{K}_R + \left(\mathbf{M}_R\mathbf{R}_a\right)\left(\mathbf{M}_R\mathbf{R}_a\right)^T\right)^{-1}\mathbf{M}_1\mathbf{P}_R\left(\mathbf{M}_2 / \mathbf{M}_R\right) \tag{C-43}$$

The interim flexibility $\tilde{\mathbf{F}}_R$ can be obtained either from the reduced flexibility $\mathbf{F}_R$ as Eq. (C-41), or from the reduced stiffness $\mathbf{K}_R$ as Eq. (C-43). In Chapter 8, the modal flexibility matrices extracted from the measured modal data and from the analytical model are both normalized with the condensed projector $\mathbf{P}_R$ for model updating purpose.

C.5 One Example

To illustrate the aforementioned properties of the free structure, the second substructure of the mass-spring model are employed here in Figure C-2.

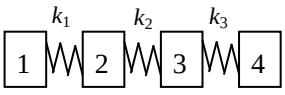

Figure C-2: 4-DOF Spring-mass Model

The 4-DOF model has the stiffness and mass matrices

$$\mathbf{K} = \begin{bmatrix} 20 & -20 & & \\ -20 & 40 & -20 & \\ & -20 & 40 & -20 \\ & & -20 & 20 \end{bmatrix}, \quad \mathbf{M} = \begin{bmatrix} 1 & & & \\ & 2 & & \\ & & 2 & \\ & & & 1 \end{bmatrix} \tag{C-44}$$

From the classical eigenequation, the eigenvalues and mass-normalized eigenvectors in modal space are obtained, which include one rigid body mode (N_R = 1) and three deformational modes (N_d = 3) as

$$\mathbf{\Lambda} = \mathrm{Diag}\left(\begin{bmatrix} \lambda_1 & \lambda_2 & \lambda_3 & \lambda_4 \end{bmatrix}\right) = \mathrm{Diag}\left(\begin{bmatrix} 0 & 10 & 30 & 40 \end{bmatrix}\right) \tag{C-45}$$

$$\mathbf{R} = \begin{bmatrix} 0.4082 \\ 0.4082 \\ 0.4082 \\ 0.4082 \end{bmatrix}, \quad \mathbf{\Phi}_d = \begin{bmatrix} -0.5774 & 0.5774 & 0.4082 \\ -0.2887 & -0.2887 & -0.4082 \\ 0.2887 & -0.2887 & 0.4082 \\ 0.5774 & 0.5774 & -0.4082 \end{bmatrix}$$

The deformational eigenmodes give the full-DOF modal flexibility as

$$\mathbf{F} = \mathbf{\Phi}_d \mathbf{\Lambda}_d^{-1} \mathbf{\Phi}_d^T = \begin{bmatrix} 0.0486 & 0.0069 & -0.0181 & -0.0264 \\ 0.0069 & 0.0153 & -0.0097 & -0.0181 \\ -0.0181 & -0.0097 & 0.0153 & 0.0069 \\ -0.0264 & -0.0181 & 0.0069 & 0.0486 \end{bmatrix} \tag{C-46}$$

It is assumed that, the third DOF is unmeasured, i.e., the 1st, 2nd, 4th DOFs are assumed to be the master DOFs, and the 3rd DOF is slave.

$$\mathbf{K} = \begin{bmatrix} 20 & -20 & & \\ -20 & 40 & -20 & \\ & -20 & 40 & -20 \\ & & -20 & 20 \end{bmatrix}$$

$$\mathbf{F} = \begin{bmatrix} 0.0437 & 0.0062 & -0.0187 \\ 0.0062 & 0.0188 & -0.0062 \\ -0.0187 & 0.0062 & 0.0187 \\ -0.0312 & 0.0187 & 0.0062 \end{bmatrix} \tag{C-47}$$

With the dynamic condensation (Xia and Lin 2004), the stiffness matrix and mass matrix are reduced to

$$\mathbf{K}_R = \begin{bmatrix} 20 & -20 & 0 \\ -20 & 30 & -10 \\ 0 & -10 & 10 \end{bmatrix}, \quad \mathbf{M}_R = \begin{bmatrix} 1.0 & 0.0 & 0.0 \\ -0.5 & 3.0 & 0.5 \\ -0.5 & 1.0 & 1.5 \end{bmatrix} \tag{C-48}$$

And the reduced modal flexibility matrix is

$$\mathbf{F}_R = \mathbf{F}_{aa} = \begin{bmatrix} 0.0486 & 0.0069 & -0.0264 \\ 0.0069 & 0.0153 & -0.0181 \\ -0.0264 & -0.0181 & 0.0486 \end{bmatrix} \tag{C-49}$$

The rigid body mode at the master DOFs is obtained as

$$\mathbf{R}_a = \begin{bmatrix} 0.4082 \\ 0.4082 \\ 0.4082 \end{bmatrix} \tag{C-50}$$

Decomposing the unsymmetrical condensed mass matrix with $\mathbf{M}_R = \mathbf{M}_1\mathbf{M}_2$, the reduced projector is constructed with

$$\mathbf{P}_R = \mathbf{I} - \mathbf{M}_2\mathbf{R}_a\left[\mathbf{M}_1^T\mathbf{R}_a\right]^T = \begin{bmatrix} 1 & 0.3015 & -0.1846 \\ 0 & 0.1818 & -0.5010 \\ 0 & 0.2969 & 0.8182 \end{bmatrix} \tag{C-51}$$

Denoting projector

$$\mathbf{P}_1 = \left(\mathbf{M}_R \setminus \mathbf{M}_1\right)\mathbf{P}_R\mathbf{M}_2, \quad \mathbf{P}_2 = \mathbf{M}_1\mathbf{P}_R\left(\mathbf{M}_2 / \mathbf{M}_R\right) \tag{C-52}$$

the interim flexibility matrix $\tilde{\mathbf{F}}_R$ can be recovered from the reduced flexibility $\mathbf{F}_R$ as

$$\tilde{\mathbf{F}}_R = \mathbf{P}_1\mathbf{F}_R\mathbf{P}_2 = \begin{bmatrix} 0.0528 & 0.0028 & -0.0306 \\ 0.0111 & 0.0111 & -0.0222 \\ -0.0222 & -0.0222 & 0.0444 \end{bmatrix} \tag{C-53}$$

or from the reduced stiffness $\mathbf{K}_R$ as

$$\tilde{\mathbf{F}}_R = \mathbf{P}_1\left(\mathbf{K}_R + \left(\mathbf{M}_R\mathbf{R}_a\right)\left(\mathbf{M}_R\mathbf{R}_a\right)^T\right)^{-1}\mathbf{P}_2 = \begin{bmatrix} 0.0528 & 0.0028 & -0.0306 \\ 0.0111 & 0.0111 & -0.0222 \\ -0.0222 & -0.0222 & 0.0444 \end{bmatrix} \tag{C-54}$$

Eq. (C-53) and Eq. (C-54) give identical results. Although it is difficult to reproduce $\mathbf{F}_R$ from the interim variable $\tilde{\mathbf{F}}_R$, one can relate the condensed stiffness matrix $\mathbf{K}_R$ and flexibility matrix $\mathbf{F}_R$ based on this term $\tilde{\mathbf{F}}_R$.

Additionally, the condensed stiffness matrix can be exactly recovered from the

reduced flexibility matrix as well.

$$\mathbf{K}_R = \mathbf{M}_1\mathbf{P}_R\left(\mathbf{M}_1 \backslash \left(\tilde{\mathbf{F}}_R + \mathbf{R}_a\left(\mathbf{R}_a^T\mathbf{R}_a\right)^{-1}\mathbf{R}_a^T\right)^{-1} / \mathbf{M}_2\right)\mathbf{P}_R\mathbf{M}_2 = \begin{bmatrix} 20 & -20 & 0 \\ -20 & 30 & -10 \\ 0 & -10 & 10 \end{bmatrix} \quad \text{(C-55)}$$

APPENDIX D

RESIDUAL FLEXIBILITY MATRIX FOR FREE STRUCTURES

Based on the aforementioned property of the stiffness and modal flexibility matrices, the residual flexibility matrix is derived for the free structures. The first-order residual flexibility matrix will be derived first, followed by the general formulae of the high-order residual flexibility matrices.

The complete eigenmodes are divided into N_m master modes $\mathbf{\Phi}_m$ and N_s slave modes $\mathbf{\Phi}_s$. The master modes $\mathbf{\Phi}_m$ include the N_r rigid body modes $\mathbf{R}$ and the (N_m-N_r) deformational master modes $\mathbf{\Phi}_{m\text{-}r}$. The deformational modes include the deformational master modes $\mathbf{\Phi}_{m\text{-}r}$ and deformational slave modes $\mathbf{\Phi}_s$. The relation between master modes, slave modes, rigid body modes, and deformational modes is illustrated in Figure D-1.

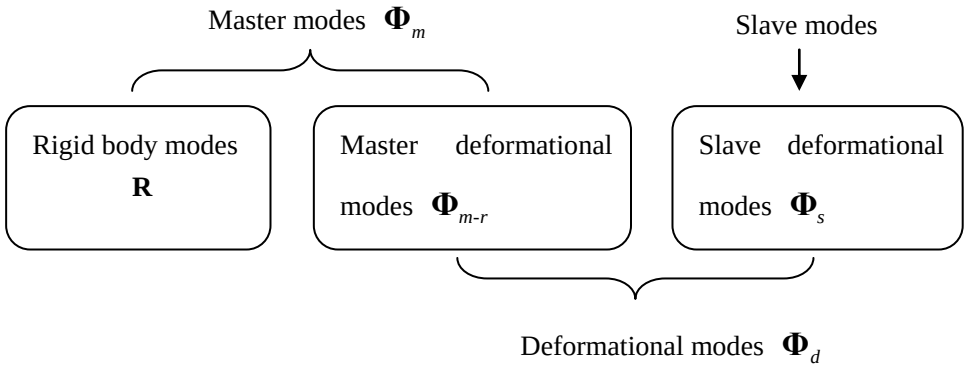

Figure D-1: Relationship between Different Kinds of Modal Modes

The generalized stiffness matrix can be expressed by the rigid body modes, master modes and slave modes as

$$\left(\mathbf{K}+\mathbf{R}\mathbf{R}^T\right)^{-1}=\sum_{\substack{i=1\\ \phi\in\boldsymbol{\Phi}_{m\text{-}r}}}^{N_m-N_r}\frac{1}{\lambda_i}\phi_i\phi_i^T+\sum_{\substack{i=1\\ \phi\in\boldsymbol{\Phi}_s}}^{N_s}\frac{1}{\lambda_i}\phi_i\phi_i^T+\mathbf{R}\mathbf{R}^T=\boldsymbol{\Phi}_{m\text{-}r}\boldsymbol{\Lambda}_{m\text{-}r}^{-1}\boldsymbol{\Phi}_{m\text{-}r}^T+\boldsymbol{\Phi}_s\boldsymbol{\Lambda}_s^{-1}\boldsymbol{\Phi}_s^T+\mathbf{R}\mathbf{R}^T \quad \text{(D-1)}$$

Therefore, the first-order residual flexibility matrix for the free structure can be expressed by the master modes as

$$\boldsymbol{\Phi}_s\boldsymbol{\Lambda}_s^{-1}\boldsymbol{\Phi}_s^T=\left(\mathbf{K}+\mathbf{R}\mathbf{R}^T\right)^{-1}-\boldsymbol{\Phi}_{m\text{-}r}\boldsymbol{\Lambda}_{m\text{-}r}^{-1}\boldsymbol{\Phi}_{m\text{-}r}^T-\mathbf{R}\mathbf{R}^T \quad \text{(D-2)}$$

Accordingly, the second-order residual flexibility matrix for the free structure is

$$\boldsymbol{\Phi}_s\boldsymbol{\Lambda}_s^{-2}\boldsymbol{\Phi}_s^T=\left(\boldsymbol{\Phi}_s\boldsymbol{\Lambda}_s^{-1}\boldsymbol{\Phi}_s^T\right)\left(\boldsymbol{\Phi}_s\boldsymbol{\Lambda}_s^{-1}\boldsymbol{\Phi}_s^T\right)=$$

$$\left(\left(\mathbf{K}+\mathbf{R}\mathbf{R}^T\right)^{-1}-\boldsymbol{\Phi}_{m\text{-}r}\boldsymbol{\Lambda}_{m\text{-}r}^{-1}\boldsymbol{\Phi}_{m\text{-}r}^T-\mathbf{R}\mathbf{R}^T\right)\left(\left(\mathbf{K}+\mathbf{R}\mathbf{R}^T\right)^{-1}-\boldsymbol{\Phi}_{m\text{-}r}\boldsymbol{\Lambda}_{m\text{-}r}^{-1}\boldsymbol{\Phi}_{m\text{-}r}^T-\mathbf{R}\mathbf{R}^T\right)$$

$$=\left(\mathbf{K}+\mathbf{R}\mathbf{R}^T\right)^{-2}-\boldsymbol{\Phi}_{m\text{-}r}\boldsymbol{\Lambda}_{m\text{-}r}^{-2}\boldsymbol{\Phi}_{m\text{-}r}^T-\mathbf{R}\mathbf{R}^T \quad \text{(D-3)}$$

which leads to

$$\boldsymbol{\Phi}_s\boldsymbol{\Lambda}_s^{-2}\boldsymbol{\Phi}_s^T=\left(\mathbf{K}+\mathbf{R}\mathbf{R}^T\right)^{-2}-\boldsymbol{\Phi}_{m\text{-}r}\boldsymbol{\Lambda}_{m\text{-}r}^{-2}\boldsymbol{\Phi}_{m\text{-}r}^T-\mathbf{R}\mathbf{R}^T \quad \text{(D-4)}$$

The general formula for the *k*-order residual flexibility is derived as

$$\boldsymbol{\Phi}_s\boldsymbol{\Lambda}_s^{-k}\boldsymbol{\Phi}_s^T=\left(\boldsymbol{\Phi}_s\boldsymbol{\Lambda}_s^{-1}\boldsymbol{\Phi}_s^T\right)\left(\boldsymbol{\Phi}_s\boldsymbol{\Lambda}_s^{-(k-1)}\boldsymbol{\Phi}_s^T\right)=$$

$$\left(\left(\mathbf{K}+\mathbf{R}\mathbf{R}^T\right)^{-1}-\boldsymbol{\Phi}_{m\text{-}r}\boldsymbol{\Lambda}_{m\text{-}r}^{-1}\boldsymbol{\Phi}_{m\text{-}r}^T-\mathbf{R}\mathbf{R}^T\right)\left(\left(\mathbf{K}+\mathbf{R}\mathbf{R}^T\right)^{-(k-1)}-\boldsymbol{\Phi}_{m\text{-}r}\boldsymbol{\Lambda}_{m\text{-}r}^{-(k-1)}\boldsymbol{\Phi}_{m\text{-}r}^T-\mathbf{R}\mathbf{R}^T\right)$$

$$=\left(\mathbf{K}+\mathbf{R}\mathbf{R}^T\right)^{-k}-\boldsymbol{\Phi}_{m\text{-}r}\boldsymbol{\Lambda}_{m\text{-}r}^{-k}\boldsymbol{\Phi}_{m\text{-}r}^T-\mathbf{R}\mathbf{R}^T \quad \text{(D-5)}$$

i.e.,

$$\boldsymbol{\Phi}_s\boldsymbol{\Lambda}_s^{-k}\boldsymbol{\Phi}_s^T==\left(\mathbf{K}+\mathbf{R}\mathbf{R}^T\right)^{-k}-\boldsymbol{\Phi}_{m\text{-}r}\boldsymbol{\Lambda}_{m\text{-}r}^{-k}\boldsymbol{\Phi}_{m\text{-}r}^T-\mathbf{R}\mathbf{R}^T \quad \text{(D-6)}$$

If the mass-normalized eigenvectors are considered, the first-order residual flexibility matrix for the free structure is

$$\boldsymbol{\Phi}_s\boldsymbol{\Lambda}_s^{-1}\boldsymbol{\Phi}_s^T=\left(\mathbf{K}+\left(\mathbf{M}\mathbf{R}\right)\left(\mathbf{M}\mathbf{R}\right)^T\right)^{-1}-\boldsymbol{\Phi}_{m\text{-}r}\boldsymbol{\Lambda}_{m\text{-}r}^{-1}\boldsymbol{\Phi}_{m\text{-}r}^T-\mathbf{R}\mathbf{R}^T \quad \text{(D-7)}$$

The second-order residual flexibility matrix can be obtained with the master modes as

$$\boldsymbol{\Phi}_s\boldsymbol{\Lambda}_s^{-2}\boldsymbol{\Phi}_s^T=\left(\boldsymbol{\Phi}_s\boldsymbol{\Lambda}_s^{-1}\boldsymbol{\Phi}_s^T\right)\mathbf{M}\left(\boldsymbol{\Phi}_s\boldsymbol{\Lambda}_s^{-1}\boldsymbol{\Phi}_s^T\right)=$$

$$\left(\mathbf{K}+\left(\mathbf{M}\mathbf{R}\right)\left(\mathbf{M}\mathbf{R}\right)^T\right)^{-1}\mathbf{M}\left(\mathbf{K}+\left(\mathbf{M}\mathbf{R}\right)\left(\mathbf{M}\mathbf{R}\right)^T\right)^{-1}-\boldsymbol{\Phi}_{m\text{-}r}\boldsymbol{\Lambda}_{m\text{-}r}^{-2}\boldsymbol{\Phi}_{m\text{-}r}^T-\mathbf{R}\mathbf{R}^T \quad \text{(D-8)}$$

Generally, the *k*-order residual flexibility is given by

$$\boldsymbol{\Phi}_s \boldsymbol{\Lambda}_s^{-k} \boldsymbol{\Phi}_s^T = \left(\boldsymbol{\Phi}_s \boldsymbol{\Lambda}_s^{-1} \boldsymbol{\Phi}_s^T\right)\left(\mathbf{M}\left(\boldsymbol{\Phi}_s \boldsymbol{\Lambda}_s^{-1} \boldsymbol{\Phi}_s^T\right)\right)^{k-1} =$$

$$\left(\mathbf{K} + (\mathbf{MR})(\mathbf{MR})^T\right)^{-1}\left(\mathbf{M}\left(\mathbf{K} + (\mathbf{MR})(\mathbf{MR})^T\right)^{-1}\right)^{k-1} - \boldsymbol{\Phi}_{m\text{-}r} \boldsymbol{\Lambda}_{m\text{-}r}^{-k} \boldsymbol{\Phi}_{m\text{-}r}^T - \mathbf{R}\mathbf{R}^T \qquad \text{(D-9)}$$

APPENDIX E

DERIVATIVE OF RESIDUAL FLEXIBILITY MATRIX

Differentiating the first-order residual flexibility (Eq. (D-2)) with respect to an elemental parameter *r*, the derivative matrix has the form of

$$\frac{\partial\left(\boldsymbol{\Phi}_s\boldsymbol{\Lambda}_s^{-1}\boldsymbol{\Phi}_s^T\right)}{\partial r}=\frac{\partial\left(\mathbf{K}+\mathbf{R}\mathbf{R}^T\right)^{-1}}{\partial r}-\frac{\partial\left(\boldsymbol{\Phi}_{m\text{-}r}\boldsymbol{\Lambda}_{m\text{-}r}^{-1}\boldsymbol{\Phi}_{m\text{-}r}^T\right)}{\partial r}$$

$$=-\left(\mathbf{K}+\mathbf{R}\mathbf{R}^T\right)^{-2}\frac{\partial\mathbf{K}}{\partial r}-\left(2\boldsymbol{\Phi}_{m\text{-}r}\boldsymbol{\Lambda}_{m\text{-}r}^{-1}\frac{\partial\left(\boldsymbol{\Phi}_{m\text{-}r}^T\right)}{\partial r}+\boldsymbol{\Phi}_{m\text{-}r}\frac{\partial\left(\boldsymbol{\Lambda}_{m\text{-}r}^{-1}\right)}{\partial r}\boldsymbol{\Phi}_{m\text{-}r}^T\right) \tag{E-1}$$

Accordingly, the second-order residual flexibility (Eq. (D-4)) is differentiated as

$$\frac{\partial\left(\boldsymbol{\Phi}_s\boldsymbol{\Lambda}_s^{-2}\boldsymbol{\Phi}_s^T\right)}{\partial r}=\frac{\partial\left(\mathbf{K}+\mathbf{R}\mathbf{R}^T\right)^{-2}}{\partial r}-\frac{\partial\left(\boldsymbol{\Phi}_{m\text{-}r}\boldsymbol{\Lambda}_{m\text{-}r}^{-2}\boldsymbol{\Phi}_{m\text{-}r}^T\right)}{\partial r}$$

$$=-2\left(\mathbf{K}+\mathbf{R}\mathbf{R}^T\right)^{-3}\frac{\partial\mathbf{K}}{\partial r}-\left(2\boldsymbol{\Phi}_{m\text{-}r}\boldsymbol{\Lambda}_{m\text{-}r}^{-2}\frac{\partial\left(\boldsymbol{\Phi}_{m\text{-}r}^T\right)}{\partial r}+\boldsymbol{\Phi}_{m\text{-}r}\frac{\partial\left(\boldsymbol{\Lambda}_{m\text{-}r}^{-2}\right)}{\partial r}\boldsymbol{\Phi}_{m\text{-}r}^T\right) \tag{E-2}$$

In general, the *k*th-order residual flexibility (Eq. (D-6)) has the derivative matrix

$$\frac{\partial\left(\boldsymbol{\Phi}_s\boldsymbol{\Lambda}_s^{-k}\boldsymbol{\Phi}_s^T\right)}{\partial r}=\frac{\partial\left(\mathbf{K}+\mathbf{R}\mathbf{R}^T\right)^{-k}}{\partial r}-\frac{\partial\left(\boldsymbol{\Phi}_{m\text{-}r}\boldsymbol{\Lambda}_{m\text{-}r}^{-k}\boldsymbol{\Phi}_{m\text{-}r}^T\right)}{\partial r}$$

$$=-k\left(\mathbf{K}+\mathbf{R}\mathbf{R}^T\right)^{-(k-1)}\frac{\partial\mathbf{K}}{\partial r}-\left(2\boldsymbol{\Phi}_{m\text{-}r}\boldsymbol{\Lambda}_{m\text{-}r}^{-k}\frac{\partial\left(\boldsymbol{\Phi}_{m\text{-}r}^T\right)}{\partial r}+\boldsymbol{\Phi}_{m\text{-}r}\frac{\partial\left(\boldsymbol{\Lambda}_{m\text{-}r}^{-k}\right)}{\partial r}\boldsymbol{\Phi}_{m\text{-}r}^T\right) \tag{E-3}$$

If considering the mass-normalized eigenmodes, the derivative matrix of the *k*th-order residual flexibility has the form of

$$\frac{\partial\left(\boldsymbol{\Phi}_s\boldsymbol{\Lambda}_s^{-k}\boldsymbol{\Phi}_s^T\right)}{\partial r}=\frac{\partial\left(\left(\mathbf{K}+(\mathbf{MR})(\mathbf{MR})^T\right)^{-1}\left(\mathbf{M}\left(\mathbf{K}+(\mathbf{MR})(\mathbf{MR})^T\right)^{-1}\right)^{k-1}\right)}{\partial r}$$

$$-\left(2\boldsymbol{\Phi}_{m\text{-}r}\boldsymbol{\Lambda}_{m\text{-}r}^{-k}\frac{\partial\left(\boldsymbol{\Phi}_{m\text{-}r}^T\right)}{\partial r}+\boldsymbol{\Phi}_{m\text{-}r}\frac{\partial\left(\boldsymbol{\Lambda}_{m\text{-}r}^{-k}\right)}{\partial r}\boldsymbol{\Phi}_{m\text{-}r}^T\right) \tag{E-4}$$

REFERENCES

Abdalla, M. O., Grigoriadis, K. M. and Zimmerman, D. C., (1998), "Enhanced structural damage detection using alternating projection methods", AIAA Journal, **36**(7), 1305-1311.

Abdalla, M. O., Grigoriadis, K. M. and Zimmerman, D. C., (2000), "Structural damage detection using linear matrix inequality methods", Journal of Vibration and Acoustics, **122**(4), 448-455.

Abdel Wahab, M. M. and De Roeck, G., (1999), "Damage detection in bridges using modal curvatures: application to a real damage scenario", Journal of Sound and Vibration, **226**(2), 217-235.

Ahmadian, H., Gladwell, G. M. L. and Ismail, F., (1997), "Parameter selection strategies in finite element model updating", Journal of Vibration and Acoustics, **119**(1), 37-45.

Aktan, A. E., Lee, K. L., Chuntavan, C. and Aksel, T., (1994), "Modal testing for structural identification and condition assessment of constructed facilities", Proceedings of the 12th International Modal Analysis Conference, Honolulu, Hawaii, 462-468.

Aldraihem, O. J., (2007), "Analysis of the dynamic stability of collar-stiffened pipes conveying fluid", Journal of Sound and Vibration, **300**(3-5), 453-465.

Allemang, R. J. and Brown, D. L., (1982), "A correlation coefficient for modal vector analysis", Proceedings of the 1st International Modal Analysis Conference, Orlando, Florida, 110-116.

Allemang, R. J., (2003), "The modal assurance criterion-twenty years of use and abuse", Sound and Vibration, **8**, 14-21.

Alvin, K. F. and Park, K. C., (1994), "Second-order structural identification procedure via state-space-based system identification", AIAA Journal, **32**(2), 397–406.

Alvin, K. F. and Park, K. C., (1999), "Extraction of substructural flexibility from global frequencies and mode shapes", AIAA Journal, **37**(11), 1444-1451.

Alvin, K. F., (1997), "Efficient computation of eigenvector sensitivities for structural dynamics", Journal of Sound and Vibration, **35**(11), 1760-1766.

Arora, J. S. and Nguyen, D. T., (1980), "Eigensolution for large structural systems with substructures", International Journal for Numerical Methods in Engineering, **15**(3), 333-341.

Bakir, P. G., Reynders, E. and De Roeck, G., (2007), "Sensitivity-based finite element model updating using constrained optimization with a trust region algorithm", Journal of Sound and Vibration, **305**(1-2), 211-225.

Baruch, M. and Bar-Itzhack, I. Y., (1978), "Optimal weighted orthogonalization of measured modes", AIAA Journal, **16**(4), 346-351.

Bathe, K. J., (1982), Finite Element Procedures in Engineering Analysis, Prentice-Hall, Englewood Cliffs, New Jersey.

Bathe, K. J. and Wilson, E. L., (1973), "Solution method for eigenvalue problems in structural mechanics", International Journal for Numerical Methods in Engineering, **6**, 213-226.

Bathe, K. J. and Ramaswamy, S., (1980), "An accelerated subspace iteration method", Computer Methods in Applied Mechanics and Engineering, **23**, 313-341.

Beck, J. L. and Karafygiotis, L. S., (1998), "Updating models and their uncertainties. I: Bayesian statistical framework", Journal of Engineering Mechanics, **124**(4), 455-461.

Bennighof, J. K. and Lehoucq, R. B., (2004), "An automated multilevel substructuring method for eigenspace computation in linear elastodynamics", Society for Industrial and Applied Mathematics, **25**(6), 2084-2106.

Berman, A., and Nagy, E. J., (1983), "Improvement of large analytical model using test data", AIAA Journal, **21**(8), 1168-1173.

Biondi, B. and Muscolino, G., (2003), "Component-mode synthesis method for coupled continuous and FE discretized substructures", Engineering Structures, **25**(4), 419-433.

Biondi, B., Muscolino, G. and Sofi, A., (2005), "A substructure approach for the dynamic analysis of train-track-bridge system", Computers and structures, **83**, 2271-2281.

Bohle, K. and Fritzen, C. P., (2003), "Results obtained by minimising natural frequency and MAC-values errors of a plate model", Mechanical Systems and Signal Processing, **17**(1), 55-64.

Brownjohn, J. M. W., (2007), "Structural health monitoring of civil infrastructure", Philosophical Transactions of the Royal Society A: Mathematical, Physical and Engineering Sciences, **365**(2), 589-622.

Brownjohn, J. M. W., Xia, P. Q., Hao, H. and Xia, Y., (2001), "Civil structure condition assessment by FE model updating: methodology and case studies", Finite Elements in Analysis and Design, **37**(10), 761-775.

Caesar, B., (1987), "Updating system matrices using modal test data", Proceedings of the 5th International Modal Analysis Conference, London, England, 453-459.

Cai, Y., Sun, H. and Xu, C., (2008), "Three-dimensional analyses of dynamic responses of track-ground system subjected to a moving train load", Computers and Structures, **86**(7-8), 816-824.

Caicedo, J. M. and Dyke, S. J., (2005), "Experimental validation of structural health monitoring for flexible bridge structures", Structural Control and Health Monitoring, **12**(3), 425-443.

Carden, E. P. and Fanning, P., (2004), "Vibration based condition monitoring: A review", Structural Health Monitoring, **3**(4), 355-377.

Carvalho, J., Datta, B. N., Gupta, A. and Lagadapati, M., (2006), "Finite element model updating: a close look at the computational aspects of direct methods", Proceedings of the 24th International Modal Analysis Conference, Louis, MO, 1-18.

Carvalho, J., Datta, B. N., Gupta, A. and Lagadapati, M., (2007), "A direct method for model updating with incomplete measured data and without spurious modes", Mechanical Systems and Signal Processing, **21**(7), 2715-2731.

Catbas, F. N., Gul, M. and Burkett, J. L., (2008), "Damage assessment using flexibility and flexibility-based curvature for structural health monitoring", Smart Materials and Structures, **17**(1), 1-12.

Cawley, P. and Adams, R. D., (1979), "The location of defects in structures from measurements of natural frequencies", Journal of Strain Analysis, **14**, 49-57.

Chen, H. M. and Archer, G. C., (2005), "New domain decomposition algorithm for nonlinear substructures", Journal of Computing in Civil Engineering, **19**(2), 148-159.

Cheung, S. H. and Beck, J. L., (2009), "Bayesian model updating using hybrid Monte Carlo simulation with application to structural dynamic models with many uncertain parameters", Journal of Engineering Mechanics, **135**(4), 243-255.

Choi, D., Kim, H. and Cho, M., (2008), "Iterative method for dynamic condensation combined with substructuring scheme", Journal of Sound and Vibration, **317**(1-2), 199-218.

Choi, K. K. and Kim, N. H., (2005), Structural Sensitivity Analysis and Optimization I: Linear Systems, Springer Science+Business Media, Inc., New York.

Choi, K. M., Cho, S. W., Ko, M. G. and Lee, I. W., (2004), "Higher order eigensensitivity analysis of damped systems with repeated eigenvalues", Computers and Structures, **82**(1), 63-69.

Christodoulou, K. and Papadimitriou, C., (2007), "Structural identification based on optimally weighted modal residuals", Mechanical Systems and Signal Processing, **21**(1), 4-23.

Clough, R. W. and Wilson, E. L., (1979), "Dynamic analysis of large structural systems with local nonlinearities", Computer Methods in Applied Mechanics and Engineering, **17**, 107-129.

Cottin, N. and Reetz, J., (2006), "Accuracy of multiparameter eigenvalues used for dynamic model updating with measured natural frequencies only", Mechanical Systems and Signal Processing, **20**(1), 65-77.

Craig, R. R. and Bampton, M. M. C., (1968), "Coupling of substructures for dynamic analysis", AIAA Journal, **6**(7), 1313-1319.

Craig, R. R., (2000), "Coupling of substructures for dynamic analyses: An overview", AIAA/ASME/ASCE/AHS/ASC the 41st Structures, Structural Dynamics, and Materials Conference, Atlanta, GA, 3-14.

D'Ambrogio, W. and Sestieri, A., (2004), "A unified approach to substructuring and structural modification problems", Shock and Vibration, **11**(3-4), 295-309.

Dailey, R. L., (1989), "Eigenvector derivatives with repeated eigenvalues", AIAA Journal, **27**(4), 486-491.

Daniell, W. E. and Macdonald, J. H. G., (2007), "Improved finite element modelling of a cable-stayed bridge through systematic manual tuning", Engineering Structures, **29**(3), 358-371.

Di, W. and Law, S. S., (2007), "Eigen-parameter decomposition of element matrices for structural damage detection", Engineering Structures, **29**(4), 519-528.

Dimarogonas, A. (1996). Vibration for Engineers, Prentice-Hall, Englewood Cliffs, New Jersey.

Doebling, S. W., (1995), Measurement of structural flexibility matrices for experiments with incomplete reciprocity, Ph.D dissertation, University of Colorado, America.

Doebling, S. W., (1996a), Damage identification and health monitoring of structural and mechanical systems from changes in their vibration characteristics: a literature review, Los Alamos National Laboratory, Report LA-13070-MS.

Doebling, S. W., (1996b), "Minimum-rank optimal update of elemental stiffness parameters for structural damage identification", AIAA Journal, **34**(12), 2615-2621.

Doebling, S. W., Farrar, C. R. and Cornwell, P. J., (1997), "DIAMOND: a graphical user interface toolbox for comparative modal analysis and damage identification", Proceedings of the 6th International Conference on Recent Advances in Structural Dynamics, Southampton, UK, 399-412.

Doebling, S. W., Peterson, L. D. and Alvin, K. F., (1996), "Estimation of reciprocal residual flexibility from experimental modal data", AIAA Journal, **34**(8), 1678-1685.

Doebling, S. W., Peterson, L. D. and Alvin, K. F., (1998), "Experimental determination of local structural stiffness by disassembly of measured flexibility matrices", Journal of Vibration and Acoustics, **120**(4), 949-957.

Duan, Z., Yan, G., Ou, J. and Spencer, B. F., (2005), "Damage detection in ambient vibration using proportional flexibility matrix with incomplete measured DOFs", Structural Control and Health Monitoring, **14**(2), 186-196.

Esfandiari, A., Bakhtiari-Nejad, F., Rahai, A. and Sanayei, M., (2009), "Structural model updating using frequency response function and quasi-linear sensitivity equation", Journal of Sound and Vibration, **326**(3-5), 557-573.

Eun, H.C., (2005), "A study on the structural analysis for structural synthesis of substructures", The Structural Design of Tall and Special Buildings, **14**, 131-141.

Farhat, C. and Geradin, M., (1994), "On a component mode synthesis method and its application to incompatible substructures", Computers and Structures, **51**(5), 459-473.

Farrar, C. R. and Worden, K., (2007), "An introduction to structural health monitoring", Philosophical Transactions of the Royal Society A: Mathematical, Physical and Engineering Sciences, **365**(2), 589-622.

Farrar, C. R., Doebling, S. W., Cornwell, P. J. and Straser, E. G., (1997), "Variability of modal parameters measured on the Alamosa Canyon bridge", Proceedings of the 15th International Modal Analysis Conference, Orlando, FL, 257-263.

Felippa, C. A. and Park, K. C., (1997), "A direct flexibility method", Computer Methods in Applied Mechanics and Engineering, **149**(1-4), 319-337.

Felippa, C. A. and Park, K. C., (2002), "The construction of free-free flexibility matrices for multilevel structural analysis", Computer Methods in Applied Mechanics and Engineering, **191**(19-20), 2111-2140.

Felippa, C. A., Park, K. C. and Filho, M. R. J., (1998), "The construction of free-free flexibility matrices as generalized stiffness inverses", Computers and Structures, **68**(4),

411-418.

Formenti, D. L. and Richardson, M. H., (2002), "Parameter estimation from frequency response measurements using rational fraction polynomials ", Proceedings of the 20th International Modal Analysis Conference, Los Angeles, CA, 1-10.

Fox, R. L. and Kapoor, M. P., (1968), "Rate of change of eigenvalues and eigenvectors", AIAA Journal, **6**(12), 2426-2429.

Friswell, M. I., Penny, J. E. T. and Wilson, D. A. L., (1994), "Using vibration data and statistical measures to locate damage in structures", Modal Analysis: The International Journal of Analytical and Experimental Modal Analysis, **9**(4), 239-254.

Friswell, M. I. and Mottershead, J. E., (1995), Finite Element Model Updating in Structural Dynamics, Kluwer Academic Publishers, Norwell, MA.

Friswell, M. I., (1995), "Calculation of second- and higher order eigenvector derivatives", Journal of Guidance, Control, and Dynamics, **18**(4), 919-921.

Friswell, M. I., (2007), "Damage identification using inverse methods", Philosophical Transactions of the Royal Society A: Mathematical, Physical and Engineering Sciences, **365**(1), 393-410.

Friswell, M. I., Garvey, S. D. and Penny, J. E. T., (1995), "Model reduction using dynamic and iterated IRS techniques", Journal of Sound and Vibration, **186**(2), 311-323.

Friswell, M. I., Garvey, S. D. and Penny, J. E. T., (1998a), "The convergence of the iterated IRS method ", Journal of Sound and Vibration, **211**(1), 123-132.

Friswell, M. I., Mottershead, J. E. and Ahmadian, H., (1998b), "Combining subset selection and parameter constraints in model updating", Journal of Vibration and Acoustics,

Transactions of the ASME, **120**(4), 854-859.

Friswell, M. I., Mottershead, J. E. and Smart, M. G., (1998c), "Dynamic models of golf clubs", Sports Engineering, **1**, 41-50.

Friswell, M. I., Penny, J. E. T. and Garvey, S. D., (1998d), "A combined genetic and eigensensitivity algorithm for the location of damage in structures", Computers and Structures, **69**(5), 547-556.

Friswell, M., Mottershead, J. E. and Ahmadian, H., (1997), "Combining subset selection and parameter constraints in model updating", Proceedings of the 16th ASME Biennial Conference on Mechanical Vibration and Noise, Sacramento, California, 41-47.

Friswell, M. I., Mottershead, J. E. and Ahmadian, H., (2007), "Finite-element model updating using experimental test data: parametrization and regularization", Philosophical Transactions of the Royal Society A: Mathematical, Physical and Engineering Sciences, **359**, 169-186.

Gao, Y., Spencer, B. F. and Bernal, D., (2007), "Experimental verification of the flexibility-based damage locating vector method", Journal of Engineering Mechanics, **133**(10), 1043-1049.

Garvey, S. D. and Penny, J. E. T., (1994), "Representing periodic structures efficiently as substructures", Journal of Sound and Vibration, **178**(1), 79-94.

Givoli, D., Barbone, P. E. and Patlashenko, I., (2004), "Which are the important modes of a subsystem?", International Journal for Numerical Methods in Engineering, **59**(12), 1657-1678.

Gladwell, G. M. L. and Ahmadian, H., (1995), "Generic element matrices suitable for finite element model updating", Mechanical Systems and Signal Processing, **9**(6), 601-614.

Goge, D. and Link, M., (2003), "Results obtained by minimizing natural frequency and mode shape errors of a beam model", Mechanical Systems and Signal Processing, **17**(1), 21-27.

Gordis, J. H., (1997), "On the analytical disassembly of structural matrices", Proceedings of the 15th International Modal Analysis Conference, Society for Experimental Mechanics, Bethel, CT, 1292-1297.

Gordis, J. H., Bielawa, R. L. and Flannelly, W. G., (1991), "A general theory for frequency domain structural synthesis", Journal of Sound and Vibration, **150**(1), 139-158.

Govers, Y. and Link, M., (2010), "Stochastic model updating--covariance matrix adjustment from uncertain experimental modal data", Mechanical Systems and Signal Processing, **24**(3), 696-706.

Grimes, R., Lewis, J. and Simon. H. (1994), "A shifted block Lanczos algorithm for solving symmetric generalized eigenproblems", SIAM Journal on Matrix Analysis and Applications, **15**(1), 228-272.

Guedria, N., Chouchane, M. and Smaoui, H., (2007), "Second-order eigensensitivity analysis of asymmetric damped systems using Nelson's method", Journal of Sound and Vibration, **300**(3-5), 974-992.

Guyan, R. J., (1965), "Reduction of stiffness and mass matrices", AIAA Journal, **3**(2), 380.

Hajela, P. and Soeiro, F. J., (1990), "Structural damage detection based on static and modal analysis", AIAA Journal, **28**(4), 1110-1115.

Han, T. and Abel, J. F., (1985), "Computational strategies for nonlinear and fracture mechanics problems", Computers and Structures, **20**(3), 181-192.

Hassis, H., (2000), "Proposition of a new approach for the substructure method", Journal of Sound and Vibration, **232**(4), 659-668.

Hua, X. G., Ni, Y. Q., Chen, Z. Q. and Ko, J. M., (2008), "An improved perturbation method for stochastic finite element model updating ", International Journal for Numerical Method in Engineering, **73**(3), 1845-1864.

Hua, X. G., (2006), Structural health monitoring and condition assessment of bridge structures, Ph.D dissertation, The HongKong Polytechnic University, Hong Kong.

Huang, B. C., Leung, A. Y. T., Lam, K. M. and Cheung, Y. K., (1996), "Analytical determination of equivalent modal damping ratios of a composite tower in wind-induced vibrations", Computers and Structures, **59**(2), 311-316.

Huang, H. W. and Yang, J. N., (2008), "Damage identification of substructure for local health monitoring", Smart Structures and Systems, **4**(6), 795-807.

Huang, N. E., (2000), "New method for nonlinear and nonstationary time series analysis: Empirical mode decomposition and Hilbert spectral analysis", Proceedings of SPIE - The International Society for Optical Engineering,197-209.

Humar, J., Bagchi, A. and Xu, H., (2006), "Performance of vibration-based techniques for the identification of structural damage", Structural Health Monitoring, **5**(3), 215-227.

Hurty, W. C. (1965). "Dynamic analysis of structural systems using component modes." AIAA Journal, **3**(4): 678-685.

Imregun, M. and Ewins, D. J., (1993), "An investigation into mode shape expansion techniques", Proceedings of the 11th International Modal Analysis Conference, Kissimmee, FL, 168-175.

Imregun, M. and Robb, D., (1992), "Structural modification via FRF coupling using measured data", Proceedings of the 10th International Modal Analysis Conference, Society for Experimental Mechanics, Bethel, CT, 1095–1099.

Imregun, M., Visser, W. J. and Ewins, D. J., (1995), "Finite element model updating using frequency response function data: I. Theory and initial investigation", Mechanical Systems and Signal Processing, **9**(2), 187-202.

Jaishi, B. and Ren, W. X., (2005), "Structural finite element model updating using ambient vibration test results", Journal of Structural Engineering, **131**(4), 617-628.

Jaishi, B. and Ren, W. X., (2006), "Damage detection by finite element model updating using modal flexibility residual", Journal of Sound and Vibration, **290**(1-2), 369-387.

Jaishi, B. and Ren, W. X., (2007), "Finite element model updating based on eigenvalue and strain energy residuals using multiobjective optimisation technique", Mechanical Systems and Signal Processing, **21**(5), 2295-2317.

Jaishi, B., Kim, H. J., Kim, M. K., Ren, W. X. and Lee, S. H., (2007), "Finite element model updating of concrete-filled steel tubular arch bridge under operational condition using modal flexibility", Mechanical Systems and Signal Processing, **21**(6), 2406-2426.

Jia, H. S., (1999), "On the bending coupled natural frequencies of a spinning, multispan timoshenko shaft carrying elastic disks", Journal of Sound and Vibration, **221**(4), 623-649.

Johnson, D. A., (2003), "A re-examination of geometric compatibility and shape function admissibility in Rayleigh-Ritz based substructure synthesis", Journal of Sound and Vibration, **267**(5), 1175-1183.

Johnson, E. A., Lam, H. F., Katafygiotis, L. S. and Beck, J. L., (2004), "Phase I IASC-ASCE structural health monitoring benchmark problem using simulated data", Journal of

Engineering Mechanics, **130**(1), 3-15.

Josson, J., Krenk, S. and Damkilde, L., (1995), "Recursive substructuring of finite elements", Computers and Structures, **54**(3), 395-404.

Kabe, A. M., (1985), "Stiffness matrix adjustment using mode data", Earthquake Engineering and Structural Dynamics, **24**(5), 747-759.

Kandil, A. and El-Rayes, K., (2005), "Parallel computing framework for optimizing construction planning in large-scale projects", Journal of Computing in Civil Engineering, **19**(3), 304-312.

Kaouk, M., Zimmerman, D. C. and Simmermacher, T. W., (2000), "Assessment of damage affecting all structural properties using experimental modal parameters", Journal of Vibration and Acoustics, Transactions of the ASME, **122**(4), 456-462.

Karafygiotis, L. S. and Beck, J. L., (1998), "Updating models and their uncertainties. II: model identifiability", Journal of Engineering Mechanics, **124**(4), 463-467.

Katafygiotis, L. S., Yuen, K. V. and Chen, J. C., (2001), "Bayesian modal updating by use of ambient data", AIAA Journal, **39**(2), 271-278.

Kenigsbuch, R. and Halevi, Y., (1998), "Model updating in structural dynamics: a generalised reference basis approach", Mechanical Systems and Signal Processing, **12**(1), 75-90.

Khodaparast, H. H., Mottershead, J. E. and Friswell, M. I., (2008), "Perturbation methods for the estimation of parameter variability in stochastic model updating", Mechanical Systems and Signal Processing, **22**(8), 1751-1773.

Kidder, R. I., (1973), "Reduction of structural frequency equation", AIAA Journal, **11**,

892-893.

Klerk, D. d., Rixen, D. J. and Voormeeren, S. N., (2008), "General framework for dynamic substructuring: history, review, and classification of techniques", AIAA Journal, **46**(5), 1169-1181.

Koh, C. G. and Perry, M. J., (2010), Structural Identification and Damage Detection Using Genetic Algorithms, CRC Press, Leiden, Netherlands.

Koh, C. G. and Shankar, K., (2003), "Substructural identification method without interface measurement", Journal of Engineering Mechanics, **129**(7), 769-776.

Koh, C. G., Hong, B. and Liaw, C. Y., (2003), "Substructural and progressive structural identification methods", Engineering Structures, **25**(12), 1551-1563.

Koh, C. G., See, L. M. and Balendra, T., (1991), "Estimation of structural parameters in time domain: A substructure approach", Earthquake Engineering and Structural Dynamics, **20**(8), 787-801.

Koh, C. G., Tee, K. F. and Quek, S. T., (2006), "Condensed model identification and recovery for structural damage assessment", Journal of Structural Engineering, **132**(12), 2018-2026.

Kron, G., (1963), Diakoptics, Macdonald and Co., London.

Kwon, K. S. and Lin, R. M., (2004), "Frequency selection method for FRF-based model updating", Journal of Sound and Vibration, **278**(1-2), 285-306.

Lam, H. F., Katafygiotis, L. S. and Mickleborough, N. C., (2004), "Application of a statistical model updating approach on Phase I of the IASC-ASCE structural health monitoring benchmark study", Journal of Engineering Mechanics, **130**(1), 34-48.

Lanczos, C., (1950), "An iteration method for the solution of the eigenvalue problem of

linear differential and integral operators", Journal of Research of the National Bureau of Standards, **45**(4), 255-282.

Law, S. S., Chan, T. H. T. and Wu, D., (2001), "Super-element with semi-rigid joints in model updating", Journal of Sound and Vibration, **239**(1), 19-39.

Lee, I. W. and Jung, G. H., (1995), "A combination of the Lanczos algorithm with the substructure technique", Journal of Sound and Vibration, **186**(4), 607-616.

Liew, K. M., Hung, K. C. and Lam, K. Y., (1993), "On the use of the substructure method for vibration analysis of rectangular plates with discontinuous boundary conditions", Journal of Sound and Vibration, **163**(3), 451-462.

Liew, K. M., Leek, S. E. and Liu, A. Q., (1996), "Mixed-interface substructures for dynamic analysis of flexible multibody systems", Engineering Structures, **18**(7), 495-503.

Lin, R. M. and Ewins, D. J., (1994), "Analytical model improvement using frequency response functions", Mechanical Systems and Signal Processing, **8**(4), 437-458.

Lin, R. M. and Lim, M. K., (1995), "Structural sensitivity analysis via reduced-order analytical model", Computer Methods in Applied Mechanics and Engineering, **121**(1-4), 345-359.

Lin, R. M. and Lim, M. K., (1996), "Eigenvector derivatives of structures with rigid body modes", AIAA Journal, **34**(5), 1083-1085.

Lin, R. M., Wang, Z. and Lim, M. K., (1996), "A practical algorithm for efficient computation of eigenvector sensitivities", Computer Methods in Applied Mechanics and Engineering, **130**(3-4), 355-367.

Lipkins, J. and Vandeurzen, U., (1987), "The use of smoothing techniques for structural

modification application", Proceedings of the 12th International Seminar on Modal Analysis, Leuven, Belgium, 1-3.

Liu, B., Riemenschneider, S. and Xu, Y., (2006), "Gearbox fault diagnosis using empirical mode decomposition and Hilbert spectrum", Mechanical Systems and Signal Processing, **20**(3), 718-734.

Liu, P. L., (1995), "Identification and damage detection of trusses using modal data", Journal of Structural Engineering, **121**(4), 599-608.

Ljung, L. and Glover, K., (1981), "Frequency domain versus time domain methods in system identification", Automatica, **17**(1), 71-86.

Lui, S. H., (1998), "Kron's method for symmetric eigenvalue problems", Journal of Computational and Applied Mathematics, **98**, 35-48.

Mackenzie, I. W., (1974), Computational methods for the eigenvalue analysis of large structures by component synthesis, Ph.D dissertation, University of London, London, UK.

MacNeal, R. H., (1971), "A hybrid method of component mode synthesis", Computers and Structures, **1**, 581-601.

Mares, C., Mottershead, J. E. and Friswell, M. I., (2006), "Stochastic model updating: Part 1--theory and simulated example", Mechanical Systems and Signal Processing, **20**(7), 1674-1695.

Markovic, D., Park, K. C. and Ibrahimbegovic, A., (2007), "Reduction of substructural interface degrees of freedom in flexibility-based component mode synthesis", International Journal for Numerical Method in Engineering, **70**(2), 163-180.

Matthies, H. G., (1985), "A Subspace Lanczos method for the generalized symmetric

eigenproblem", Computers and Structures, **21**(1~2), 319-325.

McGowan, P. E., Smith, S. W. and Javeed, M., (1990), "Experiments for locating damage members in a truss structure", Proceedings of the 2nd USAF/NASA Workshop on System Identification and Health Monitoring of Precision Space Structures, 571-615.

Meirovitch, L. and Kwak, M. K., (1990), "On the convergence of the classical Rayleigh-Ritz method and the finite element method", AIAA Journal, **28**(8), 1509-1516.

Meirovitch, L. and Kwak, M. K., (1991), "Rayleigh-Ritz based substructure synthesis method for flexible multibody systems", AIAA Journal, **29**(10), 1709-1719.

Meirovitch, L. and Kwak, M. K., (1992), "Inclusion principle for the Rayleigh-Ritz based substructure synthesis", AIAA Journal, **30**(5), 1344-1351.

Meirovitch, L., (1997), Principles and Techniques of Vibrations, Prentice-Hall, Englewood Cliffs, New Jersey.

Mills-Curran, W. C., (1988), "Calculation of eigenvector derivatives for structures with repeated eigenvalues", AIAA Journal, **26**(7), 867-871.

Modak, S. V., Kundra, T. K. and Nakra, B. C., (2002), "Prediction of dynamic characteristics using updated finite element models", Journal of Sound and Vibration, **254**(3), 447-467.

Morales, C., (2000), "Rayleigh-Ritz based substructure synthesis for multiply supported structures", Journal of Vibration and Acoustics, **122**(1), 2-6.

Morand, H. P. J. and Ohayon, R., (1979), "Substructure variational analysis for the vibrations of coupled fluid-structure systems", International Journal for Numerical Method in Engineering, **14**(5), 741-755.

Morgan, J. A., Pierre, C. and Hulbert, G. M., (2003), "Baseband methods of component mode

synthesis for non-proportionally damped systems", Mechanical Systems and Signal Processing, **17**(3), 589-598.

Mosegaard, K. and Tarantola, A., (2002), Probabilistic approach to inverse problems, International Handbook of Earthquake and Engineering Seismology, Academic Press, New York.

Mottershead, J. E. and Friswell, M. I., (1993), "Model updating in structural dynamics: A survey", Journal of Sound and Vibration, **167**(2), 347-375.

Mottershead, J. E., Friswell, M. I., Ng, G. H. T. and Brandon, J. A., (1996), "Geometric parameters for finite element model updating of joints and constraints", Mechanical Systems and Signal Processing, **10**(2), 171-182.

Mottershead, J. E., Mares, C., James, S. and Friswell, M. I., (2006), "Stochastic model updating: Part 2--application to a set of physical structures", Mechanical Systems and Signal Processing, **20**(8), 2171-2185.

Neal, R. M., (1993), Probabilistic inference using Markov chain Monte Carlo methods, Ph.D dissertation, Department of Computer Science, University of Toronto, Canada.

Neidbal, W., Klusowski, E. and Luber, W., (1990), "Updating a finite element model by means of normal mode parameters", Proceedings of the 8th International Modal Analysis Conference, Orlando, FL, 961-967.

Nelson, R. B., (1976), "Simplified calculation of eigenvector derivatives", AIAA Journal, **14**(9), 1201-1205.

Ng'andu, A. N., Fox, C. H. J. and Williams, E. G., (1995), "On the estimation of rotational degrees of freedom using spline functions", Proceedings of the 13th International Modal Analysis Conference, Nashville, TN, 791-797.

Ng'andu, A. N., Fox, C. H. J. and Williams, E. J., (1993), "Estimation of rotational degrees of freedom using curve and surface fitting", Proceedings of the 11th International Modal Analysis Conference, Kissimmee, FL, 620-626.

Ni, Y. Q., Zhou, X. T. and Ko, J. M., (2006), "Experimental investigation of seismic damage identification using PCA-compressed frequency response functions and neural networks", Journal of Sound and Vibration, **290**(1-2), 242-263.

Ni, Y. Q., Zhou, H. F. and Ko, J. M., (2009), "Generalization capability of neural network models for temperature-frequency correlation using monitoring data", Journal of Structural Engineering, **135**(10), 1290-1300.

Nour-Omid, B., Parlett, B. N., Taylor, R. L, (1983), "Lanczos versus subspace iteration for solution of eigenvalue problems", International Journal for Numerical Methods in Engineering, **19**(6), 859-871.

O'Callahan, J., (1989), "A processing for an Improved Reduced System (IRS) model", Proceedings of the 7th International Modal Analysis Conference, Las Vegas, NV, 17-21.

O'Callahan, J., Avitabile, P. and Riemer, R., (1989), "System equivalent reduction expansion process (SEREP)", Proceedings of the 7th International Modal Analysis Conference, Vegas, NV, 349-354.

Ojalvo, I. U., (1988), "Efficient computation of modal sensitivities for systems with repeated frequencies", AIAA Journal, **26**(3), 361-366.

Pandey, A. K. and Biswas, M., (1994), "Damage detection in structures using changes in flexibility", Journal of Sound and Vibration, **169**(1), 3-17.

Pandey, A. K., Biswas, M. and Samman, M. M., (1991), "Damage detection from changes in curvature mode shapes", Journal of Sound and Vibration, **145**(2), 321-332.

Park, K. C. and Reich, G. W., (1998), "Structural damage detection using localized flexibilities", Journal of Intelligent Material Systems and Structures, **9**(11), 911-919.

Park, K. C., Justino, J. M. and Felippa, C. A., (1997), "An algebraically partitioned FETI method for parallel structural analysis: algorithm description", International Journal for Numerical Method in Engineering, **40**(15), 2717-2737.

Parlett, B. N., (1987), The Symmetric Eigenvalue Problem, Prentice-Hall, Englewood Cliffs, New Jersey.

Parloo, E., Guillaume, P. and Van Overmeire, M., (2003), "Damage assessment using mode shape sensitivities", Mechanical Systems and Signal Processing, **17**(3), 499-518.

Peeters, B. and Roeck, G. D., (2001), "One-year monitoring of the Z24-Bridge: environmental effects versus damage events", Earthquake Engineering and Structural Dynamics, **30**(2), 149-171.

Perera, R. and Ruiz, A., (2008), "A multistage FE updating procedure for damage identification in large-scale structures based on multiobjective evolutionary optimization", Mechanical Systems and Signal Processing, **22**(4), 970-991.

Qian, Y. and Dhatt, G., (1995), "An accelerated subspace method for generalized eigenproblems", Computers and Structures, **54**(6), 1127-1134.

Qiu, J. B., Williams, F. W. and Qiu, R. X., (2003), "A new exact substructure method using mixed modes", Journal of Sound and Vibration, **266**(4), 737-757.

Qiu, J.-B., Ying, Z. G. and Williams, F. W., (1997), "Exact modal synthesis techniques using residual constraint modes", International Journal for Numerical Method in Engineering, **40**(13), 2475-2492.

Rade, D. A. and Lallement, G., (1998), "A strategy for the enrichment of experimental data as applied to an inverse eigensensitivity-based FE model updating method", Mechanical Systems and Signal Processing, **12**(2), 293-307.

Ratcliffe, M. J. and Lieven, N. A. J., (2000), "A generic element-based method for joint identification", Mechanical Systems and Signal Processing, **14**(1), 3-28.

Reda Taha, M. M., Noureldin, A., Lucero, J. L. and Baca, T. J., (2006), "Wavelet transform for structural health monitoring: A compendium of uses and features", Structural Health Monitoring, **5**(3), 267-295.

Reich, G. W. and Park, K. C., (2000), "Experimental application of a structural health monitoring methodology", Proceedings of the SPIE 3988, California, 143-153.

Ricles, J. M. and Kosmatka, J. B., (1992), "Damage detection in elastic structures using vibratory residual forces and weighted sensitivity", AIAA Journal, **30**(7), 2310-2316.

Rixen, D. J. D. J., (2004), "A dual Craig-Bampton method for dynamic substructuring", Journal of Computational and Applied Mathematics, **168**(1-2), 383-391.

Roberts, G. P. and Pearson, A. J. (1998), "Health monitoring of structures-towards a stethoscope for bridges", Proceedings of the 23th International Conference on Noise and Vibration Engineering, Leuven, Belgium, 885-889.

Rubin, S., (1975), "Improved component-mode representation for structural dynamic analysis", AIAA Journal, **8**(8), 995-1005.

Salawu, O. S., (1997), "Detection of structural damage through changes in frequency: a review", Engineering Structures, **19**(9), 718-723.

Sanayei, M. and Saletnik, M. J., (1996a), "Parameter estimation of structures from static

strain measurements, Part I: formulation", Journal of Structural Engineering, **122**(5), 555-562.

Sanayei, M. and Saletnik, M. J., (1996b), "Parameter estimation of structures from static strain measurements, Part II: error sensitivity analysis", Journal of Structural Engineering, **122**(5), 563-572.

Schueller, G. I. and Jensen, H. A., (2008), "Computational methods in optimization considering uncertainties - An overview", Computer Methods in Applied Mechanics and Engineering, **198**(1), 2-13.

Schwarz, B. and Richardson, M., (2003), "Scaling mode shapes obtained from operating data", Sound and Vibration, **11**, 18-22.

Sehmi, N. S., (1985), "A Newtonian procedure for the solution of the Kron characteristic value problem", Journal of Sound and Vibration, **100**(3), 409-421.

Sehmi, N. S., (1986), "The Lanczos algorithm applied to Kron's method", International Journal for Numerical Method in Engineering, **23**(10), 1857-1872.

Sehmi, N. S., (1989), Large Order Structural Eigenanalysis Techniques Algorithms for Finite Element Systems, Ellis Horwood Limited, Chichester, England.

Shanmugam, A. and Padmanabhan, C., (2006), "A fixed-free interface component mode synthesis method for rotordynamic analysis", Journal of Sound and Vibration, **297**(3-5), 664-679.

Shi, Z. Y., Law, S. S. and Zhang, L. M., (2000), "Structural damage detection from modal strain energy change", Journal of Engineering Mechanics, **126**(12), 1216-1223.

Shi, Z. Y., Law, S. S. and Zhang, L. M., (2002), "Improved damage quantification

from elemental modal strain energy change", Journal of Engineering Mechanics, **128**(5), 521-529.

Shyu, W.-H., Ma, Z. D. and Hulbert, G. M., (1997), "A new component mode synthesis method: Quasi-static mode compensation", Finite Elements in Analysis and Design, **24**(4), 271-281.

Simon, H. D. (1984), "Analysis for the symmetric Lanczos algorithm with reorthogonalization", Linear Algebra and Its Applications, **61**, 101-131.

Simpson, A. (1974), "Scanning Kron's determinant", Quarterly Journal of Mechanics and Applied Mathematics, **27**, 27-43.

Simpson, A. and Tabarrok, B., (1968), "On Kron's eigenvalue procedure and related methods of frequency analysis", Quarterly Journal of Mechanics and Applied Mathematics, **21**, 1039-1048.

Simpson, A., (1973a), "Eigenvalue and vector sensitivity in Kron's method", Journal of Sound and Vibration, **31**(1), 73-87.

Simpson, A., (1973b), "A generalization of Kron's eigenvalue procedure", Journal of Sound and Vibration, **26**(1), 129-139.

Simpson, A., (1982), "A Newtonian procedure for the solutions of Ex=Ax", Journal of Sound and Vibration, **82**(2), 161-170.

Smith, S. W. and Beattie, C. A., (1991), "Model correlation and damage location for large space truss structures: secant method development and evaluation", NASA Report NASA-CR-188102.

Smith, S. W. and Beattie, C. A., (1990), "Simultaneous expansion and orthogonalization of

measured modes for structure identification", Proceedings of the AIAA SEM Dynamic Specialists Conference, Long Beach, California, 71-76.

Smith, S. W., (1992), "Iterative use of direct matrix updates: connectivity and convergence", Proceedings of the 33rd AIAA Structures, Structural Dynamics and Materials Conference, Dallas, TX, 1797-1806.

Smith, S. W., (1998), "Iterative matrix approximation for model updating", Mechanical Systems and Signal Processing, **12**(1), 187-201.

Sohn, H., (2007), "Effects of environmental and operational variability on structural health monitoring", Philosophical Transactions of the Royal Society A: Mathematical, Physical and Engineering Sciences, **365**(2), 539-560.

Sohn, H., Dzwonczyk, M., Straser, E. G., Kiremidjian, A. S., Law, K. H. and Meng, T., (1999), "An experimental study of temperature effect on modal parameters of the Alamosa Canyon bridge", Earthquake Engineering and Structural Dynamics, **28**(8), 879-897.

Song, D. T., Han, W. Z., Chen, S. H. and Qiu, Z. P., (1996), "Simplified calculation of eigenvector derivatives with repeated eigenvalues", AIAA Journal, **34**(4), 859-861.

Spanos, J. T. and Tsuha, W. S., (1991), "Selection of component modes for flexible multibody simulation", Journal of Guidance, **14**(2), 278-286.

Suarez, L. E. and Singh, M. P., (1992), "Improved fixed interface method for modal synthesis ", AIAA Journal, **30**(12), 2952-2958.

Sunar, M. and Rao, S. S., (1997), "A substructure method for the active control design of large periodic structure", Computers and Structures, **65**(5), 695-701.

Sutter, T. R., Camarda, C. J., Walsh, J. L. and Adelman, W. M., (1988), "A comparison of

several methods for the calculation of vibration mode shape derivatives", AIAA Journal, **26**(12), 1506-1511.

Synn, S. Y. and Fulton, R. E., (1995), "Practical strategy for concurrent substructure analysis", Computers and Structures, **54**(5), 939-944.

Takewaki, I. and Uetani, K., (2000), "Inverse component-mode synthesis method for damped large structural systems", Computers and Structures, **78**(1-3), 415-423.

Tee, K. F., Koh, C. G. and Quek, S. T., (2005), "Substructural first- and second-order model identification for structural damage assessment", Earthquake Engineering and Structural Dynamics, **34**(15), 1755-1775.

Tee, K. F., Koh, C. G. and Quek, S. T., (2009), "Numerical and experimental studies of a substructural identification strategy", Structural Health Monitoring, **8**(5), 397-410.

Terrell, M. J., Friswell, M. I. and Lieven, N. A. J., (2007), "Constrained generic substructure transformations in finite element model updating", Journal of Sound and Vibration, **300**, 265-279.

Teughels, A. and De Roeck, G., (2004), "Structural damage identification of the highway bridge Z24 by FE model updating", Journal of Sound and Vibration, **278**(3), 589-610.

Thonon, C. and Golinval, J. C., (2003), "Results obtained by minimising natural frequency and MAC value errors of a beam model", Mechanical Systems and Signal Processing, **17**(1), 65-72.

Titurus, B., Friswell, M. I. and Starek, L., (2003), "Damage detection using generic elements: part I model updating", Computers and Structures, **81**, 2273-2286.

To, W. M., Lin, R. M. and Ewins, D. J., (1990), "A criterion for the localisation of structural

modification sites using modal data", Proceedings of the 8th International Modal Analysis Conference, Orlando, FL, 804-811.

Topole, K., (1997), "Damage evaluation via flexibility formulation, smart systems for bridges, structures and highways", Proceedings of the SPIE 3043, San Diego, CA 145-154.

Tournour, M. A., Atalla, N., Chiello, O. and Sgard, F., (2001), "Validation, performance, convergence and application of free interface component mode synthesis", Computers and Structures, **79**(20-21), 1861-1876.

Turner, G. L., (1983), Finite element modeling and dynamic substructuring for prediction of diesel engine vibration, Ph.D. dissertation, Loughborough University of Technology, England.

Umesha, P. K., Venuraju, M. T., Hartmann, D. and Leimbach, K. R., (2007), "Parallel computing techniques for sensitivity analysis in optimum structural design", Journal of Computing in Civil Engineering, **21**(6), 463-477.

Wang, B. P., (1985), "An improved approximate method for computing eigenvector derivatives", Proceedings of the AIAA/ASME/ASCE/AHS 20th Structures, Structural Dynamics and Materials Conference, Orlando, FL, 381-392.

Wang, B. P., (1991), "Improved approximate methods for computing eigenvector derivatives in structural dynamics", AIAA Journal, **29**(6), 1018-1020.

Wang, Q. and Deng, X., (1999), "Damage detection with spatial wavelets", International Journal of Solids and Structures, **36**(23), 3443-3468.

Weber, B. and Paultre, P., (2010), "Damage identification in a truss tower by regularized model updating", Journal of Structural Engineering, **136**(3), 307-316.

Wegner, J. L., Yao, M. M. and Zhang, X., (2005), "Dynamic wave-soil-structure interaction analysis in the time domain", Computers and Structures, **83**(27), 2206-2214.

Williams, E. G. and Green, J. S., (1990), "A spatial curve fitting technique for estimating rotational degrees of freedom", Proceedings of the 8th International Modal Analysis Conference (IMAC 8), Kissimmee, FL, 376-391.

Williams, E. J., Contursi, T. and Messina, A., (1996), "Damage detection and localization using natural frequencies sensitivity", Proceedings of Conference on Identification in Engineering Systems, Swansea, UK, 368-376.

Williams, F. W. and Kennedy, D., (1988), "Reliable use of determinants to solve non-linear structural eigenvalue problems efficiently", International Journal for Numerical Methods in Engineering, **26**(8), 1825-1841.

Wu, B. S., Xu, Z. H. and Li, Z. G., (2007), "Improved nelson's method for computing eigenvector derivatives with distinct and repeated eigenvalues", AIAA Journal, **45**(4), 950-952.

Wu, B., Xu, Z. and Li, Z., (2006), "A note on computing eigenvector derivatives with distinct and repeated eigenvalues", Communications in Numerical Methods in Engineering, **23**(3), 241-251.

Wu, D. and Law, S. S., (2004a), "Model error correction from truncated modal flexibility sensitivity and generic parameters. II: experimental verification", Mechanical Systems and Signal Processing, **18**(6), 1401-1419.

Wu, D. and Law, S. S., (2004b), "Model error correction from truncated modal flexibility sensitivity and generic parameters. I: simulation", Mechanical Systems and Signal Processing, **18**(6), 1381-1399.

Wu, J. R. and Li, Q. S., (2004), "Finite element model updating for a high-rise structure based on ambient vibration measurements", Engineering Structures, **26**(7), 979-990.

Xia, Y. and Hao, H., (2003), "Statistical damage identification of structures with frequency changes", Journal of Sound and Vibration, **263**, 853-870.

Xia, Y. and Lin, R., (2004a), "Improvement on the iterated IRS method for structural eigensolutions", Journal of Sound and Vibration, **270**(4-5), 713-727.

Xia, Y. and Lin, R., (2004b), "A new iterative order reduction (IOR) method for eigensolutions of large structures", International Journal for Numerical Method in Engineering, **59**(1), 153-172.

Xia, Y., Hao, H., Brownjohn, J. M. W. and Xia, P. Q., (2002), "Damage identification of structures with uncertain frequency and mode shape data", Earthquake Engineering and Structural Dynamics, **31**(5), 1053-1066.

Xia, Y., Hao, H., Deeks, A. J. and Zhu, X., (2008), "Condition assessment of shear connectors in slab-girder bridges via vibration measurements", Journal of Bridge Engineering, **13**(1), 43-54.

Xia, Y., Hao, H., Zanardo, G. and Deeks, A., (2006), "Long term vibration monitoring of an RC slab: Temperature and humidity effect", Engineering Structures, **28**(3), 441-452.

Yamamoto, Y. and Ohtsubo, H. (1976), "Subspace iteration accelerated by using Chebyshev polynomials for eigenvalue problems with symmetric matrices", International Journal for Numerical Methods in Engineering, **10**(4), 935-944.

Yang, J. N. and Huang, H. W., (2007), "Substructure damage identification using a damage tracking technique", Proceedings of SPIE - The International Society for Optical Engineering, San Diego, California, USA, Article No. 65292R.

Yang, Q. W. and Liu, J. K., (2009), "Damage identification by the eigenparameter decomposition of structural flexibility change", International Journal for Numerical Method in Engineering, **78**(4), 444-459.

Yuen, K. V. and Katafygiotis, L. S., (2001), "Bayesian time-domain approach for modal updating using ambient data", Probabilistic Engineering Mechanics, **16**(3), 219-231.

Yuen, K. V. and Katafygiotis, L. S., (2002), "Bayesian modal updating using complete input and incomplete response noisy measurements", Journal of Engineering Mechanics, **128**(3).

Yuen, K. V. and Katafygiotis, L. S., (2005), "Model updating using noisy response measurements without knowledge of the input spectrum", Earthquake Engineering and Structural Dynamics, **34**(2), 167-187.

Yuen, K. V. and Katafygiotis, L. S., (2006), "Substructure identification and health monitoring using noisy response measurements only", Computer-Aided Civil and Infrastructure Engineering, **21**(4), 280-291.

Yun, C. B. and Bahng, E. Y., (2000), "Substructural identification using neural networks", Computers and Structures, **77**(1), 41-52.

Yun, C. B. and Lee, H. J., (1997), "Substructural identification for damage estimation of structures", Structural Safety, **19**(1), 121-140.

Zhang, Q. W., Chang, C. C. and Chang, T. Y. P., (2000), "Finite element model updating for structures with parametric constraints", Earthquake Engineering and Structural Dynamics, **29**(7), 927-944.

Zhao, J. and Dewolf, J. T., (1999), "Sensitivity study for vibrational parameters used in damage detection", Journal of Structural Engineering, **125**(4), 410-416.

Zhao, X. and Simpson, A., (1988), "Kron's procedure for a freely vibrating spinning structure", Quarterly Journal of Mechanics and Applied Mathematics, **41**(4), 597-618.

Ziaei-Rad, S., (1997), Methods for Updating Numerical Models in Structural Dynamics, Ph.D. dissertation, Imperial College, University of London, London, UK.

Zimmerman, D. C. and Kaouk, M., (1994), "Structural damage detection using a minimum rank update theory", Journal of Vibration and Acoustics, **116**(2), 222-230.

Zimmerman, D., James, I. G. and Cao, T., (1999), "An experimental study of damage detection using modal, strain, and Ritz properties", Proceedings of the 17th International Modal Analysis Conference, Orlando, Florida, 586-592.

Zivanovic, S., Pavic, A. and Reynolds, P., (2007), "Finite element modelling and updating of a lively footbridge: the complete process", Journal of Sound and Vibration, **301**(1-2), 126-145.